UNIVERSITY OF
OXFORD

Immune Regulatory Networks in Inflammation-driven Cancer

Fanny Franchini

University of Oxford

Merton College

Nuffield Department of Medicine

A thesis submitted for the degree of *Doctor of Philosophy*,

Michaelmas Term, 2017

Abstract

Fanny Franchini | DPhil Thesis Abstract | Merton College | Trinity 2017

Immune Regulatory Betworks in Inflammation-driven Cancer

The incidence of colorectal cancer (CRC) is increasing and the prognosis for patients with advanced or metastatic disease is relatively poor. Immunotherapies hold great promise, but deploying them effectively in CRC patients will require further knowledge of the complex cellular and molecular interactions that occur between intestinal tumours and the host immune system. The objective of this study is to understand the mechanisms by which lack of immune cell regulation in the gut can drive formation of colon adenocarcinomas. In addition, this work aims to identify new mechanisms involved in progression to metastatic disease.

Using mouse model systems, we found that aberrant activity of Treg cells deficient in IL-10 can promote inflammation-driven CRC. IL-10 deficient Tregs have increased capacity to drive tumourigenesis compared to their $CD4^+$ effector T cell counterparts. RNA sequencing revealed specific upregulation of *Meteorin-like* in tumour-promoting Tregs, which is a recently described cytokine uncharacterised in Treg cells. We explored cytokine regulation and the tumour microenvironment, and show that the inflammatory cytokine IL-6 and TGFβ are necessary for tumour formation in this model. Moreover, disease is associated with a marked stromal cell signature that is induced as a consequence of Treg deficiency in IL-10 production. $Gp38^+$ stromal cells are dominant producers of IL-6, and potent ECM modellers. Furthermore, tumours driven by IL-10 deficient Tregs express high amounts of the pro-mesenchymal transcription factor Sox4. Using combined *in vitro* and *in vivo* analyses, we confirm that Sox4 is involved in tumour growth and characterise its expression in CRC patients.

Collectively, our findings suggest that Tregs and stromal cells act together to foster a microenvironment that promotes disease progression, notably through the expression of Sox4 in tumour cells. These findings open an exciting avenue to explore the phenotype of tumour-promoting Tregs and to study Sox4 function in metastatic disease.

Acknowledgements

I would like to express my deepest gratitude to my supervisor Professor Fiona Powrie for her continuous support and guidance, but also for the freedom to explore new ideas that she has given me throughout this DPhil. I am also grateful to CR-UK for the generous funding, for opening me the doors of public engagement, and for the opportunity to meet patients and fundraisers.

I am forever grateful to the members of the Powrie Lab who have made this experience unforgettable and truly amazing. Thank you to Nathan, Sarah, Matthias, Claire, Sam and Julie for reading parts of this thesis. I am also truly embedded to the members of the old and new Powrie Lab for their support in and outside the lab. Isabelle and Julie, thank you for your support when I needed it the most and for teaching me the ins and outs of takedowns. I will never forget the music-late-night-good-food times with you. Thank you Aga for your friendship and your enthusiasm, I enjoyed so much working with you outside the cancer realm! Thank you Camille for the fun in the lab and with the Green Impact Team. Thank you to Nate and Grisha for involving me on the Alpk1 project, you have taught me a lot. Grisha, your friendship, honesty and immense knowledge have brought me so many happy moments – thank you! Thank you Claire, Julia, Emily and Stefanie for being there from the very start. Claire, I cannot count how many times you have solved all the little disasters, I am truly thankful for your help throughout these years. Finally, thank you to Alina and Nicole – you have taught me more than I could ever hope to teach you during our short crossroads. Much luck and happy DPhil to Andrea and Yisu!

Coming to Oxford has changed my life and Merton College has been an inspiring place to be. Victor, I am truly thankful for your love and endless support, the memories we have made in Oxford will last forever. This journey has separated me from my family for so many years, and I have no words to express my deepest gratitude for the continuous support received over all these years. To my Dad, Grandpa and Sister, who have been lifelong sources of love, support and inspiration – merci.

Contributions

Dr. Stefanie Kirchberger for her guidance at the beginning of my DPhil, and first experiments performed together to investigate the role of IL-22 in our mouse models.

Dr. Nathaniel West for the initial analysis of SOX4 expression in primary tumours and liver and lung metastases in colorectal cancer patients.

Dr. John Buzzelli for the analysis of SOX4 mRNA and protein expression in normal liver and metastastic liver from colorectal cancer patients.

Table of contents

List of abbreviations

Abbreviations	
AMP	Antimicrobial Peptide
AOM	Azoxymethane
APC	Antigen-Presenting Cell
APC	Adenomatous polyposis coli gene
Areg	Amphiregulin
CAC	Colitis-Associated Cancer
CAF	Cancer associated fibroblast
CD	Cluster of Differentiation
CFU	Colony-Forming Units
CNS	Conserved Noncoding Sequence
CRC	Colorectal Cancer
CTL	Cytotoxic T lymphocyte
DAMP	Damage-Associated Molecular Pattern
DAPI	4',6-Diamidino-2-Phenylindole
DC	Dendritic Cell
DSS	Dextran Sulfate Sodium
ELISA	Enzyme-Linked Immunosorbent Assay
EMT	Epithelial-mesenchymal transitio
FACS	Fluorescence-Activated Cell Sorting
Foxp3	Forkhead Box P3
GALT	Gut-Associated Lymphoid Tissue
GF	Germ Free
GFP	Green Fluorescent Protein
GI	Gastrointestinal
gMFI	Geometric Mean Fluorescent Intensity
Hh	*Helicobacter hepaticus*
i.p.	Intraperitoneal
i.v.	Intravenous
IBD	Inflammatory Bowel Disease
IEC	Intestinal Epithelial Cell
IFN	Interferon
Ig	Immunoglobulin
IHC	Immunohistochemistry
IL	Interleukin
ILC	Innate Lymphoid Cell
IPEX	Immunodysregulation Polyendocrinopathy Enteropathy X-Linked Syndrome
KO	Knockout
LP	Lamina Propria
mAb	Monoclonal Antibody
MHC	Major Histocompatibility Complex
MLN	Mesenteric Lymph Node
MSI	Microsatellite instable
MSS	Microsatellite stable
NK	Natural Killer Cell
OD	Optical Density
PAMP	Pathogen-Associated Molecular Pattern
PDGFR	Platelet-Derived Growth Factor Receptor
PRR	Pattern Recognition Receptor
pTreg	Peripheral Treg

Abbreviations	
RA	Retinoic Acid
RIN	RNA Integrity Number
Rorγt	RAR-related orphan receptor-γt
RT-qPCR	Real-Time Quantitative Polymerase Chain Reaction
SEM	Standard Error of the Mean
SOX4	SRY (sex determining region Y)-box 4
SPF	Specific Pathogen-Free
STAT	Signal Transducer and Activator of Transcription
TAM	Tumour associated macrophage
TCR	T Cell Receptor
Tfh	Follicular T Helper Cell
TGF	Transforming Growth Factor
Th	Helper T Cell
TLR	Toll-Like Receptor
TNF	Tumor Necrosis Factor
Treg	Regulatory T Cell
tTreg	Thymic Treg
UC	Ulcerative Colitis
VAT	Visceral Adipose Tissue
WT	Wild Type

1 Introduction

The immune system represents a network of cells, tissues and organs that has evolved to protect the host from cellular damage caused by acute inflammation or sterile injury, as well as to coordinate responses against a wide range of pathogens (Shalapour and Karin, 2015). While the robust response of the immune system is critical for the host's protection, hyperactive responses towards external antigens as well as self-molecules are a signature of many immune diseases. Apart from its recognition of pathogens, the immune system is also able to recognise abnormal cells or tissues, such as tumours, which has long sparked an interest in harnessing its ability to promote anti-tumour responses in cancer patients. Tumourigenesis is the result of a complex interplay between cell intrinsic and extrinsic processes that promote sustained proliferation, resistance to apoptosis, reprogramming and reorganisation of the stromal environment, and genomic instability. Inflammation, although necessary for damage repair and anti-tumour immunity, can influence these processes to favour neoplasia. As such, inflammation is now perceived as an enabling characteristic for the acquisition of the core hallmarks of cancer. (Hanahan and Weinberg, 2011).

1.1 The Intestine: home of friends and potential foes

The gastrointestinal tract is one of the major sites of immunological challenge to the host immune system. It is characterised by an abundance of dietary antigens and enteric flora, but is also a major site of pathogen entry. Therefore, immune reactivity must be tightly regulated to promote tolerance towards commensals, as well as to mount appropriate responses towards pathogens. Dysregulated immune responses towards bacterial antigens in the intestine in a genetically susceptible host are a

hallmark of inflammatory bowel disease (IBD) (Maloy and Powrie, 2011). Regulatory networks controlling intestinal homeostasis are complex and involve different cell populations, including regulatory T cell (Tregs), which play a critical role in maintaining this fine balance (Maloy and Powrie, 2011).

1.1.1 The architecture of the intestine

The intestine is one of the largest immune compartments and represents a large surface area exposed to the outside world. While food digestion occurs in the small intestine, the colon is the primary site of water absorption and contains the highest density of commensal bacteria within the gastrointestinal tract. The intestine can be divided into distinct cellular compartments: the epithelium, lamina propria (LP), the muscularis mucosae, which is a thin muscle layer, the submucosal layer of connective tissue, and another thick muscle layer that is involved in peristalsis (**Figure 1.1**). Most immune cells are found in the epithelium, LP, and the underlining muscularis mucosae. Immune responses are initiated in gut-associated lymphoid tissue (GALT), which are similar structures to draining lymph nodes, and in the mesenteric lymph nodes (MLNs). (Buettner and Lochner, 2016; Mowat, 2003).

1.1.2 The intestinal microbiota

The colon contains a diverse community of microorganisms, including protozoa, fungi, viruses, archaea and the most prevalent group, bacteria (Knight, 2011). Collectively these microorganisms are termed the gut microbiota. The total amount and diversity of bacteria increase down the length of the GI tract, with a gradient in concentration along the colon itself, and approximately 10^{11} bacteria per gram measured in human stool (Sender et al., 2016). Commensal bacteria are an critical part of the mammalian body, and through aeons of co-evolution, a symbiotic and

mutualistic relationship with the host was established. The microbiota yield several benefits to the host, including breakdown, absorption and storage of nutrients, regulation of gut maturation and integrity, modulation of immune responses, but also restriction of pathogenic bacteria outgrowth through niche competition (reviewed in Ivanov and Honda, 2012). Perturbations to microbiota-host interactions may lead to dysbiosis, which has been suggested to play an essential role in the pathogenesis of multiple diseases, including IBD and colorectal cancer (Brennan and Garrett, 2016; Hansen, 2015).

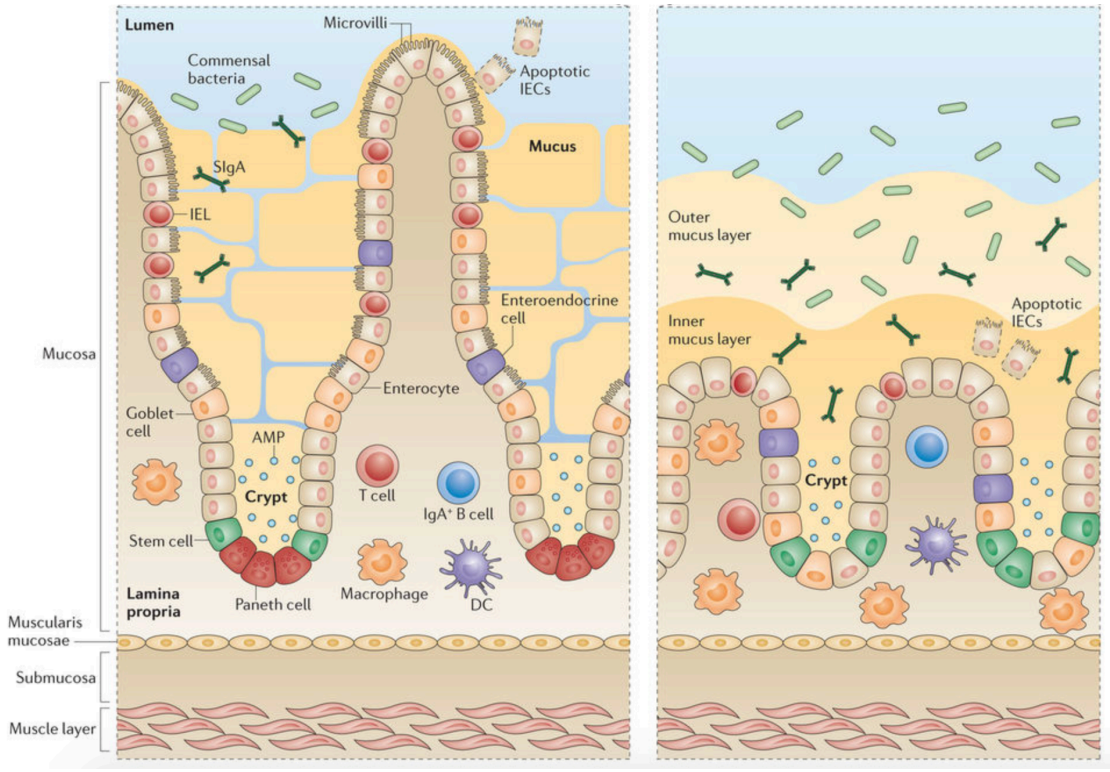

Figure 1.1: The intestinal immune system

Schematics of the small intestine (left) and the colon (right), representing major components of the tissue architecture and of the intestinal immune system.

Bacteria and luminal contents are found in the lumen (top), and a mucus layer overlies the single-cell intestinal barrier composed of epithelial cells. Intestinal stem cells lie in the crypts. The lamina propria is found right below the intestinal barrier, and is separated from the submucosa and the muscle layer by a thin layer of muscle cells called muscularis mucosae. Numerous different immune cell populations are found in the lamina propria, while the submucosa is mainly composed of non-haematopoietic cells.

AMP, antimicrobial peptide; DC, dendritic cell; IEL, intraepithelial lymphocytes; SIgA, secretory immunoglobulin A. Figure reproduced with the authorisation from Nature Publishing Group, NRI (Mowat and Agace, 2014).

1.1.3 The physiology of the epithelial barrier

A single-cell layer of columnar epithelial cells separates the microbiota from the colonic lamina propria and therefore represents a physical barrier between the luminal content and the host. The surface of the epithelium forms glandular invaginations that protrude into the underlying connective tissue, and are called crypts of Lieberkühn. These crypts are the basic functional unit of the gut and harbour the stem-cell niche at their base. The intestinal epithelium turns over rapidly and is continually replaced from the intestinal stem cell (ISC) pool. Over the past decade, signals that regulate intestinal stem cell renewal and proliferation have been extensively characterised. The WNT, EGFR/MAPK and NOTCH pathways promote the undifferentiated proliferative state of ISCs in the niche, whereas BMP and TGF-β signalling induce differentiation into sublineages (Clevers, 2013). Specifically, stem cells give rise to progenitor cells that spend approximately two days in the crypt, where they undergo rapid proliferation and terminally differentiate into the different intestinal epithelial cell (IEC) lineages as they migrate from the crypt to the luminal surface. Enterocytes, a specialised cell type that absorbs nutrients constitute the majority of IECs, complemented by goblet cells, Paneth cells, microfold cells and enteroendocrine cells. (Biswas et al., 2015; van der Flier and Clevers, 2009). Finally, to maintain the intestinal barrier while regulating the permeability of ions, nutrients and water, IECs are connected to each other through tight junctions. These junctions are dynamic multi-protein complexes that form a selectively permeable seal between adjacent epithelial cells and establish the apical-basolateral axis of the cells (Shen and Turner, 2006).

Upon cell injury, which occurs in several ways, such as exposure to toxic luminal substances, normal digestion processes, inflammation or pharmaceuticals (Iizuka, 2011), the wound healing response is triggered. This represents a highly dynamic process involving immune-epithelial-fibroblast cell interactions (Leoni et al., 2015). The coordination of the migration and proliferation of epithelial cells establishes the wound healing process. First, epithelial cells surrounding the injury lose their columnar polarity and rapidly migrate as a sheet that covers the denuded area to restore barrier integrity, in a process called “epithelial restitution” (Iizuka, 2011; Nusrat et al., 1992). This process occurs very quickly and is independent of cell proliferation, but rather involves cellular reorganisation whereby epithelial cells develop filamentous-actin-rich protrusions that adhere to the matrix and mediate forward movement of the epithelial sheet (Leoni et al., 2015; Lotz et al., 1997). Subsequently, and especially when the wound is large, epithelial cells proliferate and differentiate from the stem cell pool to increase the number of cells that populate the wound, thereby contributing to wound closure. As wound healing progresses, fibroblasts play critical roles in synthesising a newly formed matrix, enriched in collagen, and facilitating the contracting and repair of the mucosa, notably through the expression of smooth muscle actin that generates contractile forces (Leoni et al., 2015). The immune system controls and establishes the coordination of wound healing through the expression of various cytokines, such as TGF-β, IL-1β, and IL-6, as well as processes such as clearance of bacteria and cell debris, leading to a restoration of homeostasis (Beck et al., 2010; Kuhn et al., 2014; Leoni et al., 2015).

1.1.4 The epithelial barrier as a physical safeguard

Intestinal epithelial cells have a critical role in segregating host and microbes, and chronic disruption of the epithelium leads to colonic inflammation, due to bacterial translocation into the colonic tissue (Maloy and Powrie, 2011). Several subpopulations of IECs reside in the colon and employ different mechanisms to maintain intestinal homeostasis. For instance, goblet cells secrete mucins, forming a thick mucus composed of two layers, of which the inner part prevents close contact between the microbiota and the host, while the outer layer confers an ecological niche to commensals in the form of biofilms (Johansson et al., 2008). Microfold cells (M cells) represent another specialised lineage of IECs that sample and deliver microbial antigens, from the luminal contents across the epithelium via transcytosis, to various immune cell populations, such as antigen-presenting cells (APCs). (Lorenz and Newberry, 2004; Mabbott et al., 2013). Paneth cells secrete several anti-microbial peptides (AMPs), such as Defensins and Cathelicidins, the latter being specifically expressed at the surface and the top of the colonic crypts (Hase, 2002). These AMPs possess bactericidal activity towards gram-negative and gram-positive bacteria, and can also attract immune cells, as they possess effective chemo-attractant activities (Yang, 1999). Finally, IECs are able to sense the microbiota through the expression of pattern recognition receptors (PRRs), which include Toll-like receptors (TLRs), nuclear oligomerisation domain (NOD)-like receptors (NLRs) and RIG-I-like receptors (RLRs). These PRRs recognise pathogen-associated molecular patterns (PAMPs), which include a wide range of microbe-derived molecules (i.e. lipopolysaccharide, peptidoglycans, flagella, microbial nucleic acids), as well as damage-associated molecular patterns (DAMPs), which are components of host cells

released upon acute injury and death. (Abreu, 2010; Elinav et al., 2013; Seong and Matzinger, 2004). Although IECs are equipped with various mechanisms that are critical for the initiation of an immune response towards pathogens, commensals usually do not trigger hyperresponses in the intestine. In fact, these mechanisms are kept in balance by the expression of negative regulators of PRR-dependent pro-inflammatory signalling, such as single Ig IL-1-related receptor (SIGIRR), which maintains the microbial tolerance of the colonic epithelium (Xiao et al., 2007). Moreover, depending on the anatomical location of TLRs, a differential response is triggered. For instance, the apical exposure of IECs to TLR9 ligands results in a tolerogenic response, while the basolateral exposure leads to NF-κB activation (Lee et al., 2006). All these mechanisms enable the intestine to remain hyporesponsive to the microbiota yet able to quickly initiate a response upon a barrier breach.

1.2 The colonic immune response

Inflammation is a complex and dynamic biological response to cellular damage that is caused either by sterile injury (i.e. cell death) or infection. Following damage, the immune system fosters a coordinated response that eliminates or neutralises harmful stimuli and initiates the healing and regenerative processes (Shalapour and Karin, 2015).

1.2.1 The innate immune system

The innate immune system, which is more evolutionarily ancient than the adaptive immune system, forms the first line of defence once physical and chemical barriers are compromised.

1.2.1.1 The basics of the immune response

Similarly to IECs, the innate immune system recognises sequences of PAMPs or DAMPs (termed antigens) and can respond to a variety of cytokines emitted by IECs. Upon recognition of these signals, a variety of tissue-resident cells are activated, such as resident monocytes, which produce cytokines and chemokines, thereby attracting other innate cell populations that are involved in the destruction of pathogens (Iwasaki and Medzhitov, 2015).

Although innate immune cells ensure the initial response and restrain the proliferation of pathogens for the first few days, antigen-presenting cells (APCs), dendritic cells and macrophages, initiate a series of events that are central to the host's antigen driven adaptive immune response (Janeway, 1989). Thus, once activated, they upregulate major histocompatibility complex (MHC) class I and class II, as well as costimulatory molecules. Secondly, they migrate to the lymph nodes and activate T cells to direct the adaptive immune response. Activated adaptive immune cells, T cells and B cells, undergo rapid clonal expansion and migrate towards the site of infection, where they amplify the initial inflammatory response and participate to the pathogen clearing (Iwasaki and Medzhitov, 2015).

1.2.1.2 Mononuclear phagocytes

Mononuclear phagocytes (MNPs) represent a heterogeneous population in the colonic LP. Two main subtypes can be identified under homeostatic conditions based on the expression of cluster of differentiation (CD) 103 and CX3-chemokine-receptor 1 (CX3CR1): the $CD11c^{+}$ $CD103^{+}$ $CX3CR1^{-}$ dendritic cells and the $CD11c^{low}CX3CR1^{hi}$ intestinal resident macrophages (reviewed in Persson et al., 2013). Both populations

can uptake, process and present antigens on MHC class I and MHC class II, but differ in their function and migratory capacity (Schulz et al., 2009).

Following recognition of the antigen, activated $CD103^+$ DCs migrate to the mesenteric lymph nodes where they influence the differentiation of naïve $CD4^+$ T cells and the secretion of immunoglobulin A (IgA) by B cells (Macpherson, 2004). Upon activation of $CD4^+$ T cells, DCs also promote the expression of homing receptors, such as CCR9 and $\alpha4\beta7$, which allows T lymphocytes to traffic back to the lamina propria (Johansson-Lindbom et al., 2005). Importantly, $CD103^+$ DCs are potent inducers of forkhead box $P3^+$ (Foxp3) regulatory T cells (Tregs) through their production of transforming growth factor beta (TGFβ) and retinoic acid (RA) (Coombes et al., 2007; Sun et al., 2007).

By contrast to the migratory $CD103^+$ DCs, $CXCR3^+$ macrophages reside in the colonic LP close to IECs (Niess et al., 2005; Schulz et al., 2009), which allows sampling of luminal antigens through the formation of transepithelial dendrites, and where they can effectively clear pathogens by phagocytosis in the event of a breach (Niess et al., 2005). $CX3CR1^+$ macrophages produce high amounts of interleukin 10 (IL-10), thereby suppressing effector responses and promoting Treg survival and function (Kayama et al., 2012; Murai et al., 2009).

1.2.1.3 Innate lymphoid cells

Innate lymphoid cells (ILCs) are the most recently discovered group of immune cells that share striking similarities with T cell subsets in the transcription factors that govern their differentiation and the cytokines they produce. Due to these shared effector functions, it has been suggested that ILCs are the innate counterparts of T cells. (Vivier et al., 2016). ILCs are tissue-resident cells and encompass Natural Killer (NK) cells, Lymphoid tissue-inducer (LTi) cells, as well as group 1 ILCs (ILC1), group 2 ILCs (ILC2), and group 3 ILCs (ILC3). Group 1, 2 and 3 ILCs are similar to Th1, Th2, and Th17 cells respectively, through the expression of T-bet, Gata3 and Rorγt and production of IL-12/18, IL-5 /13 and IL-17/22 (Spits et al., 2013). Althought first identified and primarily studied in Rag (recombination activating genes)-deficient animals, where they are enriched, ILCs are also found in humans, and it is now recognised that Innate and adaptive lymphocytes exhibit both complementary and redundant functions in ensuring immunity. At mucosal sites particularly, ILCs serve unique and critical functions in host defense against infection, such as against *Citrobacter rodentium* (Satoh-Takayama et al., 2008; Sonnenberg et al., 2012) and in tissue repair (Monticelli et al., 2015). Although the search for an ILC with regulatory properties has not led to the identification of Foxp3 expressing ILCs, a recent study has suggested that ILCregs exist in the mouse and human intestines. These cells secrete TGFβ and IL-10, which suppresses the activation of ILC1s and ILC3s, and promote protection against innate colitis. These findings remain to be validated by other groups. Particularly, it remains unknown whether these cells are able to control inflammation elicited by ILCs when Tregs are present (Wang et al., 2017). Importantly, ILC3s are also involved in disease-driving responses as demonstrated in

experimental models of colitis and human IBD (Buonocore et al., 2010; Geremia et al., 2011; Pearson et al., 2016) and colitis-associated cancer (Kirchberger et al., 2013).

1.2.1.4 Other innate cells

Other innate cells are also abundant in the intestinal mucosa and act together to destroy pathogens and contain the infection until the adaptive response is generated.

Neutrophils are one of the first responders and are capable of forming substantial amounts of reactive oxygen species and other toxic molecules, and can also produce antimicrobial “prisons” termed neutrophil extracellular traps (NETs) (Fournier and Parkos, 2012).

Eosinophils are critical effectors of allergic reactions in the lung and essential regulators of parasitic infection, and are intestine-resident cells (Rothenberg and Hogan, 2006). Recently, it has become clear that eosinophils are pleiotropic multifunctional cells involved in initiation and propagation of diverse inflammatory responses, as well as modulators of innate and adaptive immunity. In the colonic mucosa, eosinophils secrete various inflammatory mediators, such as Tumour necrosis factor (TNF) and Interleukin-13 (IL-13), and are implicated in activation of DCs and neutrophils (Rosenberg et al., 2012). They can also release anti-microbial compounds and cytotoxic mediators such as eosinophil peroxidase (EPO) and eosinophil cationic protein (ECP) that promote clearence of viruses and bacteria, and promote plasma cells survival and switch to IgA immunoglobulin A (IgA)-secreting plasma cells in the intestine (Chu et al., 2014; Rosenberg et al., 2012).

1.2.2 The adaptive immune system

While the innate immune response relies on PAMPs and DAMPs to detect pathogens, lymphocytes are characterised by the expression of T cell antigen receptor or B cell antigen receptor (TCR or BCR respectively), which enables T and B cell to recognise antigens. This antigen-recognition system is highly specific and diverse, and has evolved in response to the high mutation rate of pathogens and the intracellular replication of various microorganisms. T and B cell have evolved differently in the way they mediate their immune function.

Upon recognition of a specific antigen, B cells proliferate and differentiate into plasma cells, which produce significant amounts of antibodies, or immunoglobulins, of a given specificity. B cells represent an important axis in mucosal homeostasis, primarily via production of secretory IgA. Secreted IgA is found in high concentration in the mucus layer and coats bacteria, thereby interfering with pathogen adherence to or penetration through the mucosal barrier (Mestecky and Russell, 2009). Interestingly, IgA can bind to microbes in a specific fashion, which facilitates fine-tuning of immune responses (Hapfelmeier et al., 2010). Finally, bacteria that are highly IgA coated belong to species that display a high colitogenic potential in germ-free mice, suggesting that the B cell-mediated immune responses are preferentially directed at specific members of the intestinal microbiota with disease potential (Palm et al., 2014).

The predominant pool of peripheral T cells express the αβ TCR and are represented by two lineages, expressing the co-receptors CD4 or CD8, which recognise the ligands of the TCR in the context of MHC class I or II respectively (Janeway, 1992).

MHC class I is expressed on all nucleated cells and presents peptides of intracellular origin to the cell surface, thereby allowing $CD8^+$ T cells (cytotoxic T lymphocytes) to scan and detect intracellular infections while preserving cell integrity. Upon recognition of a specific antigen, activated $CD8^+$ T cells exert a direct cell-killing function via the production of perforin and granzymes, or inhibit intracellular pathogen replication through secretion of TNF or interferons.

MHC class II presents antigens that originate from extracellular proteins and is expressed by specialised cells of the immune system. $CD4^+$ T cells recognise specific antigens presented by APCs, and upon activation orchestrate an immune response against extracellular infections (Sher and Coffman, 1992). Activated $CD4^+$ T cells differentiate into various sublineages and deploy an extensive range of immunological effector functions that are further detailed below.

Finally, the adaptive immunity is characterised by its long-lived immunological memory. This response protects the host against future encounter with a pathogen, a property that is harnessed for vaccination.

1.2.2.1 Effector $CD4^+$ T cell subsets

Although this study focuses on effector $CD4^+$ T cells, the intestine contains multiple specialised T cell populations that will not be discussed in extensive detail. For example, unconventional T cells, known as intraepithelial lymphocytes (IELs) are epithelial-resident cells and include TCR $\gamma\sigma^+$ T cells, $CD8\alpha\alpha^+$ cells, and double

negative T cells that neither express CD4 nor CD8. Invariant T cells, such as mucosal-associated invariant T cells (MAIT cells) and invariant natural killer T cells (iNKT cells) are also found in the colonic mucosa. These populations contribute to the maintenance of intestinal homeostasis and are involved in inflammatory responses (reviewed in Cheroutre et al., 2011; Hayday and Gibbons, 2008).

Conventional $CD4^+$ T (T helper, Th) cells are critical components of the effector immune response, responsible for host protection. Differentiation of naïve $CD4^+$ T cells into sublineages of helper cells is governed partly by TCR and co-stimulatory signals, but most importantly by cytokines that are present upon activation (DuPage and Bluestone, 2016). Several of these cytokines are produced by APCs themselves, while others are produced in the microenvironment. The different cytokines involved in the differentiation of specific $CD4^+$ T cell subsets are called inductive cytokines. These cytokines regulate the expression of critical transcription factors, which then define a specific cell programme that governs the production of effector cytokines. Each subset produces effector cytokines that are involved in the specific control of certain types of pathogen or damage, but they also limit immune pathology in the case of Tregs (detailed subsequently) (DuPage and Bluestone, 2016). Initially, two subsets of $CD4^+$ T cells were described in the 1980s: T-helper 1 (Th1) and T-helper 2 (Th2) cells, based on their capacity to produce interferon γ (IFNγ) and interleukin 4 (IL-4) respectively, and their specialisation in immune responses associated with intracellular pathogens and extracellular parasites, respectively (Mosmann et al., 1986). However, it is now well appreciated that several additional $CD4^+$ T cell subsets exist and account for the diversity of observed immune responses (**Figure 1.2**).

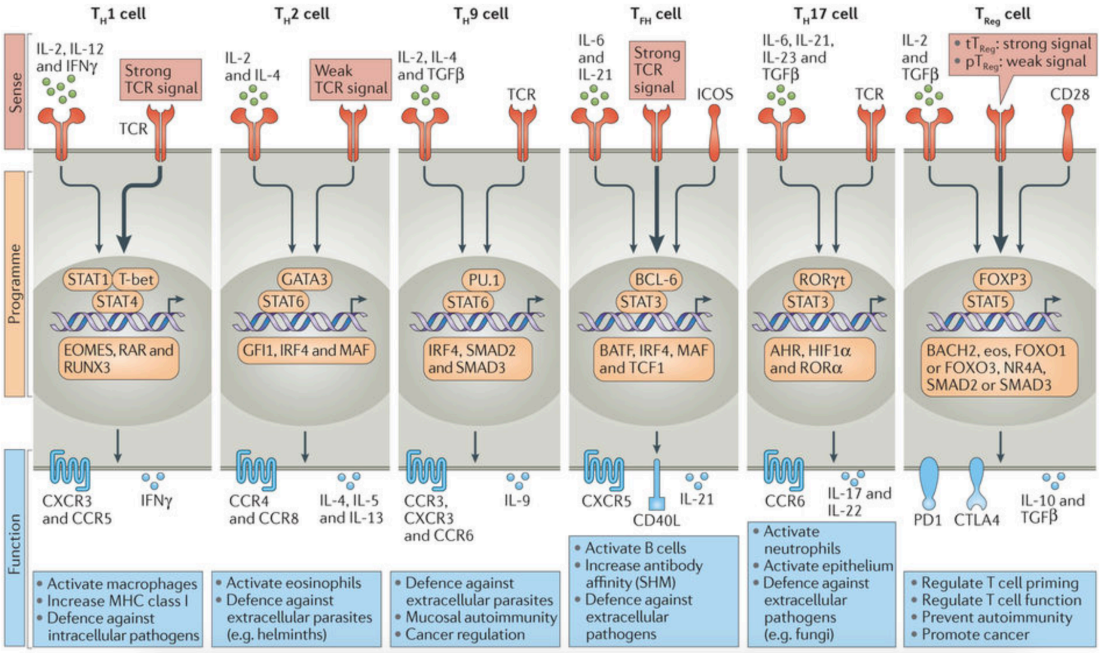

Figure 1.2: Differentiation of CD4$^+$ T cell subsets: inductive cytokines, defining transcription factors, and effector cytokines.

Upon uptake, processing and presentation of an antigen, an APC primes naïve CD4$^+$ T cell. According to the presence of specific inductive cytokines (Sense, red), differentiation into different subsets is directed by specific master transcriptional regulators (Programme, orange).

Each subet is endowed with a unique transcriptional program, which regulates the production of characteristic effector cytokines (Function, blue) that are important in the control of specific forms of immune defence.

Figure reproduced with the authorisation from Nature Publishing Group, NRI (DuPage and Bluestone, 2016).

1.2.2.1.1 Th1 and Th2 cells

Th1 cells are particularly important in mediating effector responses against intracellular bacteria and viruses, and orchestrate cellular immunity by promoting the expansion and activation of macrophage, NK cell and cytotoxic T cell activities (Murphy et al., 2000). Th1 cells differentiate in the presence of IL-12 and IFNγ, whose signalling lead to the expression of the T-box transcription factor T-bet, and subsequent production of high amounts of IFNγ (Lighvani et al., 2001).

By contrast, Th2 cells are critical in defense against gastrointestinal pathogens, such as helminths, and mediate allergic reactions. Th2 cells coordinate humoral immune responses, notably by promoting B-cell antibody class switching, and attracting innate cells, such as eosinophils and mast cells (Nakayama et al., 2017). Differentiation of naïve $CD4^+$ T cells into Th2 cells is mediated by IL-4, and Th2 cells are characterised by the expression of Gata3 and secretion of IL-4, IL-5 and IL-13 (Zhang et al., 1997). Colonic Th2 cells are not abundant in the absence of a relevant microbial driver, such as a parasite infection (Artis et al., 2005).

1.2.2.1.2 Th17 cells

Th17 cells were identified as another major player in the coordination of immune responses (Cua et al., 2003), particularly at mucosal sites. They mediate protection against extracellular bacterial and fungal infections. Th17 cells are polarised by a combination of transforming growth factor β (TGF-β), IL-1β, IL-6 and IL-21 (Veldhoen et al., 2006). Although IL-23 was originally thought to be essential for Th17 cell differentiation (Langrish et al., 2005), it is now recognised that IL-23 is dispensible for Th17 differentation and rather promotes the effector functions of these cells. Interestingly, IL-23 signalling endows Th17 cells with a pathogenic potential (Awasthi et al., 2009; Ghoreschi et al., 2010; McGeachy et al., 2009). Th17 cells are defined by expression of Rorγt and secretion of IL-17A, IL-17F, IL-21 and IL-22 (Ivanov et al., 2007). Several of these cytokines are involved in mediating pro-inflammatory responses, such as IL-17A and F, while IL-22 is primarily involved in promoting barrier integrity and AMP secretion (Maloy and Kullberg, 2008).

Several other T helper subsets have since been described, such as Th9, Th22 (producing IL-9 and IL-22 respectively) and follicular Th (Tfh) cells (involved in the development of humoral immunity), but are not detailed in this thesis.

1.2.3 Regulation of immune responses by Tregs

The function of regulatory T cells (Tregs) is to maintain immune tolerance and prevent unnecessary inflammatory responses by modulating both the innate and adaptive immune responses. Balanced control of immune responses by Tregs is central to preventing autoimmune diseases, maintaining homeostasis at barrier sites and limiting effector responses in transplantation settings. (Powrie et al., 1993; Sakaguchi et al., 1982; Wing et al., 2008). Tregs are defined by the expression of high amounts of CD25 (i.e. the IL-2Rα chain), expression of the transcription factor Foxp3, and production of immunosuppressive cytokines, such as IL-10 and TGFβ.

It was long suggested that a distinct subset of T cells was responsible for immune suppression (Gershon and Kondo, 1970; Nishizuka and Sakakura, 1969), but lack of tools and failure to identify a distinct lineage of suppressor T cells led many to question the existence of such lymphocytes (Green and Webb, 1993; Möller, 1988). In the 1990s, pioneering studies led to the discovery of a population of $CD4^+$ T cells with an antigen-experienced phenotype that could suppress effector responses of naïve $CD4^+$ $CD45RB^{high}$ T cells transferred into immunodeficient animals (Morrissey et al., 1993; Powrie and Mason, 1990), suggesting that the subset of cells could not only regulate responses to self-antigens but also to dietary and microbial antigens in the gut. In a landmark study, these cells were identified as expressing CD4 and CD25, and were critical to prevent inflammatory responses in multiple settings, including in

thymectomised mice and transplant rejection, as well as intestinal inflammation (Sakaguchi et al., 1995). The identification of Foxp3 as the molecular marker for the suppressive $CD4^+$ $CD25^+$ T cell population confirmed their status as a *bona fide* lineage (Hori et al., 2003), (reviewed in Shevach, 2011). Subsequent mouse studies demonstrated that the expression of Foxp3 endows Tregs with their immunosuppressive phenotype and is indispensable for their regulatory function (Fontenot et al., 2003; Hori et al., 2003; Khattri et al., 2003). Scurfy mice carry a mutation in the *Foxp3* gene and develop a fatal lymphoproliferative disease with multiorgan inflammation, emphasising the critical role of Foxp3 expression in Treg function (Brunkow et al., 2001; Wildin et al., 2001). In humans, a loss-of-function variant of the *FOXP3* gene results in the development of the Immunodysregulation Polyendocrinopathy Enteropathy X-linked Syndrome (IPEX), a severe autoimmune disorder, affecting various organs such as the skin, the intestines, the thyroid and lymph nodes (Bennett et al., 2001; Wildin et al., 2001).

1.2.3.1 Treg development

The majority of $Foxp3^+$ Tregs develop in the thymus and are referred as thymic-Tregs (tTregs) (Abbas et al., 2013; Itoh et al., 1999). Thymic antigen-presenting cells, including medullary thymic epithelial cells and various dendritic cell subsets, express and present a diverse array of self-antigens that are recognised by $CD4^-$ $CD8^-$ thymocytes, in the context of MHC class II and co-stimulatory signal via CD28. The affinity, specificity and cytokine signalling that induces Foxp3 expression and governs tTreg development is reviewed in (Hsieh et al., 2012).

In the periphery, naïve $CD4^+$ T cells can differentiate into Foxp3-expressing Tregs and acquire immunosuppressive function in the presence of IL-2 and TGF-β (Chen et al.,

2003; Kretschmer et al., 2005), and these cells are referred to as peripherally-derived Tregs (pTregs) (Abbas et al., 2013).

Numerous studies have attempted to identify differentially expressed markers between tTregs and pTregs, as well as to decipher whether they control different types of immune responses. The surface marker Neuropilin 1 (Nrp-1) and the transcription factor Helios have been suggested to be preferentially expressed by tTregs (Thornton et al., 2010; Weiss et al., 2012). However, it was questioned whether Helios and Nrp-1 are reliable markers of tTregs in mice (Singh et al., 2015; Szurek et al., 2015). A recent abstract from Immunology 2016™ Meeting revealed that Helios could indeed differentiate pTregs from tTregs, as assessed by sequencing Helios positive and negative Tregs from HeliosGFP reporter mice (Thornton et al., 2016). However, as this study is not published so far, Helios expression in tTregs is not yet definitive.

The selective genetic deletion of specific conserved noncoding sequences (CNSs) that are found in the regulatory regions of the *Foxp3* gene locus has emphasised the potential division of labour of tTreg and pTreg. Depletion of CNS1 leads to the preferential ablation of pTregs, notably at mucosal sites, while the depletion of CNS3 impedes the development of tTregs. Studies of CNS1 deficient mice have shown that pTregs may specifically regulate effector responses in mucosal tissues, as revealed by the Th2-driven inflammation that develops in both the intestine and lungs, which develops in these animals (Zheng et al., 2010).

1.2.3.2 Treg-mediated suppression

Tregs mediate their suppressive function through several mechanisms that can occur in both cell-dependent and -independent ways. Importantly, while the initial activation of Tregs is dependent on antigen stimulation, they then control immune responses in an antigen-nonspecific manner (Sakaguchi et al., 1995). Tregs can suppress immune responses generated by various effector cell populations, including but not limited to effector and memory $CD4^+$ T cells, cytotoxic T cells, NK and NKT cells, B cells and DCs (Shevach, 2009). It is proposed that depending on the circumstances (i.e. the nature of the immune response and the type of effector cells) and their surroundings (i.e. the site of suppression), certain mechanisms may be preferentially employed by Tregs *in vivo*, to efficiently control immune responses (Tang and Bluestone, 2008).

First, Tregs inhibit effector immune responses in a cell-contact-dependent fashion through the increased expression of inhibitory molecules on their cell surface. Engagement of these molecules can directly modulate the effector cells or induce an immunosuppressive phenotype in APCs, thereby indirectly inhibiting the activation of effector T cells (Shevach, 2009). CTLA-4, PD-1, OX-40, ICOS, GITR, LAG-3 and TIGIT are amongst the surface markers enriched on Tregs (Griseri et al., 2010; Herman et al., 2004; Liang et al., 2008; McHugh et al., 2002; Shimizu et al., 2002; Totsuka et al., 2005; Wing et al., 2008).

CTLA-4 binds to CD80 and CD86 expressed by APCs, preventing them from costimulating CD28 receptors on other T cells, and specific deletion of CTLA-4 in the Treg compartment of mice is fatal, with animals developing systemic autoimmune

disorder (Wing et al., 2008). Moreover, blocking CTLA-4 with a monoclonal antibody (mAb) abrogates Treg-mediated suppression of colitis in a mouse model of IBD (Read et al., 2006). Cancer patients receiving a CTLA-4 blocking antibody ipilimumab can develop underlying autoimmunity, with over 20% of patients developing enterocolitis, thus emphasising the critical requirement of CTLA-4 expression in maintaining intestinal homeostasis (Beck et al., 2006). However, whether CTLA-4's role is primarily mediated through Tregs is unclear, as ipilimumab also limits CTLA-4 engagement on activated T cells. Similar to CTLA-4, PD-1 is an inhibitory receptor that binds to PD-L1 and PD-L2 expressed on APCs, which negatively regulates effector T cells and CTL function, and is also a target for cancer immunotherapy. PD-L1 was shown to regulate the development, maintenance and function of peripheral-derived Treg in homeostatic conditions (Francisco LM et al., 2009). In cancer however, despite evidence of a role for PD-1/PD-L1 and PD-L2, little is known on the mechanism by which PD-1 blocks T-cell activation. In cancer patients, PD-1 blockade causes intestinal inflammation in less than 10% of the patients (Brahmer et al., 2010; Gibney et al., 2015). TIGIT, another inhibitory receptor, is also expressed on activated Tregs and is involved in the specific control of Th1 and Th17 cells, but not Th2 cells (Joller et al., 2014). Mechanistically, TIGIT induces the secretion of fibrinogen-like protein 2, which hampers effector T cell proliferation (Joller et al., 2014). Recently, tTreg were specifically shown to regulate Th1 responses through binding of CD27 to CD70, which is expressed by DCs (Dhainaut et al., 2015). This CD27-CD70 interaction resulted in internalisation and degradation of the CD27/CD70 complex by DCs, which were then unable to prime naïve $CD4^+$ T cells (Dhainaut et al., 2015). Furthermore, increased expression of galectin-1, a member of the family of

beta-galactoside-binding proteins, has been observed in both human and mouse Treg cells, and could inhibit effector responses *in vitro* (Garín et al., 2007).

Secondly, Tregs produce immunosuppressive cytokines, such as IL- 10, TGF-β and IL-35. IL-10 is a cytokine critically required for homeostasis at mucosal sites, such as in the intestine. Mice harbouring a specific deletion of IL-10 in Foxp3$^+$ Treg cells develop spontaneous inflammation in the colon and lungs (Rubtsov et al., 2008). In addition, the control of established colitis and experimental autoimmune encephalomyelitis is mediated by Treg-derived locally produced IL-10 (McGeachy et al., 2005; Uhlig et al., 2006). TGF-β is another broadly immunosuppressive cytokine that is produced in the intestines. TGF-β deficiency in mice is fatal from day 20 of life, as animals suffer from a lymphoproliferative autoimmune disorder (Shull et al., 1992). Both IL-10 and TGF-β act in a feedback loop to maintain Foxp3 expression and Treg function (Chen et al., 2003; Murai et al., 2009), highlighting that beyond suppression of effector cells, these cytokines also amplify the immunoregulatory functions of Tregs themselves. IL-35, an IL-12 family immunosuppressive cytokine, was recently described as specifically enriched in Foxp3$^+$ Tregs (Collison et al., 2007). IL-35 is composed of two subunits, IL-12α and IL-27β, which are encoded by *Il12a* and *Ebi3*. Ebi3- and Il12a-deficient Tregs exhibited reduced regulatory activity both *in vitro* and *in vivo*, highlighting IL-35 as another mechanism of immunosuppression employed by Tregs (Collison et al., 2007).

Thirdly, metabolic disruption has been described as an immunosuppressive mechanism of effector responses. Tregs consume IL-2 in their microenvironment, thereby competing with effector T cells for IL-2, which is a growth and survival factor (Pandiyan et al., 2007). Tregs also express high amounts of the endonucleases CD39 and CD73 that produce adenosine (Deaglio et al., 2007; Kobie et al., 2006), which is responsible for the inhibition of T cell effector responses upon binding to its receptor A2A (Bono et al., 2015).

Finally, in addition to regulation by suppression, Treg cells can also mediate their activity by killing effector cells. Tregs can release granzyme A/B and perforin, and exert cytolysis *in vitro*, but *in vivo* studies are lacking so far. Production of granzyme A and B by Tregs results in cytolysis of T cells and APCs *in vitro*, both in mouse and human (Gondek et al., 2005; Grossman et al., 2004; Zhao, 2006).

1.2.3.3 Tissue adaptation of Tregs

Considering that Tregs exploit different mechanisms to regulate immune responses, it is logical to assume that they may adapt to their microenvironment to mediate their functions. Recently, several studies have highlighted the function and adaptation of Tregs in peripheral tissues (tissue-Tregs), compared to their lymphoid counterparts. Specifically, these adaptations enable tissue-Tregs to control both immune and non-immune processes in a context-dependent manner.

Tregs can enhance their ability to control inflammatory responses through co-expression of transcription factors typically associated with the differentiation program of effector Th cells, such as T-bet, Gata3, IRF4 and STAT3 (Liston and Gray,

2014). For instance, T-bet expression by Tregs regulated expression of CXCR3 by promoting homing of Tregs to sites of Th1-driven inflammation (Koch et al., 2009). Similarly, a specific deletion of IRF4 in Foxp3-expressing cells was critical for the control of Th2 responses, and mice lacking IRF4 expression in Tregs displayed typical immunopathology mediated by deregulated humoral immunity (Zheng et al., 2009). Furthermore, STAT3 expression by Tregs was required for the control of Th17-mediated intestinal inflammation (Chaudhry et al., 2009). The described studies showed that deletion of the "master transcriptional regulators" of Th cell differentiation in Tregs led to subset-specific deregulation of effector responses. This suggests that the ability of Treg cells to adapt to their surrounding inflammatory milieu is critical in preventing the development of immunopathology.

Distinct subpopulations of Tregs have now been described in many organs such as the skin, colon, lung, liver and adipose tissues. Importantly, despite being exposed to distinct environments, Tregs found in non-lymphoid tissues share certain characteristics (Panduro et al., 2016). For instance, they have been shown to express a distinct TCR repertoire when compared to lymphoid Tregs or conventional $CD4^+$ T cells isolated from the same tissue (Feuerer et al., 2009). Furthermore, tissue-Tregs exhibit a differential transcriptional profile with prominent enrichment of transcripts encoding effector molecules, chemokines and their receptors, as well as immunosuppressive cytokines such as IL-10 (Burzyn et al., 2013; Feuerer et al., 2009; Schiering et al., 2014).

Tregs, which have mostly been studied in the context of the regulation of immune responses, have now been associated with a variety of physiological functions that are unique to the tissues in which they reside. For instance, specific ablation of visceral adipose tissue (VAT) Tregs by targeting peroxisome proliferator-activated receptor gamma (PPAR-γ), which controls the development of the VAT Treg transcriptional programme, results in exacerbation of VAT inflammation and a decline in metabolic indices related to glucose metabolism (Cipolletta et al., 2012). Moreover, it has been suggested that VAT Tregs control metabolic responses to thermogenic changes (Medrikova et al., 2015). Tregs are present within skeletal muscles, both after acute and chronic injury, where they display a distinct phenotype and are critical to mediate muscle regeneration. This regeneration is partially mediated by the production of amphiregulin (Areg) (Burzyn et al., 2013). In the lungs, Tregs also produce Areg and are involved in tissue repair following acute influenza infection (Arpaia et al., 2015). Studies from our lab have also revealed that colonic Tregs express Areg (Schiering et al., 2014), although its precise function is still being investigated. Finally, in the skin, Tregs display similar tissue adapations. First, a subset of Tregs in skin facilitates wound healing through increased expression of the epidermal growth factor receptor (EGFR) (Nosbaum et al., 2016). More recently, it was demonstrated that hair follicles stem cells, responsible for hair regeneration, were in close contact with tissue-resident Tregs. Skin-Tregs specifically express Jagged 1, a member of the Notch ligand family, whose expression facilitates stem cell function and efficient hair regeneration (Ali et al., 2017).

Understanding Tregs' adaptations to specific tissues and microenvironment is critical to harness their ability to effectively suppress effector responses under certain inflammatory conditions or autoimmune diseases. Accordingly, this knowledge will also be fundamental to develop and design targeted therapies, particularly for immunotherapies aimed at suppressing Treg function as in cancer.

1.2.4 Inflammatory bowel disease

IBD is an inflammatory disorder of the GI tract, comprising Crohn's disease (CD) and ulcerative colitis (UC). The combination of genetic, environmental, microbial and immune factors play a role in the pathogenesis of IBD. The immune system is involved in the development of IBD, and it is commonly accepted that the chronic inflammation observed in patients develops as a result of dysregulated immune responses directed against the microbiota in genetically susceptible hosts (de Souza and Fiocchi, 2015).

Genetic studies together with mouse models of colitis have helped to identify several genes and fundamental molecular pathways involved in disease development. For example, the IL-23-Th17 axis is a significant driver of pathology, and polymorphisms in the *IL23R* locus, identified in GWAS, are associated with increased risks of developing CD and UC (Duerr et al., 2006). Apart from pro-inflammatory components, IBD is also characterised by deficiencies in negative regulatory pathways. For example, mutations in *IL10R* have been associated with severe early-onset IBD, suggesting that a breakdown of intestinal homeostasis due to defective immunosuppressive mechanisms might underlie IBD pathogenesis (Glocker et al.,

2009). IBD is associated with a high morbidity, as patients ultimately undergo resection of the inflamed tissue, highlighting the urgent necessity for new therapies, as to date, treatments only aim at relieving symptoms and controlling inflammation levels.

1.3 Colorectal cancer

1.3.1 Statistics and disease prevalence

Colorectal cancer (CRC) is the third most commonly diagnosed cancer and is the fourth leading cause of cancer death in the world (Arnold et al., 2017). The highest incidence is found in countries with a high human development index (HDI): Australia, New Zealand, Europe, and Northern America, although these rates and associated mortality have declined over the years, partially reflecting increased early detection and prevention (Siegel et al., 2017). Medium to high HDI countries, particularly in Eastern Europe, Asian and South America, are now characterised with increased colorectal cancer incidence and mortality, a surge that has been correlated with westernised lifestyles and rapid societal changes (Arnold et al., 2017). Colorectal cancer burden is expected to increase by 60% by 2030. The National Institute for Health and Care Excellence (NICE 2014) guidelines for the clinical management of CRC involves resection of primary tumours and adjuvant chemotherapy for locally advanced and metastatic disease.

1.3.2 Types of CRCs

CRC is not a homogenous disease and the majority of CRCs are sporadic (70 to 80%), while around 20 to 30 % of CRCs have a hereditary component. Approximately 4%-6% of hereditary CRCs are associated with highly penetrant inherited mutations and clinical presentations that have been well characterised, such as: familial adenomatous polyposis (FAP), inherited autosomal dominant germline mutation in the adenomatous polyposis coli (APC) gene, hereditary non-polyposis colorectal cancer (Lynch syndrome), or germline mutation in mismatch repair (MMR) genes. The aetiologies of the remaining 20%–30% of inherited CRCs are not completely understood. To date, genome-wide association studies (GWAS) have identified at least 21 independent loci that have been conclusively associated with CRC risk (Valle L, 2014). Specifically, single-nucleotide polymorphisms (SNPs) are thought to confer weak but cumulative and increasing effects on CRC incidence (Theodoratou E. et al, 2012; Houlston RS et al., 2012). Data suggest that only a small proportion (at most 10%) of the heritability associated with CRC can be explained by the currently identified loci (Houlston RS, 2012).

Finally, a small subset of about 1 to 2 % of CRC cases arise as a consequence chronic inflammation in the context of IBD. Patients with ulcerative colitis (UC) for example have a 2.4 fold increased risk of developing colitis-associated cancer (Jess et al., 2012). Similarly, it is appreciated that sporadic CRCs also elicit an inflammatory response that has a significant role in determining disease course (Grivennikov et al., 2010).

1.3.3 Molecular heterogeneity of colorectal cancers

Over the past decade, a large CRC Subtyping Consortium has advanced the understanding of the molecular heterogeneity of colorectal cancer, based on transcriptomic signatures, by defining four major "consensus molecular subtypes" (CMS) of colorectal cancer in 2015. Additionally, these CMS have differing prognostic implications. (Guinney et al., 2015). The CMS1 subtype is characterised by microsatellite instability and immune activation (MSI-immune, 14%), while the remaining microsatellite stable CRCs are subcategorised into CMS2: epithelial WNT and MYC signalling activation (canonical, 37 %), CM3: epithelial metabolic deregulation (metabolic, 13 %) and CMS4: stromal invasion and angiogenesis (mesenchymal, 23 %). An extra residual unclassified group is also added and contains mixed features (13 %). (Guinney et al., 2015; Müller et al., 2016a).

1.3.4 From a healthy mucosa to colorectal cancer

Colorectal cancer is a progressive disease that involves the accumulation of genetic and molecular changes over many years of life. Pre-malignant lesions, adenomas, are detected via colonoscopy, which is one of the key preventive measures against CRC development. Adenomas are categorised as either conventional adenomas or sessile serrated polyps and are common precursors of the majority of cases of colorectal cancer (Strum, 2016).

Approximately 85% of colorectal cancers are thought to evolve from conventional adenomas in a step-wise accumulation of well-documented somatic mutations. This process is referred to as the adenoma-to-carcinoma sequence and was first elucidated by Fearon and Vogelstein (Fearon and Vogelstein, 1990). Several driving

disease mutations have been characterised and occur both in tumour suppressor-genes, amongst which *APC* and *TP53* are the most common, and oncogenes, amongst which *KRAS*, *PIK3CA*, and *BRAF* are the most represented (Strum, 2016). Further mutations in genes that control DNA integrity result in microsatellite instability in 15% of colorectal tumours and chromosomal instability in the context of microsatellite stability in 80% of late stage CRCs (Grady and Carethers, 2008). This genetic instability results in somatic gene copy number alterations and the acquisition of further passenger mutations that contribute to the incredible heterogeneity observed in CRC, resulting in varied responses to therapy and escape of host control.

A minority of CRCs develop through an alternative hypermutation pathway resulting in high-frequency microsatellite instability, which renders the epithelial cells premalignant (Strum, 2016). The sequence of mutational events is termed serrated neoplasia pathway and accounts for approximately 15% of CRCs. Amongst these are the serrated pathway, characterised by a high frequency of *BRAF* mutations and colitis-associated CRC, in which early loss of *TP53* and later acquisition of *KRAS* and *APC* mutations are hallmarks. (Punt et al., 2016; Strum, 2016). **Figure 1.3** summarises the developmental sequence of sporadic CRC versus colitis-associated cancer.

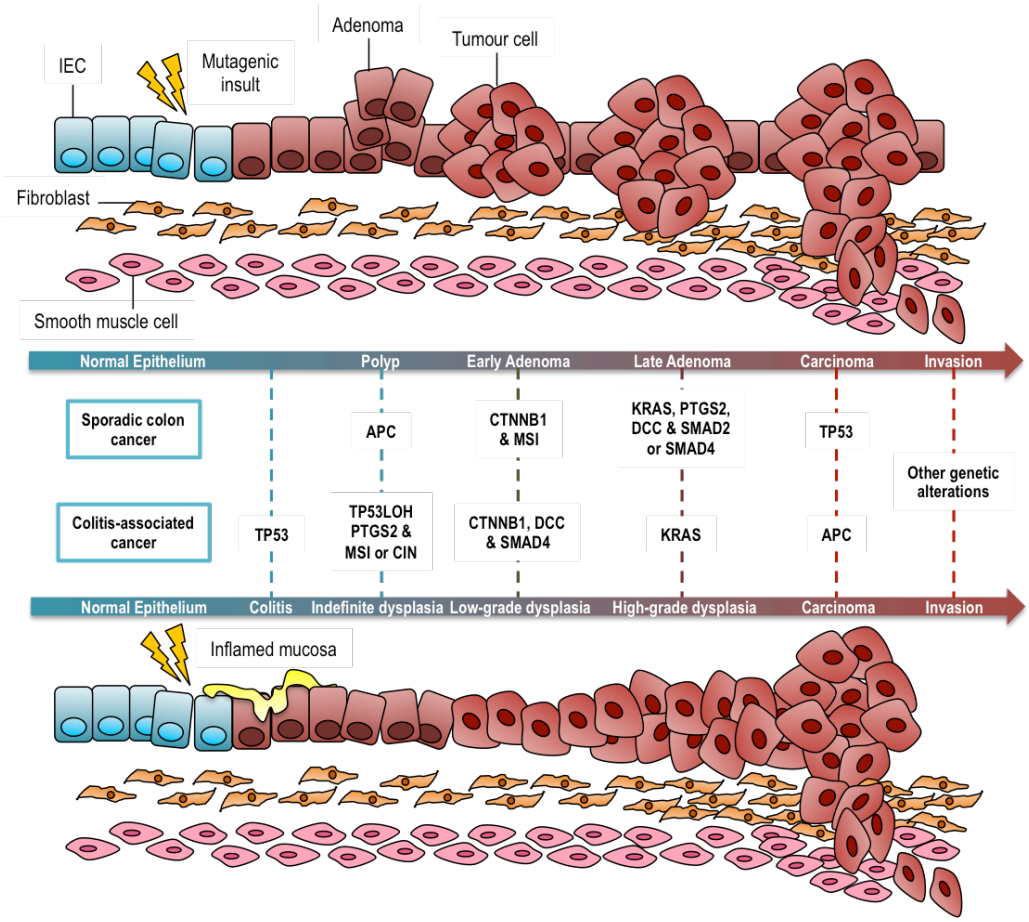

Figure 1.3: Developmental sequence of sporadic CRC versus colitis-associated cancer

Both sporadic CRC (top panel) and colitis-associated cancer (CAC) (bottom panel) are characterised by a sequence of genetic events that culminates in invasive carcinoma.

Loss of APC results in constitutive activation of the Wnt pathway and aberrant epithelial cell growth. Other driver mutations are also acquired in three major signalling pathways:

- The MAPK pathway is often hit by activating mutations in *KRAS*, *BRAF* or *PIK3CA* and provides cell autonomous mitogenic and pro-survival stimuli to cancer cells,
- The *TP53* pathway is inactivated by mutations in its protein, or less commonly in *ATM*, facilitating acquisition of genomic instability (LOH),
- The TGF-β pathway is frequently silenced by loss-of-function mutations in *TGFBR2*, *SMAD4*, *SMAD2* or *SMAD3*.
-

Mutations in deleted in colon cancer (*DCC*) loci are also observed, and activating mutations occur in β-catenin (*CTNNB1*) and cyclooxygenase 2 (COX2; encoded by PTGS2).

MSI, microsatellite instability; CIN, chromosomal instability; IEC, intestinal epithelial cell; LOH, loss of heterozygoty.

(Figure prepared for NRI by F. Franchini; (West et al., 2015).

As tumours acquire chromosomal instability or defects in the DNA mismatch repair system, hundreds to thousands of genetic alterations ultimately accumulate in these lesions (Punt et al., 2016). Amongst these, passenger mutations do not confer advantages to tumour cells, while other driver mutations give a selective advantage to the cancer cells. To date, the role of many of these mutations remains poorly understood. Collectively, the heterogeneity and complexity of CRC affect functional analysis and complicate the development of effective therapeutic approaches (Tauriello et al., 2017). As such, colorectal cancer is a prime example of a solid malignancy in which immune checkpoint blockade (Brahmer et al., 2012; Topalian et al., 2012) has been broadly ineffective, except for a small proportion of patients with microsatellite instable (MSI) CRC, whom to date are the only ones showing a beneficial response (Le et al., 2015; Llosa et al., 2015).

The first initial phase 2 study tested the efficacy of pembrolizumab (anti-PD-1 immune checkpoint inhibitor), comparing 41 CRC patients with progressive metastic carcinoma with or without mismatch-repair deficiency (Keynote-164 Le et al., 2015). This study showed an immune-related objective response rate (ORR) and 20-week progression-free survival (PFS) rate of 40% and 78%, respectively, for MMR-deficient CRCs compared with 0% and 11% for MMR-proficient CRCs. The median PFS and overall survival (OS) were not reached in patients with MMR-deficient CRC but were 2.2 and 5.0 months, respectively, for MMR-proficient CRC.

Another phase 2 study, CheckMate-142 (Overman et al., 2017), has showed the importance of immunotherapy in CRC, using nivolumab with or without ipilimumab in treatment of patients with metastatic CRC with and without high MSI-H. The 2017 updated results of the study showed that in MSI-H patients, 24 out of the 74 patients

who were treated with single-agent nivolumab had a centrally reviewed ORR, while 59 patients achieved stable disease (Overman et al., 2017; Birendra KC et al., 2017). Based on these data, the Food and Drug Administration granted accelerated approval to pembrolizumab for patients with MSI-H or MMR-deficient cancer that has progressed following standard treatment. The poor response in microsatellite stable (MSS) CRCs is likely partly explained by the reduced neoantigen load and the contribution of inflammation that is directly protumourigenic.

1.3.5 Mouse models of colorectal cancer

In vivo studies using animal models are a critical tool to dissect the complexity of CRC that arises from the mutational landscape, the colonic microenvironment and the activity of the immune system. Because of this diversity, no mouse models adequately represents all forms of the disease, thus, knowing the limitations and advantages of each model is essential in order to answer specific questions, especially in the context of immunotherapy development. **Table 1.1** displays the most commonly used mouse models to study primary tumour development.

Model	Primary Location	Invasiveness	Driver	Sporadic/CAC
DSS/AOM	Colon	Aberrant crypt foci, adenomas	Intestinal barrier dysfunction and inflammation driven by the chemical irritant DSS, combined with AOM-induced mutagenesis	CAC
Apc$^{Min/+}$ or *Apc*$^{\Delta 468}$	Small intestine	Adenomas (non-invasive)	• Mice are heterozygous for an *Apc* loss-of-function mutation • Increased WNT–β-catenin signalling occurs following allelic loss of wild-type *Apc*	Sporadic (FAP)
CPC-APC	Colon and distal small intestine	Adenomas, low frequency of carcinomas	• Colonic Cre-mediated deletion of a single *Apc* allele, causing increased WNT–β-catenin signalling upon allelic loss of wild-type *Apc* • Cre expression is driven by *Cdx2,* which is expressed preferentially by colonic epithelial cells	Sporadic (FAP)
Mkh1$^{-/-}$, *Msh2*$^{-/-}$, *Msh6*$^{-/-}$	Small intestine, skin and other tissues	Non invasive, but aggressive lymphomas	• Mice have inactivating mutations in the DNA mismatch repair genes (MMR) • Microsatellite instability leading to severely reduced lifespan and hematological malignancies	Sporadic (Lynch Syndrome)
Villin Cre, *Braf*$^{LSL-V637E/+}$	Small intestine	Small intestine adenocarcinomas, invasion to liver in some mice	*Braf* knockin allele leading to the production of the V637E mutant Braf protein expression specifically in the intestinal epithelium (Cre)	Sporadic (Serrated)
Il10$^{-/-}$	Colon & cecum	Adenocarcinoma	Loss of intestinal immune regulation, causing aggressive innate inflammation and Th1 cell responses	CAC
Rag2$^{-/-}$ *Hh* + AOM	Colon & cecum	Dysplasia, adenocarcinoma	Innate inflammation following oral infection with the commensal pathobiont *Helicobacter hepaticus*, combined with AOM-induced mutagenesis	CAC
Apc$^{Min/+}$ ETBF	Colon (distal)	Adenomas, low frequency of carcinomas	Increased WNT–β-catenin signalling and bacteria-driven Th17 cell responses	CAC
Isografts	Usually subcutaneous or orthotopic	Variable	Variable	n/a
Xenografts	Usually subcutaneous or orthotopic	Variable	Variable	n/a

Table 1.1: Mouse models of colorectal cancer

AOM, azoxymethane; APC, adenomatous polyposis coli protein; CAC, colitis-associated cancer; CRC, colorectal cancer; DSS, dextran sodium sulfate; ETBF, enterotoxigenic Bacteroides fragilis; Il10, interleukin-10; N/A, not applicable; Rag2, recombination-activating gene 2; Th, T helper.

(Table prepared for NRI by F. Franchini; (West et al., 2015).

1.3.5.1 Chemically induced colitis-associated cancer

The incidence of spontaneous CRC in wild-type (WT) mice is less than 1%, which has initiated the use of carcinogenic chemicals. These include dimethylhydrazine (DMH) and azoxymethane (AOM), both precursors of methylazoxymethanol (MAM), which is a potent carcinogen that can alkylate macromolecules such as guanine in the liver and colon, leading to tumour development (Fiala, 1977). However, the use of these carcinogens promotes tumour growth in the long term (approximately 30 weeks), and is not fully penetrant. A more commonly used model combines the

administration of AOM with dextran sodium sulfate (DSS), which results in tumour burden at earlier time points. DSS is a chemical irritant that leads to epithelial barrier dysfunction and intestinal inflammation, and is often employed as a mouse model for IBD. Tumours that arise from these models are located in the colon but are not invasive. Typically, the AOM DSS mouse model is easy to implement and can be used on a variety of mouse strains and specific knock out (KO) mice.

1.3.5.2 Mouse models for familial adenomatous polyposis (FAP)

The adenomatosis polyposis coli (*APC*) gene was identified on chromosome 5q as one of the genes commonly deleted in FAP, and is associated with activation of the Wnt pathway (Strum, 2016). Mice heterozygous for *Apc* ($Apc^{min/+}$), which carry a heterozygous germline mutation at codon 850 of *Apc*, develop multiple intestinal neoplasia (Min) or polyps that are not invasive, and are primarily located in the small intestine. These mice often die young due to anaemia and cachexia, rendering long-term studies challenging (Baltgalvis et al., 2008). Moreover, delineating the role of the immune system warrants caution as a progressive loss of immature and mature thymocytes from and subsequent complete regression of the thymus is observed in $Apc^{min/+}$ mice from day 80 of age (Coletta, 2003). Several truncated versions of the Apc gene have been generated, such as the $Apc^{\Delta 468}$ model, and have shown that polyp burden varies depending on the deleted codon.

Recently, the CPC-APC mouse model was introduced, which consists of a colonic Cre-mediated deletion of a single *Apc* allele (Xue et al., 2010). The Cre expression is driven by *Cdx2*, which is preferentially expressed by colonic epithelial cells, thus allowing tumour development to occur in the colon and distal intestine. These mice have a low frequency of carcinomas.

1.3.5.3 Mouse models for Lynch Syndrome

Patients with hereditary nonpolyposis colorectal cancer (HNPCC or Lynch syndrome) carry heterozygous germline mutations in DNA mismatch repair (MMR) genes. MMR involves the recognition of mismatched bases by MutS proteins and the recruitment of MutL proteins, which initiate the removal and re-synthesis of mutated DNA strands (Iyer et al., 2006). Failure of this system permits the persistence of mismatch mutations in repetitive regions of DNA known as microsatellites, resulting in microsatellite instability (MSI). Homozygosity in mouse homologs of MMR genes bestow early onset tumour development on the small intestine as well as other tissues, together with aggressive lymphomas that shorten lifespan.

1.3.5.4 Other models involved in the serrated pathway

With more interest in serrated models of CRC, representing an alternative route towards adenocarcinoma progression, models driven by *Kras* or *Braf* mutations were generated (Rad et al., 2013). These models lack the Apc mutation, have a long latency for tumour development and mice display high morbidity. Moreover, they are not widespread so far and also require heavy husbandry. Variations on these models and more sophisticated targeted mutations as well as combined mutations are being generated to reconstitute the mutation hallmark seen in human CRC.

Of note, the combination of several mutations on a Villin-Cre tamoxifen inducible background has led to the development of novel mouse models that represent late-stage CRC. Particularly, Owen Samson's laboratory has developed several of these models, including the KPN and BPN models, both in the process of being published. The KPN mice, $VillinCre^{ER}$ $Kras^{G12D/+}$ $p53^{fl/fl}$ $N1icd^{LSL/+}$, harbour mutations in the KRAS,

p53 and Notch pathway in the intestinal epithelium, while the BPN mice, VillinCre^{ER} Braf$^{V600E/+}$ p53$^{fl/fl}$ N1icd$^{LSL/+}$, harbour a mutation in Braf rather than in the Kras pathway. KPN mice develop spontaneous metastasis at secondary sites, including liver (82% burden), lung, peripheral lymph nodes and peritoneal cavity. These models are the first of their kind and represent an incredible advancement towards a better understanding of metastasis burden, and will allow testing various immunotherapies in this context.

1.3.5.5 Models of colitis-associated cancer

Colitis-associated cancer models generally involve the use of genetically engineered animals, which include a diversity of knockouts, such as *Il10*, *Smad3*, *Muc2* and double knockouts of *Tcrb* with *p53*, *Tgfb1* with *Rag2* and *Tgfb* with *Il10*. More models are generated every year and tend to be used to study the immune compotent of tumourigenesis. IL-10 deficient mice develop inflammatory conditions that are associated with a high incidence of colorectal adenocarcinomas in the colon and rectum (Berg et al., 1996). The enteric flora is critical for the development of colonic tumours in many KO mice, as seen by the lack of disease in IL-10 deficient animals kept under germ free conditions (Sellon et al., 1998). These studies have highlighted a critical role for the microbiota in mediating inflammation and progression to disease.

As such, other mouse models of colitis-associated cancer specifically harnessing the capacity of certain bacteria to promote disease development have been generated and represent valuable models to study the interplay between the host immune system, the microbial environment and tumourigenesis.

The mouse commensal pathobiont *Helicobacter hepaticus* (*Hh*) is widely used in both IBD and CAC models, and its infection results in colonic chronic inflammation in certain susceptible mouse strains. Infection with *H. hepaticus* is widespread in many facilities, and strict control of colonisation together with the use of specific-pathogen-free animal facilities must be enforced (Bohr et al., 2006). A typical colitis-associated cancer model involves *H. hepaticus* infection of Rag2-deficient mice, combined with injection of the carcinogen AOM (Boulard et al., 2012). Together, *Hh*-driven innate chronic inflammation and AOM-driven mutations promote tumourigenesis in the colon and cecum in susceptible RAG-deficient 129SvEv mice. Several limitations are associated with this model: the adaptive immune system component is lacking, and the 129-mouse background is restrictive as knockouts are not as widespread as compared to the B6 mouse strain. However, the lesions correspond to adenocarcinomas, which makes this model valuable to study the early steps of invasion in the context of innate regulation.

The $Apc^{Min/+}$ ETBF model represents another model involving bacteria-driven colitis-associated cancer. The human colonic bacterium, enterotoxigenic *Bacteroides fragilis* (ETBF) secretes *B. fragilis* toxin (BFT) that causes human inflammatory diarrhea in certain patients. In mice, ETBF triggers colitis and strongly induces distal colonic tumors in multiple intestinal neoplasia (Min) mice (Wu et al., 2009). Tumour development is linked to Th17 type inflammation, and the observed lesions correspond to adenomas, with a low frequency of carcinomas.

1.3.5.6 Tumour implantation models

Implantation models involve the injection of tumour cell lines of murine (isograft) or human (xenograft) origin, into immunocompetent or immunodeficient mice respectively. Cells are either injected sub-cutaneously or orthotopically. Subcutanous models are relatively easy to implement, allow longitudinal measurement of tumour growth, and are used to screen candidate therapies. However, these tumours develop in a microenvironment that is markedly different from that of the colon, which is a major limitation. Orthotopic tumours overcome the problem related to the microenvironment and can be directly injected into the colonic mucosae via endoscopic procedures. Another model involves caecal implantation, whereby the caecum is exteriorised and tumour cells are injected into the bowel wall (Tseng et al., 2007). These models are valuable as they often lead to metastasis invasion, but require precision and surgical skills.

A plethora of colorectal cancer mouse models that recapitulate certain aspects of human CRC can be used to gain valuable insights into the biology of colorectal cancer. As no mouse model encompasses the full complexity and etiology of the human disease, scientific questions must be addressed using the most suited mouse models to provide new opportunities for novel therapy discovery and development. Altogether, generated data from mouse models facilitate further translational studies.

1.4 Tumour microenvironment

Carcinogenesis is a multi-step process that requires genetic and epigenetic alterations to occur within oncogenes and tumour suppressor genes. These hallmarks of cancer include autocrine growth, avoidance of growth inhibition, evasion of apoptosis, acquisition of an infinite replicative potential, ability to stimulate angiogenesis, and development of a migratory and invasive phenotype (Hanahan & Weinberg, 2000). Understanding the molecular complexity of an evolving tumour cell is vitally important but this information needs to be considered in the context of the tumour microenvironment. Rudolf Virchow was the first to identify inflammatory infiltrates within tumours in the late nineteenth century (Grivennikov, Greten and Karin, 2010). It is now recognised that tumour cells not only interact with local stromal cells, both at the primary and the metastatic locations, but also inflammatory cells, especially at invasive front of the tumour. These tumour—immune—stromal cell interactions are able to promote invasion by multiple mechanisms (Hanahan & Weinberg, 2011). Inflammation is regarded as both beneficial and deleterious in the development and progression of colorectal cancer.

1.4.1 The rise of immunotherapy

The idea of exploiting the host's immune system to treat cancer dates back decades and relies on the insight that the immune system can detect and eliminate malignant cells during initial transformation in a process termed immune surveillance (Sharma et al., 2011). Individual human tumours arise through a combination of genetic and epigenetic changes that facilitate immortality, but at the same time create foreign antigens – neo-antigens – which render neoplastic cells detectable by the immune

system. Solid tumours are known to contain tumour antigen-specific T cells, however, a potent antitumour immune response is not always observed. This is explained by the fact that cancer cells evolve and adapt to their microenvironment, and thereby escape immune recognition by developing multiple resistance mechanisms, including local immune evasion, induction of tolerance, and systemic disruption of T cell signalling (Grivennikov et al., 2010).

After many years of trials and failures, it is now an exciting time for cancer immunotherapy: the development of clinically efficacious therapeutics that harness the capacity of the immune system to recognise and mount a response against a tumour has become a reality for many cancers (Couzin-Frankel, 2013). Such therapies harness antitumour immune reponses, which are primarily orchestrated by antigen-specific IFNγ-producing $CD4^+$ Th1 cells and CD8 cytotoxic T cells, as well as innate natural killer cells (Medler, Cotechini and Coussens, 2015). These therapies have shown durable responses in several malignancies.

For the treatment of melanoma, non-small cell lung carcinoma, bladder, and kidney cancers, therapeutic efficacy was shown through the inhibition of immune checkpoint molecules, particularly the cytotoxic T lymphocyte-associated protein 4 (CTLA-4) or the programmed death 1 (PD-1) pathways (Medler, Cotechini and Coussens, 2015). In haematological malignancies, adoptive transfer of T cells harbouring chimeric antigen receptors (CAR-T cells) has shown major success (Porter et al., 2011; Garfall et al., 2015; Brown et al., 2016). Finally, a new therapy using an oncolytic virus that selectively replicates in tumour cells and potentiates antitumour immunity has shown efficacy in a Phase III clinical trial (Andtbacka et al., 2015).

In colorectal cancer, the vast majority of patients are refractory to such therapies (Schumacher, Kesmir and van Buuren, 2015), which is potentially explained by the low neoantigen load in certain CRCs, and by the presence of immunosuppressive cells and cytokines. In colorectal cancer, immunosuppression and pro-tumourigenic inflammation work hand in hand to establish lesions and therefore represent new therapeutical opportunities (Lynch and Murphy, 2016).

1.4.2 Tumour-promoting inflammation

Inflammation inflicts tissue damage, which induces a repair response in order to heal and restore normal tissue function. This healthy tissue repair response comprises inflammation, angiogenesis, matrix deposition, and cell recruitment (Rieder et al., 2007). However, upon chronic inflammation, this response is unproductive and leads to scar formation, a process known as fibrosis (Rieder et al., 2007). In addition to fibrogenesis, chronic inflammation predisposes to cancer (Hanahan and Weinberg, 2011), and patients with ulcerative colitis in particular have an increased risk of developing colorectal cancer (CRC) by 2.4 fold (Jess et al., 2012).

Although originally thought to be exclusively involved in tumour surveillance and antitumour immunity, the presence of immune cells at tumour sites is now understood to also have a pro-tumourigenic role. Tumour-associated macrophages (TAMs) are important regulators of tumourigenesis that are either tissue resident or derived from peripheral reservoirs such as the bone marrow and spleen (Erreni et al., 2010). Although macrophages are classically regarded as critical effector cells in immune responses, numerous studies have demonstrated a role for TAMs in supporting multiple aspects of tumour progression. Mast cells, neutrophils, innate

lymphoid cells and other immune cell populations, including B cells, are now regarded as pro-tumourigenic, in certain types of cancer (Grivennikov et al., 2010).

Tumours have been deemed as “wounds that do not heal”. Indeed, the tumour niche resembles a site of chronic wound healing (Dvorak HF 1986; Barcellos-Hoff MH, Lyden D, Wang TC 2013) and the presence of myofibroblastic cells in tumours and tissue repair has emerged as a particularly common hallmark (Cirri P, Chiarugi P, 2011). Myofibroblasts are contractile mesenchymal cells that are characterised by their production of copious amounts of extracellular matrix (Eyden B, Banerjee SS, Shenjere P, Fisher C, 2009) and specific expression of AOC3 (Lin-ting Hsia et al., 2016). More recently, it has been appreciated that cancer-associated fibroblasts (CAFs) are important producers of cytokines and growth factors that modulate both neoplastic cells and the tumour microenvironment, to promote disease progression.
Alteration of the extracellular matrix (ECM) composition is a key feature of cancers, and tends to involve preferential increased deposition of Col-I and Col-III (Wynn TA, Ramalingam TR, 2012). The presence of a dense and rigid ECM has direct effects on tumour progression (reviewed in Butcher DT, Alliston T, Weaver VM, 2009), but also amplifies the activation of myofibroblasts, which in turn further promotes tumourigenesis, in a positive feedback loop (Barcellos-Hoff MH, Lyden D, Wang TC, 2013). Thus, myofibroblasts also enable the malignant epithelium to progress into the different layers of the intestine via dysregulation of ECM composition.

Overall, many of the cytokines produced by infiltrating tumour cells act directly on transformed cells to promote proliferation, inhibition of apoptosis, invasion,

angiogenesis, epithelial mesenchymal transition, and metastasis (Hanahan and Weinberg, 2011). Therapeutic strategies which combine potentiation of antitumour immunity with suppression of pro-tumourigenic inflammation will be necessary to harness the full anti-tumourigenic capacity of the immune system (Grivennikov et al., 2010). A list of pathogenic cytokines expressed in colorectal cancer is displayed in **Table 1.2**. A more comprehensive review on cytokine regulation in CRC is available in an NRI review (West et al., 2015).

Cytokine	Cellular Source	Cellular Responder
TNFα	Hematopoetic cells	IECs, cancer cells
TGF-β	CAFs	Cancer cells, CAFs
IL-1β	TAMs, neutrophils	IECs, cancer cells
IL-6	TAMs, CAFs, mesenchymal stem cells	IECs, cancer cells
IL-11	CAFs	Cancer cells
IL-23	DCs, TAMs (Cd11b+, Gr1+)	Hematopoietic cells
IL-17A	CD4+ αβ T cells, CD8+ (Tc17 cells), γδ T cells, ILCs, CAFs	Cancer cells, CICs, MDSCs
IL-17C	IECs	IECs, cancer cells
IL-17F	IECs	Endothelial cells
IL-22	ILC3s, CD4+ T cells	Cancer cells
IL-18	TAMs, IECs	IECs, T cells
IL-8	CD44+ cancer stem-like cells	CD11b+Gr-1+ myeloid cells
GM-CSF	Cancer cells	Cancer cells, APCs, monocytes
IL-15	Cancer cells	NK cells, CD8+ T cells, B & T cells
IL-21	CD4+ T cells, activated NK cells	NK cells, CD8 T cells

Table 1.2: Cytokines in the pathogenesis of colorectal cancer.

Cytokines produced by innate and adaptive immune cells, stromal fibroblasts and cancer epithelial cells have diverse and pleiotropic roles at different stages of colorectal cancer (CRC) progression.

IL-22, IL-17A and IL-21 are important for mucosal tissue healing, microbiota management and host defence, but can also promote tumour formation.

At early stages of tumourigenesis, IL-15 and IL-21 potentiate cytotoxic responses by $CD8^+$ T cells and NK cells; GM-CSF activates macrophages and DCs; IL-18 induces the release of IFNγ; IL-17F inhibits angiogenesis; and TGF-β impairs cancer cell growth and dissemination. All of these cytokine-mediated effects inhibit tumour progression.

However, in well-established tumours, which may have developed adaptations to resist impairment by specific cytokines, many cytokines can enhance tumour progression by promoting proliferation, inhibition of apoptosis, angiogenesis, stromal reorganisation, EMT, metastasis and suppression of antitumour immunity.

Major cytokine producers and associated responder cells for specific cytokines are listed in the accompanying table.

CAF, cancer-associated fibroblast; CIC, cancer-initiating cell; IEC, intestinal epithelial cell; TAM, tumour-associated macrophage; Tc17 cell, IL-17-producing cytotoxic T cell; TNF, tumour necrosis factor.

(Table prepared for NRI by S. McCuaig and F. Franchini; (West et al., 2015).

1.4.3 Regulatory T cells in colorectal cancer

In the colon, IL-10 production by Tregs is critical to control chronic inflammation and its deficiency is linked to IBD development. Early studies have shown that established inflammation is significantly diminished upon transfer of WT Tregs into 129.RAG$^{-/-}$ *H. hepaticus* infected mice (Maloy et al., 2003). In colon cancer, mouse models have established that IL-10-mediated production from Tregs is also a critical pathway for regulation of inflammation and its associated anti-tumourigenic function. For instance, established tumours from 129.RAG$^{-/-}$ hosts injected with IL-10$^{-/-}$ Tregs and infected with *H. hepaticus* can be eradicated following injection of recombinant IL-10 or transfer of WT Tregs (Erdman et al., 2003). Many other animal models of CRC have emphasised a role for Tregs in controlling tumour burden, and IL-10 has been repeatedly described as a critical cytokine in mediating tolerance at mucosal sites, and more importantly in controlling colonic inflammation and CRC development. For instance, IL-10 deficient mice are more susceptible to spontaneous colitis and intestinal tumour development (Berg DJ 1996), and IL-10 production by Tregs is also essential to reduce tumour burden in Apc$^{Min/+}$ mice (Erdman et al., 2005). Furthermore, in the *Apc*$^{\Delta 468}$ CRC model, similar to a global IL-10 deficiency, the number of intestinal polyps was increased in mice with a T cell-specific ablation of IL-10 and is associated with the accumulation of eosinophils in polyps (Dennis et al., 2013). Recent reports have suggested that during CRC development, Tregs lose the ability to produce IL-10 and start producing IL-17, thereby promoting polyp growth in Apc$^{Min/+}$ mice (Gounaris et al., 2009). Additionally, oral administration of IL-10 micro particles in Apc$^{Min/+}$ mice is sufficient to decrease polyposis, through the neutralisation of pathogenic IL-17-producing Tregs and restoration of conventional

Tregs (Chung et al., 2014). Collectively, these results have established that production of IL-10 by Tregs is required in order to control pro-inflammatory responses that ultimately promote tumour growth in the intestine.

Despite abundant evidence for a protective role for IL-10 and Foxp3 cells in both inflammation- and mutation-driven CRC murine models, their role in humans is more complex.

In CRC patients, several studies have linked the presence of Foxp3 Tregs to poor prognosis and survival (Sinicrope et al., 2009), while others have challenged this view and shown that infiltration of Foxp3 Tregs in CRC tumours was linked to improved prognosis and survival (Frey et al., 2010; Salama et al., 2009). Recent work from S. Sakagushi reconciled these contradictory results by identifying subpopulations of regulatory T cells in human CRC that are heterogeneous in phenotype and with suppressive and non-suppressive properties (Miyara et al., 2009). More specifically, two types of CRCs are described, and prognosis relates to the type of FOXP3 cells infiltrating the tumours. In type-A CRC, FOXP3 high expression is a marker of poor prognosis, in which tumour-infiltrating $FOXP3^+$ $CD4^+$ T cells are predominantly effector Treg cells (fraction II). By contrast, in type-B CRC, characterised by elevated transcripts for *TGFB1* and *IL-12A*, high $FOXP3^+$ in tumours correlates with better prognosis. The $FOXP3^+$ cells in type B-CRC mainly correspond to inflammatory non-Treg $FOXP3^+$ cells (fraction III) (Saito et al., 2016).

IL-10 serum levels have been shown to increase over time during disease progression in CRC patients (O'Hara et al., 1998; Stanilov et al., 2010), and high serum levels of IL-10 before surgery correlate with poor survival (Miteva et al., 2014). Altogether these data suggest a tumour-promoting role of IL-10 in CRC patients. In the tumour microenvironment, an extensive array of cells can produce IL-10, such as monocytes, macrophages, epithelial cells and T cells, including Tregs. (Krause et al., 2015; Maloy and Powrie, 2011). The discrepancy between the role of IL-10 in mouse models and CRC patients may be due to preferential signalling downstream of the receptor in CRC, which can signal via STAT1, STAT3, and STAT5 (Wehinger et al., 1996), but this requires further investigation.

In conclusion, the same Treg immunosuppresive functions that mediate protection against intestinal inflammation may have negative consequences in establishing tumour progression in the colon. Delineation of Treg development and function, depending on their sub-types, will be key to harnessing the full potential of immunotherapies. Moreover, in CRC, the bystander suppression mediated by Tregs, which corresponds to the state of suppressiveness that Tregs impose on the organ, will also have to be addressed, as it may influence the colonic tumour microenvironment.

1.5 Metastasis

Cancer-related death is predominantly caused by the metastatic spread of tumour cells. Tumour cells undergo a series of sequential, rate-limiting steps that establish metastatic malignancy, and is summarised in **Figure 1.3**. Tumour cells from a primary tumour migrate and invade the local tissue (Massagué and Obenauf, 2016). Following angiogenesis, tumour cells intravasate into lymphatic or circulatory systems and spread throughout the body. Within the circulation, tumour cells must survive by evading immune detection and by resisting the circulatory pressure. Once present within a capillary bed, tumour cells extravasate into a secondary organ. There, they must survive and proliferate in order to successfully colonise (Fidler, 2002). The 'soil and seed hypothesis' was originally proposed by Stephen Paget in 1889, when he analysed metastatic spread in deceased patients, and noticed that certain metastatic sites were more prevalent than others. This suggested that tumour cells from specific primary tumours favour specific secondary locations to establish a metastatic growth (Paget, 1889). Critically, metastatic spread is a highly inefficient process as million of tumours escape from the primary tumour but fail to colonise secondary organs. The presence of a favourable microenvironment at the secondary location enhances the rate of metastatic colonisation (Fidler, 2003), and the final colonisation step represents the major rate limiting factor (Koop et al., 1995).

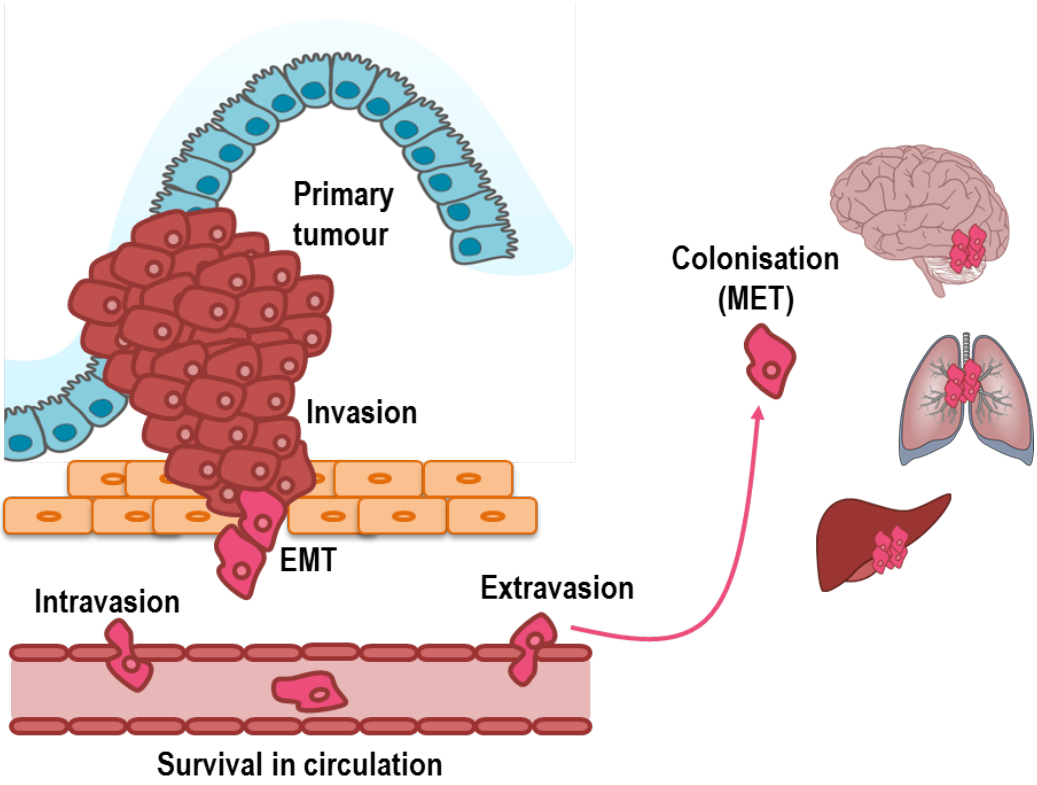

Figure 1.3: Key steps of the invasion-metastasis cascade

Metastasis is a multi-step process that starts with the infiltration of tumour cells into the adjacent tissue, representing the early (i) invasion.
Following invasion, tumour cells can ungergo EMT (ii), and enter a blood or lymphatic capillary via (iii) intravasion.
Once in the circulation, tumour cells survive immune detection and circulatory pressure (iv), and extravasate (v) into a secondary organ.
The successful colonisation process (vi) involves proliferation in the secondary organ, which may require a return to an epithelial state, notably through MET.

1.5.1 Metastases in colorectal cancer

The survival of patients with colorectal cancer has improved; however, the mortality rate still ranks third due to metastasis or recurrence (Siegel et al., 2017). Metastases are found in about 20 to 25% of patients with colorectal cancer at diagnosis, and will develop in about 50% of patients during the course of the disease. The liver is the most common site of metastasis for colorectal cancer, and only 15 to 20% of patients with liver metastases are suitable candidates for surgical resection. (Siegel et al., 2017). Other organs are specifically targeted by CRC metastases: the peritoneal cavity, the lungs, and more rarely, the brain and the bones (Damiens et al., 2012;

Riihimäki et al., 2016). Recently, it was shown that nervous system metastases occurred more frequently together with respiratory metastases than with liver metastases, which may relate to the origine of escape route, or to specific adaptations that are favourable for colonising these organs. Patients with sole liver metastases dominating could represent a subset where the tumour is immunologically distinct from those cases where tumour load is smaller and lung and bone metastases are present. These findings have clinical implications as specific treatments may be employed to treat different types of metastases, and further hints that not all colorectal tumours are alike immunologically or metastatically. (Riihimäki et al., 2016).

1.5.2 Epithelial to mesenchymal transition as a primary step towards metastasis

Epithelial cells are morphologically rounded, polarised cells, with an apical and basal site. They form layered structures, which contain highly organised cellular junctions that connect neighbouring cells, and are characterised by the expression of E-cadherin. By contrast, mesenchymal cells have a spindle, fibroblast-like morphology, and lack organised cellular junctions. Additionally, mesenchymal cells have the potential to be highly migratory, and these cells express N-cadherin. The epithelial-mesenchymal transition (EMT) is a highly complex and dynamic process whereby epithelial cells gain a mesenchymal phenotype, both at the morphological and transcriptional level. The reverse process, a mesenchymal-epithelial transition (MET), allows the reversion of mesenchymal cells to epithelial cells (Thiery & Sleeman, 2006). Classically, loss of E-cadherin is considered as a hallmark of EMT.

The process of EMT, originally identified during chicken embryogenesis, is vital at multiple stages of life and formation of various tissues, as well as during normal wound healing process (Kalluri & Weinberg, 2009). Several types of EMTs are defined depending on the processes they regulate, although they have a common set of genetic and biochemical pathways. The EMT type 1 describes processed involved during embryogenesis and organ formation, type 2 relates to wound healing and fibrosis, while type 3 concerns cancer-related events. In cancers, the process of EMT is triggered by multiple extracellular factors, including TGF-β, Notch, fibroblast growth factor (FGF) and Wnt signalling. The majority of these signals converge on a series of master EMT-inducing transcription factors (EMT-TFs), which orchestrate and coordinate this process. These EMT-TFs include the SNAIL (SNAIL1 and SNAIL2), ZEB (ZEB1 and ZEB2) and bHLH (TWIST1 and TWIST2) family members. They promote EMT by repression of epithelial genes, such as E-cadherin (Moreno-Bueno et al., 2008; Hill et al., 2013), and promote a migratory property that is critical for the escape from the primary tumour.

EMT is most prevalent within cells at the tumour invasive front (Kalluri & Weinberg, 2009), but has also been linked to the formation of tumour cells with stem-like capacities. These cells are not only highly migratory and invasive, but also have the capacity to self-renew and differentiate at the metastatic site, aiding in the formation of macro-metastases (Mani et al., 2008). Finally, although EMT is described as an event conferring mesenchymal properties to tumour cells, it should be noted that these cells often adopt a mixed epithelial and mesenchymal phenotype.

1.5.3 SOX-4 as an emerging master regulator of EMT

The SOX4 transcription factor belongs to a large family of proteins that regulate numerous aspects of embryonic development. It is structurally characterised by a highly conserved HMG-box domain that directly binds to the minor groove of DNA helix, inducing DNA bending and alterations in chromatin architecture, thus contributing to the organisation of functional transcriptional complexes (Štros et al., 2007).

In the recent years, SOX4 activation has been linked to the control of various aspects of tumour development and progression in many cancers, including breast, lung, pancreatic, glioblastoma and prostate cancer. Several cancer-associated signaling pathways have been implicated in the activation of SOX4, including TGF-β, Wnt, TNF-α, and hypoxia/HIF-1a signalling (Lourenço and Coffer, 2017).

SOX4 activation is associated with inhibition of apoptosis, induction of cell migration and metastasis, and the generation and maintenance of cancer stem cells (CSCs), depending on the tumour type (Lourenço and Coffer, 2017). The molecular mechanisms by which SOX4 exerts its function are not fully described. SOX4 may contribute to inhibition of apoptosis and stimulation of cell survival via its transcriptional regulation of the transcription factor TEAD2, which is part of the HIPPO signaling pathway that has been implicated in the development and metastasis of various tumours (Pan, 2010). In breast cancer, ectopic expression of SOX4 in epithelial cells results in the induction of a mesenchymal phenotype associated with reduced levels of E-cadherin and increased expression of vimentin, N-cadherin, and fibronectin, as well as enhanced cell migration and invasion (Tiwari

et al., 2013). Conversely, depletion of SOX4 results in a mesenchymal-to-epithelial (MET)-like phenotype, suggesting that SOX4 is also a crucial regulator in maintaining the mesenchymal state of EMT. Moreover, in mouse xenograft experiments, SOX4 potentiated RAS-induced tumorigenesis in MCF10A cells (Zhang et al., 2012). These effects have been characterised in other cancers, but not always in an extensive manner, and rarely involving the use of *in vivo* models.

Interestingly, in pancreatic cancer, SOX4 has the opposite effect on cancer cells that are sensitive to TGF-β (David et al., 2016). Upon TGF-β signaling, the EMT program becomes lethal by converting TGF-β-induced Sox4 from an enforcer of tumourigenesis into a promoter of apoptosis. Mechanistically, this effect was mediated by a remodeling of the cellular transcription factor landscape that occurred during EMT, and included the repression of the gastrointestinal lineage-master regulator Klf5. Klf5 cooperates with SOX4 in oncogenesis and prevents SOX4-induced apoptosis (David et al., 2016). Thus, SOX4 function may be cancer-dependent and more studies are required to delineate its role in cancer progression, depending on microenviromental clues and responsiveness of tumour cells to cytokines.

Several studies have attempted to identify SOX4 transcriptional targets in human tumours, however the comparative analyses that were performed have revealed a relatively minor degree of overlap between the different cancer types (Vervoort et al., 2013). This result may imply that SOX4 transcriptional targets reflect tumour-specific and context-dependent mechanisms of gene induction. Interestingly

however, certain genes are associated with a SOX4-core signature gene expression, such as the tyrosine kinase signaling-associated EGFR and VEGF, and are present in multiple studies (Vervoort et al., 2013). Moreover, other SOX4 targets, such as SLCO5A1, CCNG2, GPR56, GRN, MGAT4B, SKP2, TRIB3 and CD24, are linked to very diverse roles in the tumourigenesis of a variety of cancers (reviewed in Vervoot et al., 2013), highlighting the requirements to study SOX4 function in a cancer specific manner.

1.6 Immune regulatory networks in colorectal cancer

1.6.1 Primary aims

The objective of this work is to understand the cellular and molecular pathways by which interleukin-10 deficient regulatory T cells contribute to the development and progression of colorectal cancer. We seek to identify new mechanisms by which lack of adequate T cell regulation in the gut can drive formation of aggressive, invasive colon adenocarcinomas. Together with cytokine networks in the intestine and tumour-infiltrating cells, we study how these components of the tumour microenvironment impact on tumour cells' adapations that enable disease invasion.

1.6.2 Thesis Outline

In Chapter 3, we compare the capacity of IL-10 deficient regulatory T cells in promoting colitis-associated cancer *in vivo* to WT Tregs and IL-$10^{-/-}$ $CD4^{+}$ effector T cells. Using RNA sequencing of WT and IL-$10^{-/-}$ Tregs, we identify a newly described cytokine, *Meteorin-like*, with unknown functions in the adaptive immune system.

In Chapter 4, we focus on the tumour microenvironment promoted by IL-$10^{-/-}$ Tregs. We screen for upregulated cytokines and their cellular sources in tumour-bearing animals. *In vivo* blockade of IL-6-R and TGF-β leads to decreased tumour burden, and we identify stromal cells as major producers of the pro-tumourigenic cytokine IL-6.

Finally, in Chapter 5, we identify Sox4 as upregulated in tumour tissue compared to matched-inflamed tissue. Sox4 expression is associated with expression of several genes involved in tumour progression and angiogenesis. We confirm SOX4 expression in primary tumours and liver metastases by employing a publically available dataset and CRC patient samples. Using a panel of colorectal cancer cell lines and *in vivo* models, we identify Sox4 as an enabling factor for tumour growth.

2 Material and Methods

2.1 *In vivo* experiments

2.1.1 Mice

Wild type C57BL/6, B6.Rag1$^{-/-}$, NOD.CB17-Prkdcscid/J, B6.Foxp3GFP, B6.IL-10$^{-/-}$, Wild type 129SvEv, 129SvEv.RAG2$^{-/-}$, 129SvEv.IL-10$^{-/-}$, 129SvEv.IL-10$^{-/-}$.Foxp3GFP and 129SvEv.Foxp3GFP mice were all bred and maintained under specific pathogen-free conditions in accredited animal facilities at the University of Oxford.

Only males were used for experiments related to Chapters 3 and 4. Both females and males were used in the experiments reported in Chapter 5. Mice were negative for *Helicobacter spp*. as well as other known intestinal pathogens and were more than 8 weeks old when first used, unless otherwise indicated. All procedures were conducted in accordance with the UK Scientific Procedures Act of 1986 by a Personal Licence holder under a Project License authorized by the UK Home office.

2.1.2 Mouse model of colitis-associated cancer

Regulatory T cells were purified from spleens and from the axillary and popliteal draining lymph nodes with a CD4 kit enrichment (Stemcell) followed by FACS sorting. When sorted from Foxp3GFP reporter mice, splenic cells were stained with a viability dye and sorted on GFP expression. For non-reporting mice, Tregs were sorted based on: live cells, CD45^{+} CD3^{+} CD4^{+} CD25^{high} CD45RB^{low}. Purified regulatory T cells were washed in sterile PBS and 3.10^{5} cells were injected intraperitoneally (i.p.) into sex-matched 129.RAG$^{-/-}$ recipient mice (day 0). Mice were subsequently gavaged with 1×10^{8} colony-forming units (CFU) of *Helicobacter hepaticus* (*Hh*) using a 22 G curved needle on day 3, day 4 and day 5. The animals were monitored for signs of colitis and weight loss once a week for the first 9 weeks, and on a daily basis from week 9 to week 12, due to signs of disease.

2.1.3 *Helicobacter hepaticus* culture

Helicobacter hepaticus NCI-Frederick isolate 1A (strain 51449; American Type Culture Collection) was grown on blood agar plates containing Trimethoprim, Vancomycin, and Polymixin B (Oxoid, TVP) for 48h at 37° under microaerophilic conditions (3-5% O_2, 10% CO_2, 10% H_2, balance N_2) in a CampyPak jar (Oxoid). *H. hepaticus* was harvested from plates using a cotton swab and transferred into liquid culture of Tryptic Soy Broth (Sigma-Aldrich, TSB) supplemented with 10% Fetal Calf Serum (Life Technologies, FCS), supplemented with TVP antibiotics in vented Erlenmeyer flasks (Corning) and continued to grow under microaerophilic conditions at 37° in a shaking incubator at 200rpm. Upon use, the optical density (OD) of the culture was read at 600nm using a BioPhotometer (Eppendorf). Bacteria were then centrifuged at 4000rpm for 20 minutes. The viability of bacteria was assessed using a fluorescent Live/Dead assay (Molecular Probes) under a fluorescent microscope Olympus CKX41.

2.1.4 Cytokine and growth factor *in vivo* blockade

129.RAG$^{-/-}$ recipients injected with IL-10$^{-/-}$ Tregs and infected with *Hh* were injected i.p. twice a week with 0.25µg neutralizing antibody for IL-6-R, TGF-β (BioXCell, respectively #BE0047 clone 15A7 and #BE0057 clone 1D11.16.8), or IL-22 (Genetech, clone 8E11.9), starting from week 9 post Treg injection, for 5 consecutive weeks. Mice were sacrificed a day after the last injection and the colons were harvested for pathohistological analysis. The 15A7 monoclonal antibody has been shown to block the binding of IL-6 to the IL-6 receptor. The 1D11.16.8 monoclonal antibody is a neutralizing antibody for TGF-β. Control mice were injected with mouse IgG1 antibody (BioXCell).

2.1.5 Histopathological analysis

Colons were harvested and cleaned in PBS before being cut open longitudinally, and gently laid down on Whatma paper with the lumen side up. Colons were then ”rolled” from the distal colon towards the proximal colon. The rolls were fixed in formalin for 24h and stored into 70% ethanol until subsequent use.

2.1.5.1 Aberrant crypt foci count

For aberrant crypt foci count (ACF) in indicated experiments, fixed colons were stained in 2% methylene blue and ACFs were measured and counted using a dissection microscope and sliding calliper. Colons were washed in 70% ethanol three times until the methylene blue staining was washed off, and re-stored until further use.

2.1.5.2 Processing for histopathological analyses and *in situ* stainings

The colon rolls were paraffin embedded into “swiss-roll” sections. The whole colon was then completely ribboned at 5um sections (between 200-300 sections per mouse) with every 10^{th} section mounted and haematoxylin and eosin stained (H&E). Other unmounted sections were used for other stainings. For collagen deposition visualisation, unstained sections were selected and stained with Pycro-Sirus red.

2.1.5.3 Colitis score

Colonic inflammation was scored in a blinded fashion by two researchers according to the scoring system outlined below (**Figure 2.1**). The average of proximal, middle and distal colon scores was calculated to obtain the total colitis score. Images of the sections were acquired on an Olympus BX51 microscope.

A.	**EPITHELIUM**	**HYPERPLASIA and/or**	**GOBLET CELL DEPLETION**
	0	**None**	**None**
	1	**Mild (1.5x)**	**Mild (25%)**
	2	**Moderate (2-3x)**	**Marked (25-50%)**
	3	**Severe (>3x)**	**Substantial (>50%)**
B.	**INFLAMMATION IN LAMINA PROPRIA**		
	0	**None - few leucocytes**	
	1	**Mild - some increase in leucos at tips of crypts OR many lymphoid follicles**	
	2	**Moderate - marked infiltrate (notable broadening of crypt)**	
	3	**Severe - dense infiltrate throughout**	
C.	**AREA AFFECTED**	**(% of section)**	
	0	**None**	
	1	**up to 25%**	
	2	**25-50%**	
	3	**>50%**	
D.	**MARKERS OF SEVERE INFLAMMATION**		
	0	**None**	
	1	**Submucosal inflammation OR Few crypt abscesses (<5)**	
	2	**Submucosal inflammation AND Few Crypt Absecesses (<5)**	
	2	**Many crypt abscesses (<5) OR Extensive submucosal inflamm OR Crypt branching (*Hh)***	
	3	**Many crypt abscesses (<5) AND Extensive submucosal inflamm / Crypt branching (*Hh)***	
	3	**Ulceration OR Extensive fibrosis**	

Figure 2.1: Criteria for the histological scoring of colonic sections

2.1.5.4 Tumour grade

H&E sections mounted for pathohistological analysis were blindly graded by Dr. Daniel Royston, using criteria for grading dysplasia and tumours as previously described (Boulard et al., 2012). Tumours were staged as per TNM classification of human CRC (Tumour, Node and Metastasis). Images of the sections containing tumour lesions were acquired on an Olympus BX51 microscope.

Two types of lesions were observed: dysplasia and adenocarcinoma. Dysplastic lesions fall into the low- or high-grade category and usually precede early tumour invasion. Low-grade dysplasia is defined as branching and elongation of crypts, and lesions contain crowded epithelial cells with low nucleus-to-cytoplasm (N/C) ratio, showing a loss of nuclear polarity. By contrast, high-grade dysplasia is characterised by a complex irregularity of glands, and epithelial cells exhibit a high N/C ratio, have irregular nuclear membranes, as well as aberrant and numerous mitoses.

Adenocarcinomas are defined as cytologically and architecturally abnormal crypts breaching the muscularis mucosae, which is the thin layer of smooth muscle that surrounds the mucosae. Adenocarcinoma stages relate to the extent of invasion: T stage referring to the invasion of the primary tumour into deeper layers of the bowel wall: stage T1 into the submucosae, stage T2 into the muscularis propria, T3 through the muscularis propria and T4 involving serosa. N stage is categorised as N0 (no nodal involvement), N1 1-3 nodes involved, N2 > 3 nodes involved. M stage refers to the absence (M0) or presence (M1) of distant metastases.

Differentiation relates to the degree which the malignant epithelium approximates to normal glandular epithelium (well, moderately or poor differentiation). Of note, tumours with extensive mucinous differentiation are referred to as mucinous adenocarcinomas.

2.1.6 Xenograft and isograft of CRC cell lines

2.1.6.1 Establishment of tumours

NOD.SCID, B6.RAG$^{-/-}$ and WT C57BL/6 mice were anaesthetised with 2% Isofluorane and injected sub-cutaneously into the right flank with 5.10^5 cells of indicated human CRC lines, or 1.10^5 MC38 cells. Tumour growth was monitored every 3 or 4 days with a digital calliper and tumour width (W) and length (L) were recorded. Tumour volume was calculated using the equation V = (L x W x W)/2. The endpoint was defined as tumour exceeding 12mm in diameter.

2.1.6.2 Monitoring for metastasis dissemination

Metastatic dissemination was monitored using the IVIS Spectrum imaging system (PerkinElmer). Initial tumour growth was monitored 4 to 5 days after initial injection, and metastatic dissemination was assessed when tumours reached the end-point.

Mice were injected i.p. with luciferin (1.5mg/mL) and anaesthetised. Mice were placed into the IVIS machine on their left flank. Bioluminescence signals were measured every 5 min for 15 minutes. Settings used: 60sec exposure, binning Medium (8 pixels), F/Stop 1 and C view.

2.2 Cell Isolation

2.2.1 Isolation of leukocytes from the spleen and lymph nodes

Spleens and peripheral lymph nodes including superficial cervical, popliteal, axillary, brachial, and inguinal lymph nodes were harvested following the sacrifice of the mice. Organs were mashed through a 70µm strainer and washed with PBS/0.1% BSA/5mM EDTA (Sigma-Aldrich) and centrifuged at 500g for 5 minutes. Splenic cells were additionally incubated with 500µl ACK (Ammonium-Chloride-Potassium) lysis buffer for 3 minutes at room temperature to lyse red blood cells, followed by a wash with PBS/0.1% BSA/5mM EDTA. Single cell suspensions were counted using a hemocytometer and resuspended in an appropriate volume of PBS/0.1% BSA/5mM EDTA for subsequent analyses.

2.2.2 Isolation of cells from the colon

Colons were removed from the animals following sacrifice. Colons were cut open longitudinally, cleaned of the remaining faeces and cut at 1cm intervals. The tissue was washed twice for 20-25 minutes in RPMI (Sigma Aldrich)/10% FCS/5mM EDTA at 37°C in a shaking incubator at 200rpm to remove epithelial cells, followed by a short wash in RPMI/10% FCS/15mM completemented with Hepes (Sigma-Aldrich) to neutralise the activity of the EDTA. The tissue was digested for 40 minutes in the presence of RPMI/10% FCS/15mM Hepes with 100U/ml collagenase VIII (Sigma-

Aldrich) at 37°C in a shaking incubator at 180rpm with tubes placed horizontally. The digested tissue was then filtered through a 70µm strainer, and the digestion was terminated by addition of ice-cold RPMI/10% FCS/5mM EDTA followed by centrifugation at 500g for 10 minutes. A three-layer (30/40/70%) Percoll (GE Healthcare) density-gradient was used to enrich for the lymphocytes or stromal fraction. Cells obtained from the digestion were layered in the 30% layer on top of the 40% and 70% layers, and centrifuged for 20 minutes at 900g with low acceleration and without brake. The 40/70% Percoll interface was isolated for lamina propria leukocytes (LPLs), and then washed with PBS/0.1% BSA/5mM EDTA. Single cell suspensions were resuspended in a required volume of PBS/0.1% BSA/5mM EDTA for the subsequent analysis. Additionally, the 30/40% Percoll interface was used to recover stromal cells in the indicated experiments. Single cell suspensions were counted using a hemocytometer and resuspended in an appropriate volume of PBS/0.1% BSA/5mM EDTA for LPLs, and PBS/0.1% BSA only for stromal cells, for subsequent analyses.

2.2.3 Isolation of cells from xenografts and isografts

Tumours were dissected out from the animals following sacrifice. Tumour volume was recorded using a digital caliper as the end-point measure. Tumours were cleaned of fat tissue and rinsed in PBS. A piece of tumour was collected for RNA in RNA*later*™ (Invitrogen) and histology in 10% formalin, and stored appropriately until subsequent use. The rest of the tumour was minced into 1mm pieces with a scapel blade and the tissue was digested for 30 min in the presence of RPMI/10% FCS with 100U/ml collagenase VIII (Sigma-Aldrich), without Hepes, at 37°C in a shaking incubator at 180rpm with tubes placed horizontally. Cells were then filtered through

a 70µm strainer, and the digestion terminated by addition of ice-cold RPMI/10% FCS/5mM EDTA followed by centrifugation at 500g for 10 minutes. A two layer (40/80%) Percoll (GE Healthcare) density-gradient was used to enrich for tumour infiltrating cells (TIC). Cells obtained from the digestion were layered in the 40% layer on top of the 80% layer, and centrifuged for 20 minutes at 900g with low acceleration and without brake. The interface Percoll interface was isolated for TIC, and then washed with PBS/0.1% BSA/5mM EDTA. Single cell suspensions were counted using a hemocytometer and resuspended in a required volume of PBS/0.1% BSA/5mM EDTA for subsequent analyses.

2.3 Flow cytometry and cell sorting

2.3.1 Restimulation of cells for intracellular cytokine staining

Single cell suspensions were plated at $1x10^6$ cells/well in a 96-well round bottom plate (Corning) in complete IMDM medium supplemented with 10% FCS, 2mM L-glutamine (Life Technologies), 100 U/ml each of penicillin and streptomycin (Sigma-Aldrich). 0.1µM phorbol 12-myristate 13-acetate (PMA) and 1µm ionomycin together with 10µg/ml brefeldin A (all from Sigma-Aldrich) were added and cells were incubated for 3.5-4 hours at 37°C before further processing for flow cytometric analysis.

2.3.2 Surface staining

All staining and washing procedures were performed in PBS/0.1% BSA/5mM EDTA. All centrifugations were performed at 500g for 5 minutes. For myeloid cell staining an initial 10-minute incubation with anti-CD16/CD32 (eBioscience) was performed to minimise any non-specific antibody binding. Appropriate antibody mixes were added

together with the Fixable Viability Dye eFluor® 780 (eBioscience) and incubated for 20 minutes at 4°C in the dark followed by two PBS washes.

When the anti-ST2 antibody was used in the primary antibody mix, cells were stained with streptavidin for additional 15 minutes at 4°C followed by two additional washes. For surface-only stainings, cells were directly analysed on a flow cytometer. All antibodies used can be found in Appendix 2.

2.3.3 Intracellular staining

Prior to the intracellular staining the surface staining protocol was performed as described in section 2.3.1. Cells were then fixed and permeabilised using the Foxp3/Transcription Factor Staining Buffer Set (eBioscience) following the manufacturer's instructions. Firstly, cells were resuspended in 50µl fixation-permeabilisation buffer for 20 minutes in the dark at ambient temperature, followed by a wash in 1X permeabilisation buffer. The antibody cocktail was prepared in the permeabilisation buffer and cells were incubated for 30 minutes at 4°C followed by two washes with the permeabilisation buffer.

Cells were analysed on a flow cytometer immediately for stainings containing transcription factors, or on the following day when other stainings were performed.

2.3.4 Flow cytometry acquisition and analysis

Cells were acquired either on LSRII or Fortessa (BD Biosciences) using FACSDiva software (BD Biosciences). Compensation, using single-coloured-stained CompBeads (BD Biosciences), was performed prior to sample acquisition. The analysis of the results was performed using FlowJo 10 (Tree Star).

2.3.5 Cell sorting (FACS) BD™

Single cells suspensions were obtained as described in section 2.2, and subsequently enriched using the MoJo Sort Mouse $CD4^+$ T Cell Enrichment Kit (BioLegend) according to the manufacturer's instructions. Cells were stained with appropriate antibody mixes for 15 minutes at 4°C in the dark, washed twice with PBS and resuspended in PBS/0.1% BSA/5mM EDTA and filtered prior to the sort. 4',6-diamidino-2-phenylindole (DAPI) was added for the viability assessment. Cells were sorted into PBS/10% FCS supplemented with 1mg/mL DNAse (Roche), or directly into RLT for RNA sequencing samples. The purity of the sorted cells was assessed by a flow cytometric analysis. Cells were sorted on FACS AriaIII (BD Biosciences) by Dr H. Ferry, J. Webber or Dr C. Pearson.

2.4 *In vitro* primary cell cultures

2.4.1 Tregs culture and supernatant generation

FACS-sorted $Foxp3^+$ cells from $Foxp3^{GFP}$ reporter mice or $CD45^+$ $CD3^+$ $CD4^+$ $CD25^{high}$ $CD45RB^{low}$ from 129.IL-$10^{-/-}$ mice were plated at a density of $1x10^5$ per well in flat-bottom 96 well plates (Corning) in 200uL of RPMI-1640 medium supplemented with 10% FCS, 2 mM L-glutamine, 0.05 mM 2-mercaptoethanol, 100 U/ml each of penicillin and streptomycin for 12h (Complete medium). IL-2 (40ng/mL, Peprotech), or 10ng/mL phorbol 12-myristate 13-acetate (PMA) (Cayman Chemical) and 1µg/mL ionomycin (Iono) (Sigma) in complete medium was then added to the cultures. After 48h (PMA/Iono) and 70h (IL-2) of stimulation, plates were centrifuged at 500g for 10 min, and the supernatants were harvested, filtered and frozen for use in stimulation

experiments with stromal cells. For each independent Treg sorts, all generated supernatants from a similar condition were pooled into a larger stock.

2.4.2 Colonic stromal culture

Colons were processed as previously described in section 2.2.2. Cells were recovered from the 30/40% interface of the Percoll density gradient and washed with PBS/0.1% BSA without EDTA for 10 min at 500g. For each colon, all cells from the stromal cell fraction was plated into one well of a 6 well plate in complete RPMI media (Sigma-Aldrich) supplemented with 100 µg/mL Primocin™ (InvivoGen). After 24 and 48 hours non-adherent cells were removed by two 1xPBS-wash steps, and the media was replaced. Adherent stromal cells were cultured for another 2 to 5 days until confluent. For the first passage, cell cultures were washed with 1xPBS, and cells dissociated using TrypLE™ Express Enzyme (1x) (Gibco) for 2 minutes at 37°C. Cultures were rinsed with 1xPBS and centrifuged at 500g for 10 minutes. Cells were counted using a hemocytometer and expanded as required.

2.4.2.1 Expansion of stromal cell cultures

For expansion, confluent cells were split into 2 similar wells or plates, so that stromal cells do not suffer from a loss of cell density. Cell cultures were washed with 1xPBS, and cells dissociated using TrypLE™ Express Enzyme (1x) (Gibco) for 2 minutes at 37°C. Cultures were rinsed with 1xPBS and centrifuged at 500g for 10 minutes and expanded until subsequent use.

2.4.2.2 Stromal cell stimulations

For stromal stimulation with Treg supernantants, cells were harvested and plated at a density of $1.5x10^4$ cells per well of a 48 well plate. After 12h, the media was

removed and replaced by the Treg supernatant diluted 1 in 5 in DMEM media (Sigma-Aldrich) supplemented with 100 µg/mL Primocin™. In indicated experiments, the Treg supernatants were pre-incubated with or without anti-TNFα (clone TN3-19.12 mAb, BioXCell). RNA and supernatants were harvested for gene expression and protein secretion.

2.4.3 Cytokine analysis of colon explants and LPL cultures

Colons were harvested from the peritoneal cavity and a 0.5cm piece was dissected from the middle or distal part (as indicated) of each colon. The weight of the tissue was recorded and the pieces were incubated in complete RPMI-1640 medium for 12 hours at 37°C 5% CO_2 in a 24 well plate (Corning). Following incubation, supernatants were collected and stored at -80°C for growth factor and cytokine analysis. Weight was used to normalise cytokine production. For LPLs, total cells recovered from the 40/70% gradient interface were plated into 96 well plate at $5x10^5$ cells per well and cultured overnight in complete RPMI medium for 12 hours at 37°C.

2.5 Colorectal cancer cell line culture and experimentation

2.5.1 Source and maintenance of cell lines used

Human Colo205 and HCT116 (ATCC) colorectal cancer cell lines were a generous gift from Dr Simon Leedham. HCT116 cells were isolated from a human colorectal carcinoma, originating from an adult male patient. HCT116 are adherent cells that carry a mutation in codon 13 of the ras proto-oncogene and express the carcinoembryonic antigen. Colo205 cells were isolated from a human ascitic fluid of a 70-year-old Caucasian male with colorectal adenocarcinoma. Colo205 cells carry

deletion in APC and p53 genes, and express the carcinoembryonic antigen, keratin and IL-10. Murine MC38 colorectal cancer cell line expressing GFP and luciferase was a generous gift from Dr Lennard Lee (Professor Ian Tomlinson's Lab). MC-38 cells were derived from C57BL6 murine colon adenocarcinoma following repeated sub-cutaneous injections of the carcinogen dimethylhydrazine (DMH), and were shown to be metastatic in a transplantation model (ref to include, but it deletes my track changes when I do so, so will insert once approved).

All lines were confirmed to be mycoplasma free by their respective labs. Colo205 cells were cultured in RPMI (Sigma) with 10% FCS and 1% penicillin-streptomycin (P/S, Sigma). HCT116 and MC38 cells were cultured in DMEM (Sigma) with 10% FBS, 1% P/S. Cultures were maintained in a humidified environment at 37°C, 5% CO_2. Experiments were conducted using cells between passages 3-8. Adherent cells were dissociated using TrypLE^{TM} (Gibco), filtered through 70uM filters, and viable cells counted by Trypan Blue exclusion using a hematocytometer.

2.5.2 Generation of lentiviral particles using lipofectamine

HEK293FT were seeded at 10^6 cells in 10cm culture dish and cultured with complete IMDM (Sigma-Aldrich). Once confluency reached 80%, the media was removed and replaced with 8mL of fresh IMDM supplemented with 10% FCS, without antibiotics. Reagents and plasmids were thawed on ice. Table 2.1 shows the plasmid quantities used per transduction. Per dish of HEK293FT to transduce, 64uL of Lipofectamine® 2000 (Thermo Fisher) was combined to 1.2mL of Opti-MEM (Thermo Fisher) at room temperature and left to incubate for 5 minutes. The different plasmids were combined into Opti-MEM media to a total volume of 1.2mL, and left to incubate at

ambient temperature for 5 minutes. Lipofectamine and plasmids were mixed together without excessive agitation and were let to incubate for 20 minutes at room temperature. All the combined Lipofectamine + Plasmids mix was added to cells drop by drop with caution. The media was gently agitated so that the mix is equally distributed, and cultured cells were placed at 37°C, 5% CO_2 for 4 hours. After incubation, media was removed and 8mL of fresh IMDM supplemented with 10% FCS only was added to the dish. Supernants were harvested and fresh media replaced accordingly on the following day (Day 1 viral particles), 24h after (Day 2 viral particles) and after another 24h (Day 3 viral particles, optional). Supernatants were kept as individual batches per day of harvest, filtered and stored at -80°C until further use. Table 2.2 indicates the different plasmids used in this thesis.

Plasmids	Quantity per 10^6 cells
Transfer plasmid	1 ug
PAX2 packaging	0.75ug
MD2.G packaging	0.25ug

Table 2.1: Quantities of plasmid used for Lipofectamine transduction

Plasmid	Source	Function
pLenti PGK V5-LUC Neo	AddGene #21471	Luciferase expression
pWPXL	AddGene #12257	GFP expression control
pWPXL-Sox4	AddGene #36984	SOX4 overexpression
pLKO.1-puro Empty Vector Control	Sigma-Aldrich MISSION®	ShRNA control
pLKO-1-puro shRNA-SOX4	Sigma-Aldrich MISSION® TRCN0000018217	Sh-SOX4 control human
pLKO-1-puro shRNA-Sox4	Sigma-Aldrich MISSION® TRCN0000012081	Sh-Sox4 control mouse

Table 2.2: List of lentiviral plasmids used in this thesis

2.5.3 CRC lines titration kill curves

Colo205, HCT116 and MC38 cells were subjected to a titration kill curve for Gentamycin and Puromycin, in order to select transduced cells. Cells were seeded at 10^5 cells per well in a flat bottom 96 well plate (Corning) and were left to adhere

overnight. Each condition was repeated in duplicate and Table 2.3 indicates the concentration used for each antibiotic.

Volume of stock solution added (ul)	Final concentration (ug/mL)
G418 (50mg/mL)	
0	0
1	50
2	100
3	150
4	200
6	300
8	400
10	500
20	1000
80	4000
120	6000
160	8000

Volume of stock solution added (ul)	Final concentration (ug/mL)
Puromycin (2.5mg/mL)	
0	0
0.2	0.5
0.4	1
0.6	1.5
0.8	2
1	2.5
1.2	3
1.6	4
1.8	4.5
2	5
2.4	6
3	7.5

Table 2.3: Range of concentration used for the killing assay, using Gentamycin (G418) and Puromycin.

Cell viability was assessed every 2 days based on cell morphology, and the media containing the antibiotics was replaced every 3 days. Colo205, HCT116 and MC38 cells were efficiently killed by 1ug/mL of Puromycin. Colo205 and MC38 cells were efficiently killed by 300ug/mL of Gentamycin, and HCT116 were killed at a concentration of 4000ug/mL.

2.5.4 CRC lines lentiviral transduction

Protocol adapted from AddGene.

Cells were seeded at $5x10^5$ cells a day prior to the procedure to allow for adherence. RPMI complete containing 10µg/mL polybrene (Sigma-Aldrich) was prepared prior the procedure. The lentiviral aliquots were thawed at 37°C and a range of dilutions of the lentivirus in RPMI complete + 10µg/mL polybrene were prepared (Table 2.4) for each transduced cell line.

Dilution	Volume of Lentivirus	Volume media + 10ug/mL polybrene
0	0	500
1:5	300	200
1:50	30	470

Table 2.4: Dilutions of lentivirus used per cell line and per transduction

Each mix of dilution was added to each 6 well plate containing cells cultured in 1mL RPMI (or DMEM depending on the cell line) containing 10% FCS and 10µg/mL polybrene. One extra well was used as a "non virus" control well. Viral particles were incubated with cells for 48h. After incubation, media was gently aspirated and 1.5mL of complete RPMI (or DMEM) containing the appropriate antibiotic was added to the culture, in order to select for a stable cell pool. After 2 days of antibiotic treatment, cells were harvested using TrypLE^{TM} and individual clones were seeded into 96 well plates (24 clones per line per transduction), and antibiotic selection was maintained for a total of one month. Clones were selected based on their expression of SOX4 levels, using gene expression and protein quantification.

2.5.5 Proliferation assays

HCT116 and MC38 sub-lines were seeded at a density of 5.000 cells, and Colo205 sub-lines were seeded at a density of 10.000 cells per well in 96 well plates (Costar) in 100uL of complete RPMI or DMEM media depending on the cell line. Cells were cultured at 37°C, 5% CO_2 for 48h. WST-1 reagent (Abcam) was added to each well, with a 1:10 dilution, and cells were incubated for one hour. A well containing media only was used a control. Absorbance was measured at 450nm on a BMG SPECTROstar NANO Microplate Reader (BMG Labtech). The OD_{450} of treated cells was substracted to the OD_{450} of the control wells to assess proliferation of the sub-lines.

The WST-1 assay is based on the cleavage of the tetrazolium salt WST-1 to formazan by cellular mitochondrial dehydrogenases. Expansion in the number of viable cells results in an increase in the activity of the mitochondrial dehydrogenases, which in turn leads to increase in the amount of formazan dye formed.

2.6 Gene expression analysis

2.6.1 RNA extraction

Tissue was firstly homogenised in soft tissue homogenising CK14 tubes (Stretton Scientific) in 700µl RLT for 30s using Precellys24 homogeniser (Precellys). Cells were directly lysed in 500ul RLT lysis buffer (Qiagen). RNA was extracted using the RNeasy Mini RNA extraction kit (Qiagen) according to the manufacturer's instructions, including the DNase digestion step. RNA was quantified using a NanoDrop spectrophotometer (Thermo Scientific) and stored at -80°C.

2.6.2 qPCR analysis

cDNA was generated using the High Capacity cDNA Reverse Transcription Kit (Applied Biosystems) with up to 2µg of RNA according to the manufacturer's instructions inclusive of the RNase Inhibitor (Applied Biosystems) in a final volume of 10µl. Synthesis was performed in a C1000 TouchTM Thermal Cycler (Biorad). cDNA was diluted 1:5 with Nuclease free water.

qPCR was performed using TaqMan Real-Time PCR assays (Life Technologies; a full list of probes used can be found in Appendix 2) and Precision Fast qPCR Mastermix with ROX at a lower level, with inert blue dye (PrimerDesign) in 384 well plates (FrameStar; clear wells). All reactions were performed in duplicates and qPCR reactions were prepared as follows:

Reagent	Volume per run (uL)
cDNA	2
Precision Fast qPCR Master Mix	3
TaqMan Real Time PCR Assay	0.2
RNAse Free DNAse Free H20	0.8
Final Volume	**6**

Table 2.5 qPCR Reaction Mix

Plates were sealed with MicroAmp® Optical Adhesive Film (Life Technologies). Plates were run on the ViiA7 Real-Time PCR System (Applied Biosystems) using the fast run method (Table 2.6).

Stage	Step	Ramp Rate	Temperature	Time
Hold Stage	1	1.9°C/s	95°C	2 min
PCR Stage	1	1.9°C/s	95°C	5 sec
Number of cyles: 40	2	1.6°C/s	60°C	20 sec

Table 2.6 Fast run method for qPCR

For murine samples, the expression levels of the gene of interest were normalised to the housekeeping gene *Hprt* levels, and the gene expression was calculated using the ΔCT method [$2^{-\Delta CT}$ with ΔCT = CT(target gene) – CT(housekeeping gene)]. For human gene expression analysis, large ribosomal protein (*RPLPO*) was used as housekeeping gene.

2.6.3 RNA sequencing sample preparation

FACS-sorted cells were lysed in the RLT lysis buffer and RNA was extracted using the RNeasy Micro Kit (Qiagen) according to the manufacturer's protocol. The quality of the RNA was tested using the Agilent RNA 6000 Pico Kit (Agilent Technologies) according to the manufacturer's protocol and analysed on the Agilent 2100 Bioanalyser (Agilent Technologies). Only samples with RNA integrity number (RIN)

above or equal to 8 were used for subsequent amplification. Samples were stored at -80°C until further processing.

2.6.4 RNA sequencing analysis

Library preparation, RNA-sequencing, and quality control were performed on a service basis by the High-Throughput Genomics Group (Wellcome Trust Centre for Human Genetics, Oxford). Libraries were prepared using the Low input SMARTer kit (ClonTech) following the manufacturer's instructions. The prepared libraries were size-selected and multiplexed and paired-end sequenced using the Illumina HiSeq4000 platform (Illumina) over three lanes of a flow cell.

Raw data was processed using a build-in pipeline by Dr. Nicholas Illot. Adapter trimming was performed using Cutadapt, alignment was performed using Hisat, adapter trimming was performed using Trimmo, and mapped reads were quantified using Htseq-count. Picard was used as part of quality control for the number of reads aligned to the genome.

2.6.4.1 Data analysis

A Variance Stabilising Transformation (VST) was applied to the count data, using "local" fitType as parameter, and DESeq2's dispersion estimates was visualised for the dataset. Clustering analysis was performed on all 28 samples using correlation distance metrics. Principal component analysis (R package *prcomp* version 3.3.1) was subsequently performed on all samples. These analyses revealed several outliners, which were identified and removed from the analysis (details in Appendix 1). Clustering analysis was performed on the samples kept for the analysis as well as principal component analysis on R.

2.6.4.2 Differential expression analysis

Differential expression analysis was performed using the generalised linear model (GLM) implemented in the *Deseq2* package (version 1.14.1). The GLM approach was used to assess the differential gene expression between samples (comparison of 2 samples per analysis). Genes from each analysis were ranked according to log2 fold change and adjusted *p* values. Genes with log2 fold change greater than 2 and $p < 0.05$ were considered to be differentially regulated.

The R code used for the differential expression analysis is included in Appendix 1.

2.7 Analysis of protein expression

2.7.1 Immunoblotting using Li-COR

Protein was extracted from adherent CRC cell lines using a solution of 50mM Tris pH 6.8, 20mM EDTA, 5% SDS, 1mM DTT, 10% glycerol. 15-20µg of protein (quantified with a nanodrop) was loaded into pre-cast NuPAGE® Novex 4-12% Bis-Tris Gels (Life Technologies), separated by SDS-PAGE and transferred onto Immobilon-FL PVDF (Millipore) membranes using a wet transfer apparatus. Non-specific background binding was blocked with pure Odyssey® Blocking Buffer (TBS). Membranes were incubated with primary antibody (Table 2.7) in Odyssey® Blocking Buffer with 0.2% Tween-20 overnight at 4°C. Membranes were washed in TBST and incubated with fluorescently conjugated secondary antibody for 1 hour at ambient temperature (Table 2.7). Membranes were washed in TBST and protein expression was detected using the Odyssey CLx detection system. Target protein was quantified by normalising the target protein fluorescence intensity to the fluorescence intensity of simultaneously stained β-actin for each sample.

Target protein	Dilution	Fluorophore	Company	Clone
Primary antibodies				
SOX4 (produced in rabbit)	1:1000	/	Sigma-Aldrich	HPA029901
Sox4 (produced in rabbit)	1:1000	/	Merk	AB5803
β-actin (produced in mouse)	1:10.000	/	Sigma-Aldrich	AC-74
Secondary antibodies				
Goat anti-rabbit-800CW	1:15.000	800CW	LiCOR	925-32211
Goat anti-mouse-680RD	1:15.000	680RD	LiCOR	925-68070

Table 2.7: Western blot primary and secondary antibodies

2.7.2 Enzyme-linked immunosorbent assays (ELISAs)

Cytokine secretion was quantified using specific ELISAs (against indicated cytokines in Table 2.8) according to the manufacturer's instructions. 50µl of samples were quantified in duplicate. The absorbance was read at 450nm by a spectrophotometric plate reader SPECTROstar Nano, and the subsequent analysis was performed using SPECTROstar Nano Data Analysis software.

Target protein	Company
Mouse IFN-gamma DuoSet	R&D System
Mouse TNF-alpha DuoSet ELISA	R&D System
Mouse Amphiregulin DuoSet ELISA	R&D System
Mouse IL-6 DuoSet ELISA	R&D System
Mouse IL-10 DuoSet ELISA	R&D System
Human SRY (sex determining region Y)-box 4 ELISA	MyBioSource

Table 2.8: List of cytokines measured by ELISA

2.7.3 Bender assays

Standards were prepared according to the manufacturer's instructions. 25uL of samples were used for concomitant detection of several cytokines (IFNγ, TNFα, IL-1β, IL-17A). For TGFβ, samples were pre-treated according to the manufacturer's instructions. In each well, cytokine-beads and biotin conjugate mixtures were added. The plate was covered in foil and left to incubate for 2 hours at ambient temperature

on a microplate shaker at 500rpm. Supernatants were aspired through the wells in a process that let the beads in. The plate was washed twice with PBS. Assay buffer and Streptavidin-PE solution were added to each well. The plate was covered in foil and left to incubate for one hour on a microplate shaker at 500rpm. The plate was washed as previously described, using PBS. Beads were resuspended in assay buffer and transferred into FACS tubes. Acquisition was performed within 24 hours of the assay on a Fortessa (BD Biosciences).

2.8 Imaging studies

2.8.1 Immunofluorescent labelling – mouse

Colons were harvested, rolled into "Swiss rolls" and fixed for 24h in 3.7% formalin. Sections were processed by Richard Stillion (Dunn School) or by the Histology Laboratory at the Kennedy Institute. 5µm sections were cut and unstained sections were provided for immunofluoresecent labelling. Antigen retrieval was performed using 350mL of 1x Dako Antigen Retrieval Solution (Dako, Agilent) and microwaving slides at full power for 15 minutes. Non-specific binding of the secondary antibody was blocked using 10% normal goat serum (Sigma-Aldrich) for 1 hour at room temperature. Primary antibody staining was performed in 10% goat serum over night at 4°C, or no primary antibody was added (secondary only control). Following incubation, slides were washed 3 times with TBS for 10 min per wash, and incubated with the fluorescent conjugated secondary antibody (Life Technologies) for one hour at ambient temperature, in the dark. Slides were washed a further 3 times with TBS, and mounted with ProLong Gold Antifade Mountant with DAPI (Life Technologies) and imaged on an Olympus BX51 microscope.

Primary and secondary antibodies used in the immunofluorescence experiments are listed in Table 2.9.

Primary antibody			Secondary antibody	
Target protein	**Clone**	**Host species**	**Reactivity**	**Fluorochrome**
Sox4	polyclonal	Rabbit	Goat anti-Rabbit	AF555
Gp38	8.1.1	Hamster	Goat anti-Hamster	AF488

Table 2.9: List of primary antibodies used in the immunofluorescence staining experiments and associated secondary antibodies.

2.8.2 Immunofluorescent labelling – human

Matched-normal and liver metastases frozen tissue sections were provided by Dr. Jon Buzzelli (Professor Ruth Muschel's Laboratory). The tissues were originally collected from the Radcliffe Biobank and the study ethics number is 14/A008. The study was registered under the ORB RTB ethics 09/H0606/5+5.

Frozen sections were allowed to thaw at ambient temperature before being washed with PBS to remove the OCT, and fixed for 5 minutes with 3.7% formalin. Antigen retrieval was performed using Dako Antigen Retrieval Solution (Dako, Agilent) and microwaving slides at full power for 15 minutes. Non-specific binding of the secondary antibody was blocked using 10% normal goat serum (Sigma-Aldrich) for 1 hour at room temperature. Sections were stained with anti-human SOX4 (0.15ug/mL [1:400], Atlas Antibodies; HPA029901) or no primary antibody (secondary only control) over night at 4°C. Following incubation, slides were washed 3 times with TBS for 10 min per wash, and incubated with a rabbit anti-goat secondary antibody (Alexa Fluor 555, Life Technologies) for one hour at ambient temperature, in the dark. Slides were washed for another 3 times with TBS, and mounted with ProLong Gold Antifade Mountant with DAPI (Life Technologies) and imaged on an Olympus BX51 microscope.

2.9 Statistical analyses

All statistical analysis was performed in Prism 7.0 (GraphPad).

The Mann Whitney U test was used to compare two unpaired samples. For comparison of more than two groups, a Kruskal-Wallis one-way analysis of variance was performed followed by a Dunn's post-hoc test. Differences were considered statistically significant when $p \leq 0.05$. Significance is indicated according to the following: * $p \leq 0.05$, ** $p \leq 0.01$, *** $p \leq 0.001$, **** $p \leq 0.0001$.

For Chapter 3 and 4, where tumour grade statisical significance was assessed, contingency analysis (Fisher's exact test, two-sided) with mentioned control group was performed. Significance is indicated according to the following: * $p \leq 0.05$, ** $p \leq 0.01$, *** $p \leq 0.001$, **** $p \leq 0.0001$.

For Chapter 5, where stastical analyses were performed comparing repeated measures over time, the repeated measures two-way ANOVA was performed, followed by a Tukey's multiple comparisons test. Significance is indicated according to the following: * $p < 0.0332$, ** $p < 0.0021$, *** $p < 0.0002$, **** $p < 0.0001$.

For Chapter 5, for the clinical outcome in the Shaffer dataset, time-to-event curves were prepared using Kaplan-Meier methods and disease-specific survival (DSS) was performed as follows:

1. For comparison of two groups, *p* values were computed using Log-rank (Mantel-Cox) tests. Hazard ratios (HR) are univariate Cox proportional hazard ratios with 95% confidence intervals.

2. For comparison of three groups, *p* trend values were computed using Logrank test for trend.

3 IL-10 deficient Regulatory T cells drive tumourigenesis in a mouse model of colorectal cancer

3.1 Introduction

Regulatory T cells play a non-redundant role in controlling immune responses and maintaining self-tolerance. They are found in most peripheral tissues under homeostatic conditions and are crucial for maintaining an adequately balanced immune response, due in part to their production of the anti-inflammatory cytokines IL-10 and transforming growth factor-β (TGF-β). The role of Tregs in cancer development and progression is complex as they potentially exhibit dual and opposite functions (Zamarron and Chen, 2011). In many cancers, Tregs accumulate in primary tumours and peripheral blood of patients, where they promote disease progression and poor prognosis through suppression of anti-tumour immune responses (Wilke et al., 2010). However, in certain cancers, such as colorectal cancer, Tregs also suppress pro-tumourigenic inflammation that could otherwise induce tissue damage and tumour progression itself (la Cruz-Merino et al., 2011).

Importantly, their ultimate role in cancer progression may rely heavily on the tumour microenvironment and the events leading to initial propagation of carcinogenesis. In tumours, Tregs interact with hematopoietic-derived immune cells, such as other T cells, DCs, and macrophages. However, recent data suggests that Tregs may also influence epithelial and stromal cells. In particular, RANKL producing Tregs were found to play a critical role in promoting metastasis in breast cancer through their interactions with tumour and stromal cells (Tan et al., 2011). In a model of *H. hepaticus* driven CAC, transfer of Tregs was shown not only to block innate inflammation (Maloy et al., 2003), but also to revert established tumours (Poutahidis et al., 2007), through the action of the anti-inflammatory cytokine IL-10. Surprisingly,

injection of IL-10 deficient $CD25^{+}$ Tregs into susceptible 129/SvEv.$RAG2^{-/-}$ mice showed that these Tregs were not only unable to resolve inflammation but actually exacerbated CAC in the presence of *H. hepaticus* (Poutahidis et al., 2007). Transcriptomic analysis comparing colonic to mesenteric lymph node (MLN) Tregs showed several genes related to repair were upregulated in colonic Tregs, including amphiregulin (Areg) (Schiering et al., 2014), an EGFR ligand involved in wound healing. We hypothesise that once in the colon, injected IL-$10^{-/-}$ Tregs, in the context of a pro-inflammatory environment, will have increased repair function, possibly through the production of AREG and TGF-β, that may promote the tumour response. Indeed, IL-10 has been shown to regulate TGFβ-mediated fibrosis in a lung inflammation model (Kitani et al., 2003). Despite current efforts to provide characterisation and associated functions of tissue-Tregs, little is known about the phenotype of tumour-infiltrating Tregs. This knowledge is critical in the context of the development of immunotherapies aiming at targeting or reprogramming Treg in the tumour microenvironment.

This Treg-accelerated model of bacteria driven CAC therefore provides an excellent system in which to study the phenotype and function of a defective Treg response driven by a microbial insult leading to promotion of tumourigenesis. In this chapter, we establish a previously published mouse model of colitis-associated cancer and:

1. Characterise the model
2. Explore the phenotype of Treg cells and investigate whether Tregs are true drivers of tumourigenesis
3. Determine how Tregs promote tumourigenesis, using RNA sequencing of Treg populations.

3.2 Results

3.2.1 IL-10 deficient Regulatory T Cell transfer is associated with increased tumourigenesis in a mouse model of colitis associated cancer

To assess the function of IL-10$^{-/-}$ Tregs, we first established the cancer model previously described by the Erdman group. Genetically susceptible 129SvEv.RAG2$^{-/-}$ mice (referred thereafter as 129.RAG$^{-/-}$) infected with the mouse microaerobic pathobiont *Helicobacter hepaticus* (*Hh*), as expected, developed colitis and typhlitis by week 4 (**Figure 3.1 A, top**). As a control group, mice were injected intraperitoneally with WT Treg, which were FACS sorted from 129 WT mice, and then orally infected with *Hh* at day 3, day 4 and day 5 (**Figure 3.1 A, middle**). Finally, IL-10$^{-/-}$ CD4^{+} CD45RB^{low} CD25^{+} Treg cells were FACS sorted from IL-10$^{-/-}$ mice and injected intraperitoneally into 129.RAG$^{-/-}$ hosts, which were then orally infected with *Hh* at day 3, day 4 and day 5 (**Figure 3.1 A, bottom**).

To assess colitis and tumour burden, mice were sacrificed at week 12, and swiss rolls were made for histology assessment (**Figure 3.1 B**). This method allowed for pathology assessment of the full-length colon in one section, for parameters including inflammation and tumour burden. Detail of the histology procedure is available in section 2.1.5 of Chapter 2.

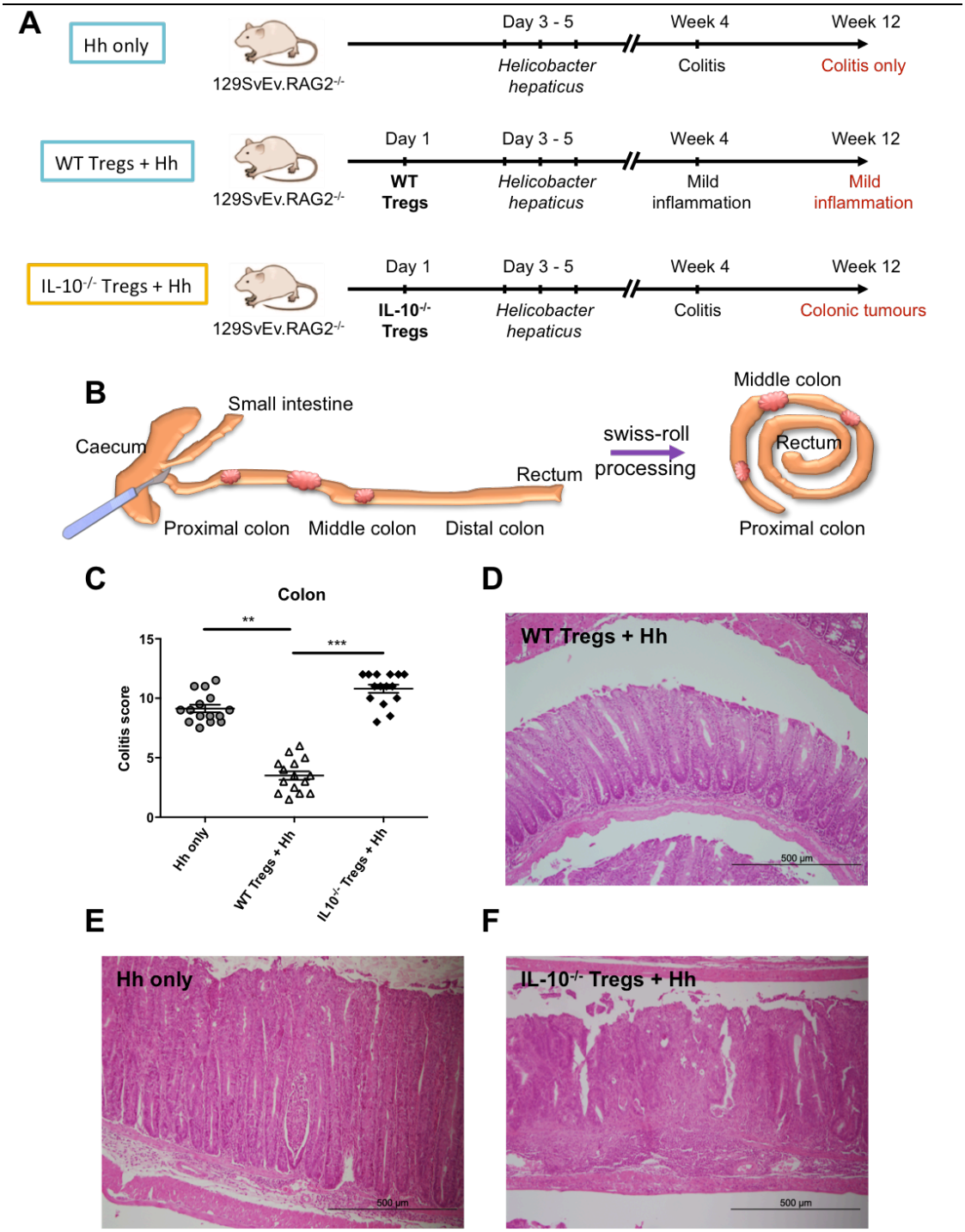

Figure 3.1: IL-10$^{-/-}$ Tregs + *Hh* group displays high colonic inflammation

129.RAG$^{-/-}$ mice were infected with *Hh* or were injected with WT or IL-10$^{-/-}$ Tregs, prior to *Hh* infection. At week 12, mice were sacrificed and colons were taken for histology.

(A) Scheme of treatment and outcome of the different experimental groups.
(B) Scheme of colonic tissue processing for histopathological analyses.
(C) Colonic inflammation quantification.
(D E F) Representative photomicrographs of middle colon H&E sections for each group.

Bars represent mean ±SEM. Data represents pooled results from three independent experiments (n=15 for each group), performed at the JR facility site.
Statistical significance was determined using a Kruskal Wallis one-way analysis of variance, followed by a Dunn's post-hoc test. ** $p \leq 0.01$, *** $p \leq 0.001$.

We first quantified colonic inflammation across the experimental groups (**Figure 3.1 C**). Mice infected with *Hh* developed severe colitis by week 12, with an average colitis score of 9 out of 12. IL-$10^{-/-}$ Tregs + *Hh* mice showed enhanced colitis, with an average score of 11, and a few mice reaching a maximum score of 12. By contrast, transfer of WT Tregs in *Hh* infected mice animals led to minimal disease, with scores ranging from 1 to 6. This highlights the ability of WT Tregs' to control inflammation driven by *H. hepaticus*.

A photomicrograph of the colon from mice transferred with WT Tregs and infected with *Hh* (WT Tregs + *Hh*) (**Figure 3.1 D**) showed a mild inflammation phenotype, where goblet cells are present in the epithelium, crypts are non-hyperplastic, and no extensive infiltration of leukocytes is detected in the lamina propria. By contrast, (**Figure 3.1 E**) photomicrographs of the colon of animals only infected with *Hh* alone displayed a loss of goblet cells, a thickening of the crypts, as well as a few abscesses. Finally, colon from the IL-$10^{-/-}$ Tregs + *Hh* group (**Figure 3.1 F**) revealed a complete loss of colonic architecture. The lamina propria was highly infiltrated by various immune cells, and the epithelium showed crypt branching as well as abscesses. We also detected an enlargement of the stromal layer and multiple markers of severe inflammation, including bleeding and oedema, were present.

We then moved on to analysing tumour burden. Adenocarcinomas of stages 1 and 2 were detected in mice, and are usually associated with a mucinous differentiation and are referred as mucinous adenocarcinomas. Representative photomicrographs of tumour lesions are provided for each experimental group. At month 3 of infection with *H. hepaticus*, 129.$RAG^{-/-}$ mice developed low-grade dysplasia, and a few mice

had T1 tumours throughout the colon and cecum of a rather small size (**Figure 3.2 A**). In chronic infection, more mice progressed to develop tumours (data not shown, months 12-24). In the WT Tregs + *Hh* group, most of the observed lesions occurred in the proximal colon and displayed a polyp-like shape, and were associated with a local inflammatory infiltration (**Figure 3.2 B**). Finally, mice from the IL-$10^{-/-}$ Treg + *Hh* group developed T1 and T2 tumours, associated with a mucinous phenotype. Most lesions were observed in the proximal and middle colon, with high amounts of inflammation but not tumourigensis in the distal colon. T1 adenocarcinomas were of slightly larger size compared to the *Hh* only group and were similarly associated with an inflammatory microenvironment. An example of a T1 adenocarcinoma is shown in **Figure 3.2 C**. The tumour crossing the muscularis mucosae in a water drop-like shape is clearly visible. In the same fashion, T2 adenocarcinomas (**Figure 3.2 D**) are associated with a high-grade inflammation and dysplasia, with a moderate differentiation towards a mucinous lesion. These lesions are usually larger, reaching 500um to 1mm in size, and multiple foci of disease are found in the area.

Interestingly, when the model is run for longer than 12 weeks, about 40-50% of the IL-$10^{-/-}$ Tregs + *Hh* mice developed a substantial tumour (1 cm in diameter) mainly arising in the middle colon, that can be directly seen from the peritoneal view. A composite photomicrograph of such a tumour is presented in **Figure 3.2 E** and revealed multiple mucinous adenocarcinomas aggregated into a large mass that is growing towards the outer muscle layer of the colon. This extreme phenotype encouraged us to investigate metastatic development, especially in the mesenteric lymph nodes, spleen and liver. However, we did not detect metastasis to these distant sites in this model (data not shown).

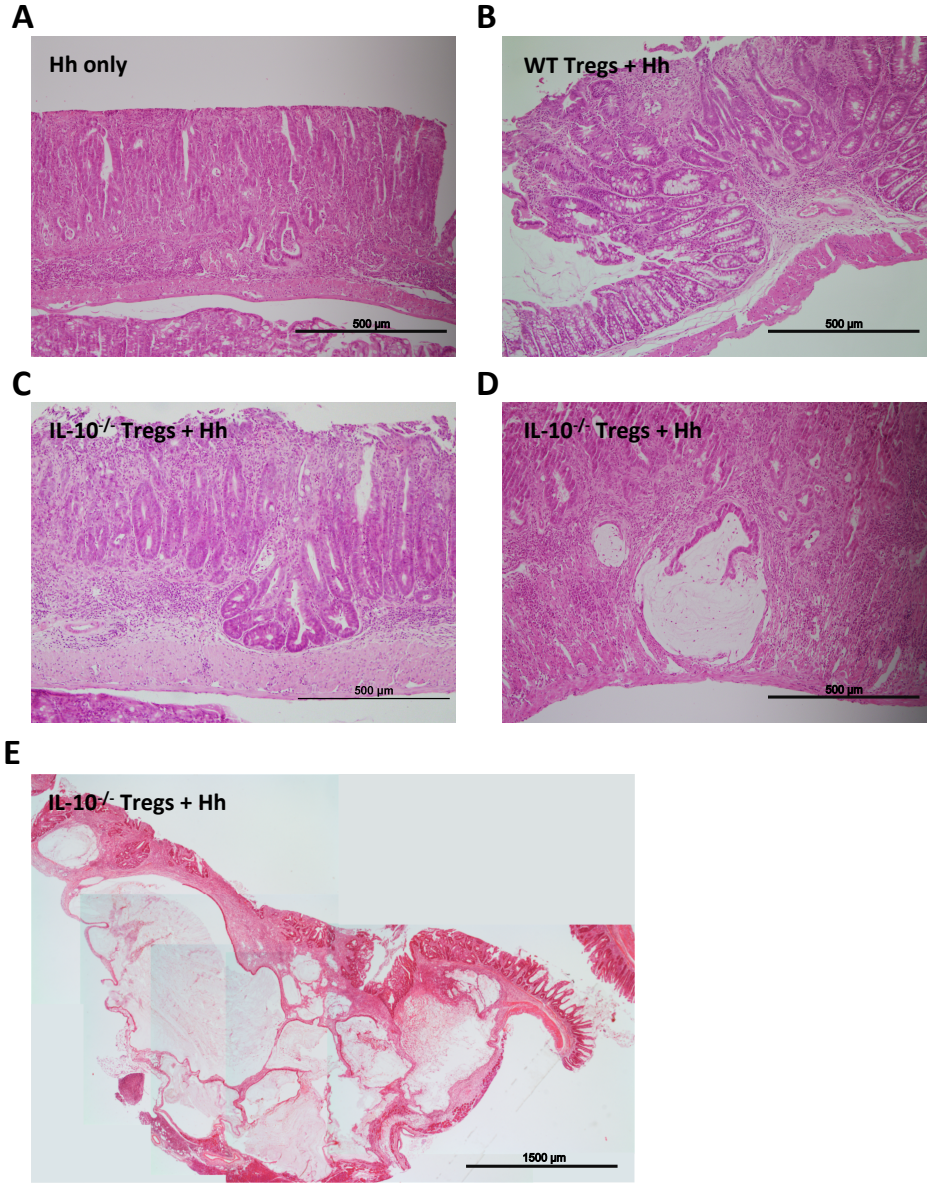

Figure 3.2: Illustration of tumour lesions across experimental groups

129.RAG$^{-/-}$ mice were infected with *Hh* or were injected with WT or IL-10$^{-/-}$ Tregs, prior to *Hh* infection. At week 12, mice were sacrificed and colons were taken for histology.
H&E stained colonic sections of tumour lesions.

(A) T1 adenocarcinoma associated with low-grade dysplasia in *Hh* only group.
(B) T1 adenocarcinoma located in proximal colon of WT Tregs + *Hh* group.
(C) T1 adenocarcinoma located in middle colon of IL-10$^{-/-}$ Tregs + *Hh* group associated with an intense infiltrate in lamina propria and inflamed submucosae.
(D) T2 mucinous adenocarcinoma in middle colon of IL-10$^{-/-}$ Tregs + *Hh* group associated with high-grade dysplasia.
(E) Composite photomicrograph of a massive formation of multiple T2 mucinous adenocarcinomas in the middle colon of IL-10$^{-/-}$ Tregs + *Hh* group, at month 6 of the model.

Tumourigenesis was quantified in various ways. First, once the colons were formalin-fixed, a short term staining with methylene blue allowed for direct visualisation of aberrant crypt foci (ACF), which were counted and measured (**Figure 3.3 A**). The mice from the IL-$10^{-/-}$ Tregs + *Hh* group developed a significantly higher number of ACF compared to the other groups. Although the ACF count is not a direct measure of tumour burden, but rather a measure of dysplastic and neoplastic lesions, it did mirror the increased number of adenocarcinomas per mouse (**Figure 3.3 B**). Of note, the size of the ACF in the *Hh* only group was larger than those in the WT Tregs + *Hh* group (data not shown). Secondly, the number of carcinoma per mouse (**Figure 3.3 B**), as well as the highest tumour stage per mouse (**Figure 3.3 C**) were directly quantified based on histopathological analysis, performed by our collaborating pathologist Dr Daniel Royston. Finally, the overall percentage of animals that developed tumours was calculated (**Figure 3.3 D**). Altogether, these data reveal that the IL-$10^{-/-}$ Tregs + *Hh* group displays a significantly higher number of carcinomas per animal and is the only group where a majority of mice developed T2 adenocarcinomas. Moreover, this group had the greatest percentage of animals with colonic tumours. Of note, a few mice in the *Hh* only and WT Tregs + *Hh* groups developed tumours, albeit exclusively T1 tumours in the *Hh* only group, and with an overall lower number of carcinomas per mouse.

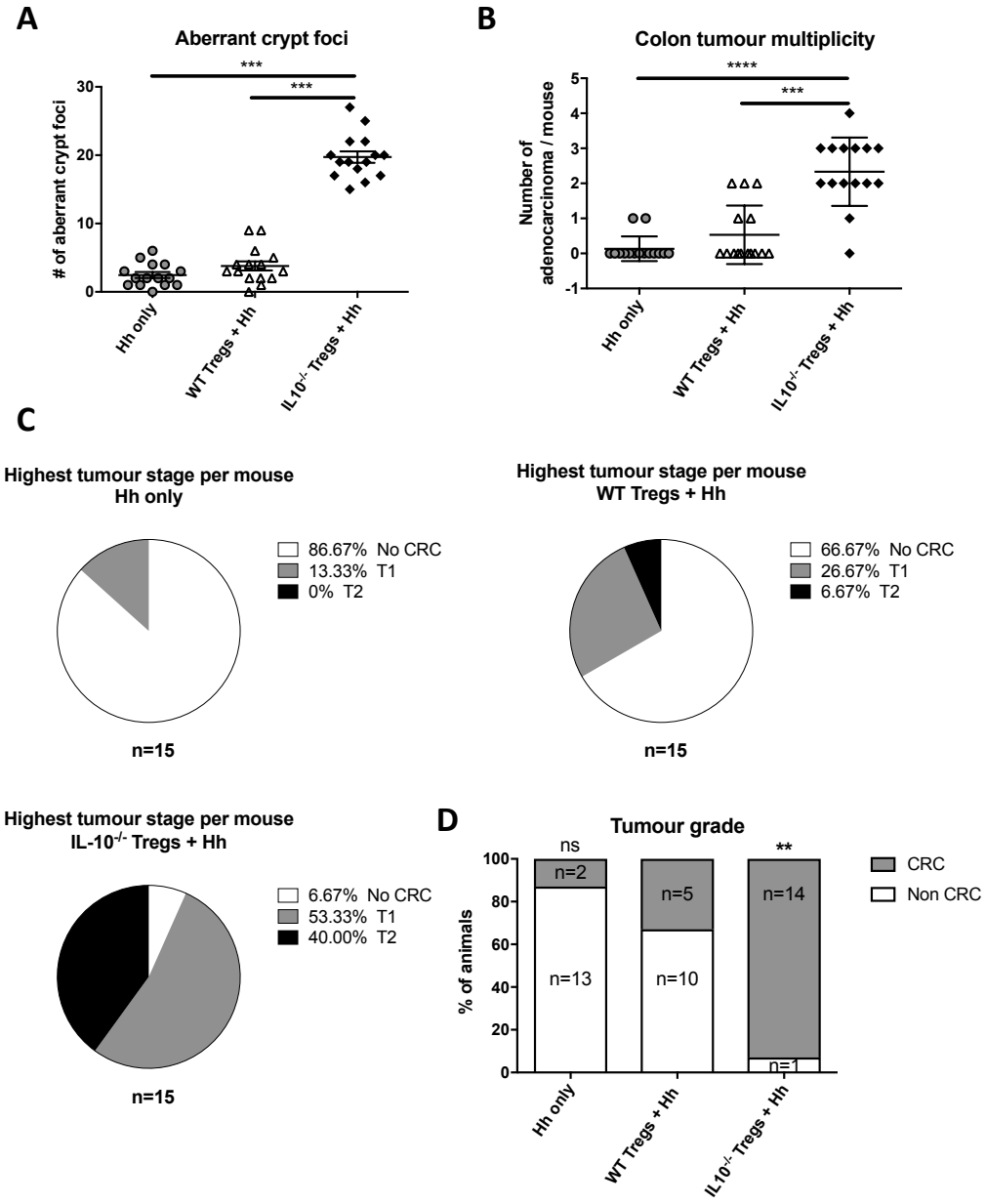

Figure 3.3: IL-10$^{-/-}$ Tregs + *Hh* group is associated with increased tumourigenesis

129.RAG$^{-/-}$ mice were infected with *Hh* or were injected with WT or IL-10$^{-/-}$ Tregs, prior to *Hh* infection. At week 12, mice were sacrificed and colons were taken for histology.

(A) Number of aberrant crypt foci per mouse and across groups, using methylene blue staining on whole colons.
(B) Number of adenocarcinoma per mouse across groups.
(C) Pie chart showing the distribution of adenocarcinoma stages across groups. When multiple tumours are found, the highest tumour stage per mouse is displayed.
(D) Percentage of mice developing colonic tumours across groups.

Bars represent mean ±SEM. Data represents pooled results from three independent experiments (n=15 for each group), performed at the JR facility site.
Statistical significance was determined using (A, B) a Kruskal-Wallis one-way analysis of variance, followed by a Dunn's post-hoc test and (D) a Fisher's exact test with WT Treg + *Hh* group as control (two sided). ** $p \leq 0.01$, *** $p \leq 0.001$.

In summary, we have successfully established this colitis-associated cancer mouse model in the lab. Within three months, mice quickly progress to tumourigenesis, which makes this model valuable as its kinetics are accelerated compared to *H. hepaticus*-driven cancer. Moreover, while chemically induced cancer models cause tumours that resemble polyps and are not invasive, this mouse model enables the study of immune responses associated with aggressive colonic adenocarcinomas and thus may more accurately reflect invasive human colorectal cancer. Finally, this model relies on the injection of IL-10$^{-/-}$ Tregs to drive tumourigenesis, providing us with the opportunity to identify new mechanisms by which lack of adequate T cell regulation in the gut can drive formation of colon adenocarcinomas.

3.2.2 Splenic IL-10$^{-/-}$ Tregs upregulate Rorγt while WT Tregs display a Gata3 phenotype

Next, we investigated whether this accelerated model of colitis-associated cancer driven by a microbial insult involved a dysregulated repair response caused by the IL-10$^{-/-}$ Tregs. To address this question, the phenotype of splenic WT and IL-10$^{-/-}$ Tregs was first analysed at steady state by gene expression and flow cytometry.

First, splenic WT Tregs, IL-10$^{-/-}$ Tregs and IL-10$^{-/-}$ CD4^{+} T cells were FACS sorted from donor mice. Foxp3 intracellular staining of the sorted population of live, CD45^{+}, TCRβ^{+}, CD4^{+}, CD45BR^{low} CD25^{high} (Tregs) before transfer showed that roughly 95-97% of the cells expressed Foxp3 when using non-Foxp3 reporter strains, indicating a relatively high purity (data not shown, Chapter 2). Moreover, when using 129.Foxp3^{GFP} mice as donors, purity levels reached 98-99%.

RNA was extracted and samples analysed for repair signature gene expression, along with other standard Treg markers. *Foxp3* expression was first assessed as a control and showed that both FACS sorted WT and IL-$10^{-/-}$ Tregs samples were enriched in *Foxp3* transcripts (**Figure 3.4 A**). Only two genes were differentially upregulated in IL-$10^{-/-}$ vs WT Tregs: *Tgfb* (**Figure 3.4 B**) and *Areg* (**Figure 3.4 C**) amongst 30 targets in our gene expression screen. Moreover, both transcripts were also upregulated in IL-$10^{-/-}$ Tregs compared to IL-$10^{-/-}$ CD4 T effector cells.

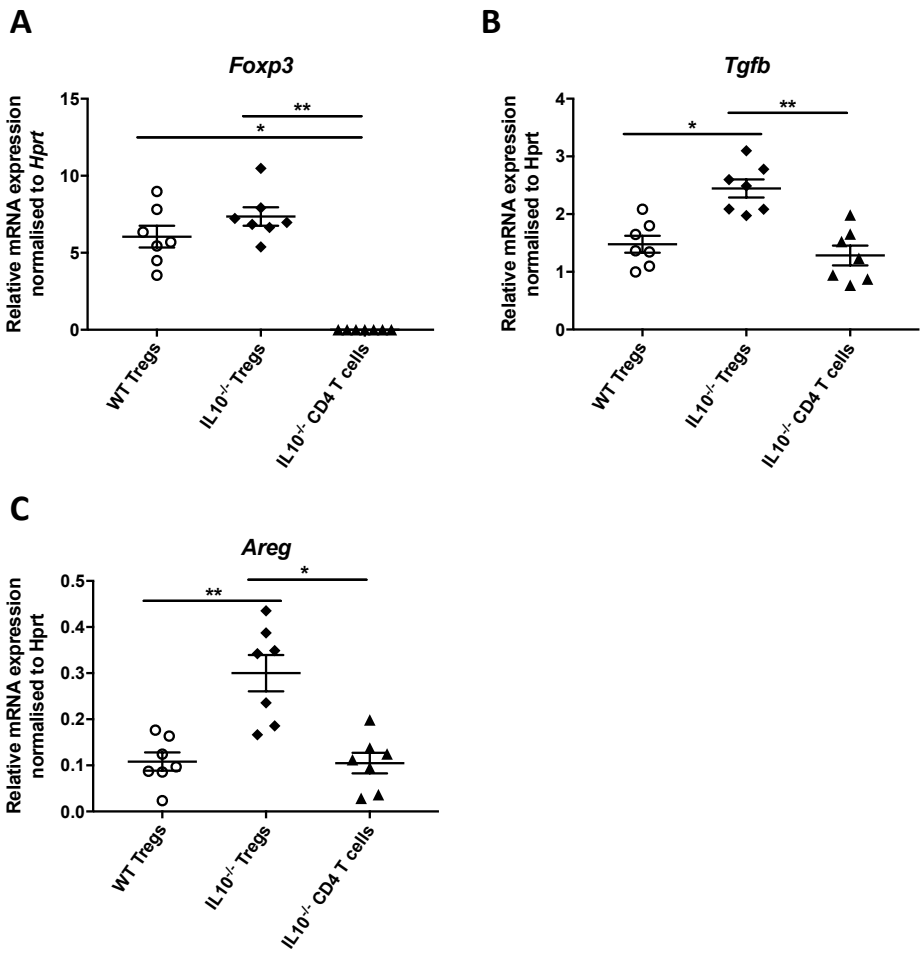

Figure 3.4: Splenic IL-10$^{-/-}$ Tregs upregulate *Tgfb* and *Areg* at the transcriptional level

129.WT and 129.IL-10$^{-/-}$ mice were sacrificed and splenic single cell suspension prepared for FACS staining and sorting. Tregs were identified as live, CD45^{+}, TCRβ^{+}, CD4^{+}, CD45BR^{low} CD25^{high}, while T cells were FACS sorted based on live, CD45^{+}, TCRβ^{+}, CD4^{+}, CD45BR^{low} CD25^{low}. RNA was extracted and gene expression was assessed by qPCR and normalised to the housekeeping gene *Hprt*.

(A B C) mRNA expression of *Foxp3*, *Tgfb1* and *Areg* for indicated cell populations. The assay was run in technical duplicates.

Each dot represents a single mouse and bars represent mean ±SEM. Data is representative of 3 independent experiments performed at the JR facility site.
Statistical significance was determined using a Kruskal-Wallis one-way analysis of variance, followed by a Dunn's post-hoc test. * $p \leq 0.05$, ** $p \leq 0.01$, *** $p \leq 0.001$.

To further investigate differences between WT and IL-10$^{-/-}$ Tregs, total splenocytes were analysed by flow cytometry. Of note, as TGF-β and other related markers are relatively challenging to stain for, and as Areg antibodies did not perform well, flow cytometry analyses for these cytokines are missing. Nonetheless, the expression of key transcription factors, as well as proliferation, was assessed. First, the Foxp3 frequency among the CD4^{+} T cell population was higher in 129.IL-10$^{-/-}$ mice compared to WT animals (**Figure 3.5 A, left**). Interestingly, the geometric mean fluorescence intensity (gMFI) of Foxp3 was significantly increased in WT Tregs (**Figure 3.5 A middle, right**), which has generally been associated with the increased potential of Tregs to produce regulatory cytokines and suppress effector T cell activation (Chauhan et al., 2009). Most WT Tregs stained positive for Helios (**Figure 3.5 B**), suggesting that this population mainly derives from tTregs. By contrast, IL-10$^{-/-}$ Tregs showed a mixed phenotype, as roughly 50% of Tregs expressed Helios, indicating that this population contains both tTregs and pTregs. A completely different transcription factor profile was uncovered between WT and IL-10$^{-/-}$ Tregs. Indeed, IL-10$^{-/-}$ Tregs showed increased frequency of Rorγt^{+} Tregs, while approximately 60% of WT Tregs stained for Gata3 (**Figure 3.5 C, E**). Furthermore, Gata3^{+} WT Tregs also expressed Helios and ST2, a component of the IL-33-R (data not shown). Of note, T-bet expression was not detected in splenic Tregs (**Figure 3.5 F**, representative plots). Proliferation assessment by Ki67 staining revealed increased MFI in IL-10$^{-/-}$ Tregs (**Figure 3.5 D**), as well as increased frequency of Ki67^{+} IL-10$^{-/-}$ Tregs compared to WT (**Figure 3.5 F**, representative plots). Finally, overall activation markers of Tregs, such as CD103, KLRG1, CD25, CTLA-4, CD44 and ICOS, tended to be slightly increased in WT Tregs (data not shown).

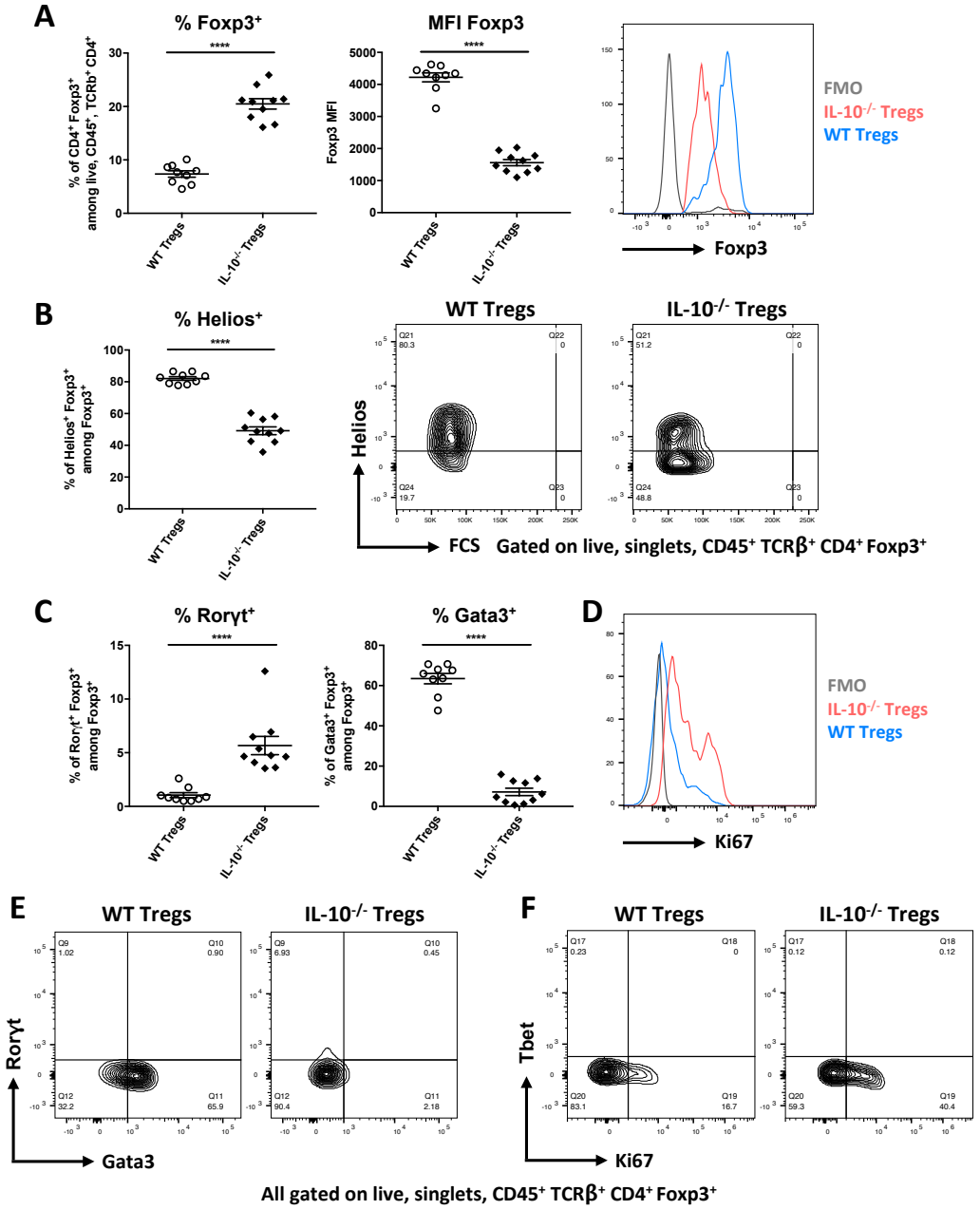

Figure 3.5: Splenic WT and IL-10$^{-/-}$ Tregs have a distinct transcriptional factor profile

129.WT and 129.IL-10$^{-/-}$ mice were sacrificed at week 8-10 of age, spleens were harvested and single cell suspensions were analysed by flow cytometry.

(A) Frequency (left panel) of Foxp3^{+} cells amongst CD4^{+} T cells, and geometric mean of fluorescence (gMFI) of Foxp3 expression amongst Foxp3+ T cells (middle panel and right panel for representative plots), reprensenting the level of expression of Foxp3 in regulatory T cells.

(B) Frequency of Helios^{+} Tregs (left) and representative plots in splenic WT and IL-10$^{-/-}$ Foxp3^{+} Tregs.

(C) Frequency of Rorγt^{+} (left), Gata3^{+} (right) Tregs in splenic WT and IL-10$^{-/-}$ Tregs.

(D) Representative histogram depicting Ki67 gMFI in FMO control (grey), WT Tregs (blue) and IL-10$^{-/-}$ Tregs (red).

(E) Representative plots for Rorγt and Gata3 in WT and IL-10$^{-/-}$ splenic Tregs.

(F) Representative plots for T-bet and Ki67 in WT and IL-10$^{-/-}$ splenic Tregs.

Each dot represents a single mouse and bars represent mean ±SEM. Data is representative of 2 independent experiments performed at the JR facility site.

Statistical significance was determined using a Mann Whitney U Test. * $p \leq 0.05$, ** $p \leq 0.01$, *** $p \leq 0.001$, **** $p \leq 0.0001$.

Collectively, these results highlight that there exist differences between splenic WT and IL-10$^{-/-}$ Tregs at time of transfer. WT Tregs represent a "classical" tTreg population Helios^{+}, primarily expressing Gata3 and high levels of Foxp3. By contrast, IL-10$^{-/-}$ Tregs are characterised by a lack of expression of transcription factors and contain a mixed population of highly proliferative tTregs and pTregs. Notably, there is an increased proportion of IL-10$^{-/-}$ Tregs expressing Rorγt, compared to WT Tregs, albeit of small frequency. Furthermore, RNA expression analysis revealed that IL-10$^{-/-}$ Tregs upregulate *Tgfb* and *Areg*.

3.2.3 At week 12, two distinct populations of T cells are found in the colon and IL-10$^{-/-}$ transferred cells are mainly T-bet positive.

Next, we assessed the fate of Treg cells transferred *in vivo*. 12 weeks following Treg transfer, mice were sacrificed and the percentage of Foxp3^{+} cells determined.

Upon initial observation, it appeared that at week 12, two distinct populations of CD4 T cells were found in the colon: CD4^{+} Foxp3^{+} Tregs as well as CD4^{+} Foxp3^{-} CD4 T cells (**Figure 3.6 A**). These populations were found both in the WT Tregs + *Hh* and IL-10$^{-/-}$ Tregs + *Hh* groups, with a similar frequency (on average 50%). Of note, while the gMFI Foxp3 was increased in splenic WT Tregs, no difference was found at week 12 in colonic Foxp3^{+} Tregs.

We first explored colonic T cell proliferation as well as the expression of main transcription factors. Ki67 staining on Foxp3^{+} cells revealed that IL-10$^{-/-}$ Tregs had increased proliferation compared to WT Tregs (**Figure 3.6 B**), similarly to splenic IL-10$^{-/-}$ Tregs. In addition, CD44 staining was significantly increased in colonic IL-10$^{-/-}$

Tregs, further highlighting their activation state (**Figure 3.6 C**). Interestingly, while the frequency of splenic Rorγt^{+} IL-10$^{-/-}$ Tregs was increased, there was a similar amount of colonic Rorγt^{+} Tregs in WT and IL-10$^{-/-}$ cells (**Figure 3.6 D, left**). Likewise splenic WT Tregs, an increased percentage of Foxp3^{+} cells were also Gata3^{+} in WT compared to IL10$^{-/-}$ colonic Tregs (**Figure 3.6 D, right**). Finally, T-bet staining revealed that colonic IL-10$^{-/-}$ Tregs were enriched in T-bet^{+} cells (**Figure 3.6 E, F**).

Similar analyses were performed on the CD4^{+} Foxp3^{-} colonic populations. Both WT and IL-10$^{-/-}$ CD4^{+} T cells displayed similar frequencies of Ki67^{+} cells (**Figure 3.7 A**). Transcription factor profiling revealed that Rorγt^{+} (**Figure 3.7 B**) and Gata3^{+} (**Figure 3.7 C**) CD4^{+} T cells frequencies were similar across groups. However, as seen in the colonic IL-10$^{-/-}$ Treg population, IL-10$^{-/-}$ CD4^{+} T cells showed significantly increased T-bet^{+} cells (**Figure 3.7 D**).

Foxp3 positive and negative cells also infiltrated the spleen. However, there was no difference between groups (data not shown).

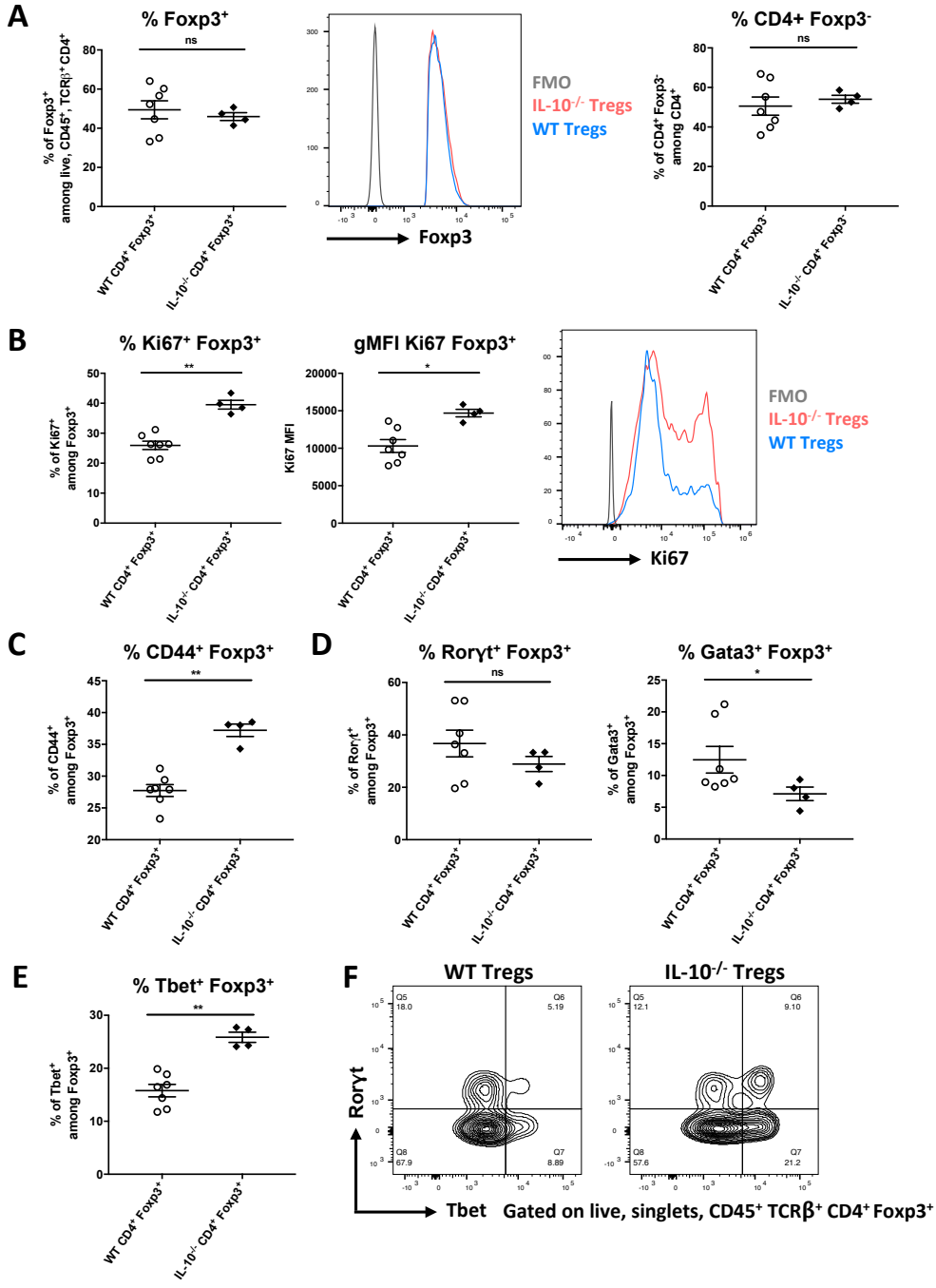

Figure 3.6: Colonic IL-10$^{-/-}$ Tregs display increased proliferation and are T-bet positive

WT Tregs + *Hh* and IL-10$^{-/-}$ Tregs + *Hh* recipients were sacrificed at week 12 of the model. Colons were harvested, and single cell suspensions were analysed by flow cytometry.

(A) Frequency of Foxp3^{+} cells (left), gMFI of Foxp3 (right, representative plots) and frequency of CD4^{+} Foxp3^{-} cells in the colon.
(B) Frequency of Ki67^{+} Tregs (left), gMFI of Ki67 (middle) with representative plots (right).
(C) Frequency of CD44^{+} colonic WT and IL-10$^{-/-}$ Tregs.
(D) Frequency of Rorγt^{+} (left) and Gata3^{+} (right) in WT and IL-10$^{-/-}$ colonic Tregs.
(E) Frequency of T-bet^{+} WT and IL-10$^{-/-}$ colonic Tregs, with representative plots in (F).

Each dot represents a single mouse and bars represent mean ±SEM. Data is representative of 2 independent experiments performed at the JR facility site.
Statistical significance was determined using a Mann Whitney U Test. * $p \leq 0.05$, ** $p \leq 0.01$.

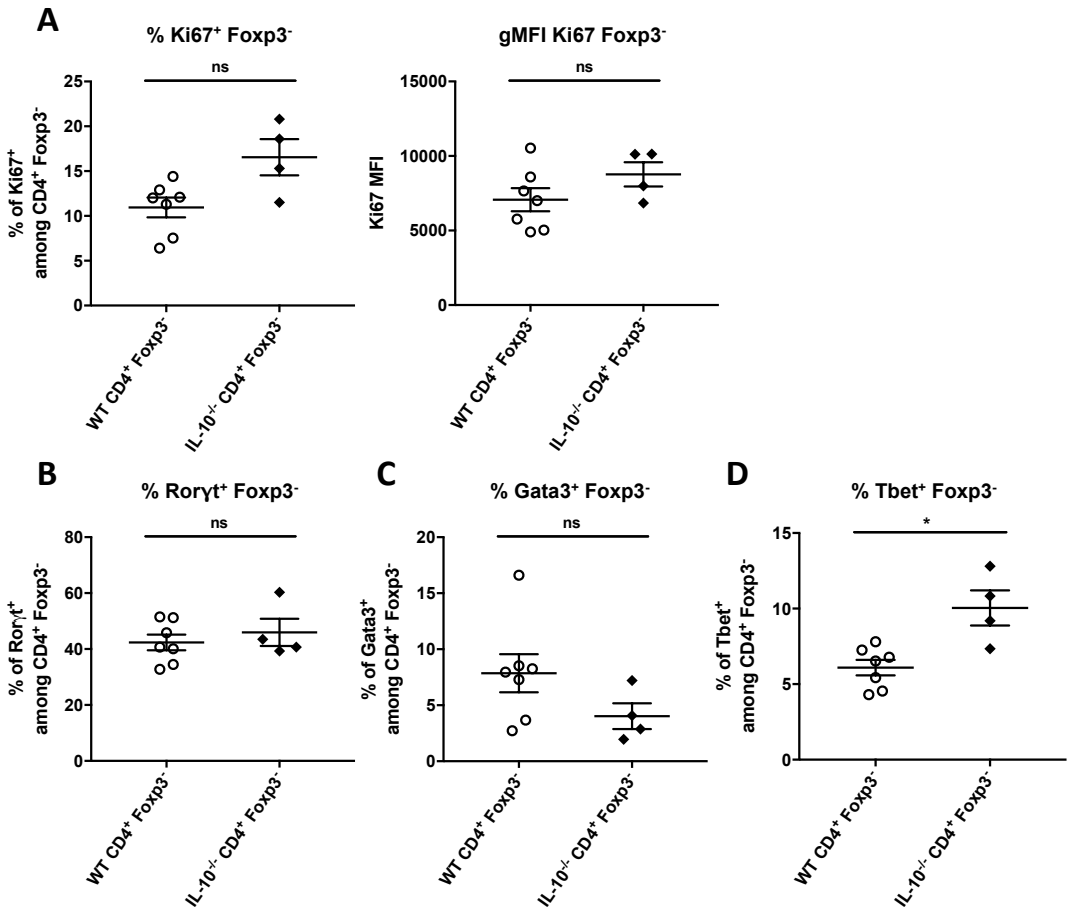

Figure 3.7: Colonic IL-10$^{-/-}$ CD4^{+} T cells are Rorγt and T-bet positive

WT Tregs + *Hh* and IL-10$^{-/-}$ Tregs + *Hh* recipients were sacrificed at week 12 of the model. Colons were harvested, and single cell suspensions were analysed by flow cytometry.

(A) Frequency of Ki67^{+} Tregs (left), gMFI of Ki67 (right) in colonic CD4^{+} Foxp3^{-} cells.
(B) Frequency of Rorγt^{+} colonic WT and IL-10$^{-/-}$ CD4^{+} T cells.
(C) Frequency of Gata3^{+} colonic WT and IL-10$^{-/-}$ CD4^{+} T cells.
(D) Frequency of T-bet^{+} colonic WT and IL-10$^{-/-}$ CD4^{+} T cells.

Each dot represents a single mouse and bars represent mean ±SEM. Data is representative of 2 independent experiments performed at the JR facility site.
Statistical significance was determined using a Mann Whitney U Test. * $p \leq 0.05$.

Total cell number of Foxp3^{+} cells was also quantified prior to cytokine phenotyping and revealed that both WT and IL-10$^{-/-}$ cells accumulated to a similar extent in the colon (**Figure 3.8 A**). We next assessed cytokine production. Both populations of colonic T cells produced inflammatory cytokines, such as IL-17A and IFNγ (**Figure 3.8 B, C, right**), and similar production was detected in Tregs, albeit to a lesser extent

(**Figure 3.8 B, C, left**), mirroring transcription factor expression. In addition, Tregs and CD4$^+$ effector cells did not express IL-22 at week 12 (**Figure 3.8 D**).

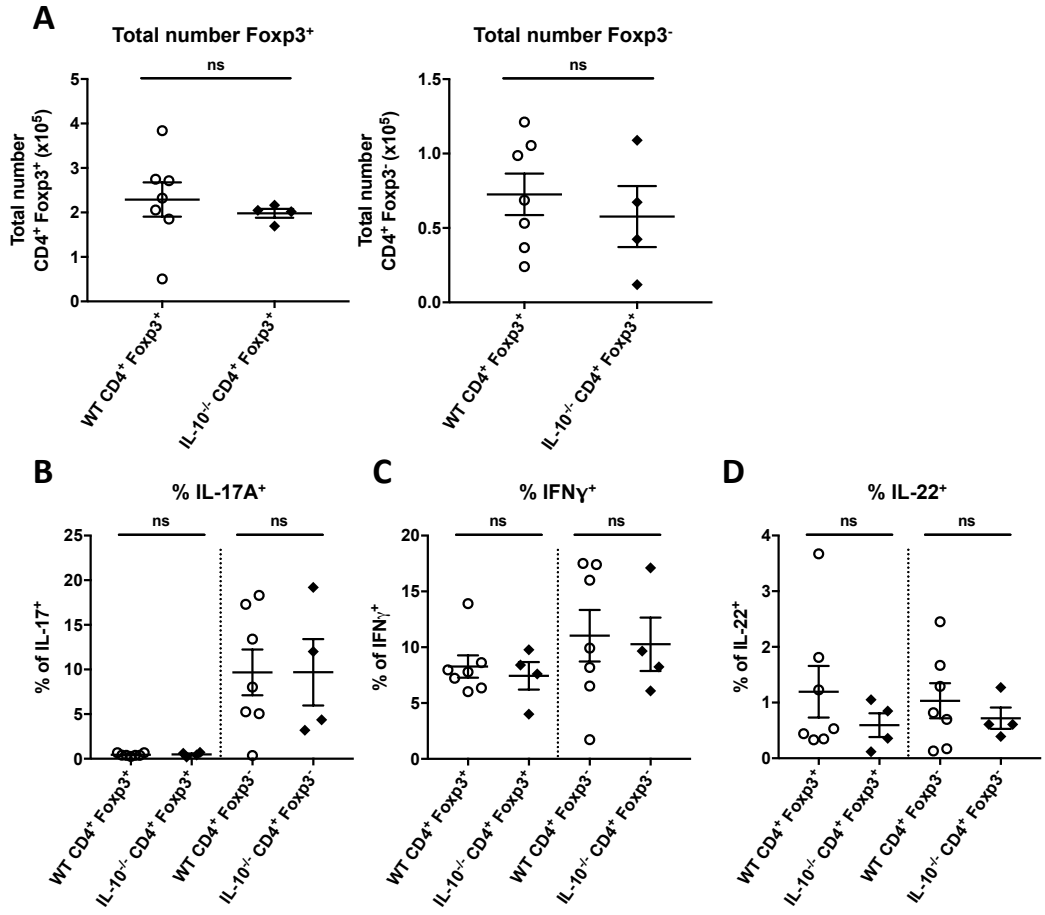

Figure 3.8: Cytokine production by colonic Foxp3$^+$ and CD4$^+$ T cells is not different across groups.

WT Tregs + *Hh* and IL-10$^{-/-}$ Tregs + *Hh* recipients were sacrificed at week 12 of the model. Colons were harvested, and single cell suspensions were analysed by flow cytometry.

(A) Total number of colonic Foxp3$^+$ (left) and CD4$^+$ Foxp3$^-$ (right) in WT and IL-10$^{-/-}$ cells.
(B) Frequency of IL-17A$^+$ Foxp3$^+$ and CD4$^+$ T cell in WT and IL-10$^{-/-}$ cells.
(C) Frequency of IFNγ$^+$ Foxp3$^+$ and CD4$^+$ T cell in WT and IL-10$^{-/-}$ cells.
(D) Frequency of IL-22$^+$ Foxp3$^+$ and CD4$^+$ T cell in WT and IL-10$^{-/-}$ cells.

Each point represents a single mouse and bars represent mean ±SEM. Data represents one experiment representative of 2 independent experiments performed at the JR facility site. Statistical significance was determined using a Mann Whitney U Test. No significant differences were found between groups.

Overall, no clear differences in cytokine production were uncovered by flow cytometry. In this setting, WT Tregs would thus be able to control colonic inflammation, while IL-10$^{-/-}$ Tregs might either be impaired in their regulatory properties or may promote disease via another pathway.

Once in the peritoneal cavity, splenic Tregs populate different tissues and are recruited in the cecum and colon following *H. hepaticus* colonisation (**Figure 3.9 A**). At week 12, given that both Tregs and CD4^{+} T effector cells are present, we investigated how quickly the population of CD4^{+} Foxp3^{-} cells arose in the colon. Three mice per group were sacrificed at different time points: week 4, week 8 and week 12. Representative FACS plots (**Figure 3.9 B**) for CD4 and Foxp3 expression are shown for the IL-10$^{-/-}$ + *Hh* group across time, highlighting the appearance of a non-Foxp3^{+} population as early as week 4. A summary of Foxp3^{+} Tregs percentage amongst total CD4^{+} cells across time highlights the gradual loss of frequency of Tregs, to a similar extent between both groups (**Figure 3.9 C**). Interestingly, after 12 weeks, only 50% of total CD4^{+} T cells expressed Foxp3.

Both WT and IL-10$^{-/-}$ Treg injection into recipients gave rise to a similar frequency of non-Foxp3 CD4^{+} effector populations and they accumulated to the same extent in the colon. Hence, we hypothesised that non-Foxp3 cells could arise from either a contamination during FACS sort, leading to a preferential expansion of non-Treg cells over time, or from the Treg population itself, which can lose Foxp3 expression under certain inflammatory conditions (Komatsu et al., 2013; Oldenhove et al., 2009; Zhou et al., 2009).

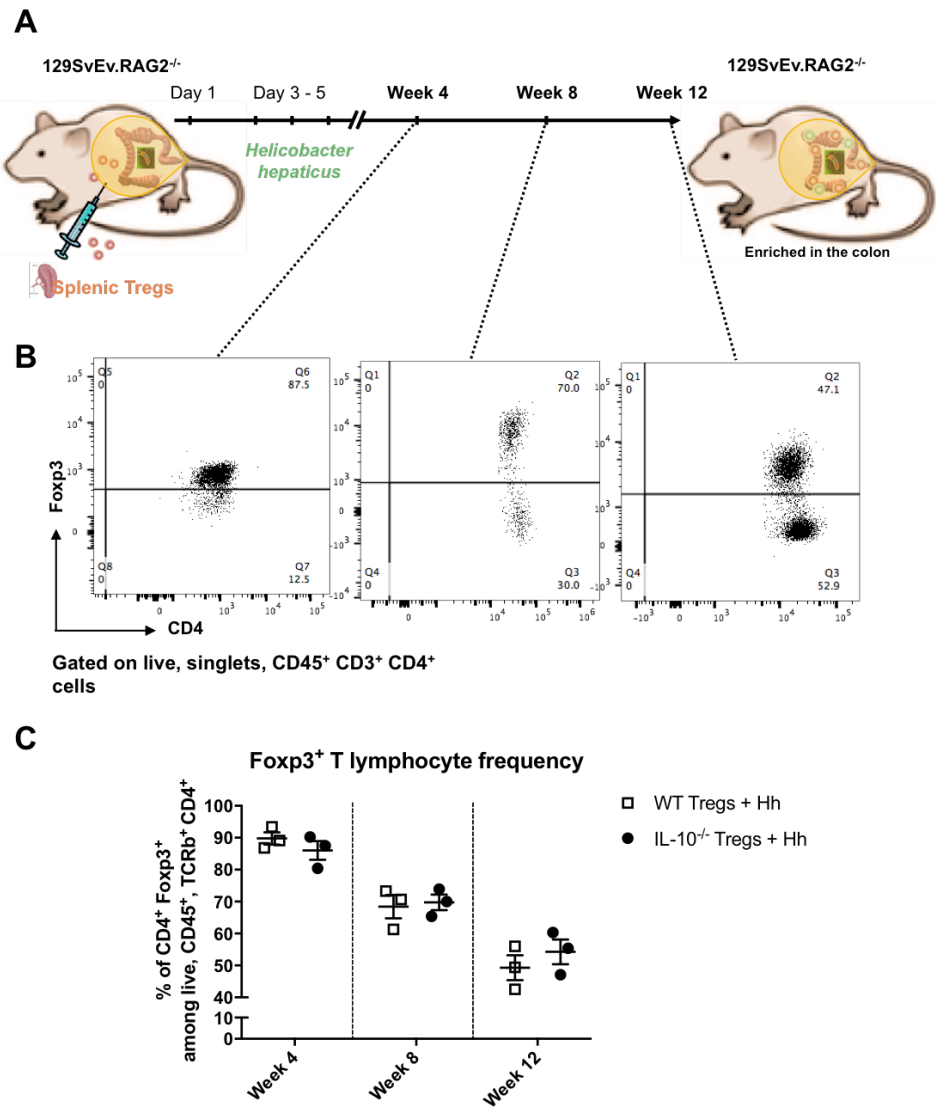

Figure 3.9: After transfer of splenic WT or IL-10$^{-/-}$ Tregs, the frequency of non-Foxp3 cells increases over time.

(A) Scheme of Regulatory T cell fate in the model. Cells are FACS sorted from donor spleens and injected intraperitoneally into 129.RAG$^{-/-}$ recipients. After *H. hepaticus* infection, cells are recruited to the colon and cecum where two populations of CD4 T cells are found as early as week 4.

(B) Representative FACS plots of CD4 versus Foxp3 gate at different time points (IL-10$^{-/-}$ Tregs + *Hh* group). Cells were gated on live, singlet, CD45^{+}, TCRβ^{+} and CD4^{+}.

(C) Summary of colonic CD4^{+} Foxp3^{+} frequency across time, comparing WT and IL-10$^{-/-}$ Tregs.

Bars represent mean ±SEM. Data represents one experiment (n=3 per group and per time point), performed at the Kennedy facility site.

3.2.4 IL-10$^{-/-}$ Regulatory T cells, rather than IL-10$^{-/-}$ CD4^{+} T cells, promote tumourigenesis

Provided that both Foxp3-expressing and non-expressing cells are found in the colon, we sought to explore whether the non-Foxp3 expressing T cell population may be involved in disease progression.

As previously described, three months after transfer, only 40 to 60% of CD4^{+} T cells still expressed Foxp3. Whether the rest of the CD4^{+} Foxp3^{-} T cells found within the colon arose from a contaminating population or originate from unstable Foxp3^{+} cells remains unclear. The definitive way to answer this question is to use a cell fate reporter system. However, in the absence of such a tool, we adopted a FACS sorting strategy to assess the tumourigenic capability of potential contaminating T cell fractions, using splenic CD4^{+} T cells from the reporter strain 129.IL-10$^{-/-}$.Foxp3^{GFP}.

Briefly, live, CD45^{+}, TCRβ^{+}, CD4^{+} cells were selected, and then utilising GFP, CD25 and CD45RB expression, 4 cell populations were identified (**Figure 3.10 B**). The population of T cells in the lower left corner, expressing CD4^{+}, CD25^{low} and CD45RB^{high}, corresponded to naïve T cells and was not used. The three other populations were FACS-sorted (**Figure 3.10 B**). The first population (red) corresponded to activated and memory T cells (GFP^{low}, CD25^{high}). The second population was GFP^{+} and CD25^{high}, which represented classical regulatory T cells (green). The last population was positive for GFP expression but lacked expression of CD25 (blue). If the phenotype seen in the IL-10$^{-/-}$ Tregs + *Hh* group was due to contaminating cells during the FACS sort, we hypothesised that this contamination might arise from the red and blue populations, as these cells would not be excluded when using a non-reporter system. Each of these populations was transferred into

129.RAG$^{-/-}$ recipient mice (**Figure 3.10 A**). Weight loss was monitored throughout the experiment (**Figure 3.10 C**) and was stable for all groups except for the activated/memory T cell group (red). This group developed a wasting disease, similar to that of IBD T cell transfer mouse model (Powrie et al., 1993). After 11 weeks, mice were sacrificed, and colons were assessed for histological signs of colitis. As shown in **Figure 3.10 D**, the majority of mice had highly inflamed colons, with overall scores ranging from 8 to 12 across groups. Mice receiving activated/memory T cells (red) displayed significantly more severe colitis compared to *Hh* only controls and the classical Treg group (green). By contrast, the highest frequency of tumours (100%, 5 out of 5 mice) developed in mice transferred with GFP^{+} CD25^{high} Treg cells (**Figure 3.10 E**). The two other experimental groups displayed tumours in only 40% of cases. Furthermore, T1 and T2 tumours were solely found in the GFP^{+} CD25^{high} Tregs group (**Figure 3.10 F**), further indicating that IL-10$^{-/-}$ Tregs might exacerbate tumour development.

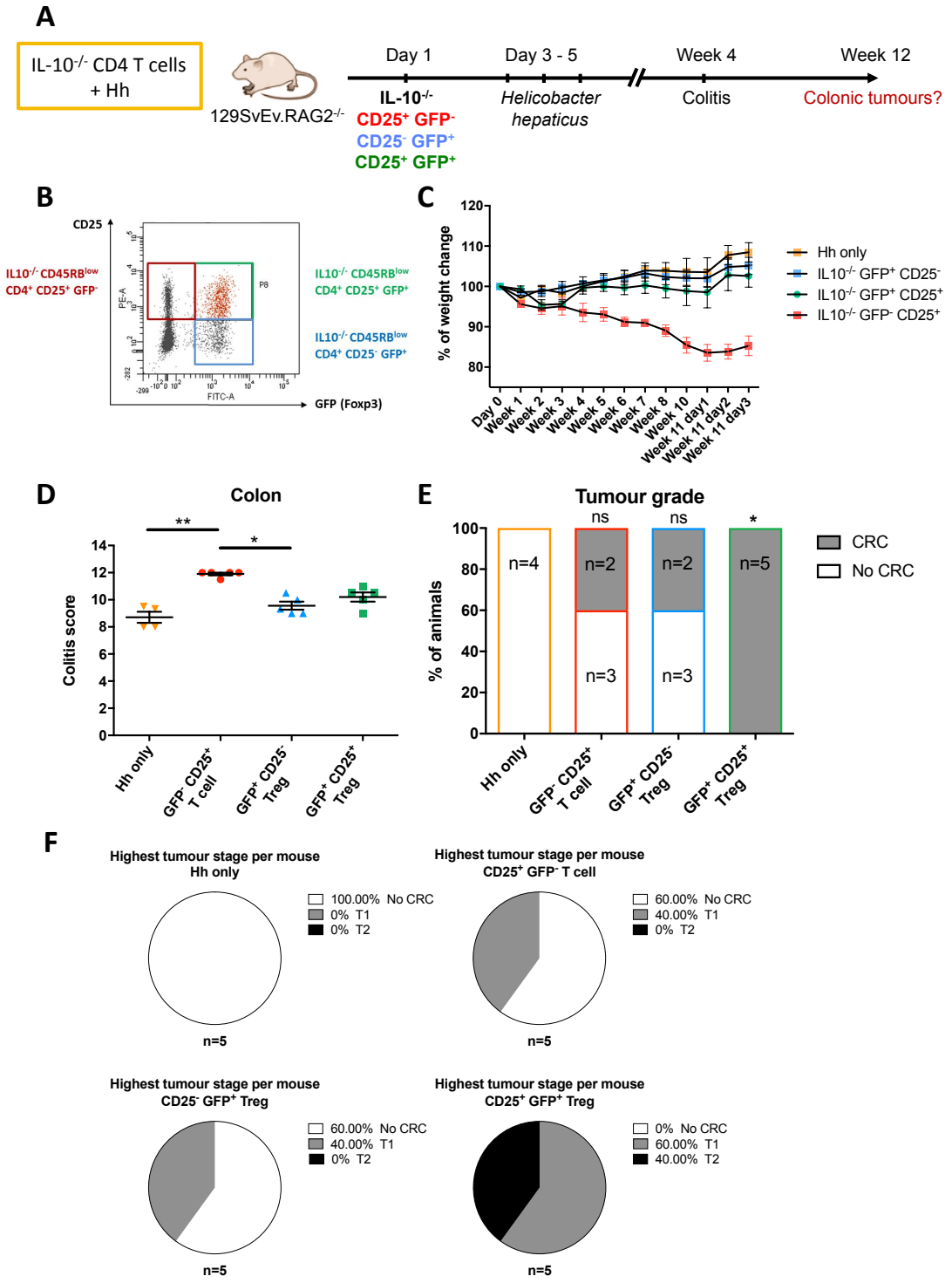

Figure 3.10: IL-10$^{-/-}$ CD25^{high} Foxp3^{GFP} Tregs may preferentially promote tumourigenesis

(A) Scheme of the experiment. 129.RAG$^{-/-}$ mice were injected with one of the indicated CD4 T cell population prior to *H. hepaticus* infection.
(B) Representative FACS plot of splenic IL-10$^{-/-}$.Foxp3^{GFP} CD4 T cell populations.
(C) Percentage of weight loss over time compared to starting weight (100%).
(D) Histological analysis of colonic inflammation.
(E) Percentage of mice developing colonic tumours across groups.
(F) Pie chart showing the distribution of adenocarcinoma stages across groups. When multiple tumours are found, the highest tumour stage per mouse is displayed.

Each dot represents a mouse and bars represent mean ±SEM. Data represents results from one experiment, performed at the JR facility site.
Statistical significance was determined using (A, B) a Kruskal-Wallis one-way analysis of variance, followed by a Dunn's post-hoc test and (D) a Fisher's exact test with *Hh* only group as control (two-sided). * $p \leq 0.05$, ** $p \leq 0.01$.

Due to health concerns, the mouse strain 129.IL-$10^{-/-}$.Foxp3^{GFP} was challenging to maintain, and a different approach was taken to further confirm our preliminary findings. Thus, using a similar experimental set-up as previously reported, we injected either splenic Tregs or splenic $CD4^+$ T effector lymphocytes, both from 129.IL-$10^{-/-}$ donors (**Figure 3.11 A**). Colonic inflammation was first analysed (**Figure 3.11 B**), showing that mice receiving IL-$10^{-/-}$ $CD4^+$ T effector cells developed as much colitis as the IL-$10^{-/-}$ Tregs + *Hh* recipients. However, analysis of tumour burden uncovered a significantly different outcome comparing the two groups. Indeed, 30% of the IL-$10^{-/-}$ $CD4^+$ T cell + *Hh* group developed tumours, compared to 90% of the mice in the IL-$10^{-/-}$ Tregs + *Hh* group (**Figure 3.11 C**). Furthermore, while T2 adenocarcinomas arose approximately 40% of the IL-$10^{-/-}$ Tregs + *Hh* mice, only T1 tumours were found when IL-$10^{-/-}$ $CD4^+$ cells were transferred into recipients, mirroring the WT Tregs + *Hh* group (**Figure 3.11 D**).

This experiment also highlighted a key role for IL-$10^{-/-}$ Tregs in promoting tumour development, as despite similar inflammation, tumours were more frequent following IL-$10^{-/-}$ Treg transfer, as opposed to transfer of effector $CD4^+$ T cells. Thus, in the event of a cell contaminant during FACS sorting, we speculate that the impact of this population is unlikely to drive tumourigenesis and disease would rather occur through the Treg population. However, provided that the non-Foxp3 population seen in the colon arises from the transferred Treg population itself, it remains unknown whether this population is involved in disease progression.

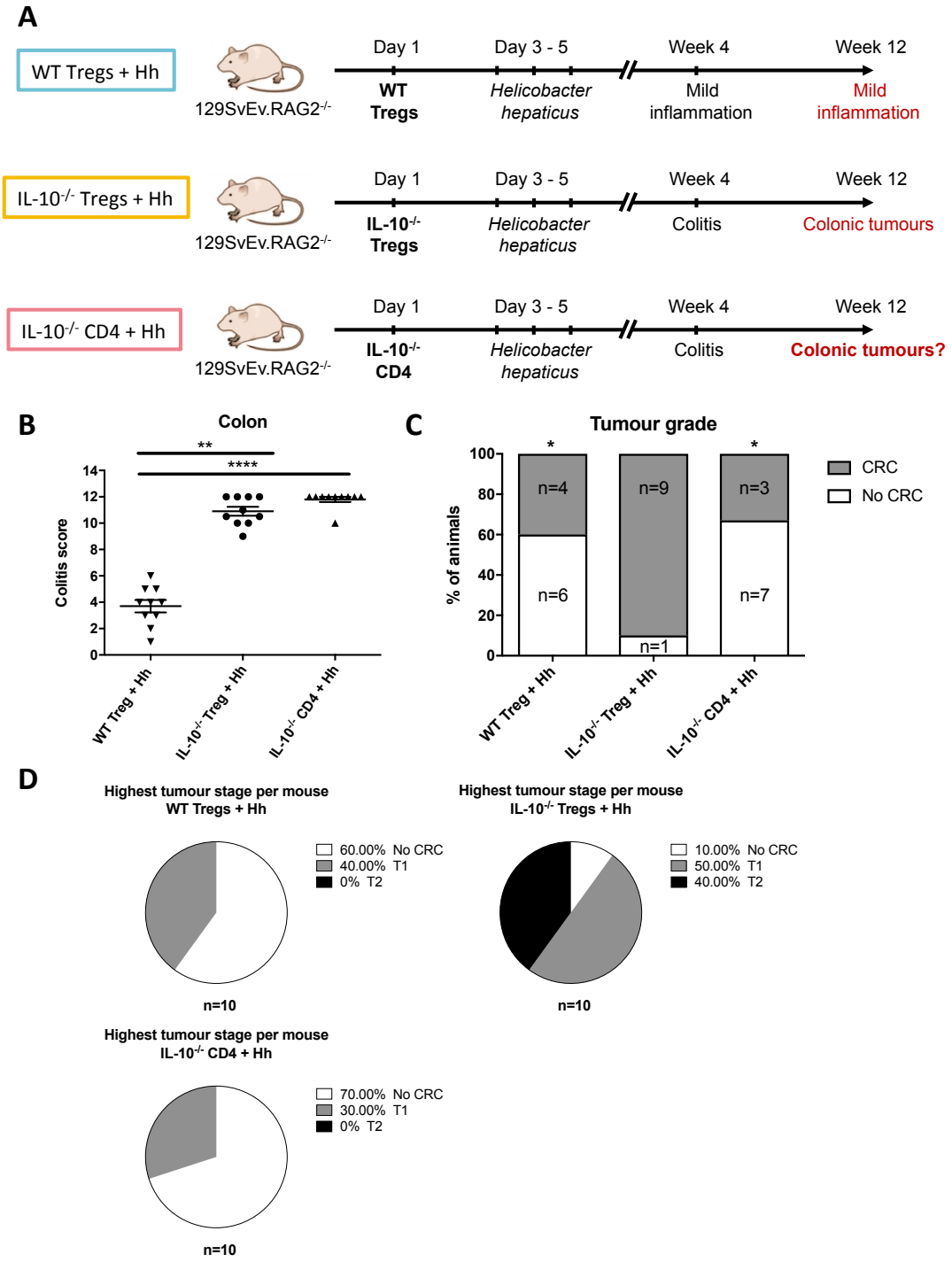

Figure 3.11: IL-10$^{-/-}$ Tregs, rather than IL-10$^{-/-}$ CD4^{+} T effector cells, promote tumourigenesis

(A) Scheme of the experiment. 129.RAG$^{-/-}$ mice were injected with either of the indicated CD4^{+} T cell populations prior to *H. hepaticus* infection.
(B) Colitis scores across groups assessed by H&E staining.
(C) Percentage of mice developing colonic tumours across groups.
(D) Pie chart showing the distribution of adenocarcinoma stages across groups. When multiple tumours are found, the highest tumour stage per mouse is displayed.

Each dot represents a mouse and bars represent mean ±SEM. Data represents one experiment (n=10 mice for each group), performed at the JR facility site.

Statistical significance was determined using (A) a Kruskal-Wallis one-way analysis of variance, followed by a Dunn's post-hoc test and (B) a Fisher's exact test with IL-10$^{-/-}$ Tregs + *Hh* group as control (two-sided). * $p \leq 0.05$, ** $p \leq 0.01$, *** $p \leq 0.001$, **** $p \leq 0.0001$.

Collectively, these results further confirm that transfer of IL-10 deficient regulatory T cells, together with a microbial insult, leads to the formation of invasive adenocarcinomas. Although the exact identity of the cells that drive tumourigenesis is not known, our study shows that transfer of IL-10$^{-/-}$ Tregs, rather than IL-10 deficient memory/activated CD4^{+} T cell population, promotes CRC. Finally, the fact that mice receiving IL-10 deficient CD4^{+} T cells do not progress to disease despite the lack of Treg-mediated immune regulation strongly suggests that in tumour-bearing mice, beyond a defect in their immunosuppressive functions, Tregs may promote tumourigenesis by employing a different mechanism.

3.2.5 RNA sequencing of splenic and colonic IL-10$^{-/-}$ Tregs revealed expression of a newly described cytokine, Meteorin-like

To provide further insights into how IL-10$^{-/-}$ Tregs drive tumourigenesis, we performed RNA sequencing to identify differences between IL-10$^{-/-}$ and WT Tregs.

Splenic WT and IL-10$^{-/-}$ Tregs were FACS sorted, and a total of 5 biological replicates per group was selected for downstream processing (**Figure 3.12 A**). 129.RAG$^{-/-}$ recipients were injected and infected with *Hh* as previously described. After 12 weeks, mice were sacrificed, and colons were taken for LPL preparation. After single cell resuspension, samples were stained for FACS sorting. As previously described, two populations of CD4^{+} T cell were detected: CD45RB^{low} CD25^{high} and CD25^{low}, and both populations were FACS sorted individually. A total of 5 biological replicates for CD25^{high} and CD25^{low} populations were chosen for downstream analysis in the WT

Tregs + *Hh* group, while 4 biological replicates were selected for the IL-$10^{-/-}$ Tregs + *Hh* group (**Figure 3.12 A**). Whole RNA was extracted from all FACS sorted samples and bio-analyser control quality revealed overall low RNA concentration in various specimens (Appendix 1). We confirmed that the $CD25^{high}$ fraction was enriched in Foxp3 transcripts from 2 samples with a low RIN but higher RNA concentration, which were not used for sequencing (data not shown). This result indicated that sequencing these populations independently might provide further insights as to their respective identity.

RNA sequencing with low-input (SMARTer kit) was thus performed at the Wellcome Trust Centre for Human Genetics sequencing facility. Three core questions were examined (**Figure 3.12 B**). First we questioned whether the splenic IL-$10^{-/-}$ Treg population may have upregulated or downregulated pathways due to lack of IL-10 production, which may be involved in disease progression. We also sought to confirm the elevated *Areg* expression we previously observed in IL-$10^{-/-}$ Tregs (**Figure 3.4 C**). The second and third question related to the colonic T lymphocyte populations. Once Tregs progress to colonising the colon, we hypothesise that they acquire a classical "gut tissue resident" cell signature. Direct comparison of colonic Treg populations may reveal upregulated or downregulated pathways that could be associated with disease progression or maintenance. Furthermore, direct comparison of colonic WT and IL-$10^{-/-}$ CD25 negative T cells will shed light on their identity and may help to understand their role in disease development.

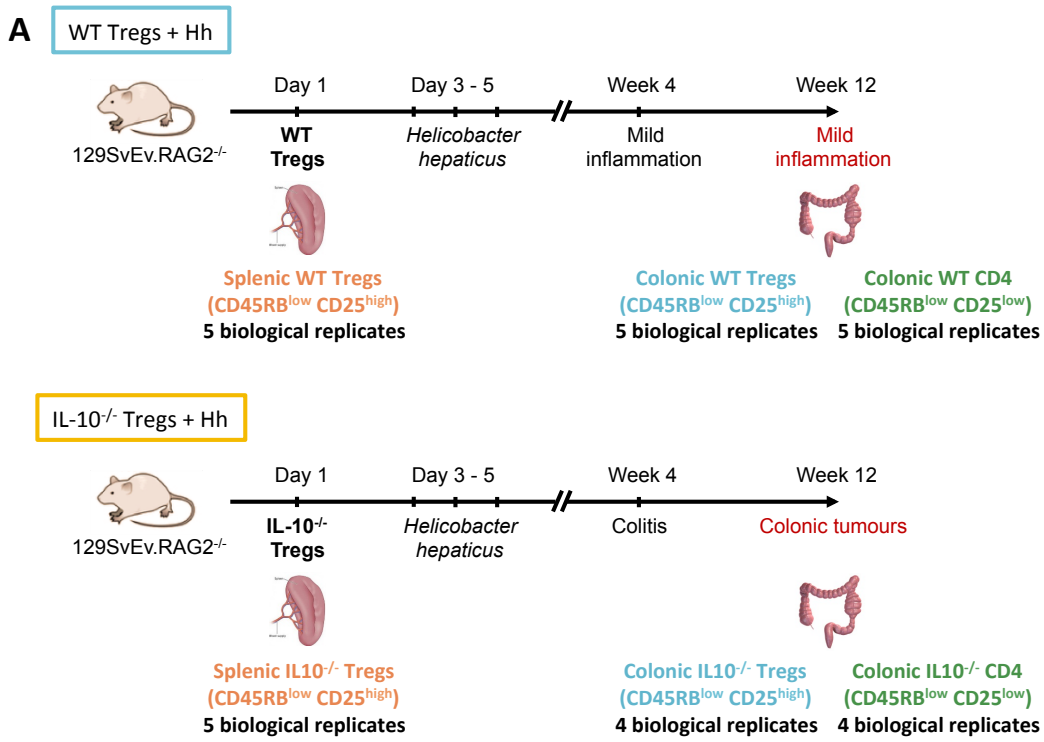

B

Questions to answer	Comparison
What is the expression profile of splenic WT and IL-10$^{-/-}$ Tregs?	Splenic WT/IL-10$^{-/-}$ Tregs (CD45RB^{low} CD25^{high})
Are colonic WT and IL-10$^{-/-}$ Tregs different?	Colonic WT/IL-10$^{-/-}$ Tregs (CD45RB^{low} CD25^{high})
Are colonic WT and IL-10$^{-/-}$ T cells different?	Colonic WT/IL-10$^{-/-}$ CD4 (CD45RB^{low} CD25^{low})

Figure 3.12: RNA sequencing strategy to unravel disease-specific pathways in IL-10$^{-/-}$ T cells.

(A) Scheme of the experimental groups and FACS sorted populations used for RNA sequencing. Splenic live, singlet, CD45^{+} TCRβ^{+} CD4^{+} CD45RB^{low} CD25^{high} WT and IL-10$^{-/-}$ Treg samples were FACS sorted individually. One population of pooled splenocytes was injected into 129.RAG$^{-/-}$ mice, prior to *H.hepaticus* infection. After 12 weeks, mice were sacrificed, and colonic single cell suspensions were prepared. Both WT and IL-10$^{-/-}$ live, singlet, CD45^{+} TCRβ^{+} CD4^{+} CD45RB^{low} CD25^{high} (Tregs) and live, singlet, CD45^{+} TCRβ^{+} CD4^{+} CD45RB^{low} CD25^{low} (T cells) were FACS sorted.

(B) Core questions assessed using RNA sequencing. Direct comparison of WT versus IL-10$^{-/-}$ populations might reveal differentially regulated pathways involved in disease development and maintenance.

For the WT samples, a total of 5 biological replicates from splenic Tregs, 5 biological replicates from colonic Tregs and 5 biological replicates from colonic T cells were chosen for sequencing. For the IL-10$^{-/-}$ samples, a total of 5 biological replicates from splenic Tregs, 4 biological replicates from colonic Tregs and 4 biological replicates from colonic T cells were chosen for sequencing.

First, initial unsupervised hierarchical clustering analysis of all RNA-sequenced samples was performed and revealed that the tissue type – spleen versus colon – drives the greatest gene expression differences overall, as all the splenic and colonic samples clustered separately (**Figure 3.13 A**). This observation was further confirmed by performing principal component analysis (PCA), in which the tissue type was the predominant mode of variation, as seen in the first principal component (PC1) (**Figure 3.13 B**). Moreover, PC1 was the component with the largest possible variance in the dataset, as shown by the Scree Plot (**Figure 3.13 C**). The second principal component (PC2) segregated colonic T cells versus colonic Tregs, with one exception. Interestingly, it was nearly impossible to further separate the samples based on following components, as PC3 versus PC4 and PC5 versus PC6 failed to show any further clustering of the samples (**Figure 3.13 C, D**). This indicates that the populations, amongst each tissue type, may not be profoundly different.

Overall, these analyses suggest that the majority of the transcriptional changes may be caused by the migration of the cells to the colon, which may relate to changes in the microenvironment. The fact that splenic and colonic Tregs do not further cluster depending on the genotype suggests that minimal transcriptional genes were discovered.

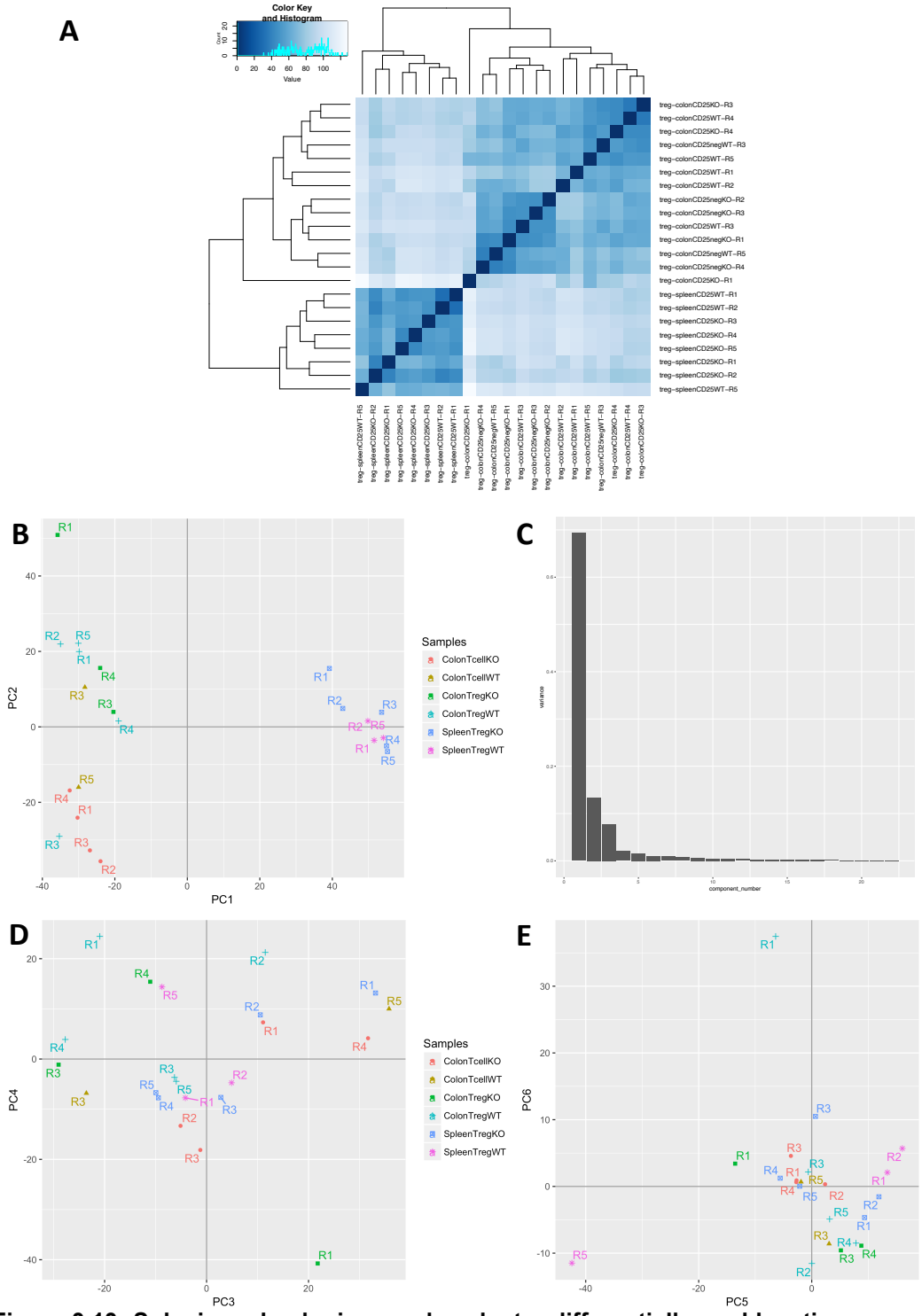

Figure 3.13: Splenic and colonic samples cluster differentially, and location represents the greatest gene expression difference.

(A) Unsupervised hierarchical clustering analysis using correlation distance metrics of all samples.

(B) Principal component analysis (PCA) on all samples (n=22) in dataset. 1st principal component (PC1) separates splenic versus colonic samples. 2nd principal component (PC2) tend to separate colonic T cells versus colonic Tregs (PC = principal component).

(C) Scree plot of all principal components, showing that PC1 represents the greatest gene expression difference amongst samples.

(D) PC3 versus PC4 on all samples (n=22), showing no further clustering of samples.

(E) PC5 versus PC6 on all samples (n=22), showing no further clustering of samples.

We also performed PCA on either splenic or colonic population separately, to remove the effect from the tissue type and potentially uncover differential clustering. **Figure 3.14 A** displays the first 4 principal components for splenic samples only, while **Figure 3.14 B** relates to the colonic samples. Except for PC3 (**Figure 3.14 A middle**), which clustered samples according to the genotype of the Tregs, the other different PCs showed that no other clustering could be detected. Interestingly, there may be a trend towards a clustering between colonic Tregs and T cells, as seen on PC1 (**Figure 3.14 B left**). Finally, no further clustering could be detected for the colonic samples by analysing other PCs. However, it is difficult to formally assess clustering of the different samples as only a few samples of WT T cells were used for this analysis, due to contamination of the other samples. Overall, these results suggest that the RNA sequencing may have revealed only a few differences in gene expression.

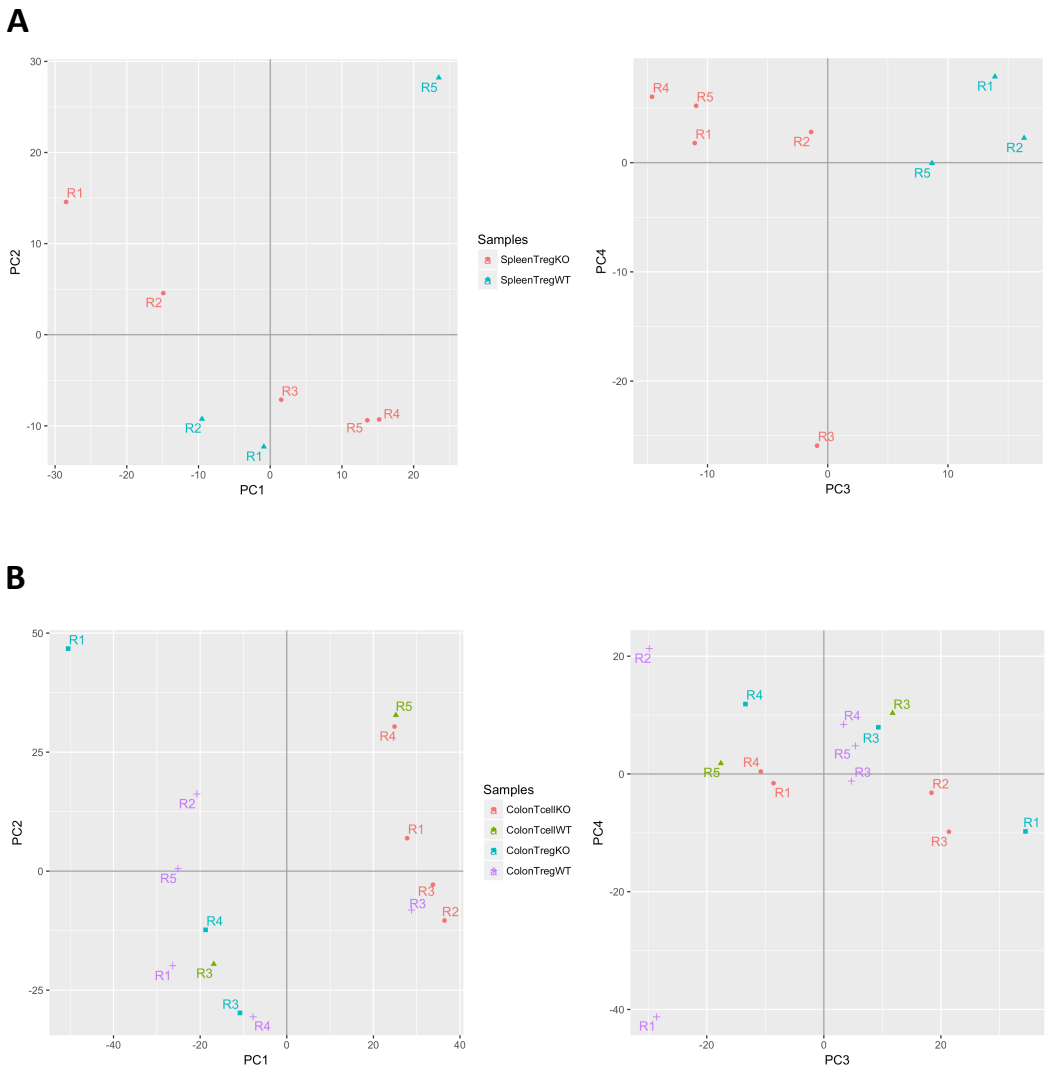

Figure 3.14: Principal component analysis of splenic and colonic samples taken separately does not reveal further clustering.

(A) Principal component analysis (PCA) on splenic samples only (n=8) in dataset. 3rd principal component (PC3) tend to separate WT versus KO Tregs. No other specific clustering is detected.

(B) Principal component analysis (PCA) on colonic samples only (n=14) in dataset. 1st principal component (PC1) tend to separate T cells versus Tregs, regardless of the genotype. No other specific clustering is detected.

3.2.5.1 A transcriptomic analysis of splenic WT and IL-10$^{-/-}$ Tregs

Next, to identify transcriptional changes at baseline, simple differential expression analysis comparing splenic WT Tregs to IL-10$^{-/-}$ Tregs was performed (**Figure 3.15**). This analysis was performed to identify critical pathways that are linked to lack of immune regulation or that promote inflammation at an early stage in the model. A volcano plot was generated in order to visualise broad differences in gene expression between splenic WT and IL-10$^{-/-}$. Significantly (adjusted *p* value ≤0.05) downregulated or upregulated genes are indicated in orange (**Figure 3.15 A**). Two vertical lines indicate a two-fold downregulation (log2 fold change=-1) and upregulation (log2 fold change=1) in the WT vs IL-10$^{-/-}$ Tregs. 19 genes were found to be downregulated in splenic IL-10$^{-/-}$ compared to WT Tregs (**Figure 3.15 B**), while 14 genes were upregulated in splenic IL-10$^{-/-}$ Tregs (**Figure 3.15 C**).

Questions to answer	Comparison
What is the expression profile of splenic WT and IL-10$^{-/-}$ Tregs?	Splenic WT/IL-10$^{-/-}$ Tregs (CD45RB^{low} CD25^{high})

A

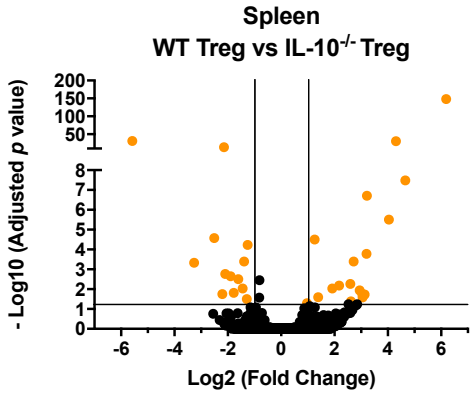

B

Fold Change (log2)	Adjusted *p* Value	Gene Name
6.186	7.07E-149	Tpm3-rs7
4.656	3.33E-08	Tubb3
4.307	4.12E-31	Gm10036
4.038	3.09E-06	Vangl1
3.213	1.95E-07	Gm9726
3.197	0.000166686	Fxyd2
3.127	0.018405359	Akr1c12
3.052	0.025821009	Srl
3.037	0.017501387	Mal2
2.941	0.011573691	Rgs4
2.914	0.040170759	Eepd1
2.717	0.00040677	Cacnb3
2.616	0.041048909	Sestd1
2.595	0.005498374	Ncald
2.176	0.006540654	Nebl
1.918	0.009325122	Nr4a2
1.388	0.025443161	Ldhb
1.26	3.17E-05	Zfp330
0.99	0.050033212	Lrrc8d

C

Fold Change (log2)	Adjusted p Value	Gene Name
-5.584	4.90E-32	Dynlt1b
-3.265	0.000466794	Fbxo41
-3.029	6.61E-09	Slc41a3
-2.507	2.65E-05	Metrnl
-2.207	0.017817765	Ptpn3
-2.142	2.91E-14	Dynlt1c
-2.098	0.001722852	Tlr1
-1.896	0.002244919	Il10
-1.774	0.015384622	Ccdc38
-1.603	0.003118912	Lilrb4a
-1.445	0.009342187	Abcb1a
-1.392	0.00040677	Tmem181a
-1.291	0.031425265	Serpina3g
-1.256	5.88E-05	Tpm3

Figure 3.15: Comparison of splenic WT and IL-10$^{-/-}$ Tregs.

Differential expression analysis comparing splenic WT and IL-10$^{-/-}$ Tregs was performed using the generalised linear model of the Deseq2 R package. WT Tregs n=3, IL-10$^{-/-}$ Tregs n=5.

(A) Volcano plot representing the top differentially expressed genes in orange (log2FC > 2, FDR < 0.05). Positive fold change corresponds to upregulated genes in WT Tregs while negative fold change relates to upregulated genes IL-10$^{-/-}$ Tregs.

(B, C) List of top differentially upregulated genes in (B) splenic WT Tregs and in (C) splenic IL-10$^{-/-}$ Tregs.

3.2.5.1.1 An exploration of genes upregulated in splenic WT Tregs

Several genes found to be upregulated in splenic WT Tregs compared to IL-10$^{-/-}$ Tregs have no function described or lack characterisation in immune populations. For instance, *Tpm3-rs7* (tropomyosin 3, related sequence 7), the top upregulated gene in splenic WT Tregs, is an uncharacterised protein that has potential functions in actin binding and filament organisation. The second top upregualted gene, *Tubb3*, is an isotype of beta-tubulin that has been described in various cell types, but its precise function in non-neuronal cells is unknown. Other poorly characterised genes and their potential function are listed in **Appendix 1** (A Treg Tale).

Certain genes that are upregulated have more defined functions. For example, *Rgs4* (regulator of G-protein signaling 4) encodes RGS4, expressed constitutively in the highest amounts in the brain and heart in both humans and mice. Genetic deletion of Rgs4 in mice results in cardiovascular abnormalities including conduction defects in the heart and a propensity for development of arrhythmias. Rgs4 deficient mice also have altered pain responses and tolerance to opioid analgesics and antidepressants. However, detailed analysis of RGS4 expression and function in leukocyte subsets has not been performed nor have prominent immune system abnormalities been reported in mice deficient in RGS4 (reviewed in Xie et al., 2015).

Lactate dehydrogenase (LDH) is a tetrameric enzyme that has two forms: LDHA, also known as the M subunit, is predominantly found in skeletal muscle, and LDHB (encoded by *Ldhb*), known as the H subunit, is predominantly found in the heart. While LDHA subunit has a higher affinity for pyruvate, thereby preferentially

converting pyruvate to lactate and NADH, the LDHB subunit possesses a higher affinity for lactate, thus preferentially converting lactate to pyruvate and NAD^+ to NADH (Valvona et al., 2015). The only study of *Lhdb* in lymphocytes explored the differential expression of the two isoforms and their dependency on cell activation state. Indeed, in resting T lymphocytes, the H-type LDH was mainly expressed, while in activated T cells, both H- and M-type LDHs were co-expressed (Pan et al., 1991).

Nr4a2 (Nuclear receptor subfamily 4, group A, member 2) deficient Tregs are prone to lose Foxp3 expression and have attenuated suppressive ability both *in vitro* and *in vivo*. Specifically, Nr4a2 binds to regulatory regions of Foxp3, where it mediates permissive histone modifications. Overall, Nr4a2 has the ability to maintain T-cell homoeostasis by regulating induction, maintenance and suppressor functions of Tregs, but also by repression of aberrant Th1 induction (Sekiya et al., 2011).

3.2.5.1.2 Splenic IL-$10^{-/-}$ Tregs upregulate *Tlr1* and *Metrnl*

Similar to their WT counterparts, a few genes that are upregulated in IL-10 deficient Tregs are poorly described and have no reported function. For example, the top upregulated gene in splenic IL-$10^{-/-}$ Tregs, *Dynlt1b,* together with *Dynlt1c* (Dynein light chain Tctex-type 1B and 1C) encode for a dynein light chain that is known to bind to various cellular and viral proteins, and can function both as a molecular clamp and as a microtubule-cargo adapter. No further functions have been described in the context of immune cells. Details of other poorly described targets are listed in **Appendix 1** (A Treg Tale).

One well-characterised gene upregulated in IL-10$^{-/-}$ Tregs is *Tlr1*. TLR1 is a member of the toll-like receptor family (TLR) of pattern recognition receptors. TLR1 recognises pathogen-associated molecular pattern with a specificity for gram-positive bacteria, and acts in concert with TLR2 to recognise bacterial triacyl lipopeptides and peptidoglycans (Medzhitov, 2001). In the gut, TRL1 expression by epithelial cells is recognised as a first line defence to pathogen detection and management. A number of studies have examined the expression of TLRs 1–10 on various subsets of purified T cells. In two studies, sorted CD4^{+} CD45RB^{high} T cells from B6 mice were found to express Tlr1, 2, 3, 6, 7 and 8 at mRNA and protein levels (Caramalho et al., 2003; Tomita et al., 2008). Treg cells deficient in the TLR adaptor-transducer MyD88 are reduced in number in the gut, which leads to the onset of inflammatory bowel disease (IBD).

Two enzymes, *Ptpn3* and *Serpina3g* are upregulated in IL-10 deficient Tregs.

Ptpn3 (Protein tyrosine phosphatase, non-receptor type 3) and *Ptpn4* encode for protein tyrosine phosphatases (PTP), which have been implicated as negative-regulators of early signal transduction through the T cell antigen receptor (TCR), acting to dephosphorylate the TCRζ chain, a component of the TCR complex. However, a recent study has shown that PTPN3 and PTPN4 are dispensable for TCR signal transduction, and that deficient mice developed normally and showed normal cytokine secretion and proliferative responses to TCR stimulation (Bauler et al., 2008). No function has been reported in Tregs. *Serpina3g* (Serine (or cysteine) peptidase inhibitor, clade A, member 3G), also known as Spi2A, is an inhibitor of lysosomal executioner proteases dependent on transcription factor NF-kappaB. Its

expression promotes the survival of cytotoxic T lymphocytes, allowing them to differentiate into memory $CD8^+$ T cells (Liu et al., 2004). To date, no specific function in CD4 T cells has been reported.

Two cytokines were also found to be upregulated in IL-$10^{-/-}$ compared to WT Tregs. The first is *Il10*, and its upregulation is likely due to a compensatory mechanism for the lack of IL-10 protein production. The second cytokine is *Metrnl* (Meteorin-like, glial cell differentiation regulator-like), which was first described as highly expressed in both muscle and fat tissues (Rao et al., 2014).

Finally, *Abcb1a* (ATP-binding cassette, sub-family B (MDR/TAP), member 1A) was also upregulated. It is a member of the superfamily of ATP-binding cassette (ABC) transporters, also part of the sub-family MDR (multi-drug resistance) proteins. *Abcb1a*, also known as *mdr1a*, encodes for P-glycoprotein (Pgp), and has been linked to colitis susceptibility in mice, where deficient mice develop a spontaneous colitis as early as 3 to 4 months of age (Panwala et al., 1998). Moreover, a polymorphism in MDR1 has been associated with ulcerative colitis susceptibility (Annese, 2006). Pgp expression by T cells is well documented, however its function is still poorly characterised.

3.2.5.2 Transcriptomic analyses of colonic Treg populations

We then compared colonic WT Tregs to IL-$10^{-/-}$ Tregs, using similar parameters. As the samples were FACS sorted at week 12 of the model, this analysis could identify key pathways that are linked to disease development and perpetuation of pro-tumourigenic inflammatory responses. Indeed, tumours usually appear around week 9 in IL-$10^{-/-}$ Tregs + *Hh* mice. Overall, a total of 9 genes were upregulated in colonic

WT Tregs (**Figure 3.15 A, B**), while 11 genes were upregulated in IL-$10^{-/-}$ Tregs (**Figure 3.15 A**) (**Figure 3.15 A, C**).

Colonic WT and IL-$10^{-/-}$ $CD4^{+}$ T effector cells were also compared by differential expression analysis. However, as 3 samples in the WT T cell population were contaminated with epithelial transcripts, we are underpowered to analyse the dataset which is not included in this thesis.

3.2.5.2.1 Colonic WT Tregs

Several genes upregulated in splenic WT Tregs were also found in colonic WT Tregs: *Tpm3-rs7*, *Vangl1*, *Ldhb*, *Nebl*, *Zfp330*. Although no protein and function have been associated with *Gm10036* and *Gm9726*, these two genes were also similarly upregulated in colonic WT Tregs.

Lrat (lecithin-retinol acyltransferase) is upregulated in WT Tregs and functions as a protein palmitoyl transferase. Lrat is essential for the retinoid cycle in visual system and vitamin A status in liver. Expression of Lrat has not been reported in T cells.

3.2.5.2.2 Colonic IL-$10^{-/-}$ Tregs

Several genes upregulated in colonic IL-$10^{-/-}$ Tregs were also upregulated in splenic cells: *Dynlt1b*, *Dynlt1c*, *Fbxo41*, *Slc41a3* and *Tlr1*. Furthermore, like splenic Tregs, a few genes have no reported function and are poorly characterised and are described in Appendix 1.

Ccr3 (Chemokine (C-C motif) receptor 3) encodes for CCR3. Early studies have demonstrated in contact dermatitis, nasal polyp and ulcerative colitis tissue that

$CCR3^+$ T lymphocytes are recruited together with eosinophils. By contrast, $CCR3^+$ T lymphocytes were absent from tissues that lack eosinophils, as demonstrated for normal skin and rheumatoid arthritis synovium (Gerber et al., 1997). More recently, it was shown that CCR3 is involved in the steady state trafficking of $CD4^+$ T cells to the human upper airway mucosa (Danilova et al., 2014). In IBD, a higher fraction of peripheral T lymphocytes were found to be positive for CCR3 in patients with ulcerative colitis (UC) compared to Crohn's disease (CD), while almost no $CCR3^+$ T cells were found in normal controls (Manousou et al., 2010). This may represent a fraction of the colonic Treg pool recirculating in the periphery or associated with eosinophil influx.

Questions to answer	Comparison
Are colonic WT and IL-10$^{-/-}$ Tregs different?	Colonic WT/IL-10$^{-/-}$ Tregs ⟷ (CD45RB^{low} CD25^{high})

A

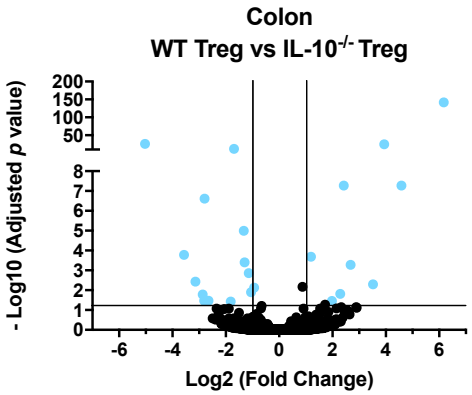

B

Fold Change (log2)	Adjusted *p* Value	Gene Name
6.175200466	2.84E-142	Tpm3-rs7
4.588368301	5.33E-08	Vangl1
3.936642397	1.58E-25	Gm10036
3.51849445	0.005110774	Lrat
2.678581918	0.000530038	Gm9726
2.422953981	5.33E-08	Ldhb
2.286958524	0.015176136	Tmod4
1.979518969	0.034453458	Nebl
1.193305751	0.000205882	Zfp330

C

Fold Change (log2)	Adjusted *p* Value	Gene Name
-5.028	1.11417E-26	Dynlt1b
-3.563	0.000165781	Fbxo41
-3.141	0.003712603	Ccr3
-2.863	0.016562551	Stra6
-2.813	0.033625355	Slc16a5
-2.797	2.41049E-07	Slc41a3
-2.651	0.033625355	Gprc5b
-1.813	0.037657049	Tlr1
-1.693	6.72394E-13	Crbn
-1.327	1.01121E-05	Trnt1
-1.295	0.000397731	Dynlt1c
-1.140	0.001383137	Fam189b
-1.051	0.012779221	Hnrnpu
-0.936	0.007395607	Pnrc2

Figure 3.16: Transcriptomic comparison of colonic WT versus IL-10$^{-/-}$ Tregs.

Differential expression analysis comparing colonic WT vs IL-10$^{-/-}$ Tregs was performed using the generalised linear model of the Deseq2 R package. WT Tregs n=5, IL-10$^{-/-}$ Tregs n=3.

(A) Volcano plot representing the top differentially expressed genes in blue (log2FC > 2, FDR < 0.05). Positive fold change corresponds to upregulated genes in WT cells, while negative fold change relates to upregulated genes IL-10$^{-/-}$ cells.

(B, C) List of top differentially upregulated genes in (B) WT Tregs, and (C) IL-10$^{-/-}$ Tregs.

3.2.5.3 A Treg tale: from the spleen to the colon

Finally, we explored the differences in gene expression between splenic and colonic cells for each genotype. Since all Tregs that are found in the colon originated from the splenic populations that were injected, we asked whether Tregs found in the colon would acquire certain genes associated with a colonic Treg gene signature, denoting their plasticity and adaption to environmental clues. A microarray analysis generated by the Powrie Lab explored gene expression differences between steady state Tregs from colons versus mesenteric lymph nodes (MLN) and allowed us to establish a colonic Treg (cTreg) gene signature (Schiering et al., 2014). In parallel, we performed differential expression analyses comparing respectively splenic versus colonic WT Tregs, and splenic versus colonic IL-10$^{-/-}$ Tregs. For the three datasets, we selected genes that were either up or downregulated and generated Venn diagrams that enabled us to identify genes at the intersection of the three groups (**Figure 3.17 A** upregulated genes, **Figure 3.17 B**, downregulated genes). A total of 71 upregulated genes and 152 downregulated genes were co-expressed in the three datasets. We retrieved the fold change values associated with these genes, both from the WT and IL-10$^{-/-}$ Tregs datasets, and graphed the fold change values associated with overall upregulated (**Figure 3.17 C**) and downregulated (**Figure 3.17 D**) genes. Several upregulated genes have been associated with a colonic and tissue-Treg phenotype, such as *Areg*, *Dgat1*, *Il10* and *Il1rl1*. Areg was upregulated in colonic WT and IL-10$^{-/-}$ Tregs, with an increased fold change in the KO population. Dgat1 encodes for Diacylglycerol O- Acyltransferase 1 (DGAT1), one of the two DGAT enzymes involved in mammalian triglyceride metabolism, and is important for lipid synthesis and storage (Harris et al., 2011). The role of IL-10 signalling in Tregs was shown to be

important for their survival and function (Chaudhry et al., 2011; Murai et al., 2009). As previously mentioned, Il10 transcripts were detected in both WT and IL-10$^{-/-}$ cells, likely produced as a compensatory mechanism related to the lack of protein production in the IL-10$^{-/-}$ cells. *Il1rl1*, encoding for ST2, promotes Treg function and adaptation to the inflammatory environment (Schiering et al., 2014).

This analysis suggests that splenic Tregs injected into 129.RAG recipients have acquired a variety of classical tissue-Treg markers by week 12 in the colon. A more detailed analysis is provided in Appendix 1.

Collectively, our RNA sequencing analyses have allowed us to discover a variety of differentially expressed genes between WT and KO populations. However, the majority of upregulated genes were poorly characterised and with unknown functions in lymphocytes. Interestingly however, splenic IL-10$^{-/-}$ Tregs display increased transcripts for *Tlr1* and *Meteorin-like*, which is a newly described cytokine. Further studies are required to test their functional relevance.

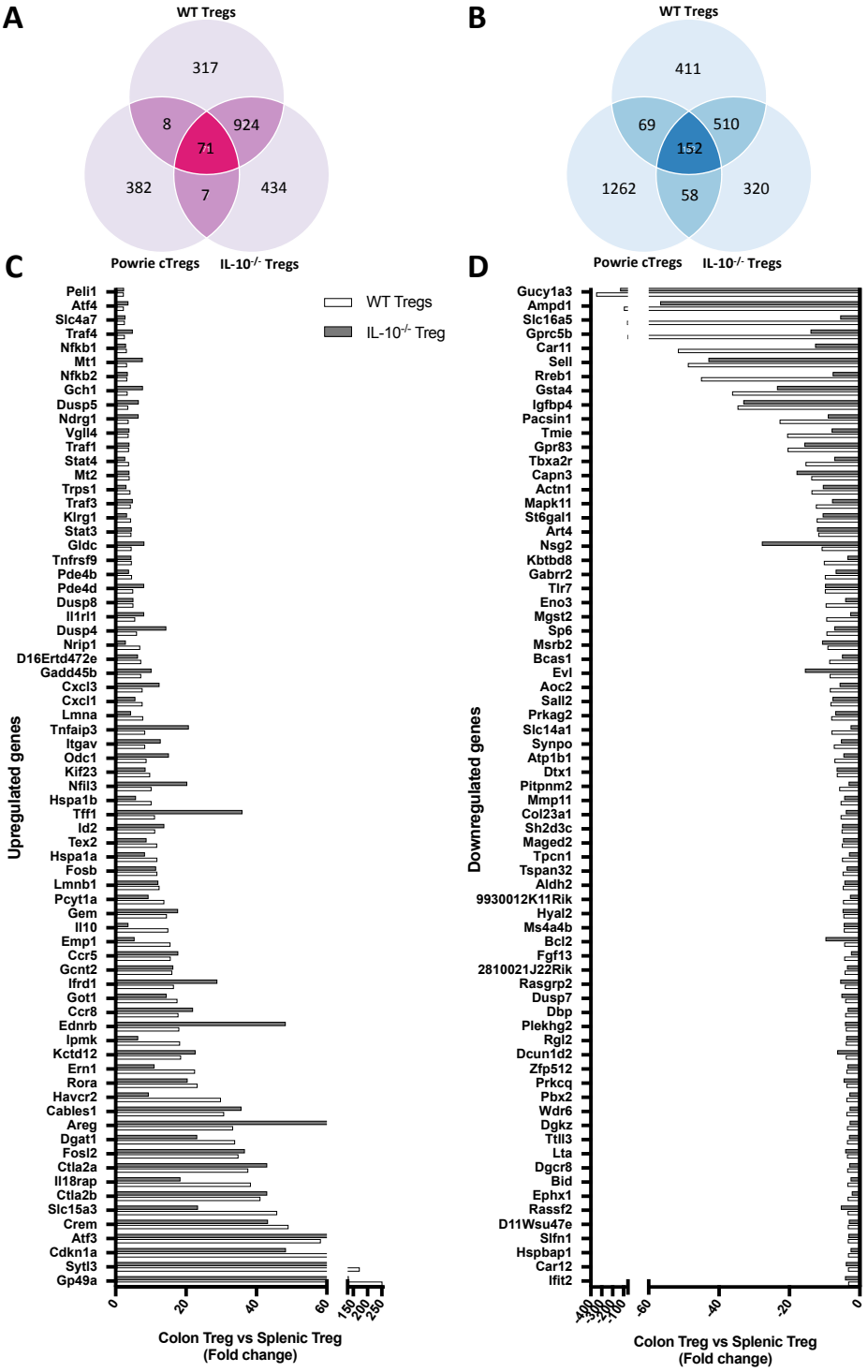

Figure 3.17: Colonic gene signature in FACS-sorted colonic Tregs

Differential expression analyses comparing Splenic vs Colonic WT Tregs and Splenic vs Colonic IL-10$^{-/-}$ Tregs were performed using the generalised linear model of the Deseq2 R package. The lists of up- and down-regulated genes were compared to data generated by the Powrie Lab, comparing colonic Tregs (cTregs) vs MLN Tregs at steady state.

(A, B) Up-regulated (A) and down-regulated (B) genes from cTregs, WT Tregs and IL-10$^{-/-}$ Tregs were compared using Venn diagrams. In total, 71 genes were similarly up-regulated, and 152 genes were similarly down-regulated.

(C, D) Fold changes (colon Tregs vs spleen Tregs condition) of similarly up- (C) and down-regulated (D) genes were computed for WT and IL-10$^{-/-}$ Tregs.

3.2.6 Validation of *Metrnl* expression in splenic IL-10$^{-/-}$ Treg cells

Next, we confirmed some of the targets identified by the RNA sequencing analysis. Splenic WT and IL-10$^{-/-}$ Tregs were FACS-sorted as previously described and gene expression was analysed by qPCR.

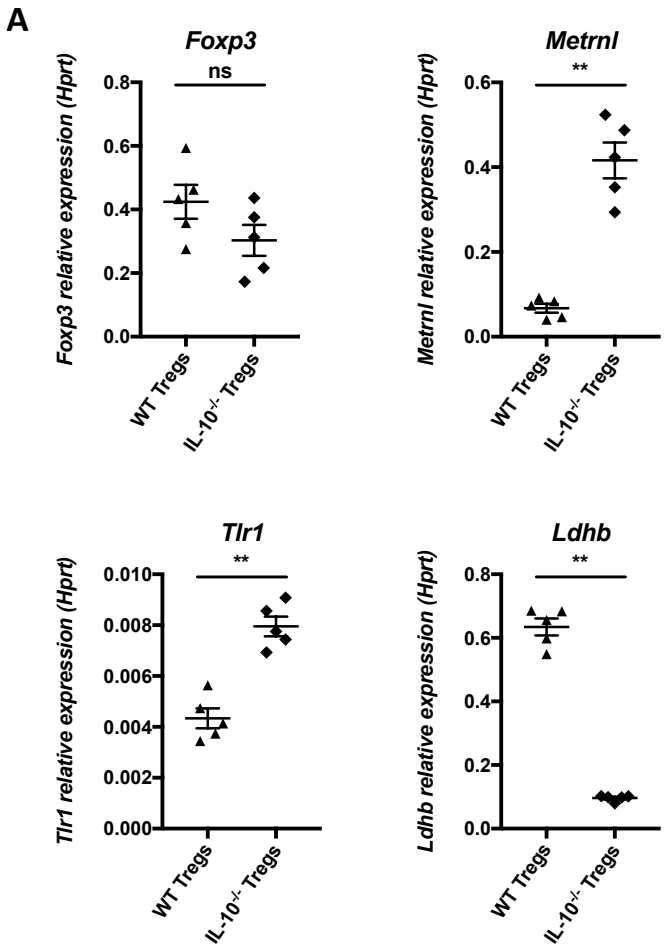

Figure 3.18: Validation of *Metrnl* and *Tlr1* expression by qPCR in splenic IL-10 deficient Tregs

Splenic WT and IL-10$^{-/-}$ Tregs were FACS-sorted from 129.WT and 129.IL-10$^{-/-}$ mice. RNA was extracted and gene analysis was performed by qPCR. Gene expression is normalised to the housekeeping gene *Hprt*.

(A) mRNA expression of *Foxp3*, *Metrnl*, *Trl1* and *Ldhb* in WT and IL-10$^{-/-}$ Tregs. The assay was run in technical duplicates.

Each dot represents a single mouse and bars represent mean ±SEM. Data represents one experiment.
Statistical significance was determined using a Mann Whitney U test. ** $p \leq 0.01$.

We confirmed that IL-10$^{-/-}$ Tregs expressed increased amounts of *Metrnl* and *Tlr1*, while they downregulate expression of *Ldhb* (**Figure 3.18 A**). Foxp3 mRNA expression was similar between Treg cells.

3.2.7 Potential dysbiosis and termination of experiments

Over the course of this thesis, the Powrie Lab moved from the John Radcliffe Hospital site to the Kennedy Institute (KIR). The move coincided with altered results in this model. Particularly, in the KIR facility, mice transferred with WT Tregs developed colonic inflammation and tumours, similarly to IL-10$^{-/-}$ Tregs transferred mice. A severe side effect associated with experimental procedures was discovered at the same time. Our 129.RAG$^{-/-}$ colony and experiments were terminated, which made it difficult to pursue this study (Chapter 3 and Chapter 4).

3.3 Discussion

3.3.1 Main conclusions

In line with published results, we show that IL-10$^{-/-}$ Tregs are unable to control *Hh*-driven innate inflammation when transferred into 129.RAG$^{-/-}$ recipients. By contrast, transfer of WT Tregs is associated with decreased tumour development and this is explained by their ability to control *H. hepaticus*-mediated inflammation. Early studies have shown that established inflammation is significantly diminished upon transfer of WT Tregs into 129.RAG$^{-/-}$ *H. hepaticus* infected mice (Maloy et al., 2003). In addition, established tumours from 129.RAG$^{-/-}$ hosts injected with IL-10$^{-/-}$ Tregs and infected with *H. hepaticus* can be eradicated following injection of recombinant IL-10 or transfer of WT Tregs (Erdman et al., 2003), further highlighting the critical role for IL-10 in controlling inflammation and its associated anti-tumourigenic function. Many other animal models of CRC have emphasised a role for Tregs in controlling tumour burden, and IL-10 has been repeatedly described as a critical cytokine in mediating tolerance at mucosal sites, and more importantly in controlling pro-tumourigenic inflammation and CRC development.

Beyond IL-10 deficiency, we confirm that IL-10$^{-/-}$ Tregs, rather than IL-10$^{-/-}$ effector CD4^{+} T cells, have increased tumourigenic potential. Mice transferred with IL-10 deficient effector CD4^{+} T cells are highly colitic, but do not progress to tumourigenesis to the same extent as mice transferred with IL-10$^{-/-}$ Tregs. Thus, our study focused on determining differences between WT and IL-10$^{-/-}$ Tregs to unravel certain pathways that may contribute to the development of colonic tumours.

Tregs can enhance their ability to control inflammatory responses through co-expression of transcription factors typically associated with the differentiation program of effector Th cells, such as T-bet, Gata3, IRF4 and STAT3 (Liston and Gray, 2014). A major difference between WT and IL-10$^{-/-}$ Tregs relates to their transcription factor expression profile. Splenic WT Tregs are primarily Gata3 positive, Helios positive, ST2 positive and express higher amounts of Foxp3, thus representing a *bona fide* thymic-derived Treg. Gata3 expression is linked to upregulation of Foxp3 expression and contributes to Treg proliferation and maintenance, making this population a classical suppressor of excessive inflammation, notably via OX40 and IL-10 production (Schiering et al., 2014; Wohlfert et al., 2011). By contrast, splenic IL-10$^{-/-}$ Tregs are mainly characterised by a lack of expression of the three transcription factors Gata3, Rorγt and Tbet. However, we detect an increased proportion of Rorγt-expressing cells compared to WT Tregs, albeit representing a small frequency, together with a small fraction of cells expressing Gata3. Globally, IL-10$^{-/-}$ Tregs are highly proliferative, express low amounts of Foxp3 and have a shared thymic and peripheral origin. The Helios-negative Rorγt-positive pTregs has been shown to develop from naive T cells in response to microbiota-derived antigens and metabolites, such as short-chain fatty acids (SCFAs). They are thought to contribute to the suppression of Th2 and Th1/Th17 responses and broad control of immune homeostasis with commensals microorganisms. (Josefowicz et al., 2012; Ohnmacht et al., 2015; Sefik et al., 2015; Yang et al., 2015). The majority of splenic IL-10$^{-/-}$ pTregs, lacking expression of Gata3, Rorγt and Tbet, are considered to be induced by dietary antigens, controlling the suppression of the immune response towards food (Kim et al., 2016). Together, our findings suggest that WT and IL-10$^{-/-}$ Tregs are

intrinsically different at the time of initial injection into 129.RAG$^{-/-}$ mice, and this difference goes beyond IL-10 deficiency.

By following the fate of the injected Treg populations in the colon of recipients over time, we discovered two populations of CD4^{+} T cells; T cells that express or not the transcription factor Foxp3, with the frequency of non-Foxp3 expresser cells increasing over time. Although we are not able to establish whether this relates to a contaminating cell population, it is interesting to note that expression of Rorγt by Tregs has also been associated with lineage plasticity, eventual loss of Treg-suppressive properties, and conversion to Th17 cells, especially under inflammatory conditions (Oldenhove et al., 2009; Zhou et al., 2009). This conversion into effector cells may explain the appearance of the non-Foxp3 population in both groups over time. Particularly, as IL-10$^{-/-}$ Tregs express low amounts of Foxp3, their stability may be further compromised upon initial transfer.

At week 12, our analyses revealed that differences between WT and IL-10$^{-/-}$ Tregs extend to the colon after transfer. Colonic WT and IL-10$^{-/-}$ Tregs both expressed high levels of Foxp3, suggesting that they acquire certain lineage stability at later stages of disease. Studies from our lab have shown that under homeostatic conditions, ST2^{+} and Gata3^{+} colonic Tregs are the major source of IL-10 among all colonic Tregs (Powrie Lab, unpublished). However, upon infection with *H. hepaticus*, the balance is reversed, and Rorγt^{+} cells become the dominant population of IL-10-expressing Tregs (Ohnmacht et al., 2015; Yang et al., 2015). In WT colonic cells, we detect expression of both Gata3^{+} and Rorγt^{+} Tregs, conferring immune suppression capabilities, notably

via IL-10 production, along with other suppressive mechanisms. Such colonic Gata3- and Rorγt-positive cells are also found in IL-$10^{-/-}$ Tregs, although their suppressive capacity is likely hampered by the lack of IL-10 secretion. Interestingly, despite being an indicator of lineage transition towards Th17 cells, Rorγt expression in Tregs at this stage of disease does not correlate with IL-17A production, suggesting that these cells are not transitioning towards a Th17 phenotype. Finally, a T-bet-positive population, significantly enriched in IL-$10^{-/-}$ cells, is also detected in the colon. T-bet expression by Tregs regulates expression of CXCR3 by promoting homing of Tregs to sites of Th1-driven inflammation (Koch et al., 2009). In effector $CD4^+$ T cells, T-bet expression mirrors IFNγ production, although there is no difference in total frequencies of $IFN\gamma^+$ cells between genotypes, similar to Rorγt expression and IL-17A expressing cells. Furthermore, differential accumulation of WT and IL-10 deficient cells most likely does not drive disease in IL-$10^{-/-}$ Tregs transferred mice, as no differences in frequencies and total numbers are found in Tregs and proinflammatory $CD4^+$ T effector cells, regardless of the genotype.

Finally, our initial gene expression screen comparing splenic Tregs revealed that IL-$10^{-/-}$ Tregs express increased amounts of *Tgfb* and *Areg*, which suggest that these Tregs may be equipped with repair capabilities, such as seen in tissue-Tregs. Secondly, taking an unbiased approach, the RNA sequencing of splenic and colonic populations of WT and IL-$10^{-/-}$ Tregs has shed light onto their gene expression profile. Although a limited amount of genes are differentially expressed, we confirm that IL-$10^{-/-}$ Tregs express increased amounts of *Tlr1*, *Metrnl* and downregulate the

expression of *Ldbh*. The expression of these genes is of interest in the context of a pathogenic Treg response and is further discussed in section 3.3.4.

Overall, the innate response towards *H. hepaticus* drives a proinflammatory milieu that may perturbe and render unstable splenic WT and IL-10$^{-/-}$ Tregs, and leads to the expansion of non-Foxp3 cells that are skewed towards a Th1/Th17 phenotype. However, as revealed by histological analyses, WT Tregs efficiently control both the innate and CD4^{+} T cell responses, while IL-10$^{-/-}$ Tregs are unable to impede these proinflammatory responses, ultimately favouring tumour development. Our study has highlighted that transfer of IL-10$^{-/-}$ Tregs preferentially promotes tumourigenesis compared to effector CD4^{+} T cells, in a mechanism that remains to be fully elucidated and represents an exciting new avenue for research.

3.3.2 Limitations of the model

Although this model has allowed us to confirm that IL-10 deficient Tregs have increased capacity to promote tumourigenesis, it holds several limitations.

First, the biggest limitation relates to the use of immunodeficient recipients. In general, immunodeficient mouse models are employed to study the initial development of tumours, as the adaptive immune system is not present to regulate tumour growth, and thus such models provide better understanding of the earlier steps and molecular pathways that lead to tumourigenesis. In our study, experiments were performed in RAG-deficient animals, where the adaptive immune component is missing and thus represents a significant drawback considering that cytokines such as IFNγ, IL-15 and IL-18 promote protective host immunity against cancer, and are primarily mediated by cytotoxic cell types, particularly CD8^{+} cytotoxic

T lymphocytes. Our model lacks critical components of the adaptive immune system and therefore does not represent a typical immunological response to tumourigenesis.

Secondly, we inject splenic Treg cells into the peritoneal cavity of immunodeficient hosts. While this model introduces a component of the adaptive immune system compared to the *Hh* innate model of CRC, it is important to note that transfer of $CD4^+$ T cells is an artificial system in which these cells are not regulated as it is the case in immunocompetent mice. Earlier studies have shown that injection of mature $CD4^+$ T cells into lymphopenic hosts home to the tissues and proliferate under homeostatic conditions, where they reconstitute a variety of immunological functions (Bell et al., 1987). Critically, this homeostatic proliferation is not a neutral event as dividing lymphocytes acquire markers associated with differentiated cells, such as effector functions, and their gene expression signature resembles that of "conventional" effector or memory T cells (Goldrath et al., 2004; Singh and Schwartz, 2006). While this proliferation and activation of T cells was deemed experimentally artifactual, recent studies have highlighted that such events occur in normal physiological processes. Similar T cell behaviour is observed when lymphocytes populate tissues and organs during the first week of life in neonatal mice, but also in adult life, where antigen-independent "spontaneous" proliferation of naïve T cells is observed in immunocompetent mice (Hataye, 2006), (reviewed in Singh and Schwartz, 2006). Thus, mouse models using lymphopenic recipients serve as a "magnifying glass", providing insights as to the function and physiological property of

certain subset of T cells, which ultimately remain to be validated in immunocompetent animals (Singh and Schwartz, 2006).

Thirdly, original publications, as well as our study, have selected Tregs as defined by expression of high CD25 and low CD45RB. Given that $CD4^+$ $Foxp3^-$ T cells upregulate CD25 upon activation, this strategy thus leaves open the possibility of injecting other contaminating activated T cell populations that may influence disease development. Although we confirmed, using Foxp3GFP reporter mice, that Tregs have increased capacity to mediate tumourigenesis compared to their effector $CD4^+$ T cells counterparts, a cell contaminant could still occur. Moreover, provided that we detect colonic $CD4^+$ T cells that do not express Foxp3, this population adds to the complexity of the transferred cells, and it is unclear whether they solely provide a pro-inflammatory microenvironment or influence tumourigenesis by direct mechanisms. Of note, although this model uses IL-10 deficient Tregs to induce pathology, it is important to note that in colorectal cancer patients, IL-10 deficiency has not been detected in Tregs. While IL-10 and IL-10R mutations in humans exist, they are not linked to increased incidence of cancer, but rather are linked to early-onset IBD, causing severe intractable enterocolitis in infants and small children (Glocker et al., 2012).

Finally, this model lacks mutational analysis. Several colorectal cancer mouse models are based on known oncogenic mutations. By contrast, in CAC models, these mutations are not always well characterised or are unknown. Our laboratory is sequencing tumours from the *Hh*-driven innate CRC model, but it remains to be determined what types of mutations are found in tumours from our mouse model.

This information is critical to better understand the relationship between our immunological observations and the type of tumours that develop *in vivo*, which may help to translate our results.

3.3.3 Relevance of the model to human colorectal cancer

Beyong the aforementioned limitations that are intrinsic to the model, it is interesting to put its features in context of human CRC. Histopathologic analysis of the tumours uncovered that lesions were predominately T1 and T2 mucinous adenocarcinomas, with roughly equal distribution between tumour stages. Most lesions were found in the proximal and middle parts of the colon, where colonic inflammation was also the highest. By contrast, the distal colon was mainly hyperplastic, and no cancerous lesions were detected. Mucinous adenocarcinoma (MC) is a subset of colorectal cancer that develops primarily in the proximal colon and is characterised by abundant mucus production, involving more than 50% of the tumour volume (Symonds and Vickery, 1976). Overall, about 10 to 15% of colorectal cancer patients are diagnosed with MC, and it is more commonly observed in patients with a history of IBD. Microsatellite instability (MSI) has been observed in MC, as is the case for instance in patients with Lynch syndrome, and some studies reported increased rates of mutations in BRAF, KRAS and PI3K/AKT (Hugen et al., 2014; Mekenkamp et al., 2012). Another common feature of patients with metastatic MC CRC is the poor response to chemotherapy and targeted therapies, and a distinct pattern of metastases. MC CRC is associated with an increased number of metastases, with extra-hepatic and peritoneal invasion, in contrast to the liver metastases observed in common adenocarcinomas (Hugen et al., 2014; Mekenkamp et al., 2012). Overall, the aetiology of MC CRC is still poorly characterised. Some

studies suggest that MC represents a genetically distinct subtype of colorectal adenocarcinoma (Melis et al., 2010) that may develop along the sessile serrated pathway (Patai, 2013)(Árpád V Patai et al., 2013), and is strongly correlated with poor prognosis and therapy resistance (Müller et al., 2016b). Therefore, it is critical to improve current understanding of molecular pathways that are perturbed in these tumours, as well as associated microenvironment. In addition to the above, the prognostic value of MC remains controversial (Catalano et al., 2009; Melis et al., 2010), likely highlighting the heterogeneity of the tumour microenvironment within the MC subtype in colorectal cancer. While the MSI and BRAF mutation status would categorise MC into the CMS1 category, a recent study has shown that differential TGF-β signalling in the microenvironment orientates tumours from the sessile serrated pathway towards different CMS (Fessler et al., 2016). Indeed, adenomas can progress to either poor-prognosis CMS4 tumours (high TGF-β signalling) or good-prognosis CMS1 tumours (low TGF-β signalling). Thus, the mouse model of colorectal cancer presented in this work may provide new insights on key pathways involved in disease progression and will further be discussed in Chapter 4.

3.3.4 Pathogenecity of Treg cells

Treg cells plasticity and adaptation to their microenvironment has been linked to acquisition of a Th17-like phenotype, conferring Treg a certain pathogenicity. For instance, a shift from IL-10 to IL-17-producing Tregs in $Apc^{Min/+}$ was shown to promote polyp growth (Gounaris et al., 2009). By contrast, our study revealed that in tumour-bearing mice, colonic IL-$10^{-/-}$ Tregs express Rorγt but do not produce IL-17A. Beyond the lack of control of proinflammatory responses due to the absence of IL-

10, we explored whether IL-10 deficient Tregs hold pathogenic potential that actively drives tumourigenesis, focusing on a plausible dysregulated repair function.

The first set of experiments that hinted towards a pathogenic role for IL-$10^{-/-}$ Tregs stemmed from the following observation: mice infected with IL-10 deficient effector $CD4^+$ T cells are highly colitic, but the progression towards tumourigenesis is preferentially enriched in mice injected with IL-$10^{-/-}$ Tregs. While mice injected with effector $CD4^+$ T cells had no Tregs to control the pro-inflammatory responses (initiated by the innate and effector T cell populations), only a few mice developed tumours, and these were restricted to T1 adenocarcinomas. This led us to hypothesise that in our model of CRC, IL-10 deficient Tregs may actively promote tumour development.

It is now broadly recognised that tissue-homing Tregs harbour a distinct phenotype from their lymphoid counterparts and have a series of specific adaptations. However, relatively little is known about tumour-adapted Tregs in colorectal cancer. Expression of high levels of *Areg* is a common trait of various tissues-Tregs, such as visceral adipose tissue (Cipolletta et al., 2012 Figure S1), skeletal muscle-resident (Burzyn et al., 2013), lung (Arpaia et al., 2015) and colonic Tregs (Schiering et al., 2014). Moreover, Areg expression is associated with the ability of Tregs to promote tissue repair processes in the lung and muscles (Arpaia et al., 2015; Burzyn et al., 2013), which correlates in this case with ST2 and Gata3 expression. Moreover, Amphiregulin has also been suggested to enhance the suppressive capacity of Tregs, upon binding to its receptor, by promoting Foxp3 expression (Zaiss et al., 2013).

Areg-producing Tregs could therefore reinforce their suppressive and repair capacities in an autocrine manner, through the expression of EGFR. During skin wound healing process, EGFR expression on Tregs facilitates repair, notably by attenuating IFN-γ production and proinflammatory macrophage accumulation (Nosbaum et al., 2016). This effect may result from their enhanced function that is acquired through the EGFR signalling pathway. In our study however, we failed to detect EGFR expression by qPCR, RNA sequencing and flow cytometry on splenic and colonic Tregs, regardless of the genotype. As *Areg* is enriched in splenic IL-10$^{-/-}$ Tregs, it suggests that these Treg cells are equipped to mediate repair processes. However, we have not been able to determine whether Areg expression in the context of the tumour microenvironment is critical for disease progression, mainly due to a lack of tools and associated functional studies.

The RNA sequencing revealed several upregulated genes that allow us to better understand the differences between WT and IL-10$^{-/-}$ Tregs.

First, WT Tregs upregulate genes with broad associations to calcium metabolism, together with metabolites and protein transport, which likely reflects their activation state, together with the production of cytokines controlling pro-inflammatory responses. Moreover, the increased expression of *Nr4a2* provides maintenance and suppressor functions to WT Tregs (Sekiya et al., 2011), which is also reflected by the increased levels of Foxp3 expressed at steady state. Upregulation of *Nr4a2* would therefore endow WT Tregs with the ability to control pro-inflammatory responses in the context of *H. hepaticus* infection. Reciprocally, its downregulation in IL-10$^{-/-}$ Tregs

renders this population prone to lose Foxp3 expression, and promotes attenuated suppressive ability (Sekiya et al., 2011).

The upregulation of *Ldhb* by WT Tregs (i.e. downregulated in IL-10 deficient Tregs) may reflect their activation state, but also signals that these cells are not engaged towards the glycolytic pathway, and would rather favour the Krebs cycle. Given that no other metabolic genes were differentially expressed, it is unclear whether splenic WT and IL-10 deficient Treg have a different metabolism. In macrophages, IL-10 inhibits LPS-induced glucose uptake and glycolysis, rather orienting the metabolism towards oxidative phosphorylation and mitophagy. The effects of IL-10 are mediated through the induction of DDIT4, an inhibitor of the mTORC1 pathway. Consequently, upon IL-10 deficiency, macrophages accumulate damaged mitochondrias that leads to dysfunctional activation of the NLRP3 inflammasome and production of IL-1β, promoting colitis *in vivo* (Ip et al., 2017). It is unknown whether IL-10 has the same effect on other immune cell types, such as Tregs, and this remains to be investigated. Given that mTORC1 inhibition promotes Tregs differentiation (Delgoffe et al., 2009), and because mTORC1 activity is modulated in Tregs upon TLR activation (Gerriets et al., 2016), it is plausible that IL-10 supports Treg development by inhibiting mTORC1 activation (Kabat and Pearce, 2017).

Conversely, IL-10 deficiency may impact on the metabolism and function of Tregs through similar pathways. The increased *Tlr1* expression detected in IL-$10^{-/-}$ Tregs puts these studies in an interesting new perspective. The TLR1/2 signalling pathway is linked to promotion of Treg cell proliferation, glycolysis and expression of Glut1, via the Akt-mTORC1 pathway (Gerriets et al., 2016). Fascinatingly, TLR-induced

mTORC1 signalling was also shown to impair Treg cell suppressive capacity. Conservely, Foxp3 opposes PI(3)K-Akt-mTORC1 signalling to diminish glycolysis and anabolic metabolism, while increasing oxidative and catabolic metabolism, establishing a balance to control the proliferation and suppressive function of Tregs upon TLR1/2 signalling. (Gerriets et al., 2016). Therefore, the upregulation of *Tlr1*, together with the lack of IL-10 production would render IL-$10^{-/-}$ Tregs entirely unable to mediate their regulatory functions. Furthermore, considering the possibility of a metabolic shift in IL-10 deficient Tregs, this may represent another way by which Tregs acquire a pathogenic function.

We report for the first time (to our knowledge) the expression of *Metrnl* in IL-10 deficient Tregs. Meteorin-like is a novel cytokine with emerging functions (reviewed in Zheng et al., 2016), and two recent studies have addressed its function *in vivo*. Overexpression of *Metrnl* in mice increases energy expenditure, promotes thermogenic gene expression, and increases the abundance of beige adipocytes. Accordingly, administration of recombinant Meteorin-like to mice stimulates thermogenic gene expression, which is accompanied by weight loss in a diet-induced model of obesity (Rao et al., 2014). More recently, a gene expression screen of *Meteorin-like* in tissue highlighted that it is highly expressed at mucosal sites and skin (Ushach et al., 2015). Specifically, both M2-type macrophages and M-CSF cultured bone marrow macrophages produce Meteorin-like, and in the skin, Metrnl is expressed by resting fibroblasts as well as IFNγ-treated keratinocytes. Over-expression of Meteorin-like in diverse skin diseases, such as psoriasis, is also reported. Additionally, *Metrnl* is also upregulated in synovial membranes of

rheumatoid arthritis patients. Overall, this study indicates that Meteorin-like represents a novel cytokine likely involved in both innate and adaptive immune responses. (Ushach et al., 2015).

So far, *Metrnl* expression has not been characterised in the colon, at steady state or during diseases such as IBD and CRC. Moreover, it remains to be determined whether Meteorin-like is secreted by Tregs and what its associated function and cellular targets are. Ultimately, the role of Meteorin-like in tumour-initiation events promoted by Tregs remains to be investigated.

Although the RNA sequencing has revealed several new avenues for research in understanding the plausible pathogenicity of IL-10 deficient Tregs, we have been generally unsuccessful at unravelling known pathways that could explain their tumour promoting capacities. Importantly, we note that whole colons were used for our analyses, including the RNA sequencing, due to cell number limitation. As a result, tumour-infiltrating Tregs and lamina propria resident Tregs were pooled, potentially leading to the dilution of a tumour-Treg signature. This highlights the necessity to explore the phenotype of Tregs that are found within colonic tumours, utilising techniques such as immunohistochemistry, immunofluorescence and RNAscope, together with single cell RNA sequencing. From a tumour-Treg perspective, it is then not unreasonable to hypothesise that the combined effects of prolonged inflammation caused by the lack of immune regulation, together with the repair function promoted by Areg expression, could mediate tumour growth or maintenance, as Tregs are close to the malignant epithelium (data not shown, and (Poutahidis et al., 2007). Since Areg plays a critical role in intestinal epithelial growth

and has been shown to drive the renewal of the intestinal epithelium following a total body irradiation (Shao and Sheng, 2010a), further renewal under pro-inflammatory conditions and microbial insults may promote malignancy, thereby establishing Tregs as an enabling factor to tumour growth. In support of this hypothesis, a recent report suggested that Areg plays pro-neoplastic roles in intestinal epithelial transformation, as decreased polyposis was seen $Areg^{-/-}.APC^{min/+}$ mice. Areg was shown to function both in autocrine- and paracrine-pathways, the latter mainly resulting from Areg production by myofibroblasts (Guzman et al., 2012). The **Figure 3.19** summarises our main findings.

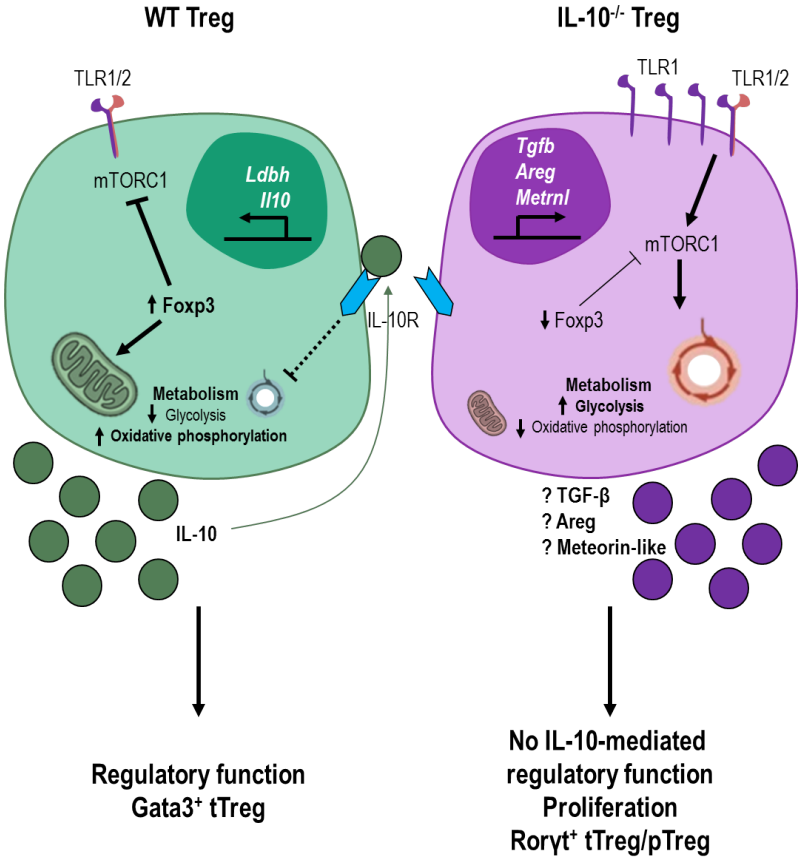

Figure 3.19: Main differences between WT and IL-10$^{-/-}$ Tregs

WT Tregs are Gata3-expressing cells of thymic origin. They are potent suppressor of colonic inflammation, which is mediated by the high amounts of Foxp3 expression, which favours the TCA and inhibits mTORC1, proliferation and glycolysis (round circle). WT Tregs mediate their immune suppression function through the production of IL-10. IL-10 may promote further inhibition of glycolysis via in an autocrine manner.

IL-10$^{-/-}$ Tregs express Rorγt and are of shared thymic and peripheral origin. These cells lack IL-10 production and therefore are unable to mediate immune regulation through this mechanism. IL-10 deficient Tregs express increased amounts of Tlr1, which may results in increased mTORC1 signalling, favouring glycolysis and increased proliferation over immune suppressive functions. Moreover, these cells express lower amounts of Foxp3, which may not allow the inhibition of the increased mTORC1 signalling. IL-10$^{-/-}$ Tregs have increased production of *Tgfb*, *Areg* and *Metrnl* whose secretion remain to be investigated.

The mitochondria represents the TCA; the circle represents glycolysis.

Finally, a few studies have highlighted the pathogenic function of Tregs in different cancers that is not a consequence of their immunosuppressive functions. First, Facciabene et al have shown that hypoxia promotes the secretion of CCL28 in ovarian cancer cells, which recruits $CD4^+CD25^+FOXP3^+$ Tregs upon ligation of the cognate receptor CCR10 (Facciabene nature 2011). Intratumoural Tregs displayed increased suppressive function due to the hypoxic environment and, surprisingly, were shown to secrete high levels of VEGF, suggesting that they may directly contribute to angiogenesis and tumour growth (Facciabene et al., 2011; Motz and Coukos, 2011). Another study conducted in breast cancer showed that Tregs infiltrating carcinoma lesions are capable of promoting metastasis of tumour cells through surface expression of the pro-metastatic TNF superfamily member RANKL (Tan et al., 2011) (Tan W 2011). Lastly, Blatner et al. described a stable Treg subset marked by the expression of RORγt in human CRC and a mouse model of hereditary polyposis, and these Tregs were not transitioning towards a Th17 effector cell type (Blatner et al., 2012). $ROR\gamma t^+$ $Foxp3^+$ T cells retained suppressive function *in vitro* but were impaired in their anti-inflammatory properties *in vivo*. Ablation of the Rorγt gene in $Foxp3^+$ cells in polyp-prone mice suppressed inflammation and severely attenuated tumourigenesis. Interestingly, loss of IL-17A had a dual effect *in vivo*: while IL-17A deficient mice had fewer polyps, the $ROR\gamma t^+$ Treg population remained and the few polyps that developed progressed to invasive cancer. Interestingly, the consequence of RORγt expression in Tregs on tumourigenesis was not completely dependent on IL-17 secretion, indicating that other effects of RORγt may contribute to disease development (Blatner et al., 2012). Further characterisation of this subset

is required to better understand the role of pathogenic Tregs in CRC, which may enable the design of new-targeted therapies.

In conclusion, several studies have emphasised that Tregs can shape the tumour microenvironment not only to promote tumour immune tolerance, but also angiogenesis, aberrant repair, and pathogenic programs. Further investigation of the function of *Meteorin-like* expression by IL-10 deficient Tregs may add a new player to the pathogenic function of these cells.

3.3.5 Concluding remarks

Collectively, our study emphasise the complex role that Tregs play in colorectal cancer. Indeed, Tregs are classically thought to enable tumour growth and progression by impeding specific anti-tumour immune responses. However, as documented by our study, other murine models of CRC and patients' studies, Tregs can also suppress inflammation-promoting cancer responses, which benefits the host. In this context, the role of Tregs in CRC will most likely depend on the tumour microenvironment and disease stage. Tregs are dominant suppressors of pro-inflammatory responses that arise upon prolonged epithelial insult driven by the microbiota and are potentially beneficial for cancer initiation. However, once tumours are established, the type of immune infiltrate and the Treg phenotype are more likely to dictate prognosis. For instance, a Th1 signature correlates with better disease-free survival, whereas a Th17 signature is associated with poor prognosis in CRC (Tosolini M, 2011a; Bindea *et al.*, 2013). In both cases, depending on the dominant T cell response, Tregs would therefore mediate either tumour escape or regression. One question that remains to be investigated is whether different

subsets of Tregs are involved in earlier versus later stages of the disease. For instance, Rorγt^{+} Tregs may be more equipped to suppress colonic inflammation driven by the microbiota at early stages, while Gata3^{+} Tregs may promote disease progression through the suppression of anti-tumour responses and potentiation of aberrant repair responses. Moreover, little is known about T-bet^{+} Tregs apart from their specific Th1 immunosuppression function. We have reported for the first time that a T-bet^{+} Treg population expands in the colon of tumour-bearing mice, which warrants further investigation as to whether and how this population supports disease progression. Overall, analysis of different Treg subtypes as well as their location in the tumour will provide further insights into their function in tumourigenesis and may help to develop better strategies for targeted immunotherapies. Furthermore, it would be interesting to explore whether the Treg suppressive mechanisms associated with inflammation are similar to those exploited in the context of colorectal cancer.

Critically, our study suggests an underappreciated function of Tregs in mediating direct tumour promotion in colorectal cancer. Such pathogenic functions have been recently emphasised in other cancers and in CRC, and we now aim at determining whether secretion of Areg and Meteorin-like confers pro-tumourigenic capacities to Treg cells.

4 Stromal cells are main producers of the pro-tumourigenic cytokine IL-6

4.1 Introduction

The tumour microenvironment, in addition to harbouring cancer cells, consists of various components that have a significant role in determining the progression and outcome of the malignancy. These components can be broadly classified into three main groups: cells of haematopoietic origin, cells of mesenchymal origin and non-cellular components. In colorectal cancer, environmental factors such as the microbiota and inflammation adds to the complexity of the microenvironment, and it is now appreciated that inflammation accompanying tumour development has a critical role in determining the course of disease. Antigen-driven, cytolytic responses can limit cancer progression, while non-specific inflammatory activity can in some circumstances promote it (Grivennikov et al., 2010).

The IL-23 axis is a critical pathway of intestinal inflammation in many mouse models (S. Hue et al. 2006) and its components IL-23R and Stat3 are not only associated with IBD susceptibility (J. C. Barrett 2008 and R. H. Duerr 2006), but also involved in inflammation-associated cancer in the skin and colon (S. I. Grivennikov 2012, J. Bollrath 2009, J. L. Langowski 2006). Recent studies have implicated IL-17 as a downstream effector of IL-23-driven tumourigenesis (S. I. Grivennikov 2012, S. Wu et al., Nat Med 2009). Furthermore, studies from the Powrie lab showed that IL-22-producing ILCs mediate CAC in *Hh*/AOM treated 129S6.RAG$^{-/-}$ mice. Depletion of ILCs or IL-22 blockade was sufficient to resolve adenocarcinomas in this model, indicating a non-redundant role for IL-22 signalling in sustaining the tumour state (Kirchberger et al., 2013).

In the Treg CAC model, it is unknown whether IL-17 or IL-22 also promotes tumourigenesis. In the *Hh*-driven innate CAC model, tumour development is associated with a marked activation of stromal cells including fibroblasts, which is further exacerbated by cotransfer of IL-10-deficient regulatory T cells (Poutahidis et al., 2007). Proliferation and activation of fibroblast are also an essential feature of CRC (D. Hanahan cancer cell 2012). Cancer-associated fibroblasts are thought to play a central role in tumourigenesis. However, the pathways involved and the interaction between these cells and cancer promoting ILCs (*Hh*/AOM) and tumoural Treg cells is not known. Thus, the Treg model of CAC represents a unique study case to dissect the cellular and molecular interactions that mediate the triangle of inflammation, cancer-associated fibroblasts and epithelial cell cancer.

Specifically, we sought to:

1. Determining whether this accelerated model of colitis-associated cancer promoted by a microbial insult involves the promotion of a specific innate response driven by IL-10$^{-/-}$ Tregs.
2. Exploring the involvement of stromal cells in tumour development.
3. Studying the upregulation of critical cytokines in tumour-bearing mice, and assess their cellular origin as well as relevance in disease development *in vivo*.

4.2 Results

4.2.1 Major immune populations of tumour-bearing mice are not different from that in colitis.

To determine whether there are distinct leukocyte populations in tumour-bearing mice, we established several comparisons between experimental groups. Uninfected mice were compared colitic mice (*Hh* only group). Colitic mice were then compared to the mice transferred with WT Tregs and infected with *Hh*, which have reduced inflammation but contain the lymphocyte fraction, and also to tumour-bearing mice.

First, we analysed the infiltrating colonic populations of *Hh* only infected mice, compared to non-inflamed controls. Next, we compared *Hh* only infected mice to mice receiving either WT or IL-10$^{-/-}$ Tregs and infected with *Hh*, to determine whether distinct cell populations are found in the colon upon Treg transfer. Finally, we compared colitic versus tumour-bearing mice to determine whether certain populations are specifically increased in the tumour setting.

We analysed the colonic $CD45^+$ cell infiltration and the innate populations by flow cytometry, looking at the frequency and total cell number of:

- Eosinophils ($CD45^+$ $CD11b^+$ $Gr1^{low}$ Siglec-F^{high}),
- Neutrophils ($CD45^+$ $CD11b^+$ $Gr1^{high}$ Siglec-F^{low}),
- $F4/80^+$ macrophages ($CD45^+$ $CD11b^+$ $Gr1^{low}$ Siglec-F^{low} $CD11c^{low}$ $F4/80^{high}$),
- $CD11b^+$ dendritic cells ($CD45^+$ $CD11b^+$ $Gr1^{low}$ Siglec-F^{low} $CD11c^{high}$ $F4/80^{low}$ $MHCII^{high}$),
- Monocytes ($CD45^+$ $CD11b^+$ $Gr1^{low}$ Siglec-F^{low}).

Monocytes were also sub-divided based on Ly6C and MHCII expression, according to the "Monocyte-waterfall gating strategy", representing a developmental series whereby extravasated Ly-$6C^{hi}$ monocytes develop to intestinal macrophages in a waterfall-shaped flow cytometric distribution (**Figure 4.1 C**, representative plots)

Figure 4.1 A represents pie charts of the average frequency of indicated colonic cell populations amongst $CD45^+$ cells, across experimental groups. All other cell populations were grouped into the "other" section, containing innate lymphoid cells, basophils, other sub-types of DCs and macrophages, NK cells, as well as injected T cell populations for the WT Tregs + *Hh* and IL-$10^{-/-}$ Tregs + *Hh* groups.

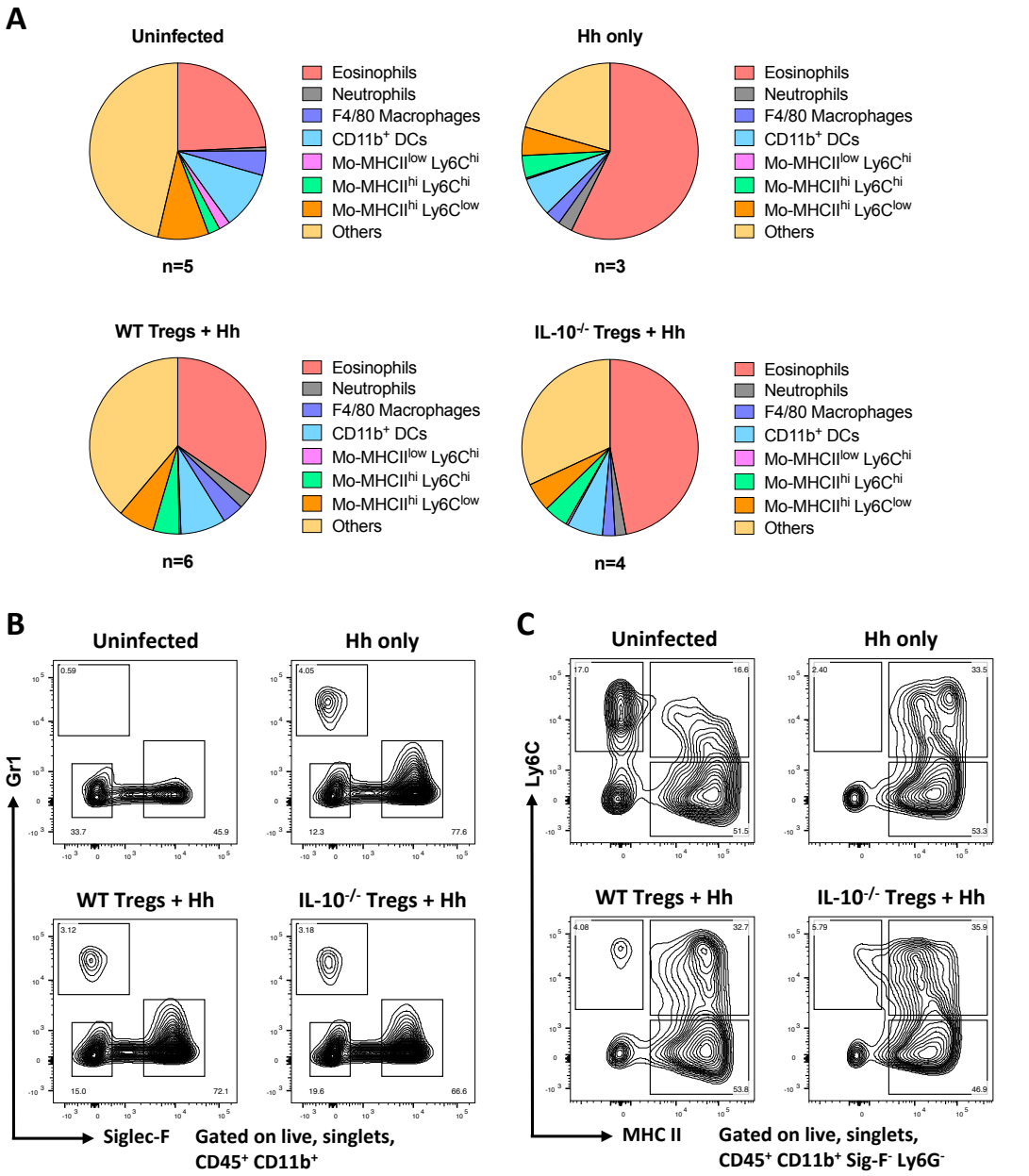

Figure 4.1: Frequencies of major colonic innate cells are similar between colitic and tumour-bearing mice.

Steady state, *Hh* infected only, WT Tregs + *Hh* and IL-10$^{-/-}$ Tregs + *Hh* recipients were sacrificed at week 12 of the model. Colons were harvested, and single cell suspensions were analysed by flow cytometry.

(A) Pie charts showing the frequencies of indicated populations for each experimental group. For each group, the average frequencies of defined populations amongst live CD45^{+} cells were calculated.

(B) Representative FACS plots displaying Gr1 and Siglec-F expression for each group. Gated on live, singlets, CD45^{+} CD11b^{+} cells.

(C) Representative FACS plots displaying the monocyte waterfall, defined by Ly6C and MHC II expression. Gated on live, singlets, CD45^{+} CD11b^{+} Gr1^{low} Siglec-F^{low} cells.

Data represents one experiment performed at the JR with the Powrie colony, representative of 2 independent experiments.

Uninfected mice were characterised by a large proportion of eosinophils (red, 24.26%), monocytes (overall 9.10%), and $CD11b^{+}$ DCs (cyan, 10.62%), which together with other immune cells represented the majority of the colonic populations. $MHCII^{low}$ $Ly6C^{high}$ monocytes were also present in the colons (pink, 2.2%).

In the colitis setting, the colons of *Hh* only infected mice were strikingly infiltrated with a large proportion of eosinophils, which represented more than 57.20% of the total infiltrating cells. Moreover, colitic mice had a lower frequency of $MHCII^{low}$ $Ly6C^{high}$ monocytes were largely depleted from colitic mice, and the population of inflammatory monocytes $MHCII^{high}$ $Ly6C^{high}$ (green, 4.3%) was increased compared to non-uninflamed animals (green, 1.8%). The frequency of neutrophils was also increased in colitic animals (grey, 2.66% compared to 0.66% in non-inflamed animals).

Upon transfer of WT Tregs and infection with *Hh*, mice were largely non inflamed. However, when compared to colitic mice, no major changes were observed. Eosinophils represented the major population (red, 34.56%), although to a lower frequency than of colitic mice. In addition, the frequency of $MHCII^{low}$ $Ly6C^{high}$ monocytes remained low, while inflammatory monocytes were present, and neutrophils also infiltrated the colons (grey, 2.66%).

Finally, we compared colitic mice to tumour-bearing mice. The same observations were made. Eosinophils accounted for the majority of the infiltrating cells in the colon, with an average of 47.25% (**Figure 4.1 B**, representative FACS plots) Neutrophils were also present (grey, 2.86%), as well as inflammatory monocytes (3.14%).

In conclusion, following *Hh* infection, there was a primarily accumulation of eosinophils and inflammatory monocytes, whereas in mice restored with Tregs, either WT or IL-10 deficient, no clear changes was discovered compared to colitic mice.

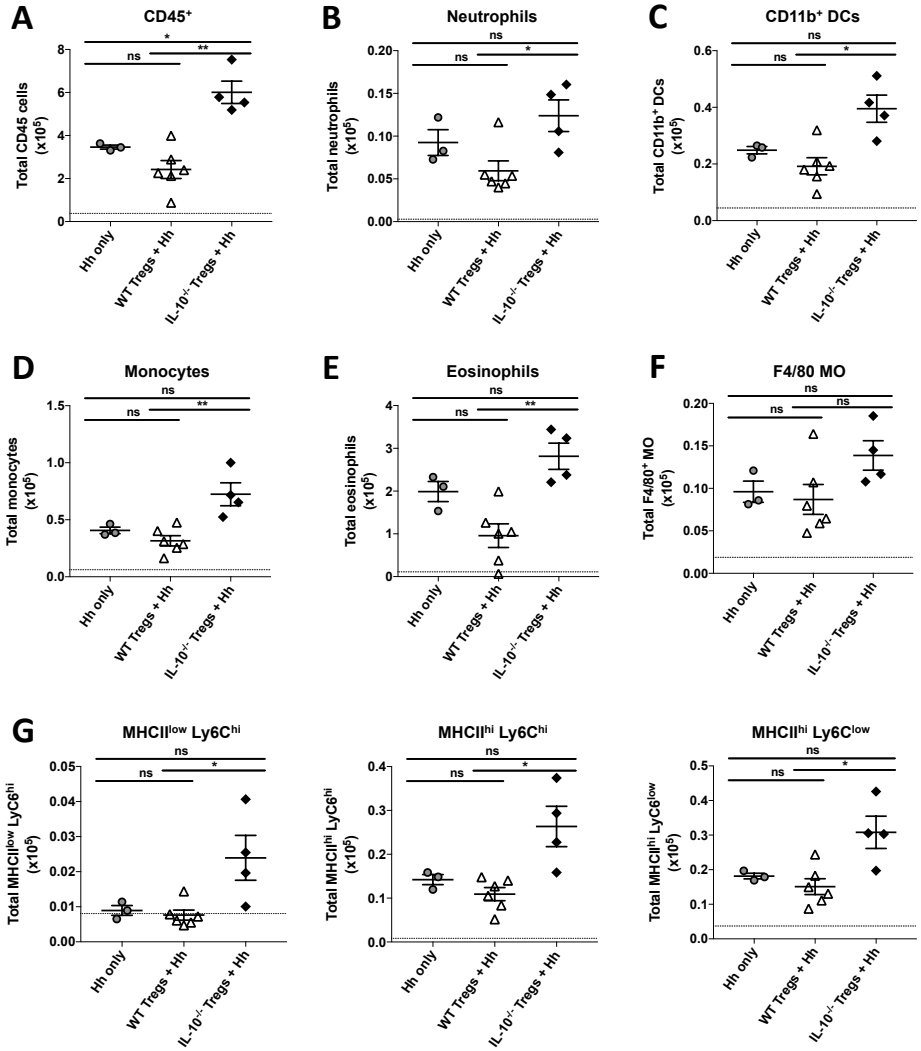

Figure 4.2: The immune compartment in the intestine of tumour-bearing mice is not different from colitis.

Uninflamed, *Hh* infected, WT Tregs + *Hh*, and IL-10$^{-/-}$ Tregs + *Hh* mice were sacrificed at week 12. Colons were harvested and single cell suspensions were analysed by FACS.

(A) Total number of live, singlet CD45^{+} colonic cells across groups.
(B-F) Total number of indicated colonic cell populations.
(G) Total number of the different monocyte-to-macrophage populations as defined by the monocyte waterfall.

Each dot represents a mouse and bars represent mean ±SEM. The dashed horizontal bar represents the mean of non-infected controls (n=5). Data represents one experiment performed at the JR, representative of 2 independent experiments.
Statistical significance was determined using a Kruskal-Wallis one-way analysis of variance, followed by a Dunn's post-hoc test. * $p \leq 0.05$.

Next, we looked at total cell number, which allowed for a better understanding of the innate cell influx in the colon.

First, we compared the total number of colonic $CD45^+$ cells (**Figure 4.2 A**). In the colitis setting, there was an increased number of colonic $CD45^+$ cells compared to uninfected mice (controls, dashed horizontal bar). Comparing colitic mice to mice transferred with WT Tregs and *Hh* infected, the total number of $CD45^+$ cells was not changed. Finally, a significant increased number of colonic $CD45^+$ cells was found in tumour-bearing mice compared to colitic mice (*Hh* only) (**Figure 4.2 A**).

Next, we compared WT Tregs + *Hh* and IL-$10^{-/-}$ Tregs + *Hh* mice for colonic cellular infiltration. The total number of all major innate cell populations in the colon was significantly increased in IL-$10^{-/-}$ Tregs + *Hh* mice (**Figure 4.2 B-G**), most likely denoting the marked inflamed environment.

Finally, we compared *Hh* only infected to IL-$10^{-/-}$ Tregs + *Hh* mice, to uncover preferential expansion of pro-tumourigenic cell populations. However, no significant increase in total cell numbers was detected when comparing inflamed *Hh* only animals to tumour-bearing mice (**Figure 4.2 B-G**), apart from the total number of $CD45^+$ cells, indicated that the experiment was most likely not powered enough.

4.2.2 The interleukin-22 pathway is not required for tumour development and maintenance

Given the evidence of a deleterious role for IL-22 in both colitis associated cancer and sporadic murine models of CRC (Huber et al., 2012; Kirchberger et al., 2013), we next investigated whether the IL-22 pathway is also critical in the IL-10$^{-/-}$ Treg + *Hh* model. Although we did not detect enrichment of innate lymphoid cell populations in tumour-bearing mice (data not shown), IL-22 production was detected (data not shown).

First, we asked whether IL-22 was involved in tumour development. Since innate lymphoid cells are the main producer of IL-22 in the innate model of colitis-associated cancer, we used 129.RAG$^{-/-}$.IL-22$^{-/-}$ mice as recipients and injected IL-10$^{-/-}$ Tregs, followed by *Hh* infection (**Figure 4.3 A**). In this setting, since ILCs or other cell populations are not able to produce IL-22, we assessed whether tumours developed to the same extent as in WT 129.RAG$^{-/-}$ recipients.

First, we compared colonic inflammation levels. *Hh* only infection led to similar colitis scores between the two genotypes (group 1 versus group 4, not significant) (**Figure 4.3 B**). As a control, we used 129.RAG$^{-/-}$ mice injected with IL-10$^{-/-}$ Tregs but not infected with *Hh*. These mice showed no signs of colitis, with an average score of approximately 2. By contrast, both 129.RAG$^{-/-}$ and 129.RAG$^{-/-}$.IL-22$^{-/-}$ mice developed colitis when injected with IL-10$^{-/-}$ Tregs and infected with *Hh* (group 3 versus group 5, not significant). Finally, colonic inflammation was similar in the 129.RAG$^{-/-}$.IL-22$^{-/-}$ recipients receiving either IL10$^{-/-}$ Tregs + *Hh* or *Hh* only (group 4 versus group 5, not significant) (**Figure 4.3 B**).

Next, tumour burden was assessed by histology (**Figure 4.3 C**). As expected from the colitis scores, no tumours developed in the mice only infected with *Hh*, irrespective of the recipients' genotype. Similarly, 129.RAG$^{-/-}$ mice that received IL-10$^{-/-}$ Tregs only did not progress to disease. However, tumours occurred in 80% of the 129.RAG$^{-/-}$.IL-22$^{-/-}$ recipients in the IL-10$^{-/-}$ Tregs + *Hh* group, which is not statistically different from the tumour burden observed in 129.RAG$^{-/-}$ recipients receiving similar treatment (83% of mice with tumours). Finally, we wanted to rule out the possibility of potential IL-22 production by the Tregs, which could promote disease development. To this end, a small part of the distal colon from 2 mice in each of the IL-10$^{-/-}$ Treg + *Hh* group was taken (i.e to preserve the rest of the tissue for histology), and were FACS stained. Representative FACS plots of CD4 and IL-22 staining on both CD4^{+} Foxp3^{-} and Foxp3^{+} populations revealed that the transferred T cells did not secrete IL-22 (**Figure 4.3 D**), which supported our previous analyses (**Chapter 3, Figure 3.8 D**).

Altogether, these results indicate that IL-22 production from the host is not required for tumour development in the IL-10$^{-/-}$ Tregs + *Hh* CRC model at the time point we analysed. Moreover, we confirmed that the injected cells do not express IL-22, indicating that this cytokine is not employed by Tregs to promote tumourigenesis.

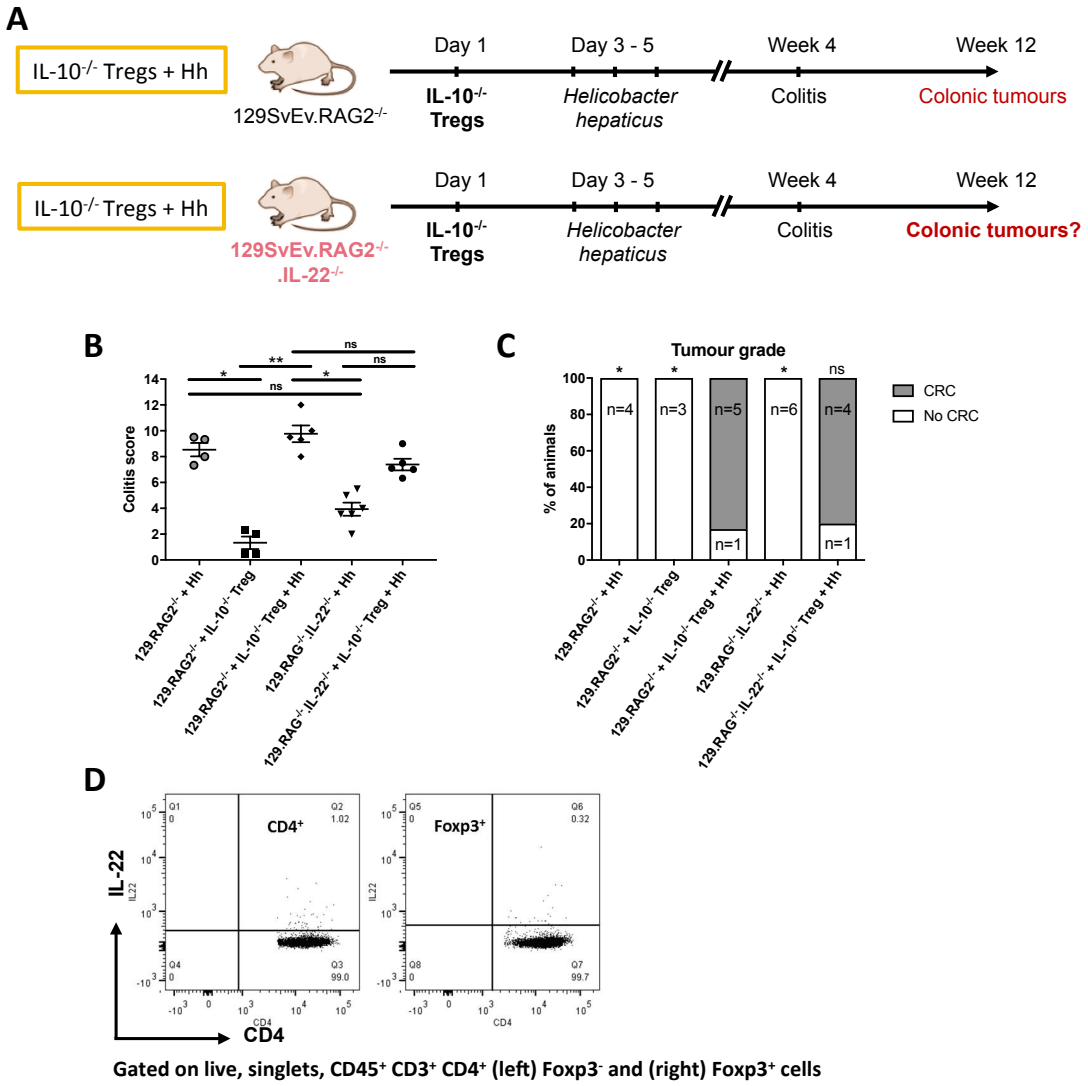

Gated on live, singlets, CD45+ CD3+ CD4+ (left) Foxp3- and (right) Foxp3+ cells

Figure 4.3: IL-22 production by the host is not required for tumour development.

129.RAG$^{-/-}$ and 129.RAG$^{-/-}$.IL-22$^{-/-}$ recipients were either infected with *Hh* only or injected with IL-10$^{-/-}$ Tregs only, or were injected with IL-10$^{-/-}$ Tregs and infected with *Hh*. After 12 weeks, mice were sacrificed and colons harvested for histopathological analyses.

(A) Scheme of the experimental set-up.
(B) Colitis score across experimental groups.
(C) Percentage of mice developing tumours for each experimental group.
(D) Representative FACS plots showing IL-22 expression against CD4. Gated for live, singlets, CD45^{+}, CD3^{+}, CD4^{+} Foxp3^{-} (left) and Foxp3^{+} (right) cells.

Each dot represents a mouse and bars represent mean ±SEM. Data represents one experiment performed at the JR with the Powrie colony.
Statistical significance was determined using a (B) Kruskal-Wallis one-way analysis of variance, followed by a Dunn's post-hoc test, and (C) Fisher's exact test with IL-10$^{-/-}$ Tregs + *Hh* group as control (two-sided). * $p \leq 0.05$.

Experiment performed by Stefanie Kirchberger and Fanny Franchini.

To further exclude a role for IL-22 in tumourigenesis, its role in tumour maintenance was next investigated using a therapeutic approach. 129.RAG$^{-/-}$ recipients were injected with IL-10$^{-/-}$ Tregs and then infected with *H. hepaticus*, as previously described. At week 9 of the model, when tumours are established, animals were divided into 3 groups: no treatment, isotype control antibody treated (isotype group), and blocking anti-IL-22 antibody treated (α-IL-22 group) (**Figure 4.4 A**). The treatment was given for 5 consecutive weeks, after which mice were sacrificed, and colons taken for histology.

Colitis was first assessed and was severe in all groups (**Figure 4.4 B**). There was a significant increase in colitis score of the IL-10$^{-/-}$ Treg + *Hh* group compared to *Hh* only animals. However, although we detected a significantly lower colitis score between untreated versus α-IL-22 treated recipients, the isotype treated group displayed a decreased score, which reached similar levels to the α-IL-22 group. This indicated that the isotype treatment might affect colitis, or might reflect that the experiment was underpowered to draw conclusions on the colitis score.

Tumour burden was next determined (**Figure 4.4 C**). Consistent with previous results, mice from the IL-10$^{-/-}$ Treg + *Hh* group and the isotype-treated group developed tumours (100% in both cases). Interestingly, mice treated with α-IL-22 equally progressed to disease, with all mice displaying colonic tumours. Finally, frequencies of T1 and T2 tumours were similar across groups, indicating that IL-22 is not involved in tumour progression (**Figure 4.4 D**). In conclusion, our results indicate a dispensable role for IL-22 in disease penetrance and maintenance.

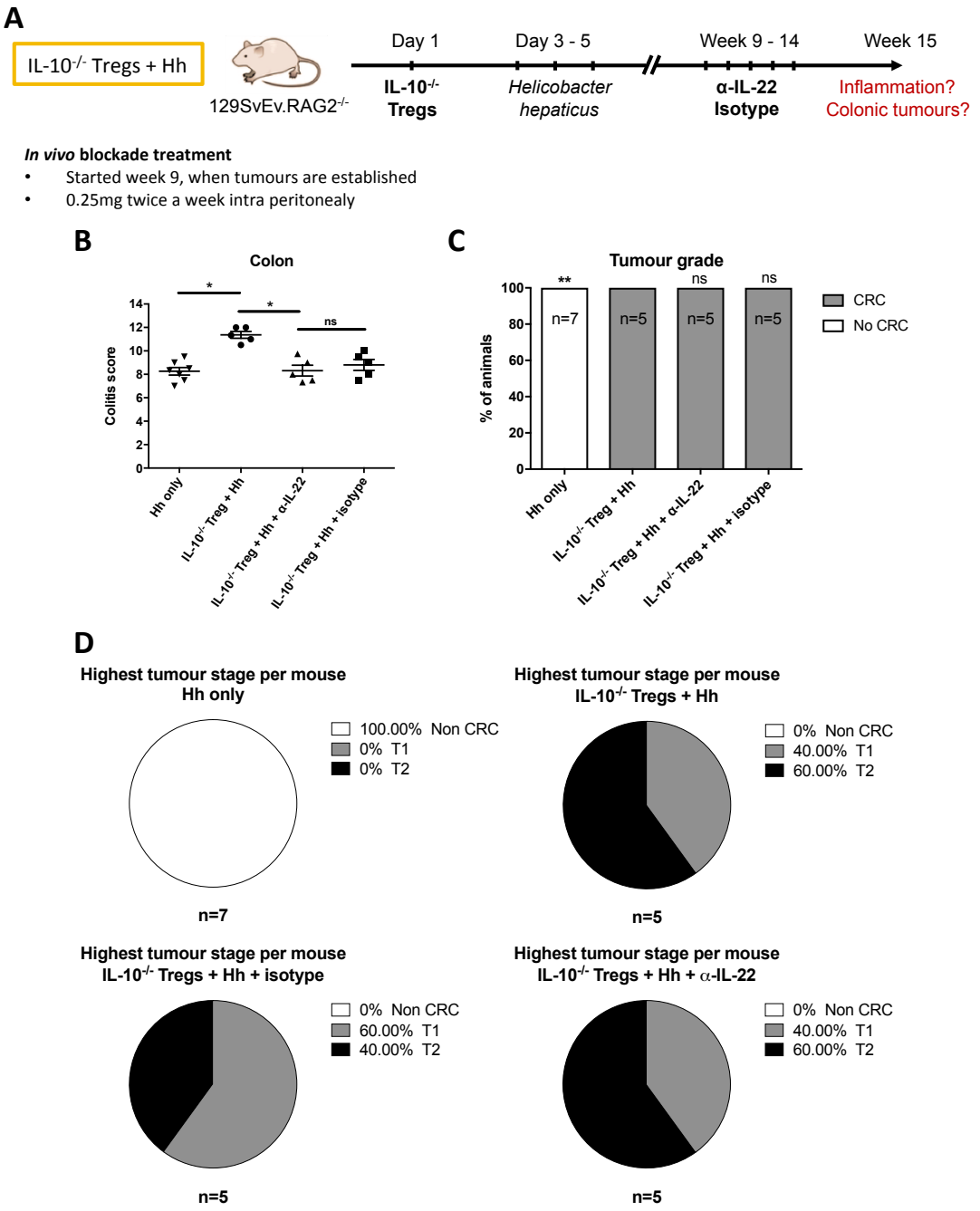

Figure 4.4: IL-22 is dispensable for tumour maintenance and progression.

129.RAG$^{-/-}$ were injected with IL-10$^{-/-}$ Tregs and infected with *Hh*. After 9 weeks, mice were treated for 5 weeks with an isotype control or an anti-IL-22 blocking antibody. At week 15, mice were sacrificed and colons harvested for histopathological analyses.

(A) Scheme of the experimental set-up and treatment.
(B) Colitis score across experimental groups.
(C) Percentage of mice developing colonic tumours across group.
(D) Pie chart showing the distribution of adenocarcinoma stages across groups. When multiple tumours are found, the highest tumour stage per mouse is displayed.

Each dot represents a mouse and bars represent mean ±SEM. Data represents one experiment performed at the KIR with the Powrie colony.
Statistical significance was determined using (B) a Kruskal-Wallis one-way analysis of variance, followed by a Dunn's post-hoc test and (C) a Fisher's exact test with IL-10$^{-/-}$ Treg + *Hh* group as control (two sided). * $p \leq 0.05$, ** $p \leq 0.01$.

4.2.3 IL-6, Areg, and TGF-β are increased in tumour-bearing mice

Given that the IL-22 pathway was dispensable for tumour development and maintenance, we next sought to explore the role of other cytokines in bacteria-driven cancer. Whole colonic tissue gene expression was assessed by qPCR, comparing *Hh* only, WT Tregs + *Hh* and IL-10$^{-/-}$ Tregs + *Hh* groups, to understand global differences between homeostasis, inflammation and malignancy.

Several cytokines were upregulated at the transcriptional level in tumour-bearing mice, when compared to non-inflamed animals (WT Tregs + *Hh* group), most likely reflecting the overall inflammatory status. Therefore, we focused on differences between inflamed and tumour-bearing animals (*Hh* only versus IL-10$^{-/-}$ Treg + *Hh*). Gene expression of *Ifng, Il17a*, *Il1b*, *Tnfa* (**Figure 4.5 A**), as well as *Tgfb* (**Figure 4.5 B, left**) did not vary between *Hh* only and IL-10$^{-/-}$ Tregs + *Hh* groups. By contrast, a significant increase of *Il6* levels was detected in tumour-bearing animals (**Figure 4.5 B, middle**). Given that *Il6* was the only upregulated cytokine detected, we next assessed expression of other *Il6* family members. *Osm* expression was significantly increased in inflamed versus non-inflamed animals, but no differences were found between inflamed and tumour-bearing mice (p=0.062) (**Figure 4.5 B, middle**). A significant increase in *Il11* levels was detected in *Hh* only infected animals, compared to the other groups (**Figure 4.5 B, right**). Finally, cytokines involved in wound repair were screened by qPCR. No significant differences were detected for expression of *Egf*, *Tgfa* and *Ereg* (**Figure 4.5 C, left & middle**). By contrast, *Areg* transcripts were specifically upregulated in tumour bearing mice, as well as in inflamed animals (i.e. *Hh* only versus WT Tregs + *Hh*) (**Figure 4.5 C, right**).

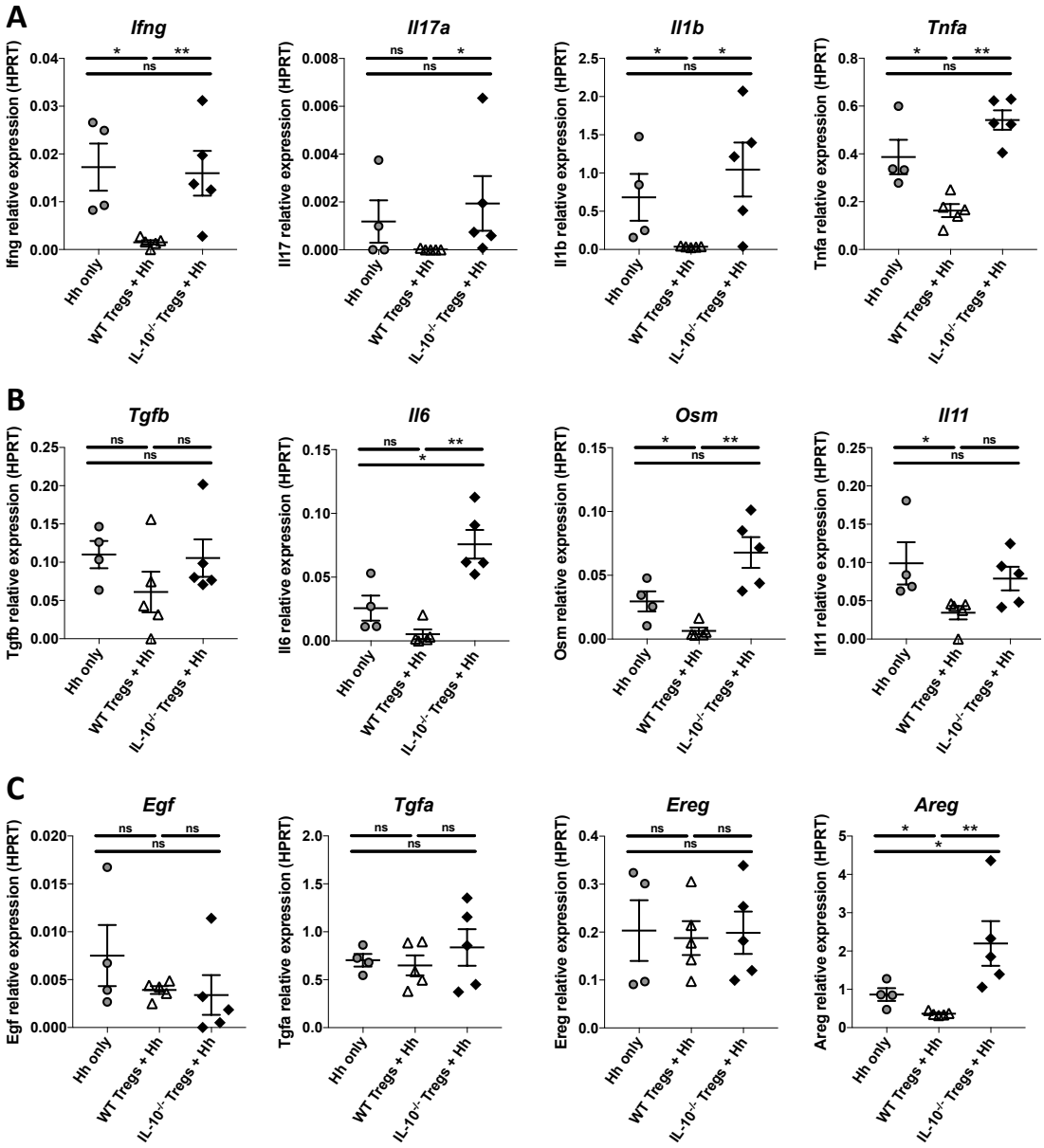

Figure 4.5: Whole tissue mRNA expression of Il6 and Areg is specifically upregulated in tumour-bearing mice.

Mice from indicated experimental groups were sacrificed, and pieces of proximal and middle colons were dissected out and stored in -80°C. RNA was extracted for subsequent RT-qPCR. Relative expression levels were calculated using the $2^{(-\Delta\Delta CT)}$ method, normalising to the housekeeping gene *Hprt*.

(A) mRNA expression of *Ifng*, *Il17*, *Il1b* and *Tnfa*.
(B) mRNA expression of *Tgfb*, *Il6*, *Osm* and *Il11*.
(C) mRNA expression of *Egf*, *Tgfa*, *Ereg* and *Areg*.

Each dot represents a mouse and bars represent mean ±SEM. Data represents one experiment performed at the JR with the Powrie colony, representative of 2.
Statistical significance was determined using a Kruskal-Wallis one-way analysis of variance, followed by a Dunn's post-hoc test. * $p \leq 0.05$, ** $p \leq 0.01$.

Next, we investigated whether these cytokines and others were similarly increased at the protein level in the IL-10$^{-/-}$ Tregs + *Hh* group. We detected cytokine secretion in the colonic lamina propria leukocyte (LPL) fraction and in whole cultured explants. Cytokines were either detected by ELISA or by Bender assays.

First, we measured IFN-γ, IL-17A, TNF-α, and IL-1β secretion. We detected significantly increased production of these cytokines in LPLs of inflamed mice, with no enrichment in tumour-bearing animals (**Figure 4.6 A and B, right**). Surprisingly, although IL-6 levels were significantly increased in inflamed animals, there was no differences between colitic and tumour-bearing mice (**Figure 4.6 B, middle**). Finally, mirroring gene expression results, Areg production was significantly increased in tumour-bearing mice (**Figure 4.6 B, left**). TGF-β was not detected in LPL supernatant (data not shown).

Although *Il6* gene expression was significantly increased in tumour-bearing mice, we failed to detect increased IL-6 production in LPLs. Given that whole colons were used to assess gene expression levels; we also measured cytokine production in whole explants. In this setting, we detected increased IL-6 production in inflamed mice compared to non-inflamed (**Figure 4.7 A**). Furthermore, a significant increased of IL-6 production was also detected in whole tissue of tumour-bearing mice, compared to *Hh* injected animals (**Figure 4.7 A**).

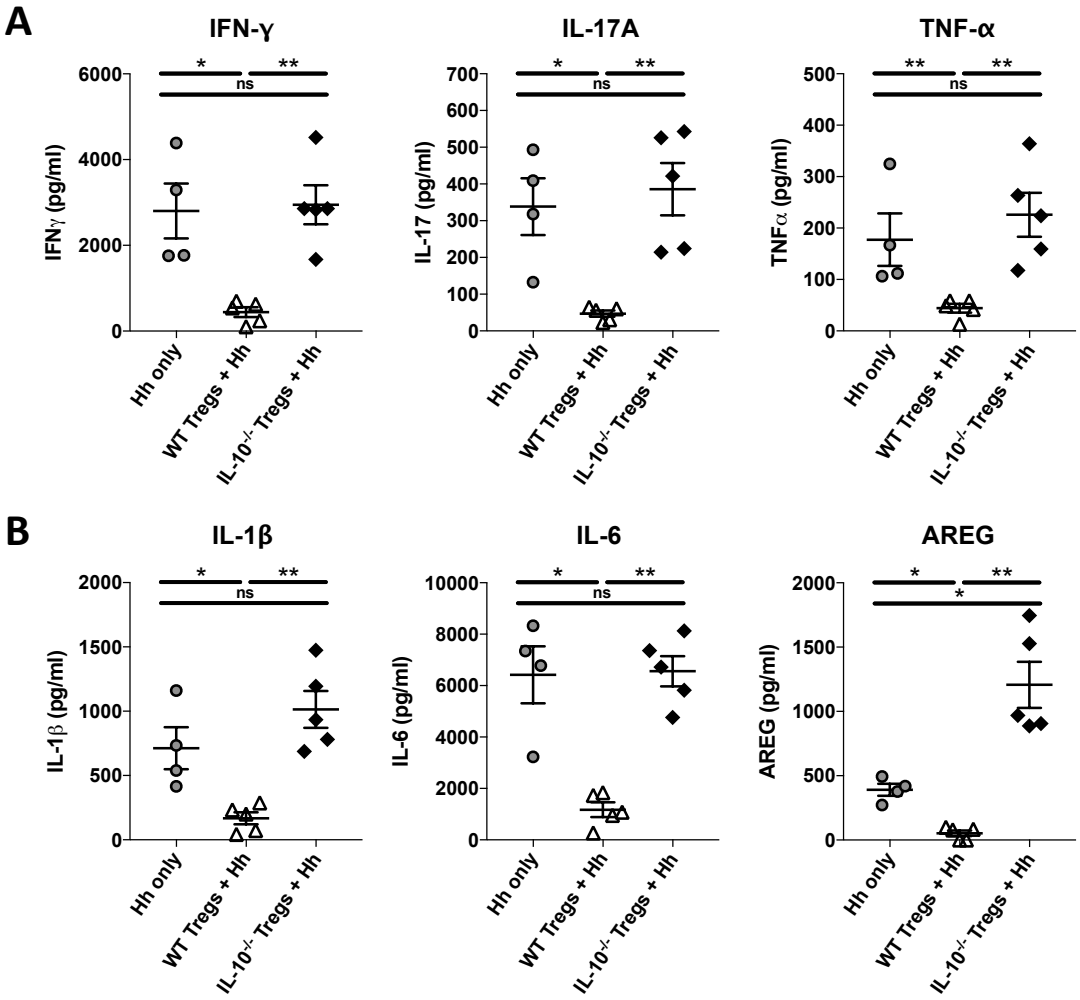

Figure 4.6: AREG production is increased in LPLs of tumour-bearing mice.

Mice from indicated experimental groups were sacrificed, and colons taken for LPL preparation. Single cell suspensions were incubated in media for 12h at 37°C. Supernatants were harvested and used for subsequent cytokine measurements by Bender assays.

(A) LPLs production of IFN-γ, IL-17A and TNF-α for the indicated experimental groups.
(B) LPLs production of IL-1β, IL-6 and AREG for the indicated experimental groups.

Each dot represents a mouse and bars represent mean ±SEM. Data represents one experiment performed at the JR with the Powrie colony and is representative of 2 performed. Statistical significance was determined using a Kruskal-Wallis one-way analysis of variance, followed by a Dunn's post-hoc test. * $p \leq 0.05$, ** $p \leq 0.01$.

Analysis of TGF-β production showed no difference between *Hh* only and WT Treg + *Hh* groups (**Figure 4.7 B**). By contrast, TGF-β was strongly produced in whole tissue of tumour-bearing mice (**Figure 4.7 B**). Finally, we sought to establish whether production of IL-10 was different in Treg transferred mice. IL-10 was detected by ELISA on whole tissue across all groups at similar levels (**Figure 4.7 C**), and is most likely produced by various cells of the immune system, which include macrophages and dendritic cells (reviewed in Margarida Saraiva and Anne O'Garra, 2010).

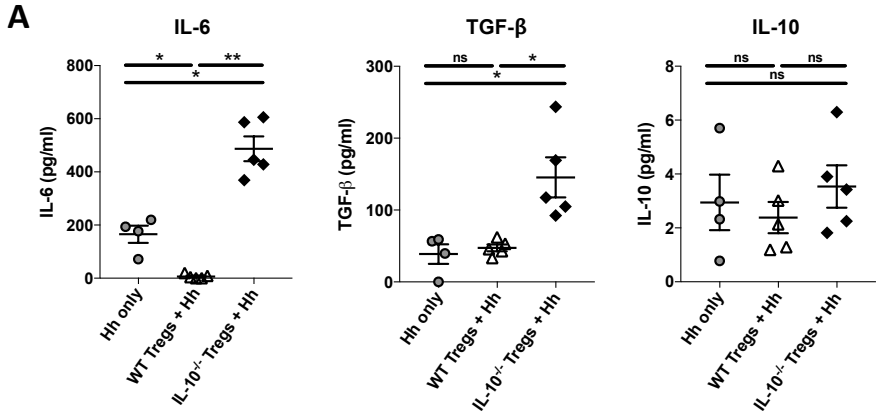

Figure 4.7: IL-6 and TGF-β production is increased in whole tissue explants of tumour-bearing mice.

Mice from indicated experimental groups were sacrificed, and pieces of proximal and middle colons were dissected out, weighed and incubated for 12h at 37°C. Supernatants were harvested and used for subsequent indicated cytokine measurements by bender assays (IL-6, TGF-β), and ELISA (IL-10), normalised to tissue weight.

Each dot represents a mouse and bars represent mean ±SEM. Data represents one experiment performed at the JR with the Powrie colony and is representative of 2 performed. Statistical significance was determined using a Kruskal-Wallis one-way analysis of variance, followed by a Dunn's post-hoc test. * $p \leq 0.05$, ** $p \leq 0.01$.

Table 4.1 summarises cytokines that are upregulated in inflammation and tumours, both at the mRNA and protein levels.

	mRNA		Protein	
	Inflammation	**Tumours**	**Inflammation**	**Tumours**
IFN-γ	+	ns	+	ns
IL-17A	ns	ns	+	ns
IL-1β	+	ns	+	ns
TNF-α	+	ns	+	ns
IL-6	ns	+	+	+
Osm	+	ns	n/a	n/a
IL-11	+	ns	n/a	n/a
TGF-β	ns	ns	ns	+
Ereg	ns	ns	n/a	n/a
TGF-α	ns	ns	n/a	n/a
EGF	ns	ns	n/a	n/a
AREG	+	+	+	+
IL-10	n/a	n/a	ns	ns

Table 4.1: Summary of upregulated cytokines in inflammation versus tumours, from whole tissue gene expression, and protein secretion from LPLs and whole tissue.

Inflammation compares differences between *Hh* and WT Tregs + *Hh* groups.
Tumours compares differences between *Hh* and IL-10$^{-/-}$ Tregs + *Hh* groups.

Legends:
- "+" denotes a significant increase in expression.
- "ns" denotes a non-significant difference in gene expression.
- "n/a" is used for assays that have not been run for the indicated cytokines.

Collectively, these results have highlighted a potential role for IL-6, Areg, and TGF-β in driving tumourigenesis in IL-10$^{-/-}$ Tregs + *Hh* mice. Other cytokines, such as IFN-γ, IL-17A, TNF-α, and IL-1β are more likely to promote a global inflammatory milieu, rather than being actively involved in tumour development.

4.2.4 Gp38^{+} stromal cells are main producers of inflammatory cytokines in tumour-bearing mice

We next focused on the cytokines that we identified to be upregulated in tumour-bearing mice. Various cell types can produce IL-6, TGF-β and Areg during inflammation and CRC. Therefore, taking a FACS sorting approach, we wanted to identify the major cellular source of each cytokine. Briefly, at week 12, mice were sacrificed and colons removed for LPL preparation and stained for FACS sorting. Endothelial cells (CD45^{-} EpCAM^{-} CD31^{+}), fibroblasts (CD45^{-} EpCAM^{-} CD31^{-} gp38^{+}), double negative cells (CD45^{-} EpCAM^{-} CD31^{-} gp38^{-}) as well as broad myeloid cells (CD45^{+} CD3^{-} MHCII^{+}) were FACS-sorted from the 40/70% gradient interphase. Eosinophils (CD45^{+} CD3^{-} CD11b^{+} Gr1^{-} Siglec-F^{+}), neutrophils (CD45^{+} CD3^{-} CD11b^{+} Gr1^{+} Siglec-F^{-}) and CD4^{+} T cells were FACS sorted from the 30/40% gradient interphase. Expression of key lineage-specific genes was assessed by qPCR to confirm the purity of FACS-sorted cell types isolated from mouse colonic tissue (**Figure 4.8 A**).

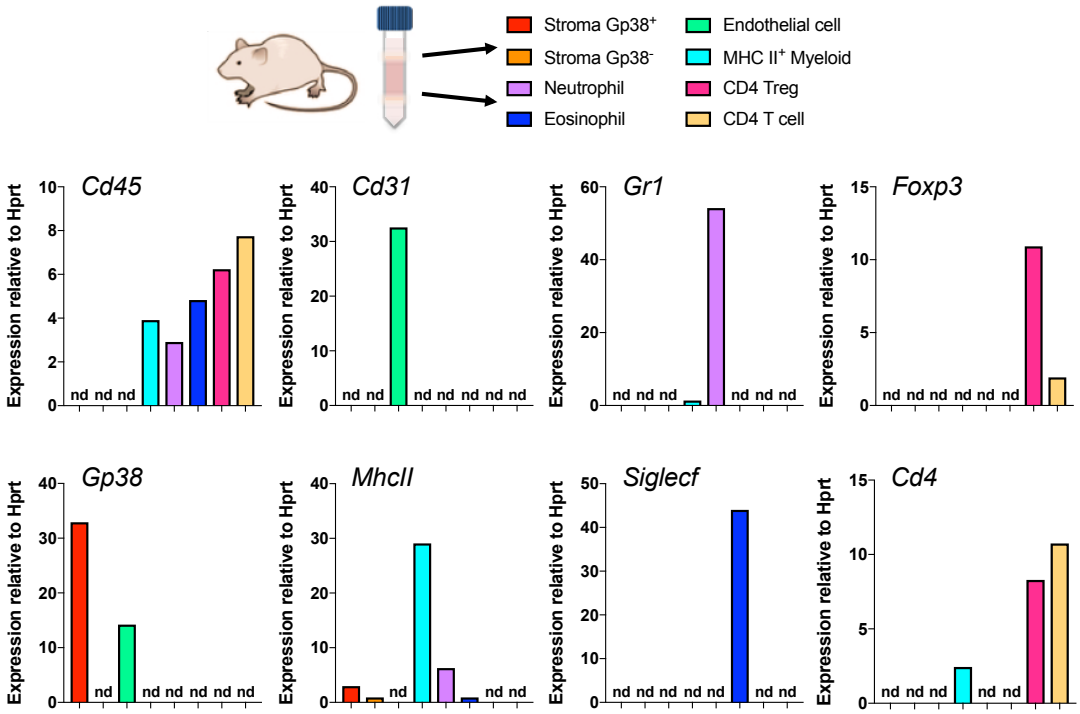

Figure 4.8: Expression of key lineage-specific genes confirms the purity of FACS-sorted cell types.

Mice from the different experimental groups were sacrificed, and colons were taken for preparation of single cell suspensions.
The 30/40% gradient interphase (enriched in stromal cells) was used to FACS-sort Gp38 positive and negative stromal cells, $CD31^{+}$ endothelial cells, and MHC II^{+} myeloid cells (including macrophages, dendritic cells, and inflammatory monocytes).
The 40/70% gradient interphase (enriched in LPLs) was used to FACS-sort $Gr1^{+}$ neutrophils, Siglec-F^{+} eosinophils, $CD4^{+}$ $CD25^{hi}$ $CD45RB^{low}$ enriched Treg fraction, and $CD4^{+}$ $CD25^{low}$ $CD45RB^{low}$ enriched CD4 T effector lymphocytes.
RNA was extracted for subsequent qPCR. Relative expression levels were calculated using the $2^{(-\Delta\Delta CT)}$ method, normalising to the housekeeper gene *Hprt*. Expression of indicated lineage-specific genes was assessed by qPCR to confirm the purity of FACS-sorted cell types isolated from mouse colon tissue, with "nd" denoting not detected.

Data represents FACS-sorted populations from pooled samples of IL-$10^{-/-}$ Tregs + *Hh* mice (n=3), and is representative of the other experimental groups.
Data is representative of two experiments performed at the KIR with the Powrie and Maloy colony (i.e. at times of potential dysbiosis).

Differences in expression of key cytokines both across sorted cell population and across experimental groups were investigated. First, we explored cytokine expression across cell populations in tumour-bearing mice. Secondly, once populations of interest were defined, we compared their cytokine expression across experimental groups, to further establish the relevance in disease pathogenesis.

In tumour-bearing mice, $Gp38^+$ stromal cells, $CD31^+$ endothelial cells, and $MHCII^+$ innate cells were major *Il6* expressers. Moreover, we found that $Gp38^+$ stromal cells have significantly increased levels of *Il6*, compared to $CD31^+$ and $MHCII^+$ cell populations (**Figure 4.9 A**). We also explored *Tnfa* gene expression amongst FACS-sorted populations as a control, and observed that $Gp38^+$ stromal cells and $MHCII^+$ myeloid cells were major producers of *Tnfa,* however, with no significant differences between the two populations (**Figure 4.9 B**). Next, we analysed *Areg* expression and detected its expression across all sorted cell populations, aside from neutrophils (**Figure 4.9 C**). Both Gp38 positive and negative stromal populations expressed high amounts of *Areg*, however the $Gp38^+$ cells showed significantly higher expression compared to other cells. Finally, we evaluated *Tgfb* expression across cell populations. Expression was variable across cell populations and no real differences were uncovered, apart from an increase in *Tgfb* expression in the $Gp38^+$ stromal cells, compared to the $Gp38^-$ cells (**Figure 4.9 D**).

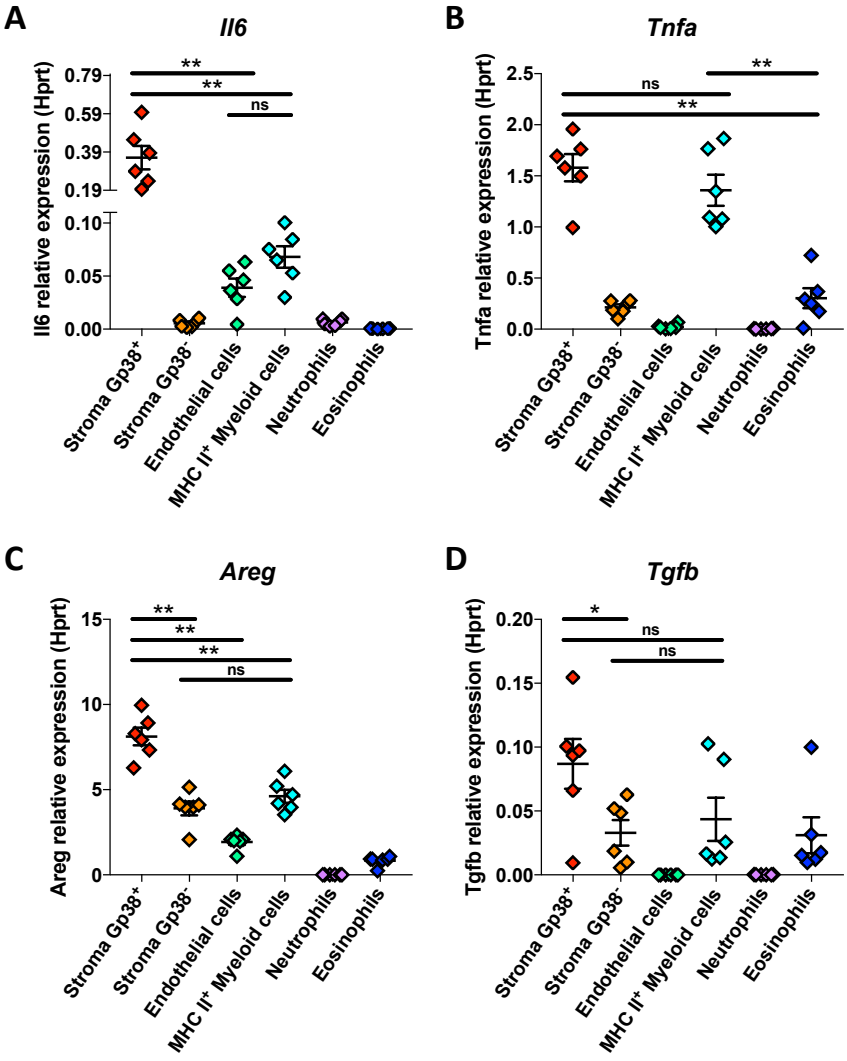

Figure 4.9: Gp38 positive stromal cells are major producers of *Il6*, *Tnfa* and *Areg*.

IL-10$^{-/-}$ Tregs + *Hh* mice were sacrificed, and colons were harvested for preparation of single cell suspensions. Indicated populations were FACS-sorted and RNA was extracted for subsequent qPCR. Relative expression levels were calculated using the $2^{(-\Delta\Delta CT)}$ method, normalised to the housekeeping gene *Hprt*.

(A-D) *Il6, Tnfa, Areg* and *Tgfb* mRNA expression across FACS-sorted populations.

Each dot represents a mouse and bars represent mean ±SEM. Data represents one experiment performed at the KIR with the Powrie colony.
Statistical significance was determined using multiple Mann–Whitney U tests. * $p \leq 0.05$, ** $p \leq 0.01$.

Having established that Gp38^{+} stromal cells and MHCII^{+} innate cells are major expressers of *Il6* and *Areg*, we sought to explore whether expression of these cytokines changes amongst the experimental groups.

Overall, *Il6* expression levels in Gp38^{+} cells were significantly increased in tumour-bearing mice (**Figure 4.10 A, left**). However, similar *Il6* expression was detected in MHCII^{+} populations across the experimental groups (**Figure 4.10 A, right**). *Tnfa* transcripts were equally expressed in Gp38^{+} and MHCII^{+} cells across experimental groups (**Figure 4.10 B**). We next investigated *Areg* expression in stromal, endothelial and innate cells. Interestingly, both Gp38^{+} and Gp38^{-} stromal cells from tumour-bearing animals displayed significant increased *Areg* expression, albeit at lower levels in Gp38^{-} cells (**Figure 4.10 C**). Although CD31^{+} endothelial cells expressed *Areg*, no significant differences were found between experimental groups (**Figure 4.10 D, right**). Finally, MHCII^{+} cells from the IL-10$^{-/-}$ Tregs + *Hh* group also displayed a significant increase in *Areg* transcripts compared to control groups (**Figure 4.10 D, left**). *Tgfb* expression was also assessed across groups, though no differences were detected between the different groups (data not shown).

Altogether, these results emphasise the potential roles for both stromal cells and MHCII^{+} innate cells in promoting tumour development through *Il6* and *Areg* expression. It remains to be determined which cell population produces TGF-β, though it is likely that tumour cells themselves may be a cellular source.

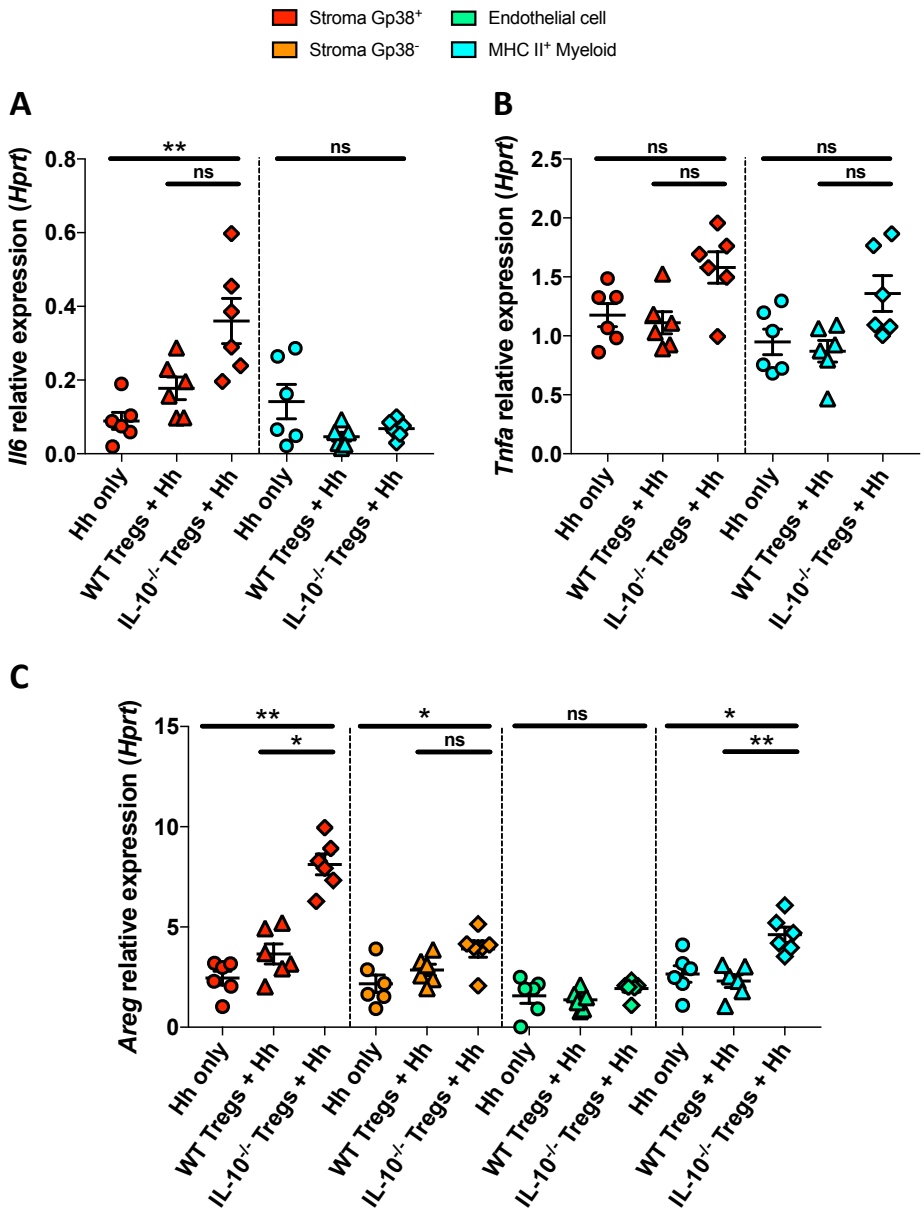

Figure 4.10: Stromal cells from tumour bearing have increased expression of *Il6* and *Areg*.

Mice from indicated experimental groups were sacrificed, and colons were harvested for preparation of single cell suspensions. Indicated cell populations were FACS-sorted and RNA was extracted for subsequent qPCR. Relative expression levels were calculated using the $2^{(-\Delta\Delta CT)}$ method, normalising to the housekeeping gene *Hprt*.

(A) *Il6* mRNA expression in Gp38$^+$ stromal cells (red) and MHCII$^+$ cells (blue) across experimental groups.
(B) *Tnfa* mRNA expression in Gp38$^+$ stromal cells (red) and MHCII$^+$ cells (blue) across experimental groups.
(C) *Areg* mRNA expression in Gp38$^+$ stromal cells (red), Gp38$^-$ stromal cells (orange), CD31$^+$ endothelial cells (green) and MHCII$^+$ cells (blue) across experimental groups.

Each dot represents a mouse and bars represent mean ±SEM. Data represents one experiment performed at the KIR with the Powrie colony.
Statistical significance was determined using a Kruskal-Wallis one-way analysis of variance, followed by a Dunn's post-hoc test. * $p \leq 0.05$, ** $p \leq 0.01$.

4.2.5 IL-6 and TGF-β *in vivo* blockade decreases tumourigenesis

Having established that IL-22 is dispensable for tumourigenesis, we next investigated whether IL-6 and TGF-β might be involved in tumourigenesis, as both of these cytokines were increased in tumour-bearing mice compared to colitic mice.

One difficulty in testing the role of these cytokines is that few KO mice are available on the 129.SvEv background. Therefore instead, we used blocking antibodies, at the time of early tumour onset (**Figure 4.11 A**). Of note, no blocking antibody for Amphiregulin was available at time of this study, and therefore it remains to be determined whether this cytokine is involved in disease promotion.

To test the functional role of IL-6 and TGF-β, 129.RAG$^{-/-}$ were injected with IL-10$^{-/-}$ Treg and infected with *H. hepaticus*. At week 9, when tumours are established, anti-IL-6-R, anti-TGF-β, or isotype control monoclonal antibodies were administered for 5 consecutive weeks. After 15 weeks, mice were sacrificed and colitis and tumourigenesis were assessed. The experimal scheme of the experiment is outlined in **Figure 4.11 A**. Of note, a general improvement of body appearance, associated with a weight gain was observed in the anti-IL-6-R treated mice.

First, we analysed the colitis score (**Figure 4.11 B**). Strikingly, only the anti-IL-6-R treatment led to a significant decrease of colitis, with an average score of approximately 3 out of 12. By contrast, anti-TGF-β treated mice displayed no significant difference in the colitis score compared to the isotype-treated group (IL-10$^{-/-}$ Tregs + *Hh* group).

Next, we investigated tumour burden following treatment. Around 90% of the animals in the IL-10$^{-/-}$ Tregs + *Hh* isotype treated group developed colonic tumours (**Figure 4.11 C**). Anti-IL-6-R treated animals showed reduced tumour burden in the colon. As 70% of the animals were tumour free, highlighting the key role of IL-6 in tumour maintenance. The anti-TGF-β treatment also led to a reduction in tumour burden, despite the relatively high colitis score in this group (**Figure 4.11 C**).

We next focused on the tumour stage distribution of mice that were not tumour-free. Mice from the anti-IL-6-R group only displayed T1 adenocarcinomas, with one tumour per mouse on average (**Figure 4.11 D**). By contrast, in the affected mice, the anti-TGF-β treatment led to the development of T2 tumours, including one T3 adenocarcinoma, with multiple tumours per colon (**Figure 4.11 D**).

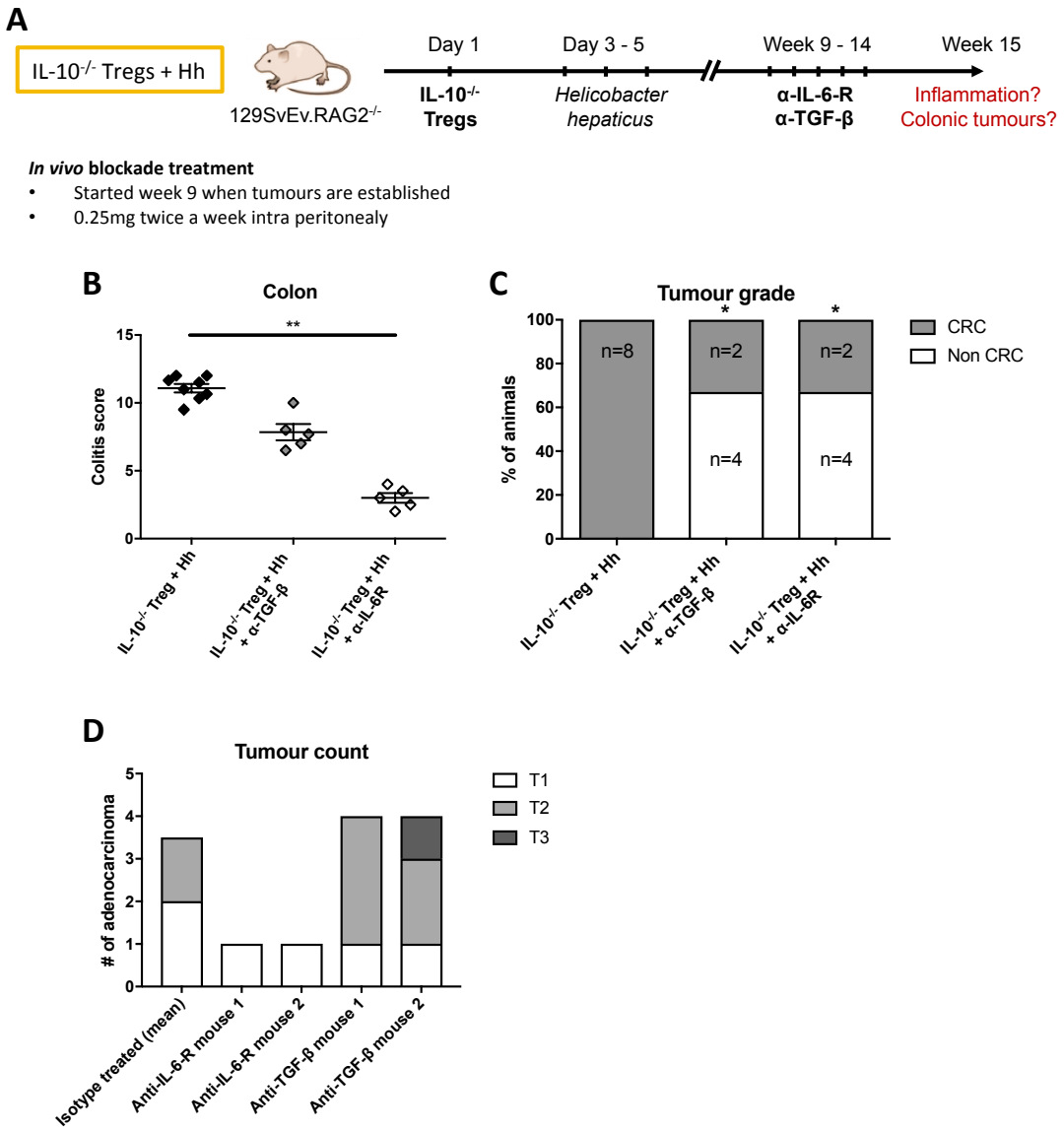

Figure 4.11: Anti-IL-6-R treatment leads to reduced colitis and tumour occurrence, while anti-TGF-β treatment leads to reduced tumour occurrence, while promoting disease progression under certain circumstances.

Mice injected with IL-10$^{-/-}$ Tregs and infected with *H. hepaticus* were treated at week 9 for 5 consecutive weeks with anti-IL-6R or anti-TGFβ blocking antibodies. After treatment, mice were sacrificed, and colons were harvested and assessed for colitis and tumour burden.

(A) Scheme of experiment with anti-IL-6R or anti-TGFβ treatment.
(B) Histological analysis of colonic inflammation in control and treated groups.
(C) Percentage of mice which developed colonic tumours across groups.
(D) Tumour count in mice of T1, T2 and T3 tumours. The average number of T1 and T2 adenocarcinomas is shown for isotype-treated mice.

Each dot represents a mouse and bars represent mean ±SEM. Data represents one experiment performed at the KIR with the Powrie colony, representative of two independent experiments.
Statistical significance was determined using a (B) Kruskal-Wallis one-way analysis of variance, followed by a Dunn's post-hoc test, and (C) a Fisher's exact test with IL-10$^{-/-}$ Tregs + *Hh* isotype group as control (two-sided). * $p \leq 0.05$, ** $p \leq 0.01$.

Altogether, these results suggest that IL-6 is a colitogenic and tumourigenic cytokine. By contrast, TGF-β has a dual action in disease development, which likely depends on its cellular targets, as well as on the disease state and progression at time of treatment.

4.2.6 Stromal cells are a source of pro-tumourigenic IL-6

In tumour-bearing mice, *Il6* transcripts were enriched in the stromal population and anti-IL-6-R *in vivo* blockade has revealed the critical role for this cytokine in sustaining tumour lesions. Therefore, next we focused on characterising IL-6-secreting stromal cells in tumour-bearing mice.

First, frequencies and total number of non-hematopoietic populations were assessed using flow cytometry. Briefly, colons of mice from the different experimental groups were taken at week 12, and the stromal layer was harvested and prepared for single cell suspension. Representative FACS plots, gated on CD45 negative cells, and displaying CD31 and EpCAM expression defined three major cell populations (**Figure 4.12 A**). Epithelial cells were defined by their expression of EpCAM, and their frequency varies accordingly to the relative purity of the colonic preparations (i.e. the epithelium is washed off). The two other populations were defined by CD31 expression: endothelial cells, and absence of expression of both EpCAM and CD31, defining stromal cells. This population of stromal cells is heterogeneous, and contains (myo)-fibroblasts, smooth muscle cells, as well as subepithelial myofibroblasts. In this study, we consider colonic stromal cells as a mixed population and focus on the functional contribution of multiple subsets to disease initiation and progression. The population of colonic stromal cells was further subdivided into

Gp38 (Podoplanin) positive and negative cells (**Figure 4.12 B**). Gp38 is known as a marker of several stromal cell subsets of the lymphoid organs, including the intestine (reviewed in Turley, 2012; Vicente-Suarez et al., 2014), however recent work from our laboratory may rather attribute its expression to an activation state of the stromal compartment.

Similar frequencies of $EpCAM^{-}$ $CD45^{-}$ mesenchymal cells were found across experimental groups (**Figure 4.12 C**), included in steady state controls (horizontal dotted bar), while total number were significantly increased in IL-$10^{-/-}$ Tregs + *Hh* mice compared to the WT Tregs + *Hh* group (**Figure 4.12 G**). We did not detect differences in frequencies and total cell number of $CD31^{+}$ endothelial cells (**Figure 4.12 D, H**) and $Gp38^{-}$ stromal cells (**Figure 4.12 F, J**). However, although there was no difference in frequencies of $Gp38^{+}$ stromal cells, their total number was increased in IL-$10^{-/-}$ Tregs + *Hh* group compared to WT Tregs + *Hh* group (**Figure 4.12 E, I**). However, a caveat of these studies is that calculated frequencies depends heavily on the efficiency of tissue digestion, and leads to discrepencies between the inflammation state of the colon as well as between independent experiments.

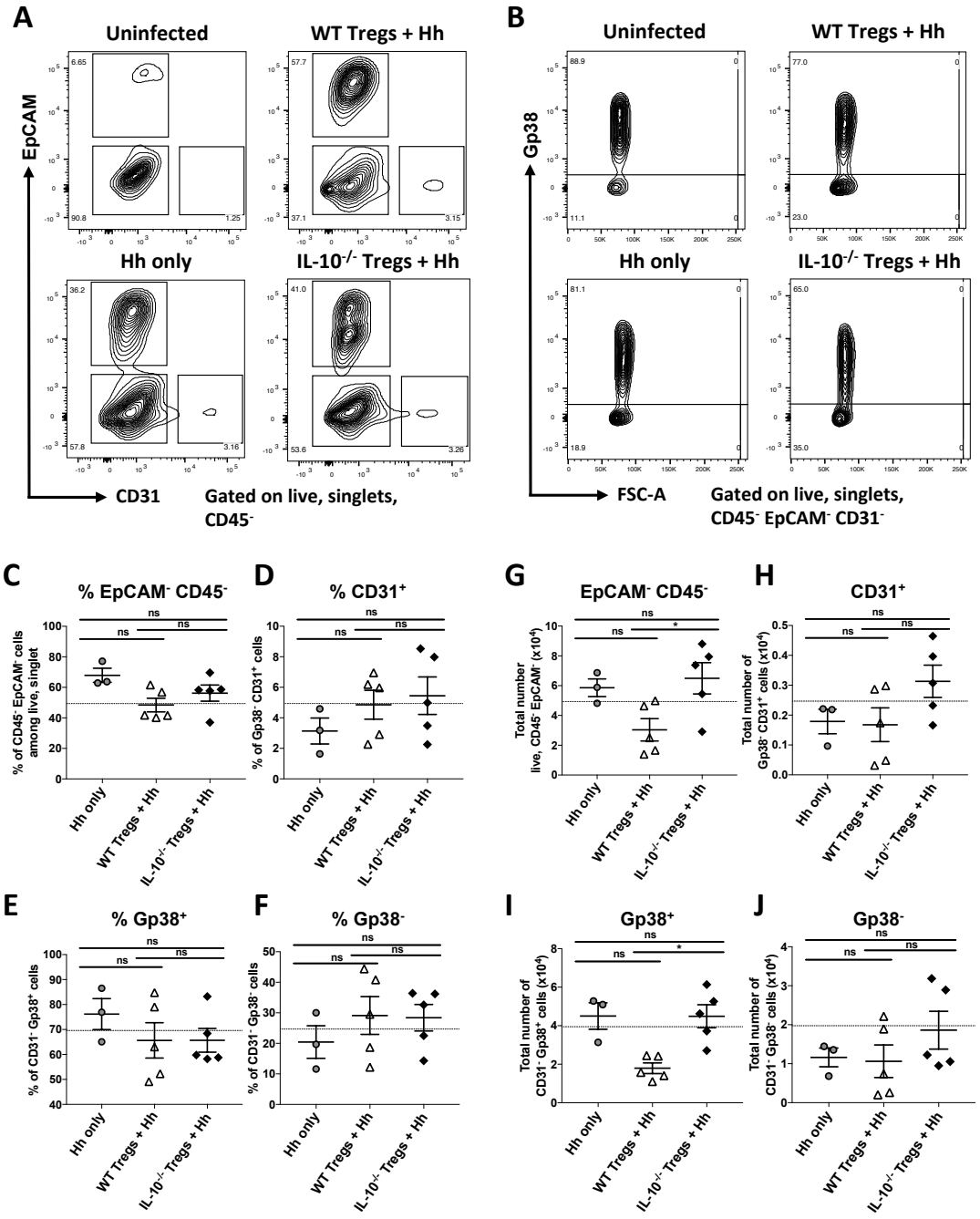

Figure 4.12: Similar frequencies and total cell number of mesenchymal cells are found between experimental groups in whole colon analysis.

Hh infected only, WT Tregs + *Hh* and IL-10$^{-/-}$ Tregs + *Hh* recipients were sacrificed at week 12. Colons were harvested, and single cell suspensions were analysed by flow cytometry.

(A) Representative FACS plots of non-hematopoietic colonic cells of indicated groups, gated on live, singlets and CD45^{-} cells. EpCAM vs CD31 defines epithelial cells (EpCAM^{+}), endothelial cells (CD31^{+}) and stromal cells (EpCAM^{-} CD31^{-}).
(B) Representative FACS plots of colonic stromal cells of indicated groups.
(C-F) Frequencies of indicated populations across experimental groups.
(G-I) Total number of indicated populations across experimental groups.

Each dot represents a mouse and bars represent mean ±SEM. Data represents one experiment performed at the KIR with the Powrie colony.
Statistical significance was determined using a Kruskal-Wallis one-way analysis of variance, followed by a Dunn's post-hoc test. * $p \leq 0.05$.

Next, we explored cytokine production, mainly focusing on IL-6. $Gp38^{+}$ stromal cells largely expressed ICAM1, and produced IL-6 (**Figure 4.13 A**). Frequencies of IL-6 producing cells revealed a significant increase in $IL\text{-}10^{-/-}$ Tregs + *Hh* mice compared to *Hh* only animals (**Figure 4.13 B**). Although a trend towards increased total number of IL-6 producing $Gp38^{+}$ cells was seen when comparing tumour-bearing versus colitic mice, the only significant difference was detected between $IL\text{-}10^{-/-}$ Tregs + *Hh* and WT Tregs + *Hh* groups (**Figure 4.13 C**). TNF-α and GM-CSF production was equally detected in $Gp38^{+}$ cells, however at similar frequencies and total number across experimental groups (data not shown). By contrast, $Gp38^{-}$ stromal cells and endothelial cells both produced small amount of IL-6 and TNF-α, but overall to similar frequencies and total numbers between groups (**Figure 4.13 D, E** and data not shown). While cytokine-producing cells mainly expressed ICAM1, there was no difference in its expression on mesenchymal populations between groups (data not shown).

We found large variation in frequencies of non-hematopoietic populations in inflamed and tumour-bearing animals across our experiments, likely indicating that tissue digestion was not always identical and potentially less efficient as inflammation increases, leading to major differences in our analyses. Accordingly, the total number of cells was also subjected to variations. Moreover, given that whole colons were used for this analysis, it is not possible to clearly determine whether the stromal compartment is enriched in tumours versus inflamed mucosae. Therefore, *in situ* approaches would be more conclusive.

Our results confirmed IL-6 production in the Gp38^{+} stromal compartment, thereby establishing this population as a critical player in inflammation and tumourigenesis.

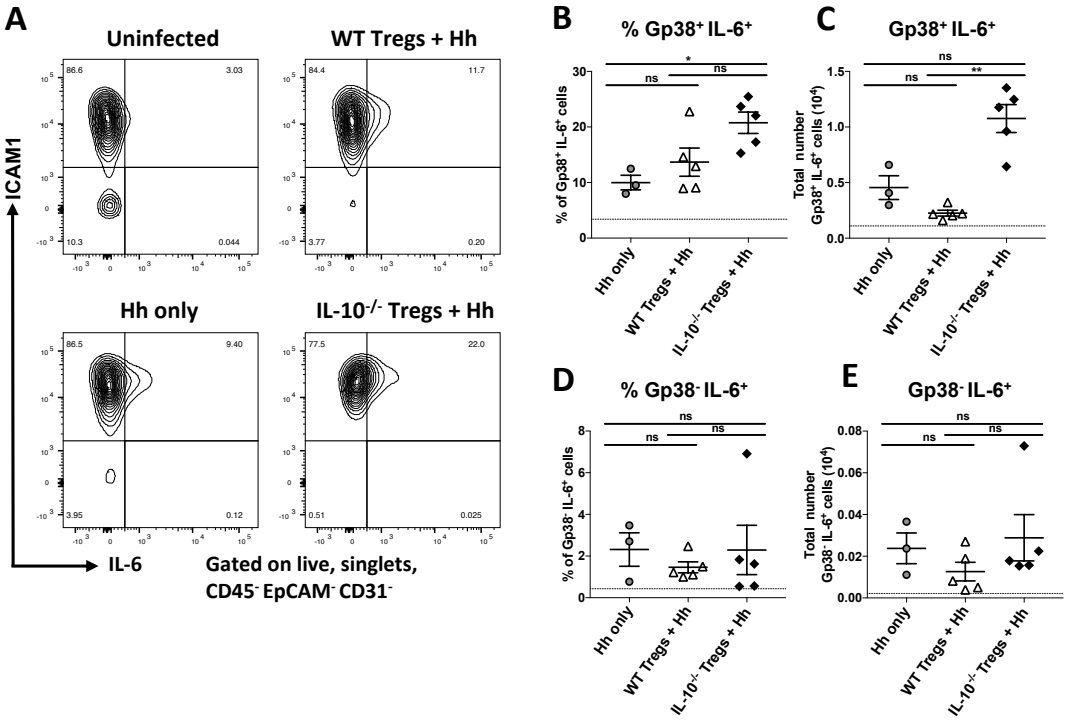

Figure 4.13: Gp38^{+} stromal cells are main producers of the pro-inflammatory and pro-tumourigenic cytokine IL-6.

Hh infected only, WT Tregs + *Hh* and IL-10$^{-/-}$ Tregs + *Hh* recipients were sacrificed at week 12. Colons were harvested, and single cell suspensions were analysed by flow cytometry.

(A) Representative FACS plots of IL-6 and ICAM1 expression in Gp38^{+} stromal cells in the colon of indicated groups.
(B, C) Frequencies (B) and total number (C) of IL-6 producing Gp38^{+} stromal cells in indicated groups.
(D, E) Frequencies (D) and total number (E) of IL-6 producing Gp38^{-} stromal cells in indicated groups.

Each dot represents a mouse and bars represent mean ±SEM. Data represents one experiment performed at the KIR with the Maloy colony.
Statistical significance was determined using a Kruskal-Wallis one-way analysis of variance, followed by a Dunn's post-hoc test. * $p \leq 0.05$, ** $p \leq 0.01$.

4.2.7 Tumours are surrounded by a network of collagen

At week 12, colons of inflamed animals displayed a loss of flexibility and general thickening of the organ, which resembled fibrosis. Moreover, histologically, markers of severe inflammation were present in inflamed and tumour-bearing mice, and corresponded to extensive submucosal inflammation, bleeding and oedemas. Therefore, we first qualitatively assessed collagen deposition in the mucosa as a measure of ECM deposition and fibroblast activation. Paraffin embedded sections were selected and stained with Picro-Sirius Red, allowing for direct visualisation of collagen deposition *in situ*. In bright field microscopy, cell components, muscular fibres and red blood cells are stained in yellow, while collagen fibres appear in red.

Uninfected 129.RAG$^{-/-}$ and WT Tregs + *Hh* animals showed a thin and sporadic collagen deposition in the lamina propria, while the muscularis mucosae displayed a thin collagen network, potentially staining basement membranes, lymphatics and blood capillaries (**Figure 4.14 A, B**). *Hh* only and IL-10$^{-/-}$ Tregs + *Hh* mice showed increased deposition of collagen in the lamina propria at sites of inflammation, attested by the presence of collagen between crypts forming a dense network (**Figure 4.14 C, D, E and F**). In highly inflamed tissue, collagen deposition was especially increased at basement membranes and in subepithelial cells, as well as in the lamina propria and submucosae, forming a dense layer of collagen (**Figure 4.14 F**).

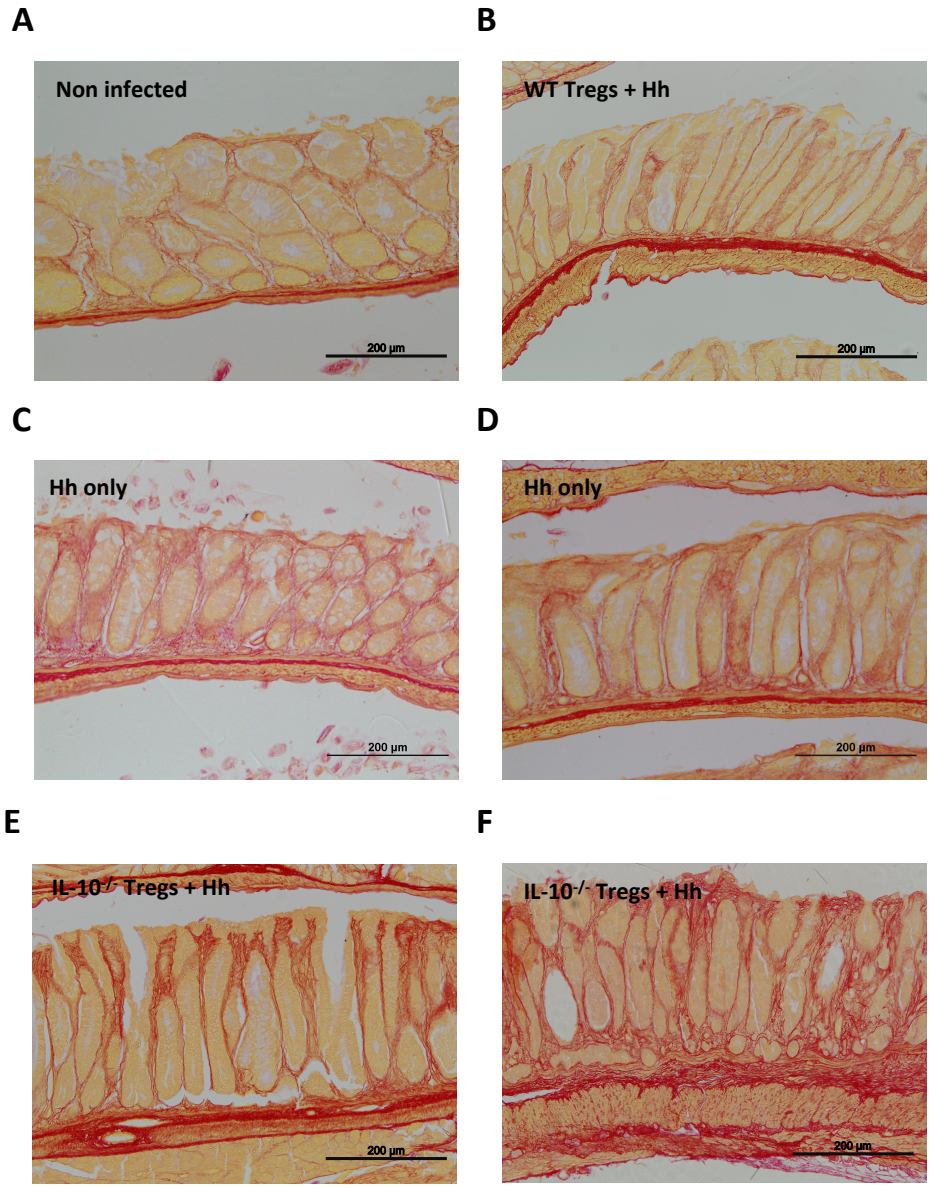

Figure 4.14: Collagen deposition is increased in the colonic epithelium, lamina propria and submucoae regions of inflamed animals.

Sirius Red staining of paraffin embedded colonic sections from indicated experimental groups. Collagen is stained in red.

(A) Representative photomicrograph of uninfected 129.RAG$^{-/-}$, n=3 mice.
(B) Representative photomicrograph of WT Tregs + *Hh* group, n=5 mice.
(C, D) Representative photomicrographs of inflamed *Hh* only animals, n=5 mice.
(E, F) Representative photomicrographs of IL-10$^{-/-}$ Tregs + *Hh* group with (F) highly inflamed portion of the colon, n=7 mice.

Finally, tumours are usually associated with increased ECM deposition, when the chronic tissue repair response arises in the setting of the genetic insult to the functional epithelium. Such enriched collagen zones were found in tumours across experimental groups (**Figure 4.15**). We observed collagen deposition within adenocarcinomas (**Figure 4.15 B-D**), regardless of the stage, including in early lesions (**Figure 4.15 A**). In the long term, mucinous adenocarcinomas seemed to be surrounded by a large collagen capsule (**Figure 4.15 E**).

Collectively, collagen deposition in the lamina propria and between crypts indicated the presence of collagen-producing cells at increased levels in the context of chronic inflammation. Furthermore, collagen was also found within tumours, potentially establishing a supporting a microenvironmental niche for disease progression. Additional experiments will aim at characterising the type of collagen deposited in inflammation versus tumours.

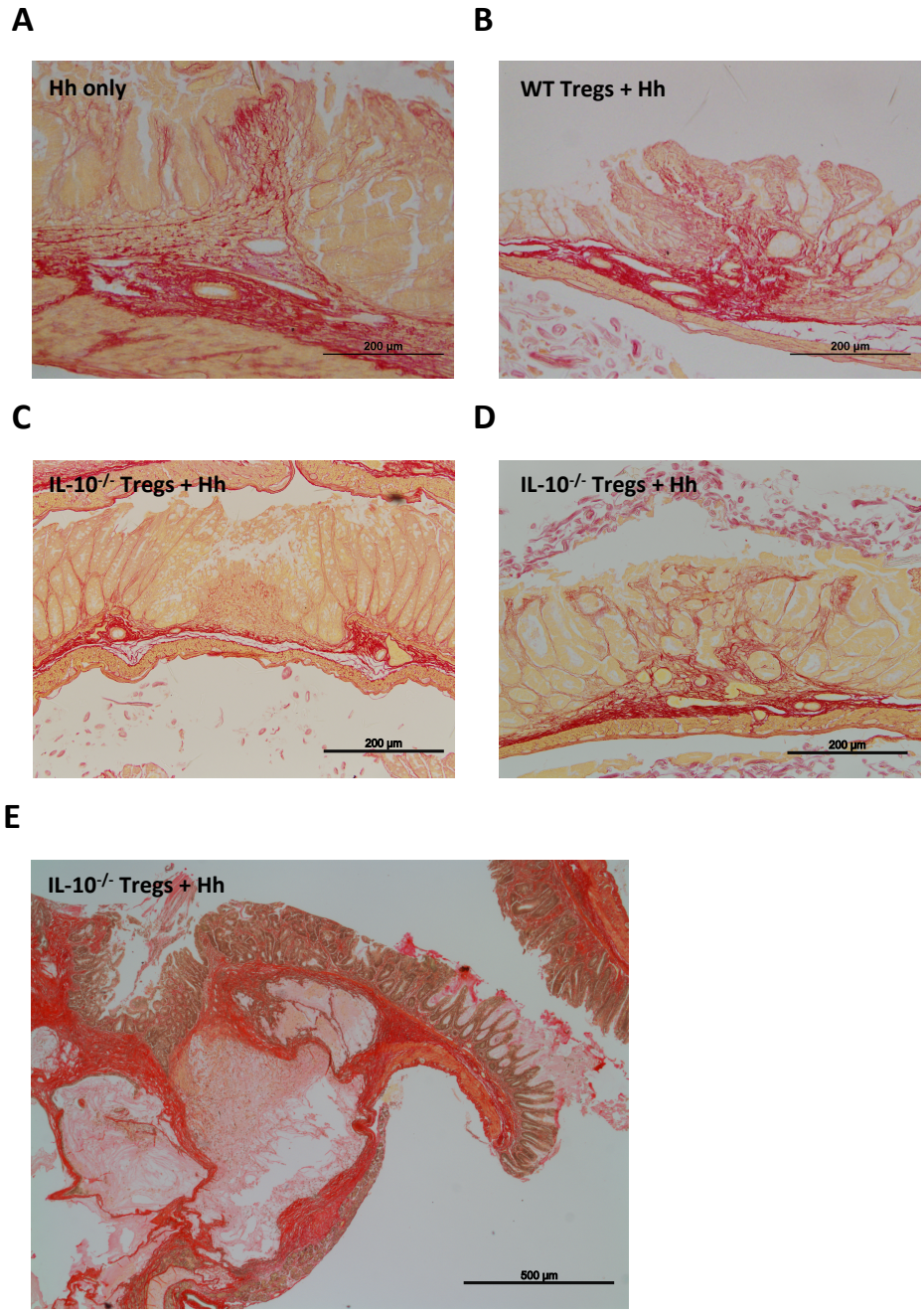

Figure 4.15: Collagen deposition is present within and surrounding tumours of various tumour stages.

Sirius Red staining of paraffin embedded colonic sections containing tumours, for indicated experimental groups. Collagen is stained in red.

(A) Early invasive lesion in *Hh* infected 129.RAG$^{-/-}$.
(B) T1 adenocarcinoma in WT Treg + *Hh* group.
(C, D) T1 adenocarcinoma (C) and T2 adenocarcinoma (D) in IL-10$^{-/-}$ Treg + *Hh* groups.
(E) Sirius Red staining of multiple T2 mucinous adenocarcinomas in the middle colon of IL-10$^{-/-}$ Tregs + *Hh* group, at month 6 of the model.

4.2.8 Gp38-expressing cells are present within adenocarcinomas

Given that tumours were clearly in contact with collagen-producing cells, and that fibroblasts are a primary source of EMT components, we next assessed whether $Gp38^+$ cells were also found in adenocarcinomas.

In situ imaging of the colon tissue provided a better insight into the expression of Gp38 in the tumour microenvironment. Gp38 expression is most intense on lymphatic endothelium and its expression has been reported in steady state colon tissue as well as during colitis (West et al., 2017). Interestingly, Gp38 is also upregulated by cancer-associated fibroblasts in the stroma surrounding various human tumours, including in colorectal cancer (Kitano et al., 2010). Gp38 expression is also upregulated on tumour cells themselves, in various cancers, although its expression has not been reported in CRC (reviewed in Astarita et al., 2012).

Gp38-expressing cells were found in various locations in the colon. Based on cell anatomy and matched-H&E sections, Gp38 staining did not correlate with location of innate infiltrate. Different populations of cells expressed Gp38. **Figure 4.16 A** represents a T1 adenocarcinoma found in the IL-$10^{-/-}$ Treg + *Hh* group, and illustrates the locations where $Gp38^+$ cells can be found within the different parts of the colon. Invasive crypts were localised between the muscularis mucosae and the submucosae, indicated by white arrows. Gp38-expressing cells were first found within the muscularis mucosa, which is normally composed of a thin layer of smooth muscle. As the tumour invaded the inner layers of the colon, we noted a large infiltrate of $Gp38^+$ cells on the sides and bottom of the invasive crypts. Gp38-

expressing cells were also found in the lamina propria (bottom part), where early invasion was also noted. The next layer of the colon corresponded to the submucosae. This part of the colon is made of connective tissue, blood and lymphatic vessels. We also observed $Gp38^+$ cells in the submucosae, most likely corresponding to lymphatics and fibroblasts. Finally, the outer layer of the colon corresponded to the longitudinal and circular muscles layer, involved in peristalsis, which contained smooth muscle cells that also expressed Gp38. The muscular layer was enlarged compared to other parts of the colon, such as seen on the top right part of **Figure 4.16 C**, which could either be caused by a strong inflammatory foci or is related to tumour progression.

Similar observations can be made for other T1 and T2 adenocarcinomas. We noticed Gp38-expressing cells in the vicinity of invasive crypts (**Figure 4.16 B, C, D**), with a dense number of $Gp38^+$ stromal cells in the muscularis mucosae and submucosae. Gp38-expressing cells were also found in the lamina propria, and lymphatics can be spotted in the submucosae, which formed round structures and were positive for Gp38 expression (**Figure 4.16 B, C**). In T2 adenocarcinomas, lymphatic vessels seemed to be more frequent and were located throughout the lesion (**Figure 4.16 D**). We noted that some tumour cells were positive for Gp38 expression, such as seen on the left part of the adecarcinoma on **Figure 4.16 B**, although overall Gp38 expression was not detected in the majority of the tumours.

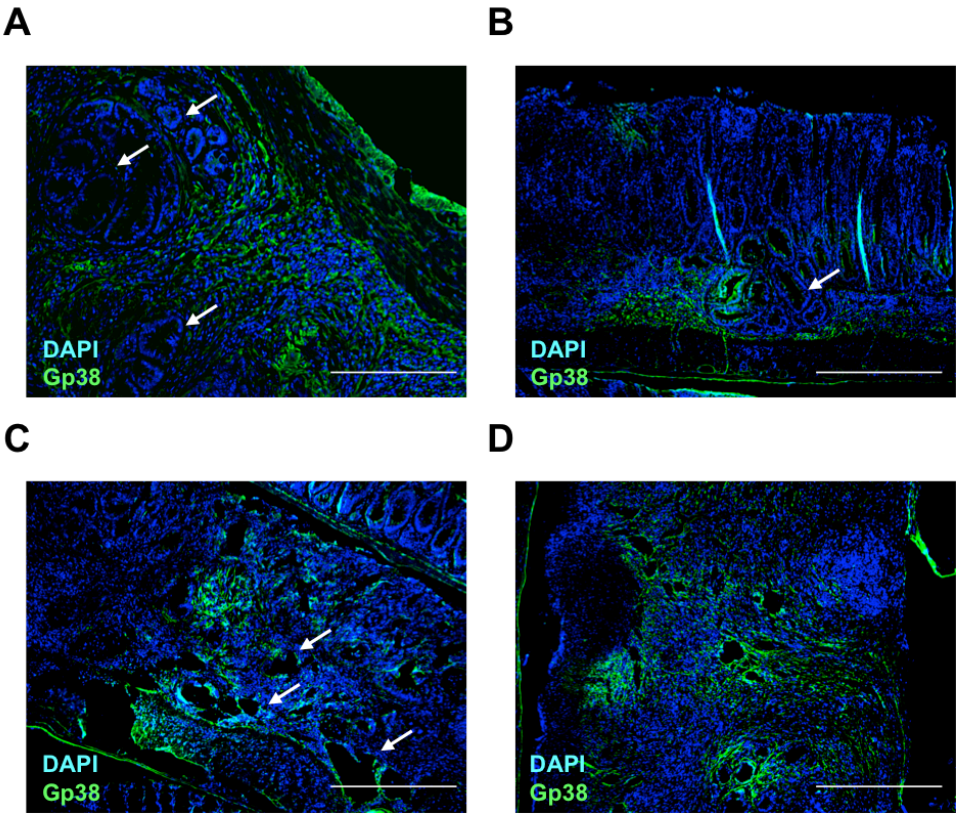

Figure 4.16: GP38^{+} cells are found within adenocarcinomas.

Colonic tumour sections were selected based on H&E staining to identify lesions, and processed for IHC staining. White arrows indicate invasive crypts.

(A) Representative image of immunofluorescence staining of Gp38-expressing cells in a T1 adenocarcinoma, invading the muscularis mucosae.
(B) Representative image of immunofluorescence staining of Gp38-expressing cells in a T1 adenocarcinoma, showing the water drop like tumour invading the muscularis mucosae (Chapter 3).
(C) Representative image of immunofluorescence staining of Gp38-expressing cells in a large T1 adenocarcinoma, invading the muscularis mucosae.
(D) Representative image of immunofluorescence staining of Gp38-expressing cells in a T2 adenocarcinoma, crossing the submucosae.

Image represents merge images from green channel (Gp38) and blue channel (nuclei, DAPI). Original magnifications – 20x (A) and 10x (B-D). Scale bar – 200μm (A) and 500μm (B-D). Staining was performed in n=9 tumours from difference mice and from 2 independent experiments. Images are shown for IL-10$^{-/-}$ Tregs + *Hh* mice.

4.2.9 Stromal cells isolated from tumour-bearing mice produce IL-6 at increased and sustained levels over time

As Gp38-expressing cells were present within tumours, we hypothesized that these may relate to the $Gp38^{+}$ stromal cells that expressed increased amounts of *Il6*. Therefore, we sought to establish *ex vivo* culture of stromal cells to probe their phenotype and function in disease progression.

First, we tested whether culture of stromal cells was feasible and would represent a useful *ex vivo* tool. As a preliminary experiment, mice were sacrificed at week 12, and colons taken for preparation of LPL single cell suspensions. Stromal cells were cultured for two weeks after isolation from tumour bearing mice and controls (**Figure 4.17 A**). RNA was then extracted, and genes of interest were screened by qPCR. While we did not detect differences in expression of *Tgfb* and *Gm-csf* transcripts in cultured cells, *Il6* and *Tnfa* expression mirrored results previously reported, with increased amounts of these cytokines in stromal cells isolated from tumour-bearing mice (**Figure 4.17 B-E**). Moreover, transcripts for contaminating epithelial cells, innate populations and endothelial cells were largely non-detected or expressed at low amounts, confirming that *ex vivo* culture is a valuable tool to study stromal biology in cancer (**Figure 4.17 F**).

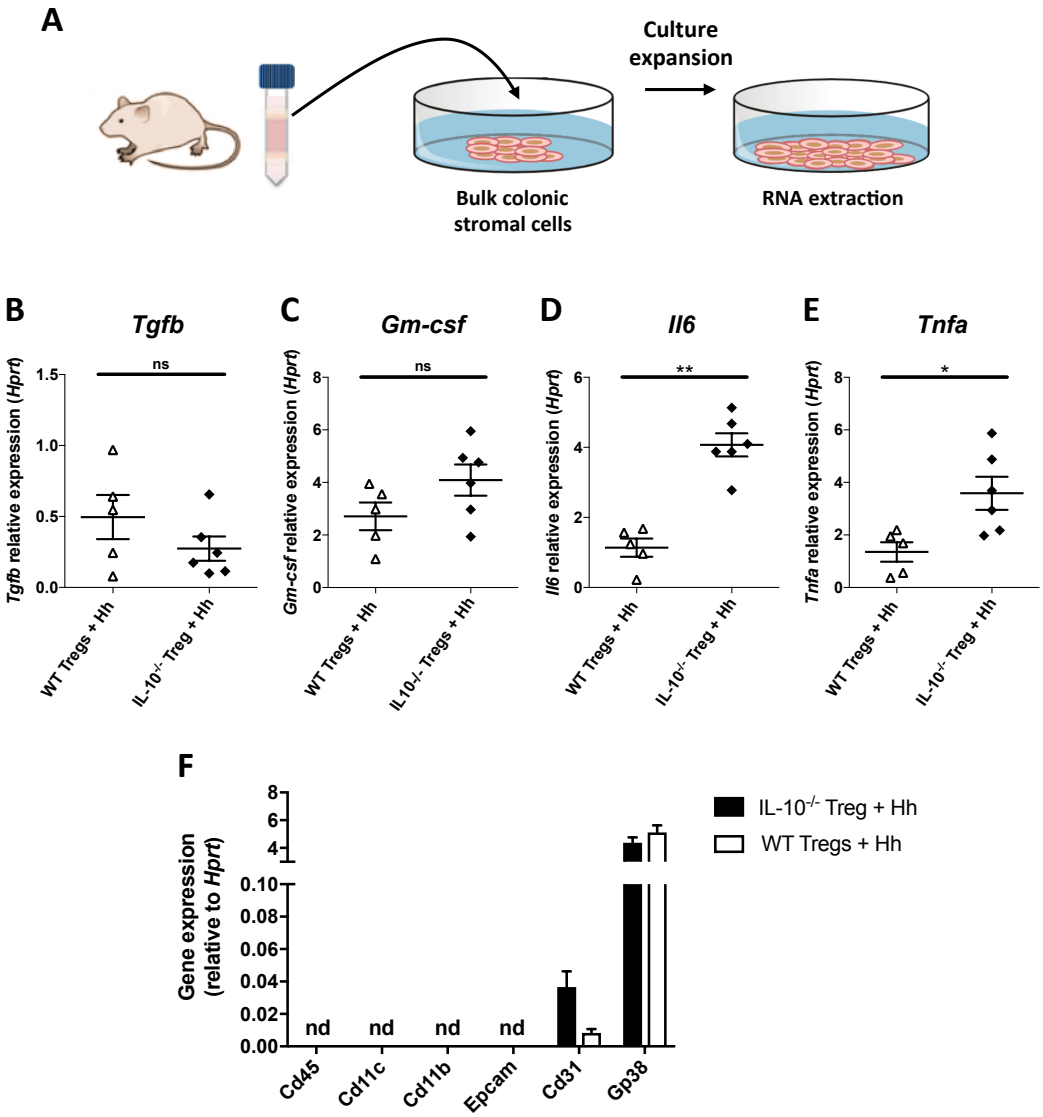

Figure 4.17: *Ex vivo* stromal cell cultures mirrors *in vivo* stromal cytokine gene expression signature.

(A) Mice from WT Treg + *Hh* and IL-10$^{-/-}$ Treg + *Hh* groups were sacrificed at week 12, and colons taken for LPL preparation. The 30/40% interphase of the gradient (enriched in stromal cells) was harvested and plated in 6 well plates. After an initial expansion of 3-4 days, cells are passaged, and were further expanded for another week. RNA was extracted for subsequent qPCR. Relative expression levels were calculated using the $2^{(-\Delta\Delta CT)}$ method, normalising to the housekeeping gene *Hprt*.

(B-E) mRNA expression of *Tgfb*, *Gm-csf*, *Il6* and *Tnfa* in indicated stromal cell groups.

(F) Expression of indicated lineage-specific genes was assessed by qPCR to confirm the purity of *ex vivo* stromal cell cultures isolated from mouse colon tissue, with "nd" denoting not detected.

Each dot represents a stromal culture originating from one mouse, and bars represent mean ±SEM. Data represents one experiment performed at the JR with the Powrie colony.
Statistical significance was determined using a Mann Whitney U Test. * $p \leq 0.05$, ** $p \leq 0.01$.

Next, we assessed IL-6 and TNF-α production by ELISA. Stromal cultures from WT Tregs + *Hh* and IL-10$^{-/-}$ Tregs + *Hh* groups were expanded for approximately 3 months. At every passage, in addition to expanding the cultures, a fixed number of cells was re-seeded into a 6 well plate and supernatants were harvested after 24h (**Figure 4.18 A**). Consequently, we were able to detect stromal IL-6 and TNF-α production in supernatants over time.

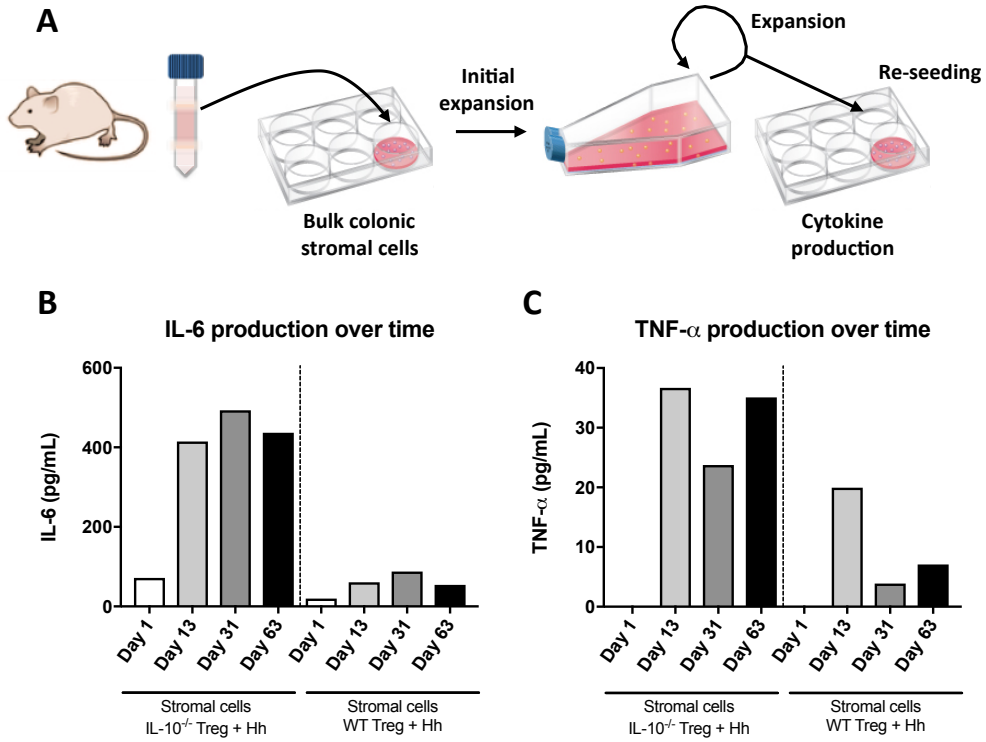

Figure 4.18: Stromal cells isolated from tumour-bearing mice produce IL-6 and TNF-α at elevated and sustained levels over time.

(A) Mice from WT Treg + *Hh* and IL-10$^{-/-}$ Treg + *Hh* groups were sacrificed at week 12, and colons taken for LPL preparation. The 30/40% interphase of the gradient (enriched in stromal cells) was harvested and plated in 6 well plates. After an initial expansion of 2-5 days, cells were passaged and cultures established.
24h after the initial passage, supernatants were harvested and stored until further use (Day 1).
Once confluency was reached, cells were re-seeded into larger flasks for expansion, and 50,000 cells were placed in a 6 well plate for cytokine measurement in supernatants after 24h (Days 13, 31, 63).
(B) IL-6 detection in supernatants of indicated stromal cell cultures over time.
(C) TNF-α detection in supernatants of indicated stromal cell cultures over time.

Stromal cell culture isolated from tumour-bearing mice represents 5 pooled stromal fractions, and stromal cell culture isolated from WT Treg + *Hh* animals represents 5 pooled stromal fractions.
Data represents one experiment performed at the KIR with the Maloy colony.

The day 1 measurement corresponded to the first re-seeding after the initial passage, and therefore contained fewer fibroblasts than the rest of the measurements, which explained to low amounts of IL-6 detected. IL-6 secretion was detected at early time points following culture of stromal cells derived from tumour-bearing mice, compared to the control group (**Figure 4.18 B, left**). Over time, and as early as day 13, IL-6 production was increased and strongly maintained over time in the IL-10$^{-/-}$ Treg + *Hh* stromal cells (**Figure 4.18 B, left**). Although sustained levels of IL-6 were also detected over time in the control group, generally the amount was reduced (**Figure 4.18 B, right**). Similarly, TNF-α production was assessed across groups and time. Comparable observations were made with TNF-α, in that stromal cells derived from tumour-bearing mice displayed increased production of TNF-α that was prolonged over time (**Figure 4.18 C, left**), and control stromal cells tended to express lower amounts of TNF-α.

In summary, these results are consistent with increased transcripts and secreted IL-6 previously found in the stromal compartment of tumour-bearing mice. Moreover, we confirmed that stromal cells isolated from tumour-bearing mice and cultured *ex vivo* have increased IL-6 and TNF-α production. Intriguingly, sustained production of these cytokines was noted over time, which may suggest an epigenetic imprint from the microenvironment.

4.2.10 Phenotyping of *ex vivo* stromal cells isolated from tumour-bearing mice revealed increased expression of collagen and chemokines.

Stromal cells isolated from tumour-bearing mice and cultured *ex vivo* over a number of passages retained their enhanced production of the pro-inflammatory and tumourigenic cytokine IL-6. Therefore, we explored the phenotype of these cells by gene expression.

As described, upon re-seeding and expansion of the stromal cultures, a portion of cells was harvested for gene expression analysis. In total, RNA was extracted from three different time points (day 13, 31 and 63) in both populations, followed by qPCR analysis. First, the purity of the stromal cultures were assessed by screening lineage-specific genes for epithelial, endothelial and hematopoietic lineages, confirming that *ex vivo* cultures solely contained cells of mesenchymal origin (**Figure 4.19 A**). Next, we analysed gene expression of common stromal and fibroblastic markers, as well as collagen expression. Stromal cells isolated from the IL-10$^{-/-}$ Treg + *Hh* group displayed significant increased transcripts for *Pdgfra* (platelet-derived growth factor receptor A) and *Acta2* (Alpha-smooth muscle actin) (**Figure 4.19 B**). Interestingly, there may also be a trend towards increased amounts of *Fap* (Fibroblast activation protein alpha) in IL-10$^{-/-}$ Treg + *Hh* isolated stromal cells, which is a classical marker of CAFs. Both populations expressed *Icam1* at similar levels, which is consistent with FACS analysis expression. Moreover, *Col1a1* and *Col3a1* expression were significantly increased in stromal cells isolated from tumour-bearing animals (**Figure 4.19 B**), while no change in expression was detected for *Col5a1*.

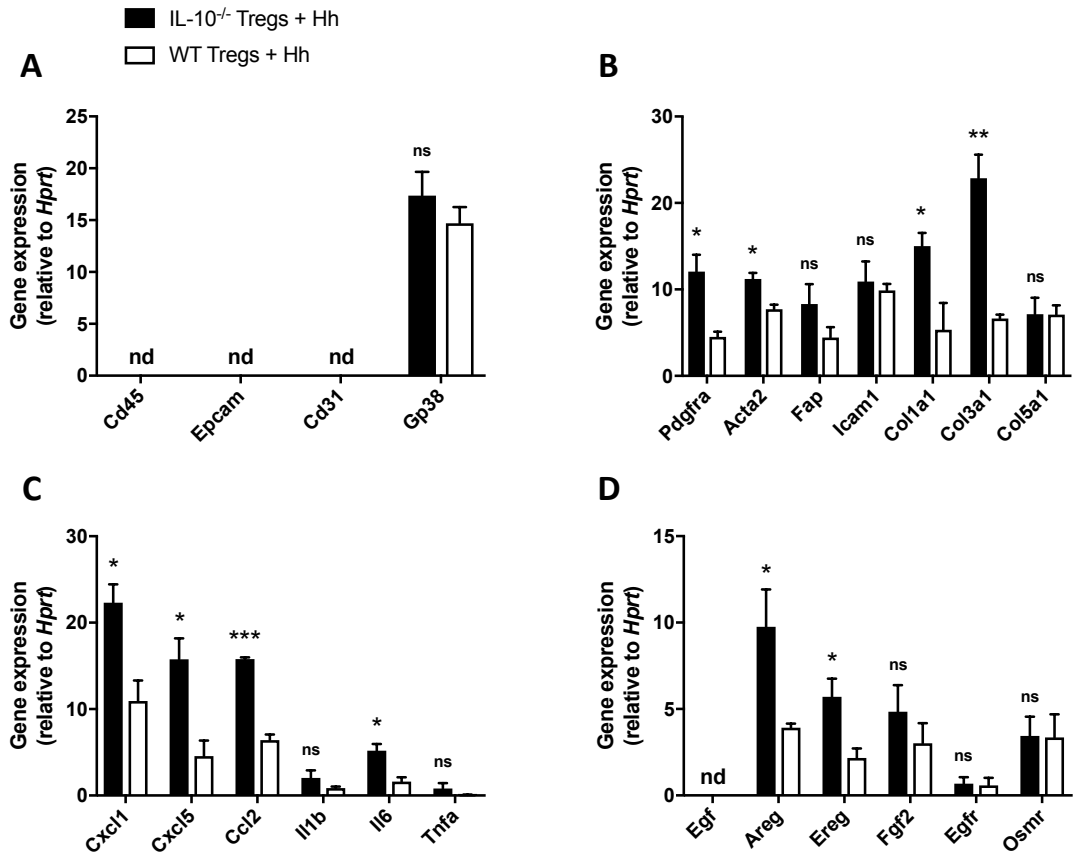

Figure 4.19: Characterisation of cultured stromal cells, isolated from WT Tregs + *Hh* and IL-10$^{-/-}$ Tregs + *Hh* groups, by gene expression analysis.

Mice from WT Treg + *Hh* and IL-10$^{-/-}$ Treg + *Hh* groups were sacrificed at week 12, and colons taken for LPL preparation. The 30/40% interphase of the gradient (enriched in stromal cells) was harvested and plated in 6 well plates. Cells were expended over time.
Once confluency was reached, cells were re-seeded into larger flasks for expansion, and 200,000 cells taken for RNA extraction. 3 time points were collected for each culture: days 13, 31 and 63. RNA was extracted for subsequent qPCR. Relative expression levels were calculated using the $2^{(-\Delta\Delta CT)}$ method, normalising to the housekeeping gene *Hprt,* with "nd" denoting not detected.

(A) Expression of indicated lineage-specific genes to confirm the purity of *ex vivo* stromal cell cultures isolated from mouse colon tissue.
(B) Expression of stromal and fibroblasts markers, *Pdgfra*, *Acta2*, *Fap*, *Icam1*, *Col1a1*, *Col3a1* and *Col5a1*.
(C) Expression of key chemokines and cytokines, *Cxcl1*, *Cxcl3*, *Ccl2*, *Il1b*, *Il6* and *Tnfa*.
(D) Expression of growth factors and associated receptors, *Egf*, *Areg*, *Ereg*, *Fgf2*, *Egfr*, *Osmr*.

Data represents gene expression at 3 time points for each stromal cultures, and bar represents ±SEM. Data represents one experiment performed at the KIR with the Maloy colony.
Statistical significance was determined using multiple t tests. * $p \leq 0.05$, ** $p \leq 0.01$, *** $p \leq 0.001$.

Chemokine and cytokine gene expression was next analysed. Stromal cells from IL-$10^{-/-}$ Treg + *Hh* expressed significantly higher amounts of *Cxcl1*, *Cxcl5* and *Ccl2* compared to controls (**Figure 4.19 C**). Consistent with our other findings, we detected increased amounts of *Il6* in IL-$10^{-/-}$ Treg + *Hh* stromal cells, but found no difference in gene expression for *Il1b* and *Tfna* (**Figure 4.19 C**).

Finally, as *Areg* was consistently upregulated in the stromal compartment of tumour-bearing mice, we explored its expression along with other EGF family members. In culture, stromal cells isolated from IL-$10^{-/-}$ Treg + *Hh* animals retained a significant upregulation of *Areg*, together with *Ereg* (**Figure 4.19 D**). *Egf* expression was not detected *ex vivo*, and *Egfr* expression was similar between groups. Additionally, *Fgf2* and *Osmr* expression was analysed but no differences were detected (**Figure 4.19 D**).

Collectively, our results point towards a phenotype of tumour-bearing mice-derived stromal cells that is of an activated phenotype that is collagen-producing, with potent abilities to recruit $Ccr2^{+}$ myeloid cells and neutrophils (i.e. via Cxcl1 secretion), and may promote angiogenesis through expression of *Cxcl1* and *Cxcl5*, which bind to Cxcr2 expressed by endothelial cells. Moreover, expression of *Il6*, *Areg*, and *Ereg* may provide tumour cells with a microenvironmental niche that allows their survival, proliferation, and maintenance of pro-inflammatory signals, ultimately promoting tumour progression.

4.2.11 Steady state stromal cells produce increased amounts of IL-6 upon stimulation with an IL-10$^{-/-}$ Treg supernatant.

IL-6 was found to be critical to promote colitis and tumour development *in vivo*, and we have demonstrated that Gp38^{+} stromal cells are a main cellular source of IL-6, highlighting this population as key in disease progression. However so far, it remains unclear what the driver of elevated IL-6 production is in this mouse model. We next sought to determine whether IL-10 deficient Tregs might directly foster a pro-inflammatory and tumourigenic phenotype in the stromal compartment.

First, we FACS-sorted IL-10$^{-/-}$ and WT Tregs as previously described in Chapter 3, and stimulated Tregs with either PMA/ionomycin for 24h, or with IL-2 alone for 70h, and supernatants were harvested and stored until further use (**Figure 20 A**). The IL-2 stimulation was used to maintain Treg cells viability over time, while the PMA/ionomycin condition was used to promote the secretion of cytokines *in vitro*. Next, we probed IL-6 and TNF-α production in Treg supernatants. Low amounts of IL-6 were detected, regardless of the stimulation and genotype of the Treg cells (**Figure 4.20 B**). TNF-α production was similarly produced at low amount by Tregs stimulated with IL-2 alone, while its production was detected in Tregs stimulated with PMA/ionomycin, albeit to lower amounts than CD4^{+} T cells controls (**Figure 4.20 C**).

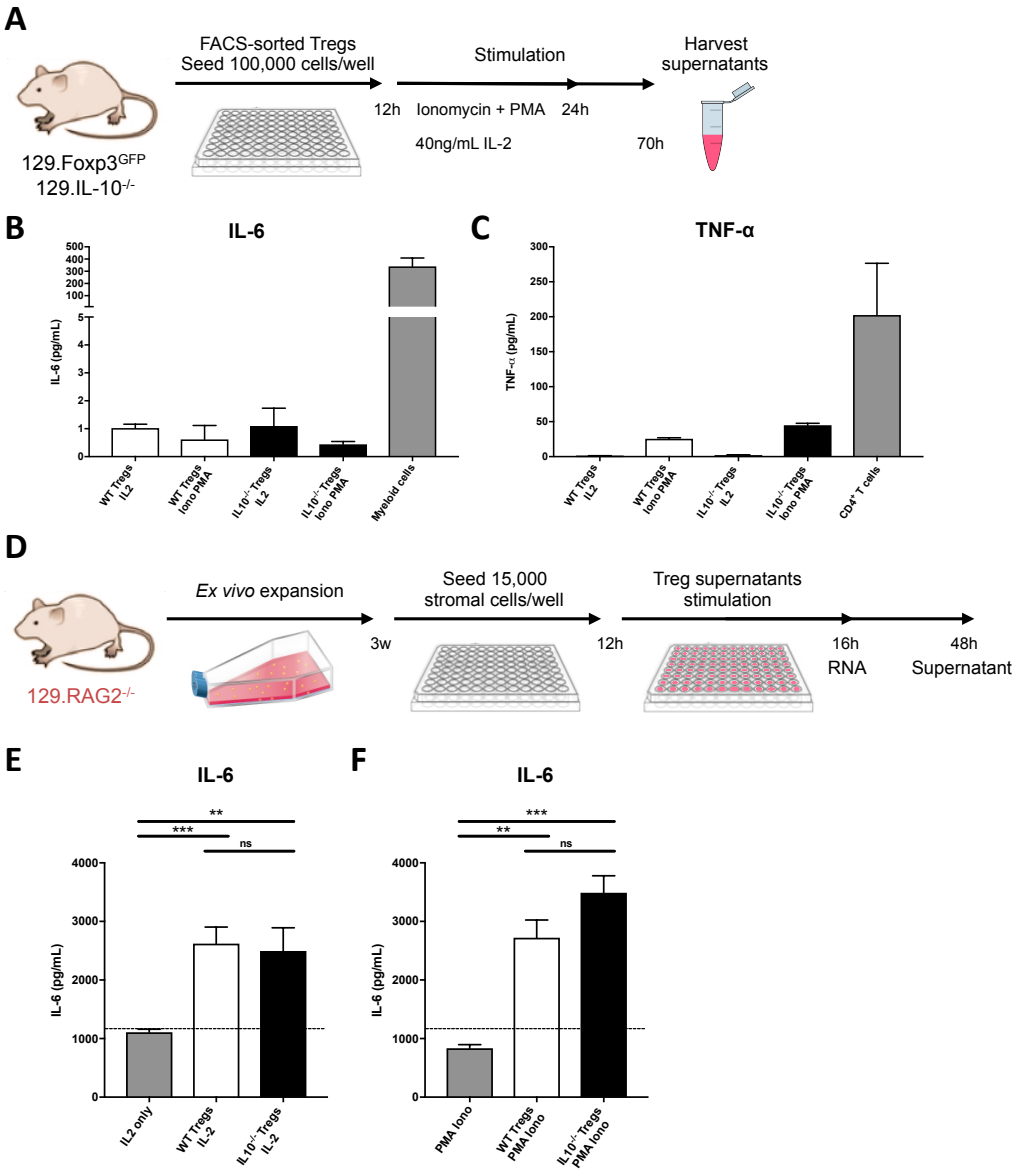

Figure 4.20: Stromal cells cultured with Treg supernatant have increased IL-6 production.

(A) Splenic WT and IL-10$^{-/-}$ Tregs were FACS-sorted from respectively 129.Foxp3^{GFP} and 129.IL10$^{-/-}$ as described in Chapter 3. Tregs were plated in 96 well plates at 100,000 cells per well and rested for 12h. Tregs were then stimulated with IL-2 only for 70h or with PMA/ionomycin for 24h. After stimulation, supernatants were harvested, and filtered sterile until further use.

(D) 129.RAG$^{-/-}$ stromal cells were harvested from steady state mice and cultured as previously described. Cells were expanded and seeded at 15,000 cells per well in a 48 well plate. After 12h, conditioned media was removed and replaced with media containing Treg supernatants (dilution 1:5). Stromal cells were stimulated for 16h (RNA) or 48h (ELISA).

(B, C) ELISA for IL-6 with myeloid cells as control (B) and TNF-α with CD4^{+} T cells as control (C) on WT and IL-10$^{-/-}$ Treg supernatants.

(E, F) IL-6 production by stromal cells cultured with Tregs stimulated with IL-2 alone (E) or with PMA/ionomycin (F).

Bar represents ±SEM. Data represents the pool of three independent experiments performed at the KIR with the Maloy colony, with each experiment using different stromal cultures and FACS-sorted Tregs.
Statistical significance was determined using a Kruskal-Wallis one-way analysis of variance, followed by a Dunn's post-hoc test. ** $p \leq 0.01$, *** $p \leq 0.001$.

Secondly, stromal cells were isolated from steady state 129.RAG$^{-/-}$ mice as previously described in this chapter. After expansion, cells were re-seeded into 48 well plates and were left in normal media for 12h. Culture media was then removed and replaced by media containing either WT or IL-10$^{-/-}$ Treg supernatant generated as described (**Figure 4.20 D**). As controls, we used media containing either IL-2 or PMA/ionomycin in stromal cultures. After 48h, supernatants were harvested and assessed for IL-6 production. Supernatants from WT and IL-10$^{-/-}$ Tregs stimulated with IL-2 alone increased IL-6 production by fibroblast cultures (**Figure 4.20 E**). Similarly, stromal cells cultured with Treg supernatants generated from PMA/ionomycin stimulation also induced high amounts of IL-6 production (**Figure 4.20 F**), although there was no significant difference between the groups.

As IL-6 production has been linked to TNF-α signalling, we hypothesised that the low amounts of TNF-α in the Treg supernatants could influence IL-6 production. Therefore, we pre-treated the Treg supernatants with an anti-TNF-α antibody, and used the pre-treated supernatant in stromal cultures (**Figure 4.21 A**), as described. IL-6 production was unaffected by blockade of TNF-α, therefore indicating a TNF-independent mechanism for IL-6 induction (**Figure 4.21 B, C**).

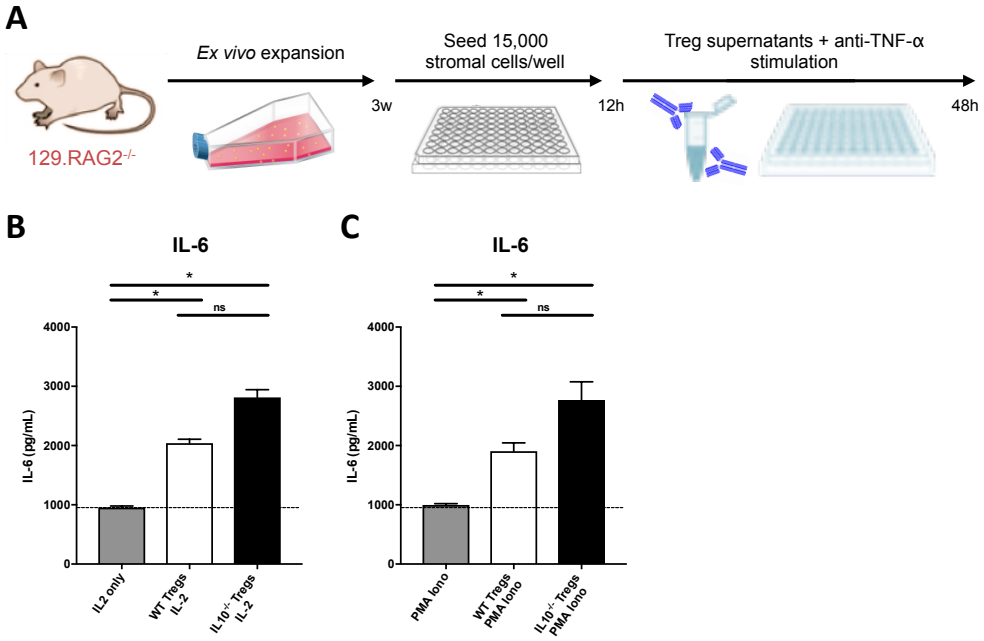

Figure 4.21: Induced IL-6 production in stromal cells is independent of TNF-α.

(A) 129.RAG$^{-/-}$ stromal cells were harvested from steady state mice and cultured as previously described. Cells were expanded and seeded at 15.000 cells per well in a 48 well plate. After 12h, conditioned media was removed and replaced with media containing Treg supernatants treated for 30 min with anti-TNF-α (dilution 1:5). Stromal cells were then stimulated for 48h.

(B, C) IL-6 production in stromal cultures with indicated stimulations.

Bar represents ±SEM. Data represents one experiment performed at the KIR with the Maloy colony, with n=3 independent stromal cultures per group.
Statistical significance was determined using a Kruskal-Wallis one-way analysis of variance, followed by a Dunn's post-hoc test. * $p \leq 0.05$.

Our results indicate that supernatants from activated Treg cells can enhance IL-6 production by stromal cell cultures. This effect was not mediated by TNF-α dependent induction of IL-6, as pre-treatment with a blocking antibody led to similar stromal IL-6 production.

4.3 Discussion

4.3.1 Main conclusions

Previous work in our lab has identified IL-22 as a major tumourigenic cytokine in *Hh*-driven colitis-associated cancer. However, using a model in where IL-10 deficient Tregs drive tumourigenesis in the presence of *Hh*, we have demonstrated that this process is independent of IL-22.

Expression and secretion of various cytokines in whole tissue and in LP cells allowed us to probe the differences between a globally inflamed colon and a malignant colon in an inflammatory context. Our combined analyses have highlighted upregulation of TGF-β, Areg and IL-6 in the colon of tumour-bearing mice. Blockade of IL-6-R and TGF-β *in vivo* led to overall decreased tumour burden.

Specifically, blockade of IL-6-R is sufficient to reduce both colitis and tumour burden, establishing IL-6 as critical for disease progression. We also discovered that $Gp38^+$ cells are present in adenocarcinomas, and that collagen is deposited within tumours. Both populations of $Gp38^+$ stromal and endothelial cells express *Il6* in inflamed and tumour-bearing animals. Importantly, *Il6* expression is significantly upregulated in $Gp38^+$ stromal cells of tumour-bearing animals, compared to inflamed controls. Altogether, these data suggest that stromal cells represent a major cell population promoting inflammation and tumourigenesis through IL-6 production. Stromal cells isolated from tumour-bearing mice retain their capacity to produce elevated amounts of IL-6 over time, suggesting imprinting from the microenvironment. This phenomenon has been described in the context of colitis, involving the production of

decoy cytokine receptor soluble ST2 by stromal cells (Powrie lab, unpublished), and is more documented in rheumatoid arthritis patients, notably through production of inflammatory cytokines and chemokines by stromal cells (reviewed in Ospelt et al., 2011). These so-called "inflammatory memories" operating at the level of the tissue stroma are proposed to be a major determinant in the chronicity of inflammation within the joint (Ospelt et al., 2011), and may potentially be contributing to other chronic inflammatory diseases and cancer.

Preliminary data showed that cultured stromal cells express a variety of cytokines, growth factors, and different types of collagens that might act together to promote a tumourigenic milieu. Importantly, these cells also express *Areg* and *Ereg*, which may add to their pro-tumourigenic capabilities. Altogether, our data suggest that $Gp38^{+}$ stromal cells represent a critical population equipped with immune properties, including IL-6 production, and abilities to reshape the ECM, promoting invasion in the colon.

The **Figure 4.22** summarises our findings.

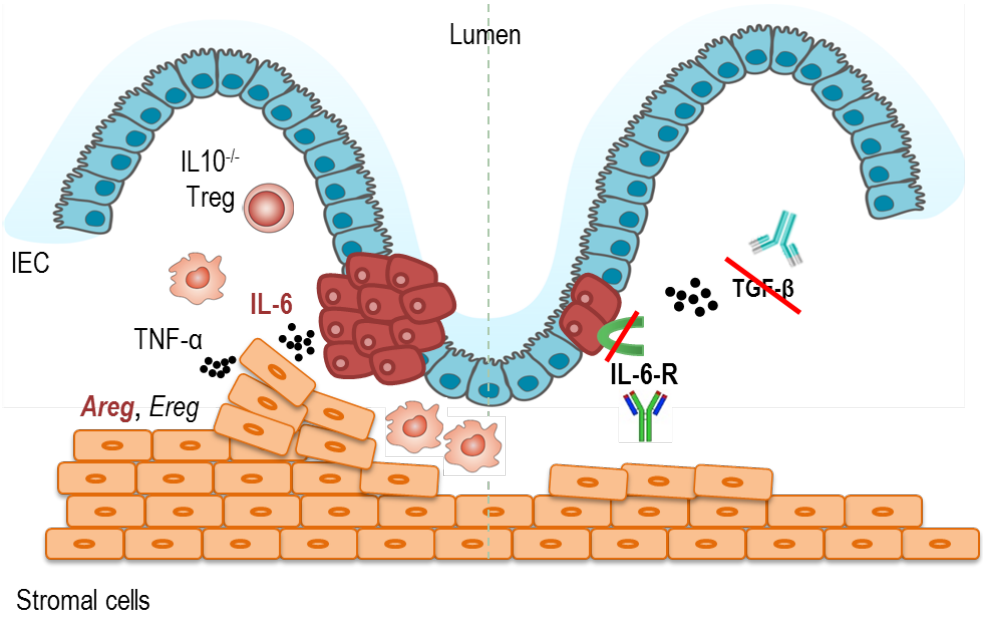

Figure 4.22: IL-6 and TGF-β promote tumour growth in the colon

Schematic of the tumour microenvironment that fosters tumour growth (left), and decreased tumourigenesis upon treatment with IL-6-R or TGF-β blocking mAbs (right).

Mice injected with IL-10$^{-/-}$ Tregs and infected with *H. hepaticus* develop colonic mucinous adenocarcinomas and have increased amounts of colonic IL-6, TGF-β and Areg. Gp38-expressing stromal cells are primary producers of IL-6 and are found within tumour lesions. Stromal cells express various collagens, thus influencing the ECM composition that may promote tumour invasion. Moreover, they also express several chemokines, thereby attracting myeloid cells, which maintain a pro-tumourigenic inflammatory milieu. Finally, these cells also express *Areg* and *Ereg*, which may favour tumour growth. The cellular source of TGF-β and primary source of Areg are unknown.

In vivo treatment with a blocking antibody against IL-6-R decreases colitis, while anti-TGF-β has no effect on the colitis levels. However, both treatments reduce tumour burden in mice injected with IL-10$^{-/-}$ Tregs and infected with *H. hepaticus.*

4.3.2 The innate immune component of tumourigenesis

Several immune populations infiltrate tumours, promoting disease development and progression. Amongst these, tumour-associated macrophages (TAM) are perhaps the most-studied pro-tumourigenic population in various cancers. They have been linked to tumour vascularisation, metastases and poor prognosis (Chanmee et al., 2014; Grivennikov et al., 2010). In our study, a number of experiments have been performed investigating whether TAMs infiltrated tumours (data not shown), however our results lacked consistency and failed to provide any definitive

conclusion. Therefore, as we did not reveal a particular enrichment in tumour-infiltrating macrophages, their phenotype and location *in situ* was not studied further. We also detected a large number of eosinophils in the lamina propria of inflamed and tumour-bearing animals. Although we did not investigate the phenotype and location of these cells any further, it is worth mentioning that tumour-associated tissue eosinophilia (TATE) has been reported *in vivo* and its prognostic value depends on the cancer type. Interestingly, in CRC, eosinophils are correlated with a good clinical outcome (Harbaum et al., 2014; Prizment et al., 2016). In retrospect, dissecting out tumours versus inflamed tissue from matched animals may have been a better strategy to explore differences by flow cytometry, and investigate the infiltration of cell populations and their phenotype associated with tumour development.

4.3.3 Cytokines and tumour development

Enrichment for TGF-β, Areg and IL-6 in the colon of tumour bearing mice has various implications for the tumour microenvironment, as these cytokines can act on tumours cells, immune cells and stromal cells, to either promote direct progression of CRC, or to maintain a pro-inflammatory milieu that ultimately favours tumour development.

4.3.3.1 TGF-β

TGF-β is a cytokine with complex roles in tissue homeostasis, wound healing and cancer (reviewed in Wrzesinski et al., 2007). Mechanistically, TGF-β activates the serine/threonine kinase receptors TBFβR1 and TGFβR2, which then activate the intracellular proteins SMAD2 and SMAD3 that subsequently interact with SMAD4 to control gene expression (Weiss and Attisano, 2012).

In vivo blockade of TGF-β provided insights into its role in tumour development and maintenance. Our study revealed that the majority of anti-TGF-β treated animals did not develop tumours, but a few mice displayed multiple tumours and T2 adenocarcinomas. Recent studies shed light on this result, as TGF-β is deemed as a double-edged sword in cancer: it promotes anti-tumour immunity at early stages of disease, which is beneficial for the host, whereas it mediates tumour growth and dissemination at later stages of the disease.

TGF-β is thought to have tumour suppressive functions in early-stage CRC (Kim *et al.*, 2000; Becker *et al.*, 2004; Biswas *et al.*, 2004), which is consistent with a high frequency of inactivating mutations in TGF-β signalling components in CRC (Fleming *et al.*, 2013). Furthermore, in concordance with a tumour-suppressive role, human CRC cell lines with high TGF-β sensitivity are weakly metastatic in orthotopic xenograft models (Simms, N. A. K. et al. 2012).

By contrast, high amounts of TGF-β in CRC patients is associated with poor prognosis, particularly in patients with advanced disease (Calon *et al.*, 2012). Rather than promoting tumourigenesis by directly affecting the malignant epithelium, TGF-β signalling into stromal cells drives gene expression signatures associated with poor prognosis in CRC (Calon *et al.*, 2015). Mechanistically, in cancer-associated fibroblasts, TGF-β induces IL-11 expression, which promotes STAT3 signalling in CRC and increases multi-organ metastasis (Calon *et al.*, 2012). Interestingly, in pancreatic cancer, expression of the pro-angiogenic factor FGF-2 in CAFs is dependent on both intact Smad3 and MAPK signalling pathways, further highlighting the role of TGF-β in shaping the stromal microenvironment (Douglas W Strand, 2014). It remains to be determined whether TGF-β shapes the stromal compartment in our mouse model.

Overall, targeting TGF-β in patients with late-stage CRC therefore represents a noteworthy therapeutic possibility (Calon *et al.*, 2012; Calon *et al.*, 2015).

Although we detected elevated levels of *Tgfb* in splenic IL-10$^{-/-}$ Tregs and in Gp38^{+} stromal cells, we were only able to confirm the TGF-β signature by protein expression in whole tissue. To date, it is unclear what the cellular source of this cytokine is. Preliminary data have shown that the malignant epithelium may be a source (protein expression analysis, data not shown). In the case of an interaction between cancer cells and stromal cells, it would be interesting to probe IL-11 production by stromal cells upon TGF-β signalling, together with other members of the IL-6 family, such as Osm. Employing techniques such as *in situ* approaches will be critical to probe cytokine expression.

4.3.3.2 Amphiregulin

Amphiregulin is a member of the epidermal growth factor (EGF) family that is constitutively expressed by various epithelial and mesenchymal cell types, and is implicated in a variety of physiological processes, including developmental processes and tissue homeostasis (Berasain and Avila, 2014). Areg expression is elicited by diverse stimuli and has been primarily associated with immune cell populations activated in type 2 inflammation, wound repair, and resolution of inflammation (reviewed by (Zaiss et al., 2015). As Areg production is implicated in wound healing, it is reasonable to assume that its function may be dysregulated in the context of chronic inflammation, but its function remains poorly defined. Interestingly, TGF-β can regulate Areg mRNA expression *in vitro* (Bennett et al., 1992), and critically, Areg mediates the development of TGF-β-induced pulmonary fibrosis (Zhou et al., 2012).

Another player in fibrosis is the cytokine IL-13, which together with TGF-β promote myofibroblast differentiation and fibrosis (Brunner et al., 2013; Fichtner-Feigl et al., 2005). It is unknown, however, whether IL-13 signalling can directly induce Areg.

Given that both TGF-β and Areg are upregulated in tumour-bearing mice, it is plausible that signalling into stromal cells induces a pro-fibrotic phenotype, which may favour disease progression in the context of the tumoural microenvironment and warrants further investigation. Initial experiments aimed at identifying cytokines involved in inflammation and tumourigenesis have not confirmed IL-13 as an interesting target. However, our analysis suffers from a major caveat, as similar remarks can be made regarding the use of whole colons rather than focusing on tumours only, which may have led to a dilution of locally expressed cytokines.

The role of Areg in anti-tumour immunity and tolerance is still poorly understood. Interestingly, the wide clinical use of EGFR antagonists in various metastatic cancers, including CRC, suggests that Areg, as well as other members of the EGF family, might play a critical role in orchestrating responses to tumours (Zaiss et al., 2015). As mentioned in Chapter 3, Areg plays a critical role in intestinal epithelial growth and has been shown to drive the renewal of the intestinal epithelium following total body irradiation (Shao and Sheng, 2010b). Further renewal under pro-inflammatory conditions and microbial insults may skew the balance towards malignancy, thereby establishing Areg as an enabling factor for tumour growth. In support of this hypothesis, a recent report suggested that Areg plays pro-neoplastic roles in intestinal epithelial transformation, denoted by the decreased polyposis in $Areg^{-/-}$

.APC$^{min/+}$ mice (Guzman et al., 2012). Importantly, this effect is partially mediated by Areg-producing myofibroblasts (Guzman et al., 2012).

In CRC patients, AREG expression in primary tumours is an important predictive factor of liver metastases (Yamada et al., 2008). In addition, the FOCUS-4 study (http://www.focus4trial.org/) aims to stratify patients for targeted therapies based on the genetic and molecular features of their disease, and strives to develop several biomarkers for EGFR dependent cohorts, which includes Areg and Ereg.

GIven the lack of available tools and inability to use an Areg deficient mouse strain due to the 129.SvEv background used in this CRC model, the *in vivo* relevance of Areg in disease progression remains to be investigated.

4.3.3.3 IL-6

Our study has revealed a major pro-inflammatory and pro-tumourigenic role of Interleukin 6. IL-6 is a crucial mediator of inflammation and immunity. In the CRC microenvironment, IL-6 is produced by diverse cell types and transduces signals via gp130 (also known as IL-6Rβ) to induce STAT3 activation (Taniguchi and Karin, 2014). IL-6 is the most well studied STAT3 activator in CRC and has been shown to drive proliferation, migration, and angiogenesis in both CAC (Bollrath *et al.*, 2009; Grivennikov *et al.*, 2009) and sporadic CRC (Nagasaki *et al.*, 2014; Taniguchi and Karin, 2014).

We aimed at identifying the cellular source of IL-6 by gene expression, protein secretion and *ex vivo* cultures. In our mouse model, IL-6 has been suggested to play a critical role in tumour development by amplifying the pro-inflammatory innate immune response (Poutahidis et al., 2007). Indeed, macrophages are historically

regarded as the primary source of IL-6 in CRC. In our study, flow cytometric analyses of tumour-bearing mice have detected IL-6 production, albeit limited, in the innate compartment (data not shown). Furthermore, increased IL-6 secretion in tumour-bearing mice is detected in whole tissues, while we do not detect increased production of IL-6 in lamina propria cells. These data suggest that IL-6 is predominantly produced in the stromal-enriched fraction of the colon.

Recent data have challenged the view that macrophages are the primary source of IL-6. Indeed, in human tumours, CAF production of IL-6 has been reported (Nagasaki *et al.*, 2014), and CAF-derived IL-6 promotes tumourigenesis in human CRC through the induction of Notch1 and CD44 expression (Lin *et al.*, 2013). Another new source of IL-6 has also recently been linked to the microbiota. Indeed, the presence of bacterial biofilms was detected on tumours in the proximal colon. Although causality remains elusive, biofilms were associated with increased IL-6 production in the lamina propria, epithelial STAT3 activation and loss of E-cadherin expression (Dejea *et al.*, 2014). Here, we show that stromal cells are a primary cellular source of IL-6, as assessed by gene expression, flow cytometry, as well as *ex vivo* cultures. Given the broad literature on IL-6 signalling into cancer cells, it is likely that similar mechanisms are in place, whereby the malignant epithelium proliferates through activation of the STAT3 signalling pathway. So far, however, we have not been able to pin down a mechanism by which the presence of IL-10$^{-/-}$ Tregs may favour a microenvironment that would promote stromal secretion of IL-6. Specific ablation of IL-6 in the stromal compartment would give further insights to the specificity of stromal-cancer cell interactions and promotion of tumourigenesis.

Overall, our results suggest that similarly to certain subtypes of CRC patients, stromal cells represent a major cellular source of IL-6, thus directly promoting tumourigenesis.

4.3.4 Bivalent functions of stromal cells in tumour development

4.3.4.1 Classical effector function of stromal cells

Tumours have been deemed as “wounds that do not heal” (Dvorak, 1986). Indeed, the tumour niche resembles a site of chronic wound healing (Barcellos-Hoff et al., 2013; Dvorak, 1986) and the presence of myofibroblastic cells in tumours and tissue repair has emerged as a particularly common hallmark (Cirri and Chiarugi, 2011).

Our results indicate that in the colonic tumoural microenvironment, collagen is produced and highly deposited around mucinous adenocarcinomas. Moreover, we confirmed that Gp38-expressing cells also infiltrated the tumoural niche. Given that these observations are qualitative, it is of utmost importance to quantify the collagen production as well as to characterise its type. The gene expression profile of *ex vivo* cultured stromal cells isolated from tumour-bearing mice has established that these cells produce increased amounts of *Col1a1* and *Col3a1*, compared to controls. Alteration of the ECM composition is a key feature of cancers, and tends to involve preferential increased deposition of Col-I and Col-III (Wynn and Ramalingam, 2012). The presence of a dense and rigid ECM has direct effects on tumour progression (reviewed in Butcher et al., 2009), but also amplifies the activation of myofibroblasts, which in turn further promotes tumourigenesis, in a positive feedback loop (Barcellos-Hoff et al., 2013). Thus, it is possible that stromal cells in the tumour microenvironment enables the malignant epithelium to progress into the different layers of the intestine via dysregulation of ECM composition. Given the similarities

between chronic fibrosis and the tumour niche, it is unclear whether we would observe differences along the lamina proria, and thus far it has not been established *in vivo* either.

Another classical function attributed to myofibroblasts in addition to wound healing, chronic fibrosis and cancer, is their ability to produce chemokines. Indeed, in normal repair processes, the coordination of the recruitment of several immune, endothelial and epithelial cells to the injured tissue is of paramount importance. This process is mediated via secretion of specific chemokines, thereby ensuring tissue integrity. Similarly, the healing response and the tumour niche share expression of chemokines. In our mouse model, several chemokines were upregulated by stromal cells isolated from tumour-bearing mice, including *Ccl2*, *Cxcl1* and *Cxcl5*.

CCL2 (MCP-10) is a classical chemokine that is expressed in CRC and is a predictive marker for liver metastasis in human CRC (Hu et al., 2009). In light of the increased expression of *Ccl2*, it suggests that the stromal compartment may perpetuate the pro-inflammatory niche by recruiting circulating monocytes to the tumour site. Accordingly, from histology, it is clear that macrophages can infiltrate both the inflamed colon and surrounding tumour microenvironment. Interestingly, a recent study found that CCL2 promotes colorectal carcinogenesis by influencing the accumulation and function of myeloid-derived suppressor cells (MDSCs), as well as shaping a tumour-permissive tissue microenvironment (Chun et al., 2015). More specifically, the authors showed that intratumoral CCL2 levels are increased in patients with colitis-associated colorectal cancer and sporadic cancer. Using different mouse models of CRC, including $APC^{min/+}$ mice and xenografts, blockade of CCL2 led

to diminished lesions that progressed to adenocarcinomas, together with a reduction in MDSCs number (Chun et al., 2015). In lung fibrosis, a recent study suggests that CCL2 mediates fibroblast survival through inhibition of apoptosis, via activation of the IL-6/STAT3 pathway, thereby providing a novel mechanism through which CCL2 may contribute to the development and maintenance of fibrosis (Liu et al., 2007). In breast cancer, primary CAFs produce higher amounts of CCL2, which in turn stimulates the stem cell-specific, sphere-forming phenotype in breast cancer cells, as well as self-renewal of cancer stem cells (Tsuyada et al., 2012).

CXCL1 and CXCL5 are CXC chemokines that bind to CXCR2 and promote angiogenesis. CXCL1 is notably produced by cancer cells and induces migration of $CXCR2^+$ endothelial cells, facilitating microvessel formation (Wang et al., 2006). More importantly, the CXCL1-CXCR2 axis promotes the formation of the pre-metastatic niche of CRC liver metastasis, whereby $CXCR2^+$ neutrophils mediate metastasis progression to the liver in a mouse model (Yamamoto et al., 2008). Although expression of CXCL1 is widely reported in murine models and CRC patients, its expression by stromal cells and relevance in disease progression remains poorly characterised. CXCL5 is mainly produced by cancer cells and is associated with promotion of metastasis and poor clinical outcomes in CRC patients (Zhao et al., 2017). To date, CXCL5-stromal derived function has not been investigated in CRC.

Overall, CAFs employ a variety of different mechanisms that shape the tumoural niche and promote disease progression, which is also mediated by their production of growth factors. So far, we have not fully investigated the phenotype of the stromal compartment isolated from tumour-bearing mice. However, single cell

sequencing of the population may represent the better strategy to investigate their phenotype and function. Besides, it will also shed light as to their identity and potential sub-populations that may be involved in different aspects of disease progression.

4.3.4.2 Stromal cells as an "immunological active" population – a new identity

Recently it has been appreciated that stromal cells are also capable of modulating immune responses (Owens and Simmons, 2012; Owens, 2015; Powell et al., 2011). Multiple characteristics make stromal cells relevant for this task. For instance, both murine and human intestinal stromal cells express TLRs, allowing them to mount a response to microbial challenge (Otte et al., 2003; Walton et al., 2009). There is also some evidence that stromal cells can express MHCII and present antigens, acting as non-professional APCs (Kain and Owens, 2013; Saada et al., 2006). Furthermore, intestinal stromal cells can influence dendritic cell function under steady state conditions, by inducing retinoic acid (RA) production in DCs in a RA- and GM-CSF-dependent fashion (Vicente-Suarez et al., 2014). Human intestinal stromal cells have also been suggested to promote $CD25^{+}$ $CD127^{-}$ $Foxp3^{+}$ T cells via secretion of prostaglandin E2 in *in vitro* co-culture systems (Pinchuk et al., 2011). Altogether, these studies highlight that intestinal stromal cells can actively contribute to the coordination of immune responses in the gut.

Recent studies have also emphasised a key role for stromal cells in orchestrating intestinal immunity and pathology. In the $TNF^{\Delta ARE}$ mouse model of IBD, in which TNF-α is continuously overexpressed and promotes colitis (Kontoyiannis et al., 2002), the ability to respond to TNF-α by mesenchymal cells is sufficient to drive intestinal

pathology (Armaka et al., 2008). In IBD, intestinal stromal cells express the OSMR and respond to OSM by producing various proinflammatory molecules, including IL-6, ICAM1, and numerous chemokines that orchestrate the migration of pro-inflammatory cells (West et al., 2017). In CRC, CAFs promote disease progression via expression of growth factors, chemokines and inflammatory cytokines. In this work, we demonstrate that intestinal stromal cells from tumour-bearing mice are a primary source of IL-6 and we report for the first time that *Areg* expression is increased in $Gp38^{+}$ stromal cells from tumour mice. Our preliminary gene expression analysis of stromal cell cultures isolated from tumour-bearing mice has shown that several stromal markers are upregulated. These include *Acta2*, *Gp38* and *Pdgfra*. Although this may suggest the presence of subepithelial fibroblasts (*Pdgfra*) and myofibroblasts (Acta2, or α-SMA) in our cultures, the upregulation of these markers may be an *in vitro* bias (Powrie lab, observations). Importantly, we detected increased amounts of *Areg* and *Ereg* mRNA in the tumour-derived stromal cultures. The fact that *Areg* and *Ereg* are significantly increased warrants further investigation, and may represent a newly described pro-tumourigenic function of stromal cells.

However, the immunological importance of intestinal stromal cells is not clear, given the lack of tools to specifically ablate certain stromal populations *in vivo*. One major unresolved issue in stromal cell biology is the lack of specific markers that can be used to generate cre-Lox mouse strains. Single-cell transcriptional profiling of stromal cell subsets from the intestine is therefore of paramount importance for identifying novel, lineage-specific markers that will enable the assessment of diverse stromal functions *in vivo*. Several groups aim at defining subsets and associated

markers, which should provide the scientific community with new insights on that front and drive stromal research forward. In CRC, this would be of particular importance given the critical role of the stromal compartment in driving disease progression and poor clinical outcome in patients with aggressive disease (Calon et al., 2015; Isella et al., 2015). Additionally, further understanding of the stromal niche in the tumour microenvironment may lead to new therapeutic strategies.

4.3.5 Regulatory T cell and stromal cell interactions

Finally, one major question remains: do IL-10$^{-/-}$ Tregs directly promote the stromal phenotype?

In an attempt to investigate whether Tregs may drive IL-6 production in stromal cells, we set up *in vitro* stromal cultures in wherein supernatants of stimulated Tregs are transferred to the cultures, and IL-6 production is measured. In that setting, we discovered that WT and IL-10$^{-/-}$ Tregs supernatants have a potent ability to increase IL-6 secretion *in vitro*. Although there may be a trend towards increased production of IL-6 using IL-10 deficient Treg supernatant, we could not confirm this effect. It is unknown whether other signals are required in order to promote the observed stromal phenotype. As such, stromal cells isolated from *H. hepaticus* animals may be activated by the inflammatory environment, and may then respond differentially to contact with the Treg supernatant. It is also possible that the acquisition of the tumour-promoting phenotype of the stromal cells requires a cellular interaction with Tregs, and therefore involves other molecules rather than, or in combination with, cytokine secretion. Mechanistically, we rule out an induction of IL-6 by TNF-α, as pre-treatment of Treg supernatants with an anti-TNF-α antibody do not block protein

secretion. Preliminary experiments have shown that EGFR blockade in the stromal cultures led to similar IL-6 production (data not shown), which might rule out this pathway as a potential mechanism. Finally, experiments aimed at blockade the JAK/STAT pathway will provide insight as to whether or not the factor promoting IL-6 production is a cytokine produced by Tregs.

4.3.6 Concluding remarks

Overall, our results suggest that our mouse model resembles certain types of colorectal cancer. We detect stromal cells in the tumour milieu, and our analyses suggest that they represent a major cellular source of IL-6, thereby promoting tumourigenesis by employing an immune effector function. Furthermore, stromal cells upregulate critical cytokines and chemokines that promote a pro-tumourigenic inflammatory setting, combined with capacities to remodel the ECM, potentially enabling tumour progression. Tumour-bearing mice also display high secretion of TGF-β and Areg in the colon, which adds to the complexity of the tumour microenvironment. Given that TGF-β endows stromal cells with a pro-tumourigenic signature in human CRC that correlates with a poor prognosis CMS4 subtype (Calon et al., 2015), we envisage that our mouse model may display features associated with a CMS4, poor-prognosis subtype of CRC. Therefore, it may provide a valuable *in vivo* tool to deepen our knowledge of the stromal biology and pro-inflammatory and tumourigenic cytokine networks in CRC. Using robust human systems, such as the use of organoids, together with interrogating patient cohort databases will enable us to translate our findings.

5 Characterisation of SOX4 and its function in colorectal cancer

5.1 Introduction

It is now evident that the tumour microenvironment is a critical driver for tumour development and progression. Consequently, it is logical to assume that tumours adapt to their environment, using growth factors and responding to cytokines in a way that will promote their growth and progression. So far, we have focused our study on tumour infiltrating immune cells as well as cytokine networks that act together to promote tumour development. We showed that IL-10 deficient Tregs preferentially promote tumourigenesis compared to WT Tregs and to their IL-10 deficient effector $CD4^+$ T cell counterparts. This was in part due to the inability of IL-$10^{-/-}$ Tregs to control *H. hepaticus*-driven inflammation, but may also involve a Treg-mediated pathological function, through an unknown mechanism that remains to be investigated (Chapter 3). *In vivo* blockade of IL-6-R as well as TGF-β revealed profound effects on tumour maintenance and progression in our model. We detected Gp38-expressing stromal cells in tumours and showed that they were a source of the pro-tumourigenic cytokine IL-6 (Chapter 4). Alongside IL-6, TGF-β and Areg represent other cytokines that were elevated in tumour-bearing mice.

Although understanding of cytokine signalling in primary tumours represents a critical step towards designing efficient therapies, targeting cytokine pathways that promote relapse by acting directly within the metastatic niche may be critical for preventing life-threatening disease progression in patients. Many CRC patients develop metastatic relapse in organs such as the liver and the lung several years after surgery, indicating that the precursors of these lesions had probably emigrated

from the primary intestinal tumour by the time of surgery (Siegel et al., 2017; West et al., 2015).

Metastasis is the process by which cancer cells escape their primary location and migrate throughout the body. Metastatic outgrowths are the primary cause of CRC-related mortality, as they are challenging to treat and compromise the function of vital organs. Several keys pathways are required for tumour cells to fully and efficiently establish secondary cancer, including the phenomenon of EMT. EMT is a complex process by which polarised epithelial cells engage in a transdifferentiation program that enables them to gain mesenchymal features. Thus, through EMT, tumour cells acquire migratory and invasive potential, which are critical steps towards disease progression and establishment of metastasis.

So-called “master regulators” of EMT have been extensively studied in various cancers, such as in CRC, and include members of the Snail, Twist, and ZEB transcription factor families (Valastyan and Weinberg, 2011). Several signalling pathways promote expression of these factors, including TGF-β, Notch and Wnt pathways, reactive oxygen species, and hypoxic stress (Zheng and Kang, 2013). TGF-β is one of the most prominent EMT inducing cytokines, and its downstream signalling activates several members of the EMT transcriptional factors. In recent years, SOX4 has emerged as another transcription factor implicated in EMT processes upon TGF-β signalling, such as in breast cancer (Tiwari et al., 2013). Moreover, elevated SOX4 expression is associated with a wide variety of human cancers, including colorectal, breast, and lung cancer (Vervoort et al., 2012).

To date, the precise function of SOX4 in CRC remains elusive and *in vivo* experiments are lacking to understand its significance and mode of action. Because TGF-β drives tumour progression in our mouse model, we hypothesised that SOX4 could be a functionally relevant mediator of the pro-tumourigenic TGF-β response. To address this hypothesis, we aimed to:

1. Characterise murine tumour gene expression compared to matched-inflamed tissue, including SOX4 expression.
2. Determine whether SOX4 exerts a pathogenic function, using *in vivo* pre-clinical models of CRC.
3. Provide an early understanding of the mechanism by which SOX4 operates in CRC.

5.2 Results

5.2.1 Sox4 is upregulated in tumours compared to inflamed tissue in a mouse model of colorectal cancer

Injection of IL-10$^{-/-}$ Tregs into 129.RAG$^{-/-}$ mice, followed by infection with *H. hepaticus*, promoted the development of stage 1 and 2 adenocarcinomas in the colon (Chapter 3 & **Figure 5.1 A**). As these tumours were large enough to be spotted by the naked eye, we dissected tumour lesions from the proximal colon and inflamed distal tissue from the distal colon of matched-animals (**Figure 5.1 B**). Histological analyses revealed that tumours did not develop in the distal colon. Given that ECM remodelling represents a critical process for tumour progression, and having determined that Gp38-expressing stromal cells upregulated the expression of Collagen type 1 and 3 (Chapter 4), we first explored the expression of different MMPs. The expression of *Mmp2* and *Mmp10* was variable between tumours and colitic tissue, and did not correlate with increased expression in tumour lesions (**Figure 5.1 C**). By contrast, we found that the expression of *Mmp9* and *Mmp13* was significantly upregulated in tumour tissue (**Figure 5.1C**). We detected *Egfr* expression in both tumours and inflamed tissue, but no differences were found. However, it highlighted the fact that Areg and other EGF family member could signal in the tumour microenvironment. Finally, the expression of *Vegfa*, *Hif1a* and *Sox4* was significantly upregulated in tumour tissue and was generally increased per mouse matched-tissues (**Figure 5.1 D**).

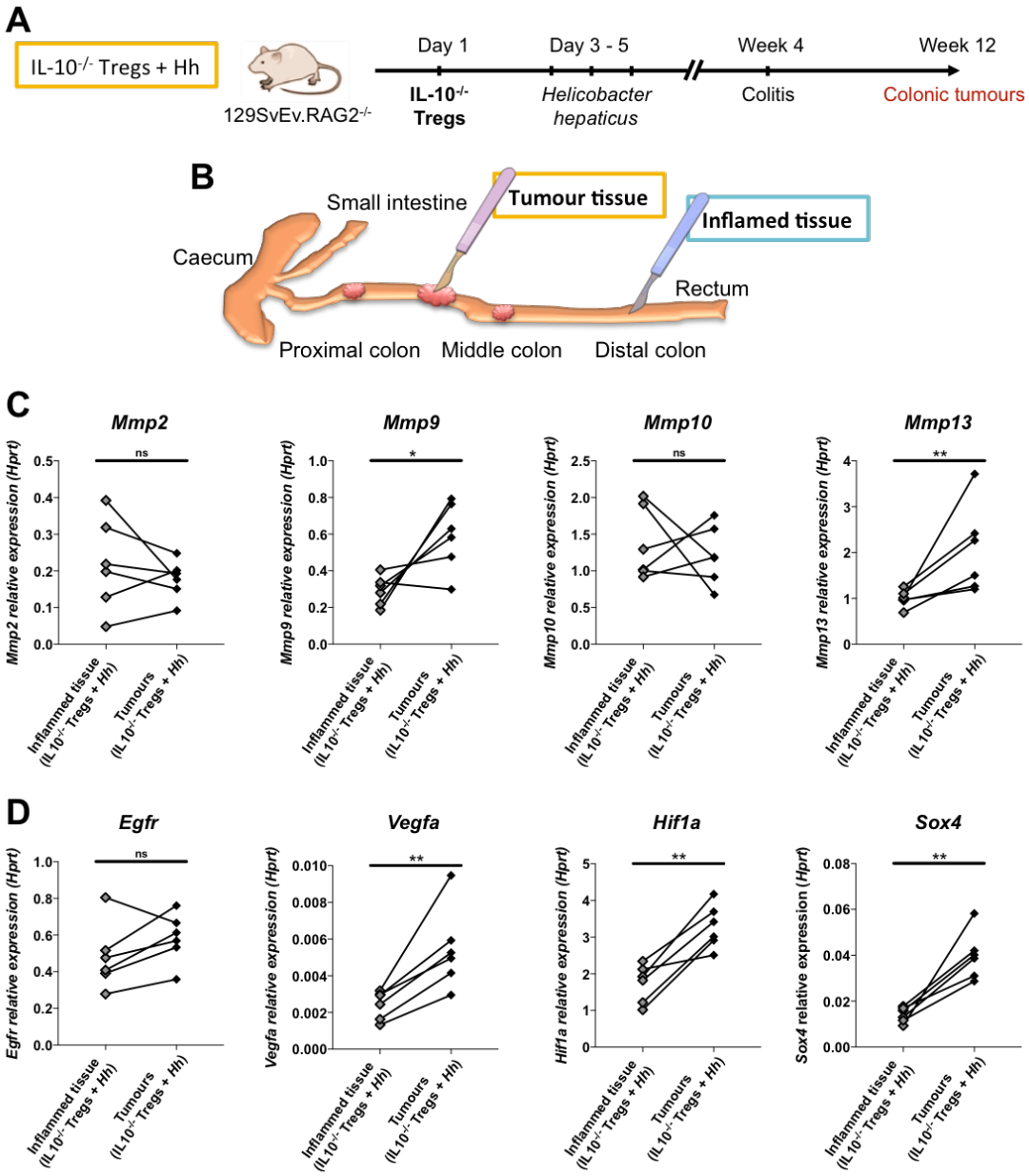

Figure 5.1: Tumour tissue shows elevated transcripts for genes associated with invasion and tissue remodelling in a mouse model of colitis-associated cancer.

129.RAG$^{-/-}$ mice were injected with IL10$^{-/-}$ Tregs and infected with *H. hepaticus*. At week 12, mice were sacrificed, and colons harvested. Whole tissue gene expression was assessed by qPCR.

(A) Scheme of treatment.
(B) Tumour tissue was selected based on tumour size (> 0.5 cm), and matched-inflamed tissue was carefully chosen from the distal part of colon, where tumours are rarely found by histopathology. Tissue was dissected out with a razor blade and directly snap frozen in liquid nitrogen.
(C, D) RNA was extracted from tissue and mRNA expression of indicated genes is shown, relative to the housekeeping gene *Hprt*.

Each dot represents a mouse and a line between dots represents paired-tissues from the same animal. Data represents one experiment representive of 2 independent experiments performed at the JR site.
Statistical significance was determined using a Mann Whitney U Test. * $p \leq 0.05$, ** $p \leq 0.01$.

Given that Sox4 expression has been linked to TGF-β signalling and promotion of EMT in breast cancer (Tiwari et al., 2013), we sought to confirm its expression in the inflamed colon and tumour lesions by immunofluorescence. Colons from 129.RAG$^{-/-}$ animals showed Sox4 expression within the epithelium, but not the lamina propria (**Figure 5.2 A**). Analysis of Sox4 expression in inflamed versus tumour sites in mice restored with IL-10$^{-/-}$ Tregs and infected with *Hh* is shown in **Figure 5.2 B and C**. In the mild (**Figure 5.2 B**) and dysplastic (**Figure 5.2 C**) inflamed tissue, Sox4 was expressed in the epithelium, with a similar pattern as steady state controls. By contrast, Sox4 was strongly expressed in the malignant epithelium, including in invasive crypts (**Figure 5.2 D, E**). The staining intensity seemed enhanced in tumours, compared to the match-inflamed sections, but requires quantification to confirm this.

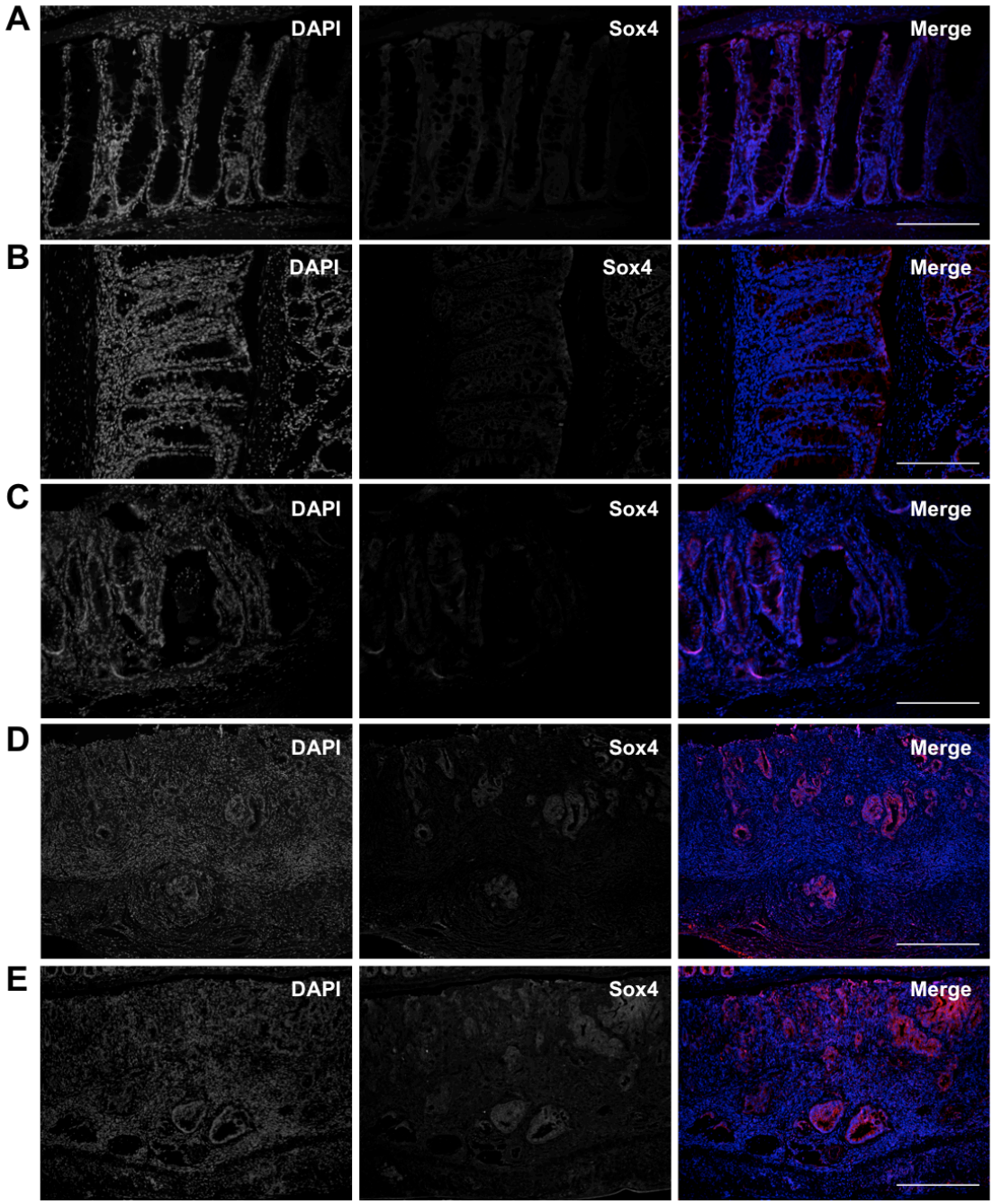

Figure 5.2: Sox4 expression is elevated in the malignant epithelium in a mouse model of colitis-associated cancer

Colonic sections from IL-10$^{-/-}$ Tregs + *Hh* mice were selected based on H&E staining to identify lesions, and then processed for immunofluoresence staining.

(A) Representative image of Sox4 staining in steady state 129.RAG$^{-/-}$.
(B, D) Representative images of Sox4 staining in same mouse, showing the inflamed epithelium (B) and a T1 adenocarcinoma invading the muscularis mucosae (D).
(C, E) Representative images of Sox4 staining in same mouse, showing the inflamed epithelium (C) and a large T2 adenocarcinoma crossing the submucosae (E).

Images represent DAPI (nuclei) and Sox4 in black and white to allow visualisation, and merged images from red channel (Sox4) and blue channel (nuclei, DAPI).
Original magnifications: 10x (A-C) and 4x (D, E). Scale bars: 200μm (A-C) and 500μm (D, E).
Staining was performed in n=4 steady state mice, and n=8 mice from 2 independent experiments.

5.2.2 SOX4 is expressed in human colorectal cancer

As Sox4 is expressed in murine tumour tissue, we explored *SOX4* gene expression in human cancers. The Human Protein Atlas represents a useful online resource to probe gene and protein expression in cancers (Uhlen et al. 2017; Uhlen et al. 2015). It computes RNA-sequencing data from The Cancer Genome Atlas (TCGA) database of 17 cancers and displays a RNA expression overview. *SOX4* expression was detected in all cancers, including colorectal cancer, and showed increased FPKM (Fragments Per Kilobase of exon per Million reads) in endometrial, ovarian, testis, breasts and lung cancers (**Figure 5.3 A**). By contrast, liver cancer showed the lowest FKPM values.

The Human Protein Atlas database also provides information regarding protein expression in tumours versus normal tissue. For each cancer, a blue-scale color-coding bar denotes the protein expression levels of high (dark blue), medium (blue), low (light blue), or not detected (white). A total of 12 patients were profiled for SOX4 expression in colorectal cancer, and showed medium expression by tumours cells (**Figure 5.3 B** "cancer staining"). In comparison, protein expression of normal colon was generally scored as low (**Figure 5.3 B** "protein expression of normal tissue).

Both tumour and normal tissues IHC stainings are also provided. In normal tissue, SOX4 expression was scored as high in endothelial cells, and low expression in glandular cells, ganglions, and the normal epithelium (**Figure 5.4 A**). However, in tumour tissues from patients with adenocarcinomas, SOX4 was more broadly expressed, and invasive crypts were positive (**Figure 5.4 B**).

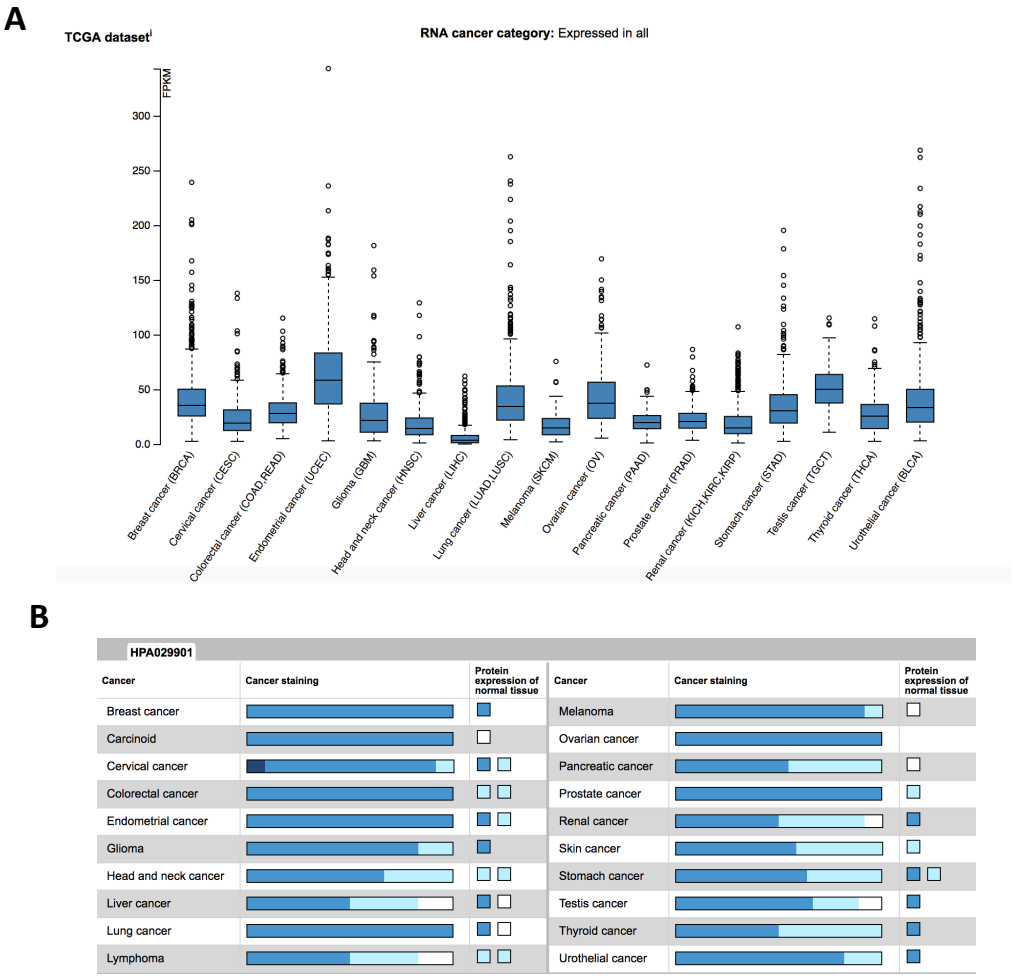

Figure 5.3: *SOX4* expression across various cancers, using the Human Protein Atlas interface.

The Pathology Atlas is built on gene expression data that includes quantitative transcriptomics data (RNA-Seq) and spatial proteomics data (immunohistochemistry on tissue microarrays). All transcriptomics data has been retrieved from The Cancer Genome Atlas (TCGA) and all proteomics data has been generated in-house using the same antibodies as in protein expression profiling in normal human tissues.

(A) RNA expression overview shows RNA-seq data from The Cancer Genome Atlas. RNA-seq data in 17 cancer types are reported as median FPKM (number of Fragments Per Kilobase of exon per Million reads), generated by The Cancer Genome Atlas (TCGA). RNA cancer tissue category is calculated based on mRNA expression levels across 17 cancer tissues and include: cancer tissue enriched, cancer group enriched, cancer tissue enhanced, expressed in all, mixed and not detected.

(B) For each cancer, the fraction of samples with protein expression level high, medium, low, or not detected are provided by the blue-scale color-coding (dark blue: high, white: not detected). The antibody used for SOX4 detection *in situ* is HPA029901.

Protein Atlas version 17.
http://www.proteinatlas.org/ENSG00000124766-SOX4/pathology

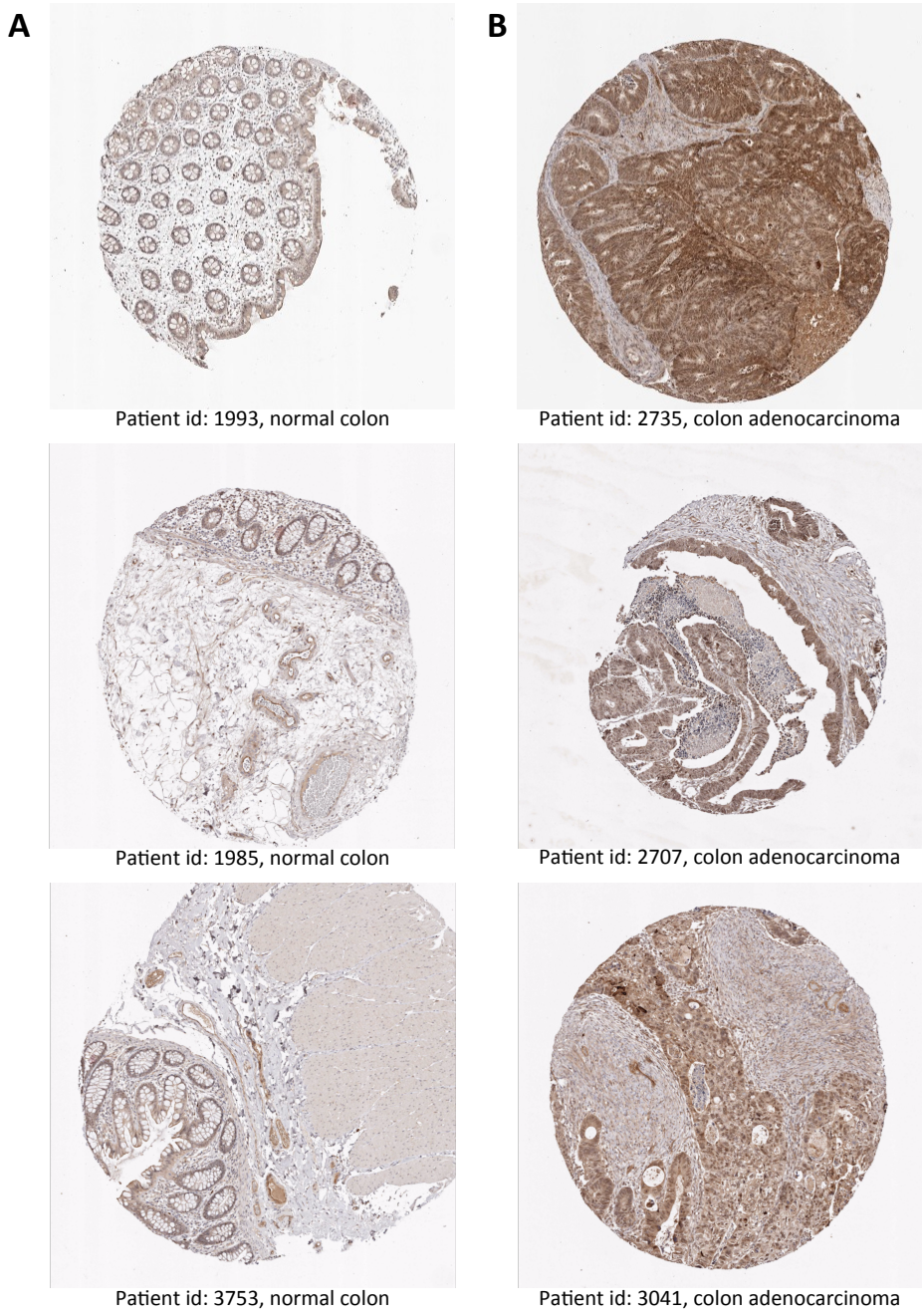

Figure 5.4: SOX4 is expressed in normal colon tissue and its expression is detected in human colon adenocarcinomas.

The Human Protein Atlas contains images of histological sections from normal and cancer tissues obtained by immunohistochemistry. Antibodies are labeled with DAB (3,3'-diaminobenzidine) and the resulting brown staining indicates where an antibody has bound to its corresponding antigen. The antibody used for SOX4 detection *in situ* is HPA029901.

(A) SOX4 staining in normal colon tissue. Image credit: Human Protein Atlas. Patients ID are indicated.
(B) SOX4 staining in colon adenocarcinoma. Image credit: Human Pathology Atlas. Patients ID are indicated.

Protein Atlas version 17.
http://www.proteinatlas.org/ENSG00000124766-SOX4/pathology

Together, these data showed that SOX4 is expressed at the mRNA and protein level in CRC patients. However, although the Human Protein Atlas represents an interesting way to probe gene and protein expression in cancers, the database does not allow for differential expression analysis and further quantification.

5.2.3 *SOX4* is upregulated in CRC and further increased in liver and lung metastases

Given Sox4 upregulation in murine adenocarcinomas and its expression in human colorectal cancer, we next assessed *SOX4* expression in tumours using a publically available transcriptomic dataset.

Shaffer et al (2009) performed a transcriptomic analysis in colorectal cancer patients across multiple disease sites. The study consisted of patients who presented at Memorial Sloan-Kettering Cancer Center (US) with a colonic neoplasm between 1992 and 2004. Biological specimens used in this study included primary colon adenocarcinomas, adenomas, metastasis and corresponding normal mucosae (Shaffer M et al., 2009). We downloaded the dataset (GEO Accession: GSE41258) and interrogated *SOX4* expression across collected samples, normalised to normal colon.

First, we found that *SOX4* expression was significantly elevated in both polyps and primary tumours compared to normal tissue (**Figure 5.5 A**). There was no difference in *SOX4* expression between polyps and primary CRC. The Shaffer et al dataset provides valuable information regarding disease progression, as samples from metastatic disease are also available. Thus, we compared *SOX4* expression in liver and lung metastases, and detected a significant increase in its expression compared

to matched-tissues, respectively normal liver and normal lung (**Figure 5.5 A**). Surprisingly, when comparing primary CRC to metastatic sites, we found that *SOX4* was significantly enriched in the latter (**Figure 5.5 A**).

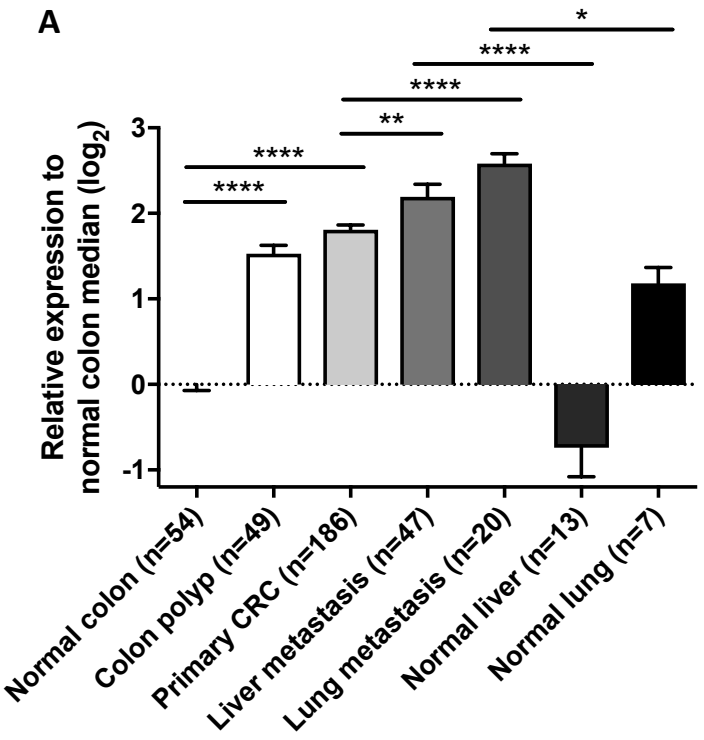

Figure 5.5: *SOX4* expression is elevated in polyps and primary tumours compared to normal colon, and is further increased in metastases compared to primary CRC.

The dataset from Shaffer et al (2009, GEO Accession: GSE41258) was used to explore *SOX4* expression in patients that were recruited with a colonic neoplasm between 1992 and 2004. Biological specimens included primary colon adenocarcinomas, adenomas, metastases and corresponding normal mucosae.

RNA was extracted and microarrays were performed. *SOX4* expression was log2 normalised across the dataset median, and was then normalised to normal colon expression.

(A) *SOX4* expression relative to normal colon in indicated samples.

5.2.4 *SOX4* high CRC patients have worsen prognosis

We next sought to determine whether *SOX4* expression impacts CRC patient survival.

First, disease-specific survival (DSS) was assessed in all cases (stage I to IV), defining *SOX4*-high and low patients, based on the top 2/3 expressers for *SOX4*-high and bottom 1/3 expressers for *SOX4*-low. *SOX4*-high patients were strongly associated with poor DSS (*HR*=1.9, 95% CI=1.175-3.237, *P*=0.0097) (**Figure 5.6 A**). Similarly, amongst stages II and III, SOX4-high expression in patients correlated with poor DSS (*HR*=3.2, 95% CI=1.024-9.754, *P*<0.05) (**Figure 5.6 B**).

Secondly, to further explore SOX4's impact on patient survival, we separated patients based on their SOX4 expression either into thirds (**Figure 5.6 C**), or defined *SOX4*-high as the top 10% expressers, *SOX4*-low as the bottom 10% expressers, and *SOX4*-int as the 80% middle expressers (**Figure 5.6 D**). In a similar fashion, *SOX4*-high expression in patients correlated with decreased DSS in both cases (*P* trend=0.0047 **C** and *P* trend=0.0008, **D**).

Altogether, these survival analyses revealed that *SOX4* high expression in CRC patients was associated with decreased disease-specific survival in disease stages I to IV, but also when considering stages II and III only.

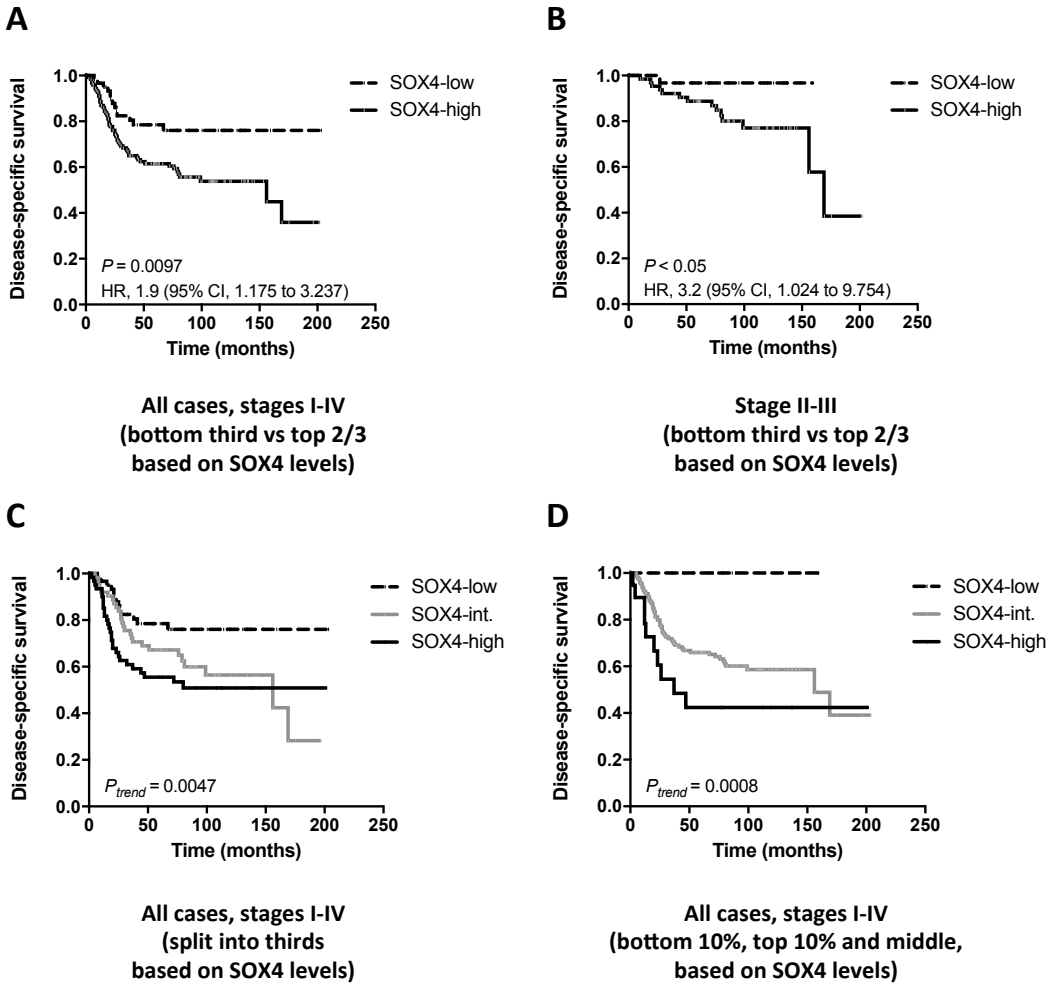

Figure 5.6: High *SOX4* expression promotes poor disease-specific survival in CRC patients.

Disease-specific survival (DSS) in indicated disease stages in the GSE41258 transcriptomic dataset, using Kaplan-Meier methods.

(A) DSS in the cohort based on *SOX4* expression for all cases (stages I to IV). *SOX4*-high is defined by the top 2/3 expressers, and low is defined by the bottom 1/3 expressers.
(B) DSS in the cohort based on *SOX4* expression for stage II and III only. *SOX4*-high is defined by the top 2/3 expressers, and low is defined by the bottom 1/3 expressers.
(C) DSS in the cohort based on *SOX4* expression for all cases (stages I to IV). *SOX4*-high, intermediate and low is defined by thirds.
(D) DSS in the cohort based on *SOX4* expression for all cases (stages I to IV). *SOX4*-high is defined by the top 2/3 expressers, and low is defined by the bottom 1/3 expressers.

For comparison of two groups (A and B), *P* values were computed using Log-rank (Mantel-Cox) tests. Hazard ratios (HR) are univariate Cox proportional hazard ratios with 95% confidence intervals.
For comparison of three groups (C and D), *P* trend values were computed using Logrank test for trend.

5.2.5 SOX4 mRNA and protein expression is increased in liver metastases originating from primary tumours in CRC patients

Given the upregulation of *SOX4* mRNA expression in metastases compared to primary tumours, and the decreased survival detected in *SOX4*-high patients, we next investigated SOX4 expression in liver metastasis.

We established a collaboration with Ruth Muschel's laboratory (Department of Oncology, Oxford UK) to determine SOX4 expression in liver metastases samples from CRC patients. *SOX4* mRNA expression was first assessed, comparing normal liver (n=7) and liver metastases (n=10). In liver metastases, *SOX4* was significantly upregulated (p=0.003) (**Figure 5.7 A**). Next, SOX4 protein expression was analysed by ELISA in whole tissue lysate (normal liver n=11 and liver metastasis n=12), and showed significant increase in SOX4 protein expression in liver metastases (p=0.021) (**Figure 5.7 B**).

Using the Human Protein Atlas, we probed SOX4 expression in normal liver tissue. SOX4 expression was scored as medium on hepatocytes in normal liver, and no expression was detected on bile duct cells (Human Protein Atlas, data not shown). Thus, to confirm that the upregulation of SOX4 in liver metastases was not biased due the presence of hepatocytes, we carried out immunofluorescence staining on normal liver and liver metastases tissue sections. In line with data from the Human Protein Atlas, SOX4 expression was detected in normal liver in the majority of the cells, possibly corresponding to hepatocytes (**Figure 5.7 C, D**). In certain areas of normal liver, SOX4 expression was not detected (**Figure 5.7 C**, middle) and potentially represented bile duct cells, as there seemed to be a tubular structure.

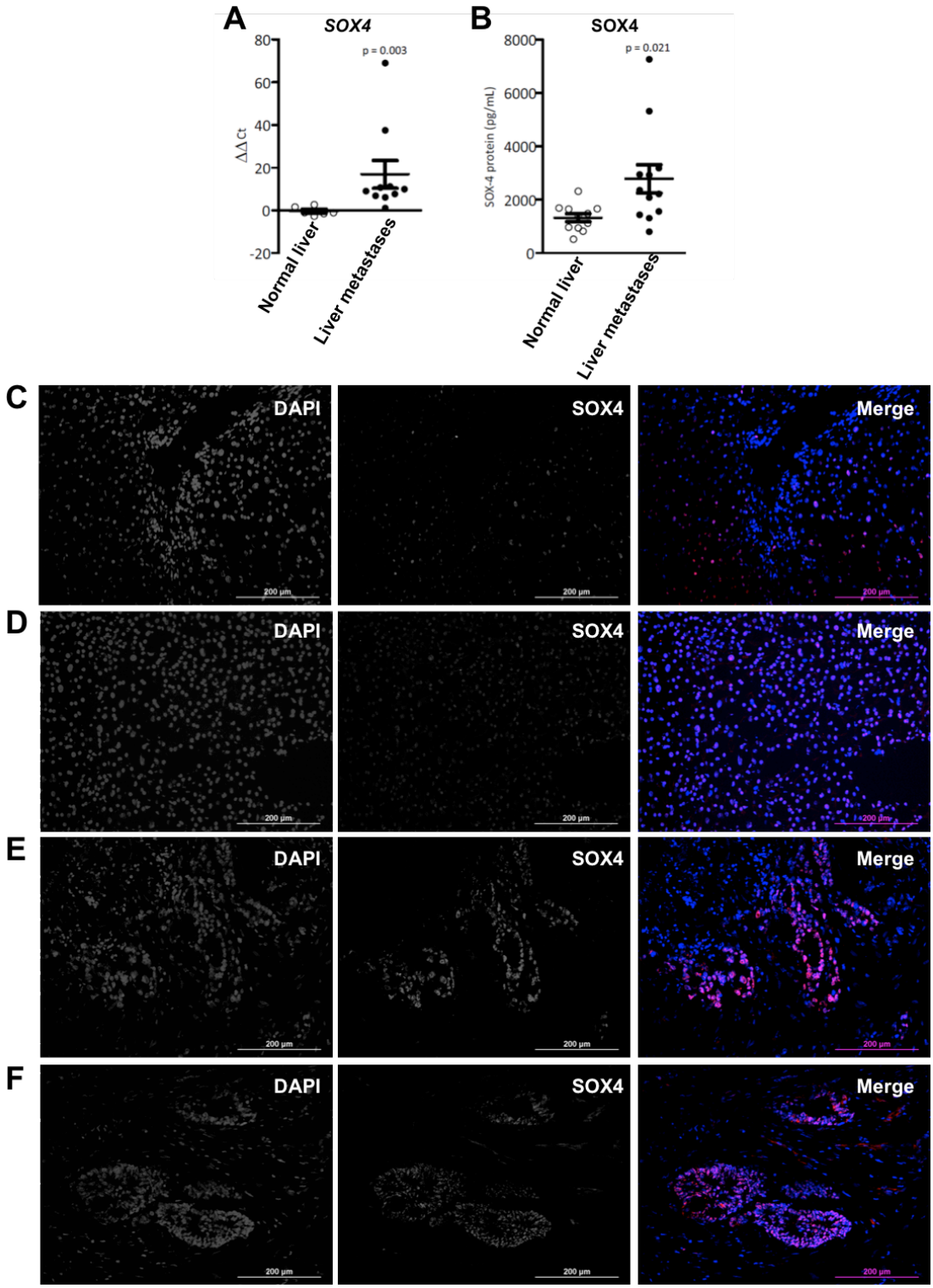

Figure 5.7: SOX4 mRNA and protein expression is elevated in liver metastases compared to normal liver in CRC patients.

(A) *SOX4* expression was measured by qPCR from indicated RNA samples.
(B) SOX4 protein concentration was measured in tissue lysate from indicated samples.
(C-F) SOX4 staining in normal liver (C, D) and liver metastases (E, F), from matched-patients (C/E & D/F). Images represent DAPI (nuclei) and SOX4 individual channels, and merged images from red channel (SOX4) and blue channel (nuclei, DAPI). Staining is representative of n=15 patients.

In liver metastases, the architecture was drastically different from that of the normal liver. Two types of structure were detected: infiltrating cells that resembled colonic crypts, and a stroma-like compartment surrounding the invasive crypts. Overall, SOX4 expression was mainly restricted to the crypt-like structures, while the stroma compartment remained largely SOX4 negative (**Figure 5.7 E, F**). In addition, although it is difficult to quantify, some crypt-like structures were partially SOX4 negative (**Figure 5.7 E**, top part). We detected SOX4 expression in 100% of the liver metastases samples from CRC patients (15 out of 15 patients).

Overall, we confirmed that SOX4 mRNA and protein expression is increased in liver metastases compared to normal liver. Furthermore, *in situ* SOX4 staining of 15 patients has revealed that liver metastases expressed SOX4, and that its expression was primarily confined within the invasive crypts.

5.2.6 *SOX4* expression is heterogeneous in different colorectal cancer cell lines

Given that SOX4 is expressed in both primary CRC tumours and liver metastases, we next determined whether *SOX4* was also expressed in different colorectal cancer cell lines, in order to select lines for *in vitro* studies.

The Shaffer et al dataset (GSE41258) also contained transcriptomics data from different CRC lines, which we analysed for *SOX4* expression. Certain lines were high expressers, such as the HTB39 and SW116 lines, while others displayed low *SOX4* levels, including DLD1 and LOVO cells (**Figure 5.8 A**). In the laboratory, a screen for *SOX4* expression was also performed on available CRC lines. We detected variability

in *SOX4* expression levels, with the HCT116 line expressing higher levels and Colo205 cells expressing lower levels at baseline (**Figure 5.8 B**).

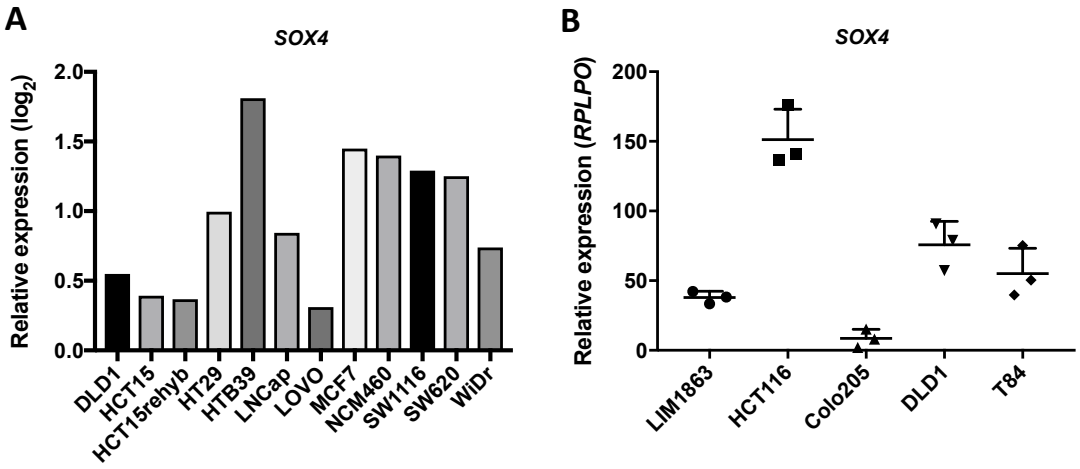

Figure 5.8: *SOX4* expression in different colorectal cancer cell lines is heterogeneous.

(A) The dataset from Sheffer et al (2009, GEO Accession: GSE41258) was used to explore *SOX4* expression in a panel of colorectal cancer cell lines. RNA was extracted and microarrays were performed. *SOX4* expression was median normalised log2 across the dataset.

(B) Indicated colorectal cancer cell lines were harvested and RNA was extracted for *SOX4* gene expression analysis by qPCR, relative to the housekeeping gene *RPLPO*. Each dot represents an independent *in vitro* culture.

5.2.7 Generation of over-expressing and knockdown CRC lines for *in vitro* and *in vivo* studies

In order to investigate SOX4 function both *in vitro* and *in vivo*, we chose two different human CRC lines and generated associated SOX4 over-expressing and knockdown lines, using lentiviral transduction.

Given that the HCT116 and Colo205 displayed a very distinct SOX4 expression profile, they were chosen for our studies. All lines were first transduced with a luciferase expressing lentiviral vector to allow *in vivo* tracking. Subsequently, a total of 4 sub-lines were generated per cell lines (**Figure 5.9 A**). Validation of overexpression and knowndown was assessed by qPCR and WB analysis (**Figure 5.9 B, C**).

A

Cell line	ID	SOX4 status
Colo205	p-GFP	control GFP for overexpression
	p-SOX4	SOX4 overexpression
	Sh-CTL	ShRNA control for knockdown
	Sh-SOX4	ShSOX4 knockdown
HCT116	p-GFP	control GFP for overexpression
	p-SOX4	SOX4 overexpression
	Sh-CTL	ShRNA control for knockdown
	Sh-SOX4	ShSOX4 knockdown

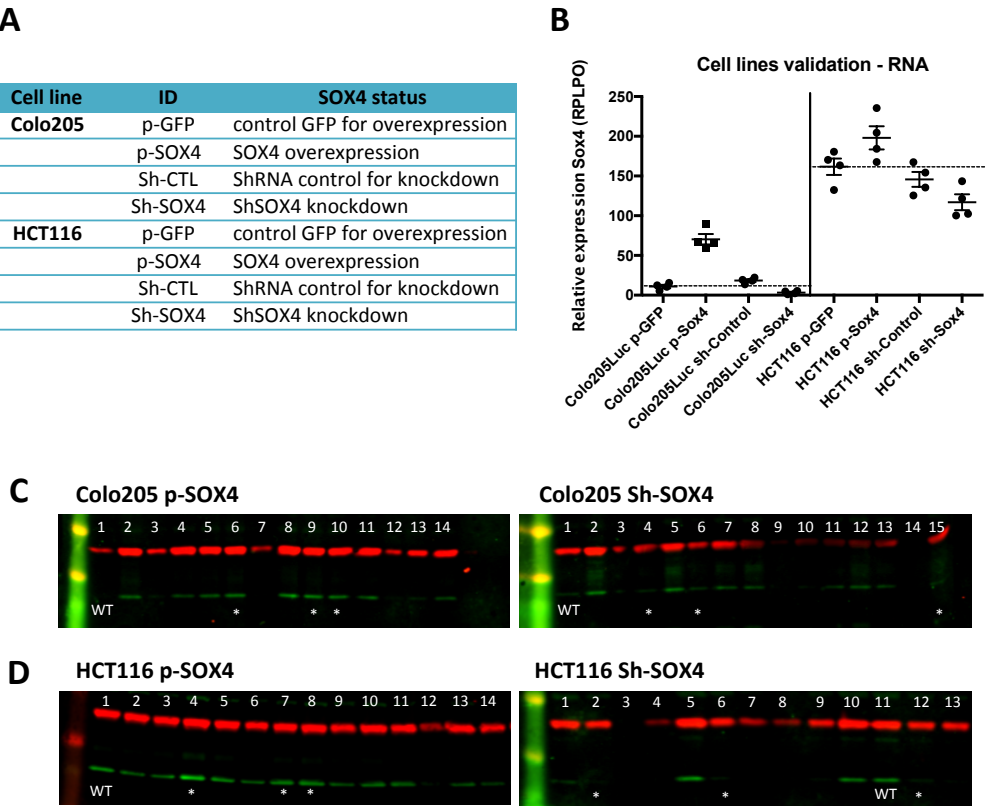

Figure 5.9: Generation of Colo205 and HCT116 sub-lines for SOX4 *in vivo* studies.

(A) For each of the cell lines, an overexpressing line (p-SOX4) was generated, including a control line overexpressing GFP (p-GFP), as well as a knockdown line (Sh-SOX4), including a knockdown control line (Sh-CTL).
(B) qPCR validation of different clones for indicated Colo205 and HCT116 sub-lines.
(C, D) SOX4 protein expression validation by LI-COR. ACTIN is displayed in the red chanel and SOX4 is detected in the green chanel. Three clones per sub-line were selected, indicated with a star, for archive and downstream applications. The WT cell line is indicated.

Protein expression generally mirrored *SOX4* gene expression, with Colo205 cells expressing low amounts of SOX4 at baseline, and the HCT116 line expressing high amounts of SOX4. Details regarding lentiviral transduction can be found in the Material & Methods section 2.6. For each sub-lines, three clones were chosen based on protein expression and were then selected using appropriate antibiotic selection or FACS-sorting strategy for GFP expression. Initial observations did not reveal a specific change in cellular shape, and cultured sub-lines did not display altered proliferation or signs of senescence (data not shown).

5.2.8 Overexpression of SOX4 in Colo205 cells promotes ectopic xenograft growth *in vivo*

To investigate whether SOX4 controls tumour growth and metastasis, rather than just being a marker of disease, we set up *in vivo* ectopic xenograft experiments. Using the Colo205 sub-lines, we hypothesised that overexpression of SOX4 might lead to enhanced tumour growth. Moreover, given that Colo205 cells expressed low amounts of SOX4 at baseline, we assumed that the overexpressing sub-line might reveal the most striking results.

Briefly, NOD.SCID mice received tumour cells by sub-cutaneous injection into the right flank (**Figure 5.10 A**). Every 3 to 4 days, tumour growth was measured using a digital calliper. Once tumour volume reached our defined end-point, mice were sacrificed and tumours measured. Tumours were subsequently dissected out for tissue histology and analysis of RNA expression.

All Colo205 sub-lines showed sign of growth from day 6 onwards. Both Colo205 Sh-CTL and Sh-SOX4 lines had a steady growth throughout the experiment, reaching an approximate tumour volume of 200mm^3 by day 21 (**Figure 5.10 B**, blue and yellow dots). By contrast, the p-GFP control sub-line showed a slightly increased volume starting from day 15 and reached a final tumour volume of 350mm3 on average, which is statistically different from the Sh-CTL and Sh-SOX4 sub-lines, **Figure 5.10 B**, green dots, $p < 0.0032$ not shown on graph). Finally, the p-SOX4 overexpressing sub-line displayed a rapid tumour growth, reaching 200mm^3 in volume on average by day 6. At day 22, tumours in the p-SOX4 sub-line grew on average to 570mm^3 (**Figure 5.10 B**, red dots). From day 12 until the end-point, p-SOX4 tumours were significantly

larger than the control sub-line p-GFP, emphasising the effect of SOX4 overexpression *in vivo*.

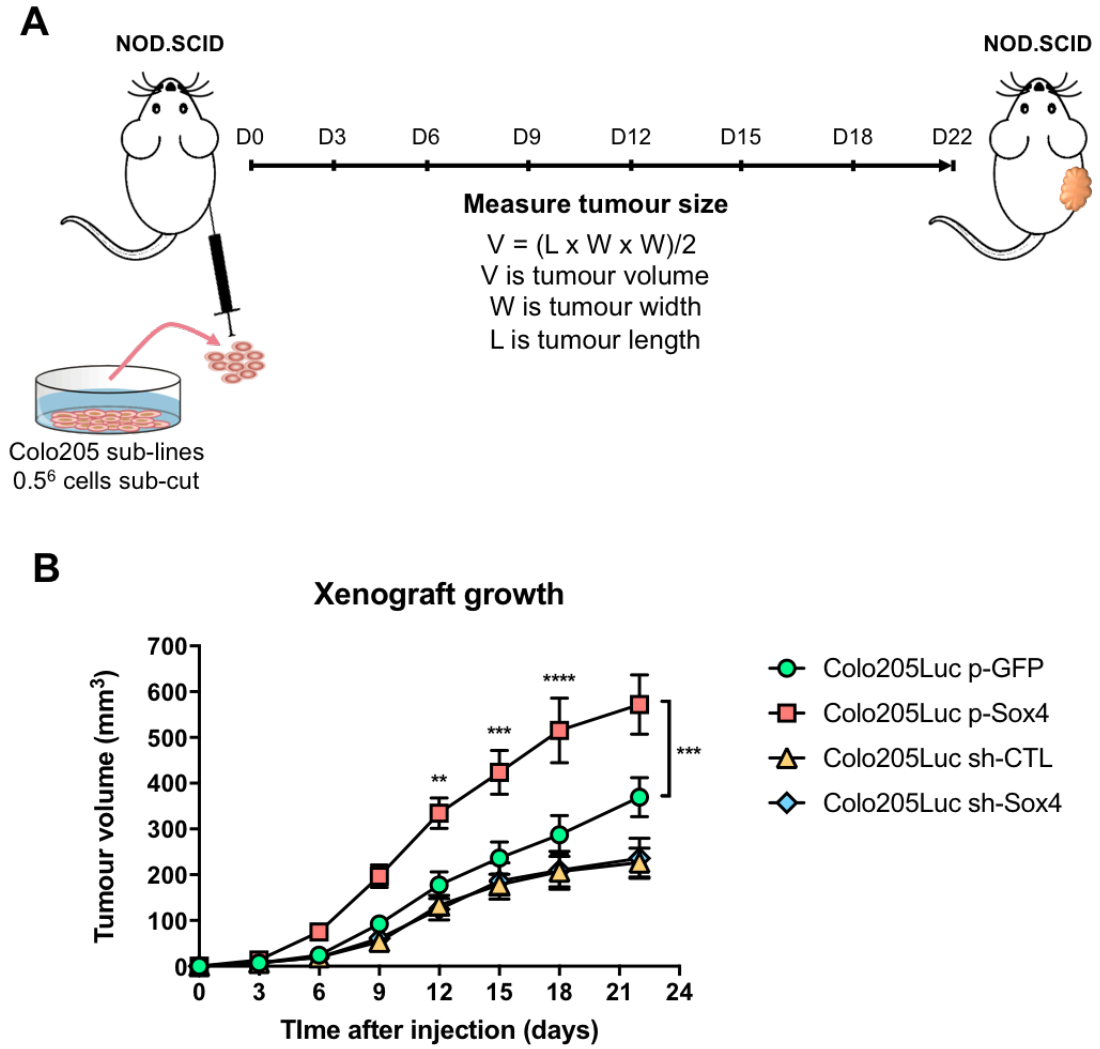

Figure 5.10: The Colo205 p-SOX4 overexpressing sub-line promotes increased tumour growth *in vivo*.

(A) Colo205 sub-lines were harvested at 80% confluency and single cell suspensions were prepared for injection into NOD.SCID hosts. 500.000 cells were injected via sub-cutaneous route per mouse, into the right flank. Tumour volume was measured every 3 or 4 days by a digital calliper. Tumour volume was calculated as indicated.

(B) Xenograft growth measurements from day of injection (day 0) until end of experiment (day 22).

Each dot represents the mean value of tumour volume per sub-line and bar represents ±SEM. Data represents one experiment performed at the KIR, with p-GFP and Sh-CTL n=5 mice per group, p-SOX4 n=7 mice, and Sh-SOX4 n=8 mice. Data is representative of 2 independent experiments.
Statistical significance was determined using a repeated measures two-way ANOVA, followed by a Tukey's multiple comparisons test. * $p < 0.0332$, ** $p < 0.0021$, *** $p < 0.0002$, **** $p < 0.0001$.

5.2.9 Knockdown of SOX4 in HCT116 cells delays ectopic xenograft growth *in vivo*

Similar experiments were performed with the HCT116 sub-lines. Considering that HCT116 cells expressed high amounts of SOX4 at baseline, we hypothesised that the knockdown sub-line (Sh-SOX4) might represent the ideal sub-line to test SOX4 function *in vivo*. Consequently, tumour growth might be reduced in the Sh-SOX4 sub-line, while the p-SOX4 sub-line might enhance tumour growth.

Briefly, NOD.SCID mice received tumour cells by sub-cutaneous injection into the right flank (**Figure 5.11 A**). Every 3 to 4 days, tumour growth was measured using a digital calliper. Once tumour volume reached the end-point, mice were sacrificed and tumours measured.

All HCT116 sub-lines showed sign of growth from day 9 onwards. Both HCT116 p-GFP and p-SOX4 lines had a steady growth throughout the experiment, reaching an approximate tumour volume of respectively 1080mm^3 and 950mm^3 by day 27 (**Figure 5.11 B**, green and red dots). No differences in growth were detected between the overexpressing and control-GFP sub-lines. Similarly, the growth curve of the Sh-CTL sub-line mirrored the growth of the p-SOX4 and p-GFP tumours (**Figure 5.11 B**, blue dots). By contrast, the Sh-SOX4 sub-line displayed a significantly delayed growth by day 18 ($p < 0.0032$), with an average tumour volume 3 times smaller, with a mean of 180mm^3 compared to 420mm^3 on average for the Sh-CTL sub-line (**Figure 5.11 B**, yellow dots). The decreased tumour volume was sustained until the end point (day 27) and was significantly different from the control Sh-CTL sub-line.

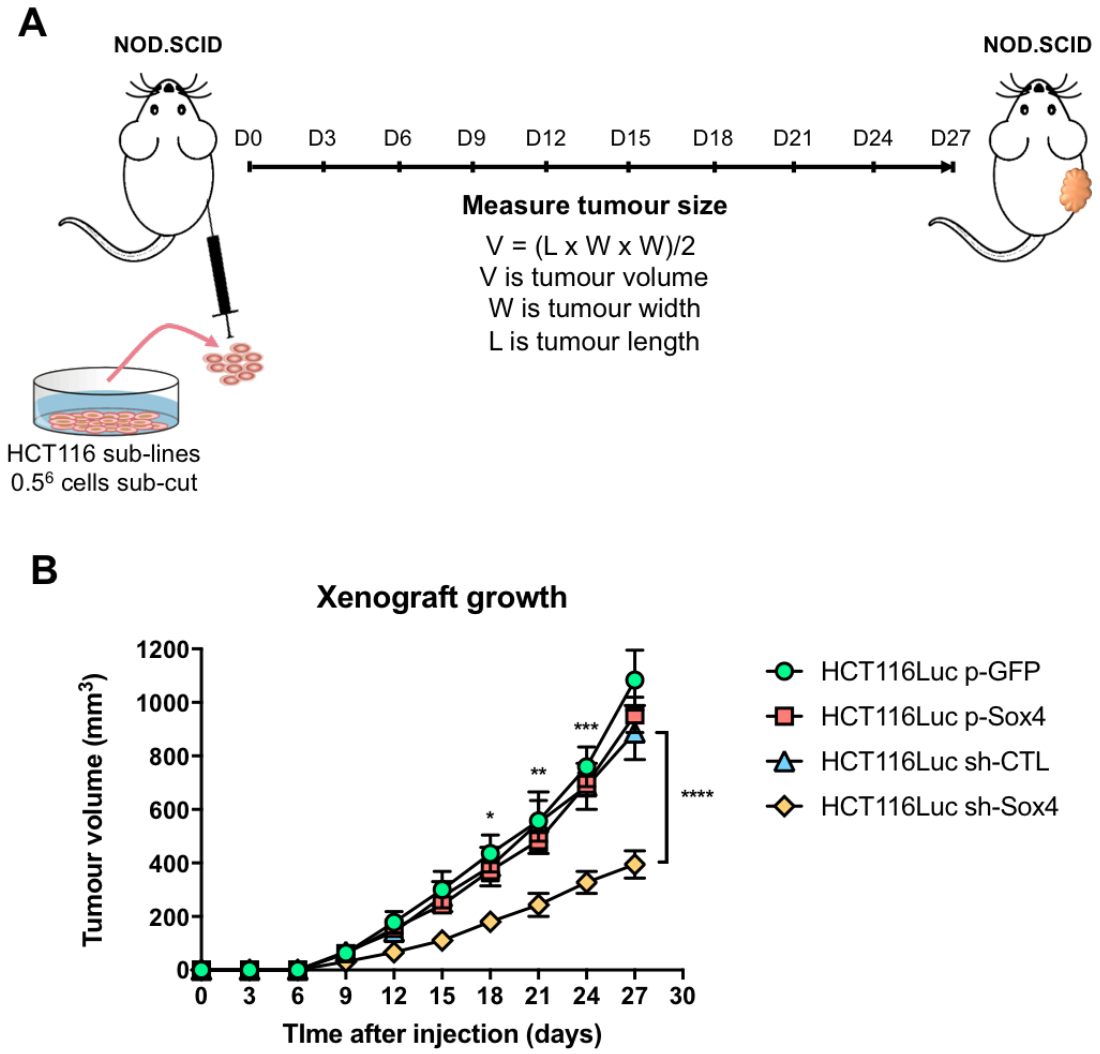

Figure 5.11: The HCT116 Sh-SOX4 knockdown sub-line displays decreased tumour growth *in vivo*.

(A) HCT116 sub-lines were harvested at 80% confluency and single cell suspensions were prepared for injection into NOD.SCID hosts. 500.000 cells were injected via sub-cutaneous route per mouse, into the right flank. Tumour volume was measured every 3 or 4 days by a digital calliper. Tumour volume was calculated as indicated.

(B) Xenograft growth measurements from day of injection (day 0) until end of experiment (day 27).

Each dot represents the mean value of tumour volume per sub-line and bar represents ±SEM. Data represents one experiment performed at the KIR, with p-GFP and Sh-CTL n=5 mice per group, p-SOX4 n=7 mice, and Sh-SOX4 n=7 mice. Data is representative of 2 independent experiments.
Statistical significance was determined using a repeated measures two-way ANOVA, followed by a Tukey's multiple comparisons test. * $p < 0.0332$, ** $p < 0.0021$, *** $p < 0.0002$, **** $p < 0.0001$.

Altogether, our xenografts experiments using two different human colorectal cancer cell sub-lines have highlighted the importance of SOX4 in regulating tumour growth *in vivo*.

Given that all sub-lines express luciferase, we were also able to track tumour cell escape to distant organs via luminescent reading using the IVIS Spectrum In Vivo Imaging System (IVIS). However, no metastasis growth was detected outside the site of injection (data not shown). These results might relate to the fact that the tumours grew relatively fast, while metastasis colonisation usually appears at later time points. Establishing experiments with fewer injected cells might allow for slower tumour growth, which would provide more time for metastasis to occur.

5.2.10 Generation of SOX4 overexpressing and knockdown MC38 sub-lines

As we detected a difference in tumour growth that was dependent on SOX4 expression, we next wanted to test this pathway in an isograft system, where cancer cells are injected into a genetically identical inbred and immune competent host.

MC38 is a cell line derived from C57BL/6 murine colonic adenocarcinoma cells, which allows the study of tumour-stroma-immune interactions in a syngenic system. MC38 cells are also known to metastasise into spleen and liver over time, providing the opportunity to SOX4 function not only in tumour growth, but also in metastasis in the context of an adaptive immune response.

The MC38 line expressing luciferase was transduced with different lentiviral vectors to generate different sub-lines: SOX4 overexpressing and SOX4 knockdown sub-lines, including overexpressing and knockdown controls. A total of 4 sub-lines were generated per cell line (**Figure 5.12 A**). Validation of overexpression and knowndown of several clones was assessed by WB analysis (**Figure 5.12 B**).

A

Cell line	ID	SOX4 status
MC38	p-GFP	control GFP for overexpression
	p-SOX4	SOX4 overexpression
	Sh-CTL	ShRNA control for knockdown
	Sh-SOX4	ShSOX4 knockdown

B

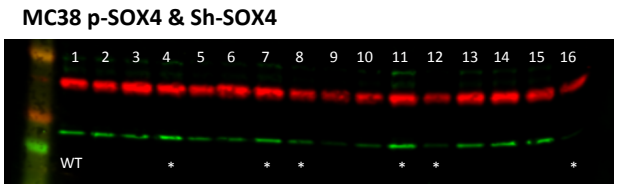

Figure 5.12: Generation of MC38 sub-lines for SOX4 *in vivo* studies.

(A) An overexpressing line (p-SOX4) was generated, including a control line overexpressing GFP (p-GFP), as well as a knockdown line (Sh-SOX4), including a knockdown control line (Sh-CTL).

(B) SOX4 protein expression validations by LI-COR. ACTIN is displayed in the red chanel and SOX4 is detected in the green chanel. Three clones per sub-line were selected, marked with a star, for archive and downstream applications. The first line corresponds to the WT cell line. Lines 2-6,10 represent different clones of p-SOX4, and lines 7-9,11-15 represent different clones of Sh-SOX4.

Protein expression revealed that MC38 expressed SOX4 at baseline, however overexpression could enhance its expression. Details regarding lentiviral transduction can be found in Material & Methods section 2.6. For each of the sub-lines, three clones were chosen based on protein expression, and were then selected using appropriate antibiotic selection or FACS-sorting strategy for GFP expression.

5.2.11 SOX4 overexpression promotes increased tumour growth in B6.RAG$^{-/-}$ mice

To test whether SOX4 expression promoted tumour growth in immune competent animals, we first validated the MC38 overexpressing sub-line's ability to promote tumour growth in B6.RAG$^{-/-}$ animals.

Briefly, B6.RAG$^{-/-}$ mice received MC38 tumour cells by sub-cutaneous injection into the right flank (**Figure 5.13 A**). Every 3 days, tumour growth was monitored using a digital calliper. Once tumour volume reached the end-point, mice were sacrificed and tumours measured.

We confirmed that MC38 p-GFP and p-SOX4 cells were able to develop in B6.RAG$^{-/-}$ recipients (**Figure 5.13 B**). We already noticed a significant difference in tumour volume between the two sub-lines by day 12, with a mean tumour volume of 246mm^3 for p-SOX4 cells compared to 123mm^3 for p-GFP tumours (**Figure 5.13 B**, $p < 0.0332$). This difference was maintained over time, out to the end of the experiment (day 18, $p < 0.0021$).

These preliminary results validated the isograft system in immunodeficient B6 mice and indicated that SOX4 overexpression in MC38 led to increased tumour growth, similarly to previous experiments using modified human CRC lines.

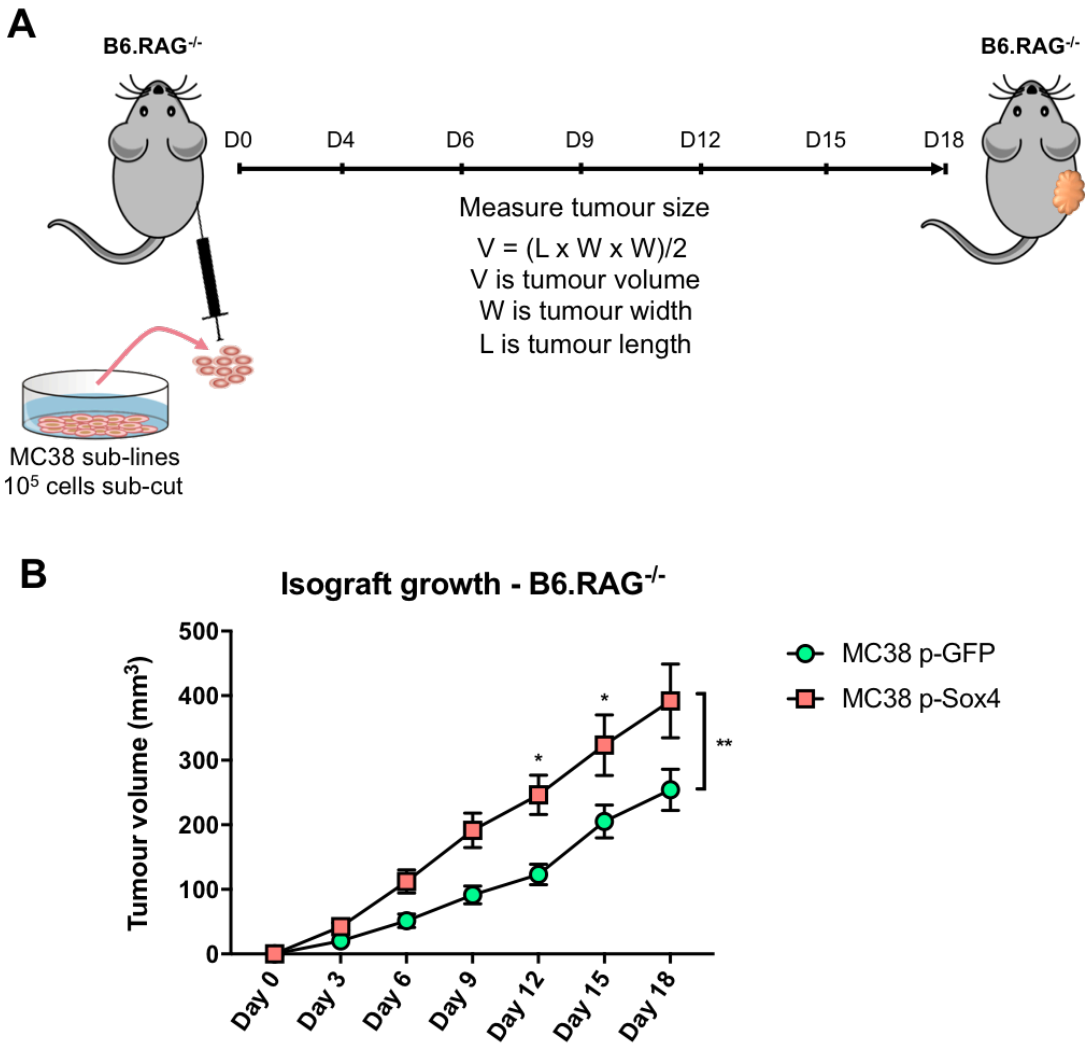

Figure 5.13: Overexpression of SOX4 in MC38 cells promotes increased tumour growth in B6.RAG$^{-/-}$ mice.

(A) MC38 sub-lines were harvested at 80% confluency and single cell suspensions were prepared for injection into B6.RAG$^{-/-}$ hosts. 100.000 cells were injected via sub-cutaneous route per mouse, into the right flank. Tumour volume was measured every 3 days by a digital calliper. Tumour volume was calculated as indicated.

(B) Isograft growth measurements from day of injection (day 0) until end of experiment (day 18).

Each dot represents the mean value of tumour volume per sub-line and bar represents ±SEM. Data represents one experiment performed at the KIR, with n=10 mice per group.
Statistical significance was determined using a repeated measures two-way ANOVA, followed by a Tukey's multiple comparisons test. * $p < 0.0332$, ** $p < 0.0021$.

5.2.12 SOX4 function in immunocompetent C57BL/6 mice

So far, we have demonstrated that SOX4 overexpression in human colorectal cancer cell lines promoted accelerated and increased tumour growth. Reciprocally, SOX4 knockdown led to delayed and reduced tumour development. In a mouse CRC cell line, overexpression of SOX4 in immunodeficient mice likewise stimulated tumour growth. However, it remains unknown whether SOX4 overexpression or knowndown would affect tumour growth in an immune competent host.

Considering that SOX4 protein expression in MC38 p-SOX4 was increased compared to WT MC38 cells and that its expression was reduced in Sh-SOX4 cells, we hypothesise that both sub-lines might reveal differences compared to the control sub-lines.

Briefly, C57BL/6 mice received tumour cells by sub-cutaneous injection into the right flank (**Figure 5.14 A**). Every 5 days, we monitored tumour growth using a digital caliper. Once a mouse reached the defined tumour volume end-point, it was sacrificed and was recorded as dead. Thus, we were able to define the percentage of survival over time for each mouse group (**Figure 5.14 A**). Upon sacrifice, tumours were collected for histology and FACS staining. In this study, we report the impact of SOX4 expression on survival that is recorded thus far, as this preliminary experiment is still ongoing. Further analyses, using FACS and histology, are not completed.

The host immune response was able to control tumour growth in the first few weeks compared to our studies using immunodeficient hosts, where the majority of mice reached end-point by days 21 to 28. In control sub-lines, p-GFP and Sh-CTL, the first animals that reached tumour volume end-point were sacrificed respectively at days 35 and 45 (**Figure 5.14 B**, green and blue curves). At day 63, 6 mice from the p-GFP group and 7 mice from the Sh-CTL group were still alive and had not reached the end-point.

By contrast, the first mice injected with MC38 p-SOX4 cells that reached the end-point were sacrificed at day 22. Moreover, only two animals from this groups out of 10 were still alive at day 63 (**Figure 5.14 B**, red curve). Finally, 9 mice out of 10 from the MC38 Sh-SOX4 group were still alive at day 63, and the only mouse that reached the end-point was sacrificed at day 45 (**Figure 5.14 B**, yellow curve).

Although not completed, this experiment provides evidence thus far that SOX4 overexpression might be linked to decreased survival, while SOX4 knockdown might improve survival, as tumour growth is delayed. The current *p*-value was provided and suggested that while there might exist a difference in survival, it remains to be determined whether the effect is confirmed after completion of the experiment.

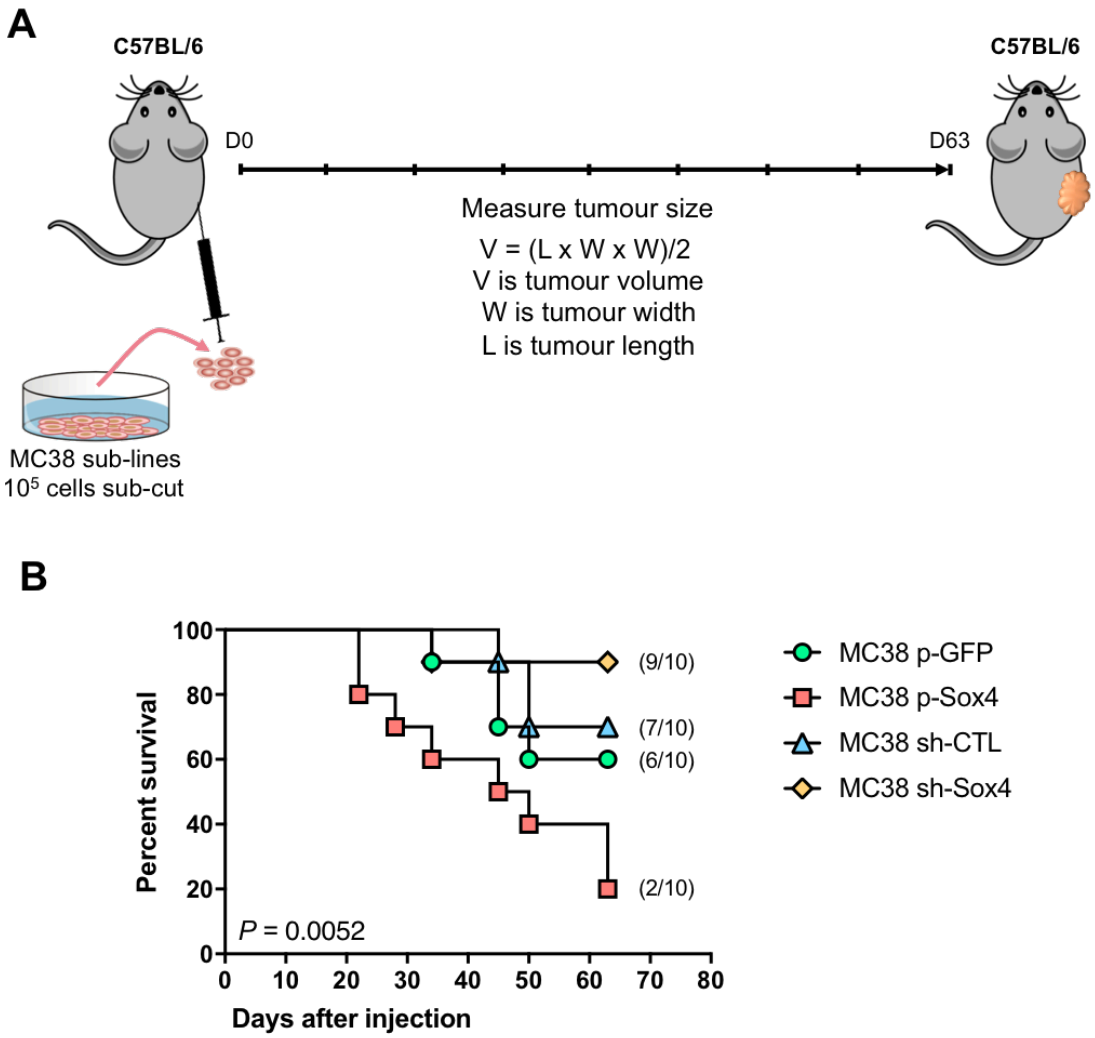

Figure 5.14: Mice receiving MC38 p-SOX4 tumour cells tend to have lower survival rate compared to controls.

(A) MC38 sub-lines were harvested at 80% confluency and single cell suspensions were prepared for injection into C56BL/6 hosts. 100.000 cells were injected via sub-cutaneous route per mouse, into the right flank. Tumour volume was measured every 3 days by a digital calliper. Tumour volume was calculated as indicated. Once the tumour volume end-point is reached, mice are sacrificed, and tumours dissected and processed for FACS analysis.

(B) Percentage of survival for each mouse group, using Kaplan-Meier methods. Death is recorded once a tumour reaches the end-point volume. Ongoing experiment (day 63 on Monday 11th September 2017).

Data represents one experiment performed at the KIR, with n=10 mice per group.
P values were computed using Log-rank (Mantel-Cox) tests.

5.2.13 Insights into the mechanism of Sox4 function

Our studies using both murine and human colorectal cancer cell lines modified to overexpress or downregulate SOX4 have provided evidence that SOX4 mediates increased tumour growth. Therefore, we employed *in vitro* cultures and assays to interrogate the SOX4-mediated tumour growth mechanisms.

First, differences in proliferation were assessed for all Colo205, HCT116 and MC38 sub-lines. WST-1 is a colorimetric assay that determines cell metabolic activity and is widely used as a method to infer cell proliferation.

In Colo205, no differences in cell proliferation were detected between the sub-lines (**Figure 5.15 A**). In HCT116 sub-lines, Sh-SOX4 cells showed increased cell proliferation compared to its respective control line Sh-CTL (**Figure 5.15 B**). Finally, in MC38 sub-lines, p-SOX4 cells cell proliferation was significantly increased compared to p-GFP cells, while we found no difference when comparing Sh-CTL and Sh-SOX4 cells (**Figure 5.15 C**).

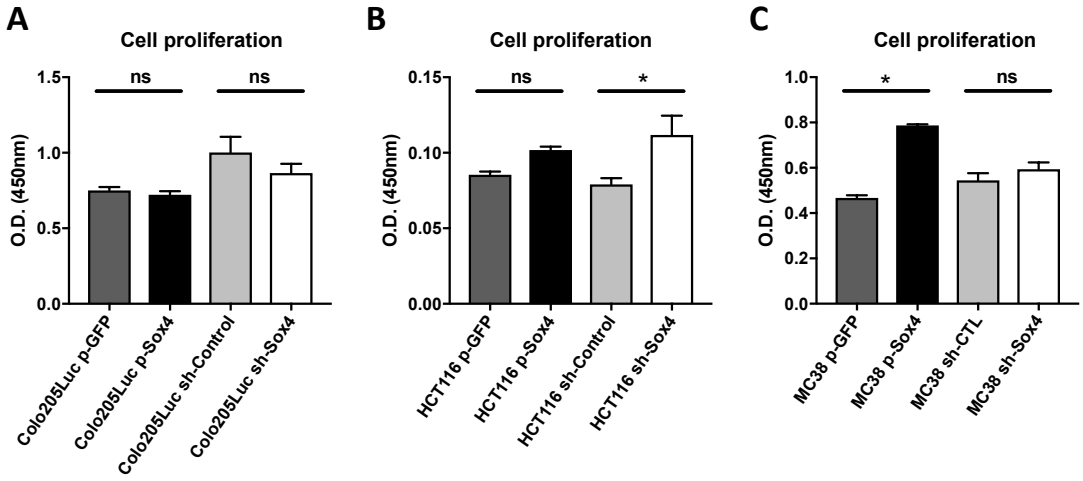

Figure 5.15: Cell proliferation in MC38 p-SOX4 is increased compared to control.

Cells were seeded in 96 well plates at a density of 5,000 (HCT116 and MC38) or 10,000 (Colo205) cells per well and left 48h in culture. WST-1 reagent was added to each well and cells were incubated for one hour. Absorbance (O.D. = 450nm) was measured in a plate reader.

(A B C) Cell proliferation in Colo205, HCT116 and MC38 sub-lines.

Bar represents ±SEM and data represents the pool of three independent experiments performed at passages 3, 4 and 5.
Statistical significance was determined using a Kruskal-Wallis one-way analysis of variance, followed by a Dunn's post-hoc test. * $p \leq 0.05$.

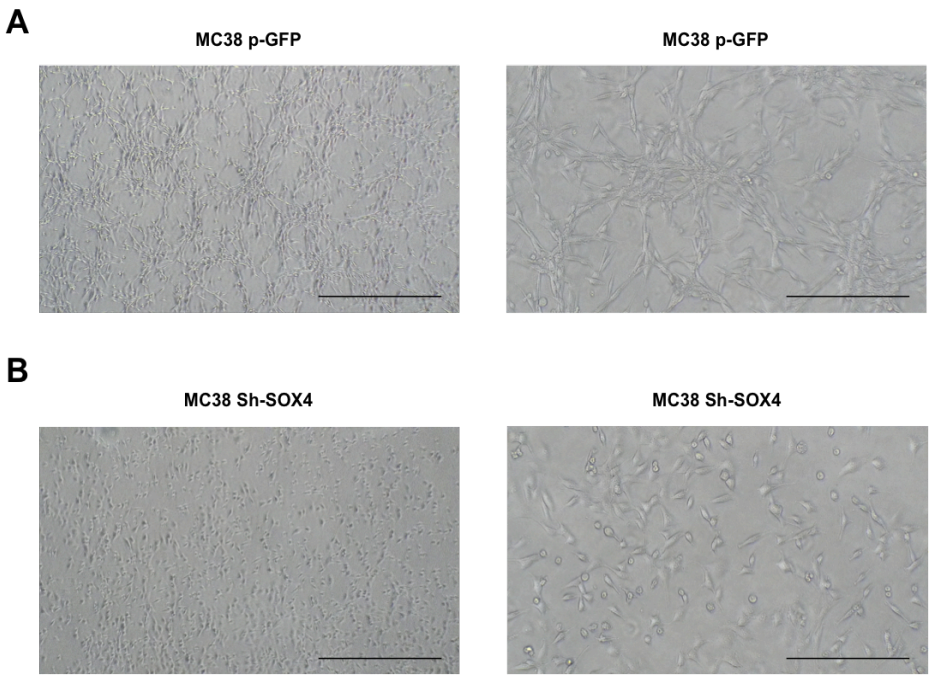

Figure 5.16: The MC38 Sh-SOX4 sub-line displays a change in cellular morphology.

(A) MC38 p-GFP sub-line *in vitro* culture in T75 flask, 10x (left) and 20x (right) magnifications, scale: 100μm.
(B) MC38 Sh-SOX4 sub-line *in vitro* culture in T75 flask, 10x (left) and 20x (right) magnifications, scale: 500μm.

Modification of SOX4 expression in the generated Colo205 and HCT116 sub-lines did not lead to a change in cellular morphology *in vitro* (data not shown). However, observation of the MC38 Sh-SOX4 sub-line to the other MC38 sub-lines revealed a change in cellular morphology. MC38 CRC cells have prolonged extensions of their cytoplasm and tend to aggregate into clusters (**Figure 5.16 A**). By contrast, MC38 Sh-SOX4 cells appeared to have lost their elongated shape and did not cluster like the other sub-lines (**Figure 5.16 B**). Cell migration was evaluated in Colo205 sub-lines; however, cells did not migrate (data not shown). HCT116 and MC38 sub-lines were able to migrate (data not shown), and differences in invasion are under investigation.

5.3 Discussion

5.3.1 Main conclusion

In the recent years, SOX4 expression in tumour cells has gained broad interest in the cancer community. In colorectal cancer, a few studies have pinned down correlations between SOX4 expression, poor prognosis and disease progression. To date, however, very little is known regarding SOX4 function *in vitro* and *in vivo*.

One study has investigated SOX4 pathogenic function in CRC, concluding that siRNA-mediated inhibition of SOX4 could suppress proliferation and invasion in two colorectal cancer cell lines *in vitro* (Wang et al., 2016). However, that study was not very well controlled and a few issues have to be noted. First, the invasion assays are not quantified, and it is unclear whether the provided pictures show similar magnification. Furthermore, the authors claim that SOX4 promotes EMT processes by looking at protein quantification in the siRNA CRC lines. SOX4 inhibition supposedly correlates with the downregulation of N-cadherin and Vimentin, and upregulation of E-cadherin. However, both modified cell lines have opposite results and the control lines also show increased levels of Vimentin expression, suggesting off-target effects of the siRNA transfection.

Using pre-clinical transplantation models of CRC, we provide a more advanced understanding of SOX4 function. We employ stable lentiviral transduction in one mouse and two human colorectal cancer cell lines to overexpress or downregulate SOX4 expression, together with overexpressing and knockdown control lines, and assess SOX4 function *in vivo*.

The two human CRC lines were chosen based on their differential expression of SOX4 at baseline, and clones were selected from all generated sub-lines, with subsequent mRNA and protein expression confirmation of the lentiviral transduction. Using NOD.SCID recipients, we confirm that SOX4 overexpression in the Colo205 human CRC line leads to a significantly increased tumour growth *in vivo*. No differences are seen upon injection of the SOX4 knockdown line compared to controls, which is consistent with the low SOX4 expression that is detected at baseline. Similarly, using HCT116 cells that express high levels of SOX4 at baseline, we confirm that SOX4 knockdown delays tumour growth *in vivo*.

Using similar lentiviral transduction methods to manipulate SOX4 expression, we generated overexpressing and knockdown sub-lines in the murine MC38 CRC line. After confirmation of SOX4 protein expression in the generated sub-lines, we validated SOX4 function in two key experiments. First, the injection of the MC38 SOX4-overexpressing line or its control GFP overexpressing line in B6.RAG$^{-/-}$ immunodeficient mice resulted in increased tumour growth when SOX4 is overexpressed, confirming our experiments using human CRC lines. Next, the MC38 sub-lines were injected into immunocompetent hosts. Contrary to B6.RAG$^{-/-}$ mice, the adaptive component of the immune system in WT mice is able to control tumour growth to a certain extent, while tumours proliferate rapidly in immunodeficient animals, reaching tumour end-point shortly after the first two to three weeks. In a preliminary experiment, we injected the MC38 sub-lines into WT B6 mice and assessed survival, which is defined as the sacrifice of a mouse when tumour volume reaches the end-point. So far, our analysis has revealed that mice injected with the SOX4 overexpressing MC38 sub-line have decreased survival compared to controls.

Furthermore, our data points towards enhanced survival and overall delayed tumour growth in mice injected with the SOX4 knockdown sub-line.

To investigate the molecular mechanisms underlying SOX4 function in CRC, we first analysed *in vitro* proliferation of various cell lines. We detected no differences in proliferation in Colo205 sub-lines, while the HCT116 Sh-SOX4 line displayed increased proliferation compared to the control line Sh-CTL. However, as the injection of the SOX4 knockdown line did not lead to increased tumour growth *in vivo*, it is plausible that *in vitro* differences do not represent a biological effect. We also detected a significant proliferation increase in the SOX4 overexpressing MC38 sub-line. Although it is possible that this result accounts for a real biological effect, we cannot exclude the possibility that it relates to a difference in metabolism. The WST-1 assay, similarly to the MTT assay, uses the metabolic activity of cells as a means of inferring proliferation. To examine the proliferation state of the MC38 sub-lines, we aim to seed the sub-lines at the same density and manually count cells after 24h, 48h and 72h in culture.

Finally, the striking change in cellular morphology in the MC38 SOX4 knockdown suggests that SOX4 confers a mesenchymal phenotype upon the expressing cells. Thus, it is tempting to speculate that SOX4 may promote EMT process in CRC. Future experiments will aim to characterise the phenotype of the SOX4 knockdown sub-lines, looking at EpCAM and E-cadherin expression. Ideally, RNA sequencing of the MC38 generated sub-lines will provide information as to SOX4's function and its molecular mechanisms that contribute to disease.

5.3.2 Tumour microenvironment and SOX4 expression in murine CRC

The tumour microenvironment is widely recognized as an enabling factor for disease progression, and its characterisation represents a global effort towards patient stratification and development of new-targeted therapies. Critically, given that tumour cells evolve and adapt to their microenvironment, bringing together the tumours' phenotype as well as the cellular and molecular signatures of the tumour microenvironment is critical to inform prognosis and a patient treatment regimen. In this chapter, we explore tumour biology in our mouse model of CRC. By dissecting out tumours and inflamed tissue, we identify several genes that are associated with the tumour response.

Matrix metalloproteinases are a family of zinc-dependent proteases that are capable of cleaving various components of extracellular matrix. They are produced by tumour cells, stromal cells and infiltrating inflammatory cells. In our mouse model, *Mmp9* and *Mmp13* expression is increased in tumour tissue and may thus, along with the selective production of certain collagen types (Chapter 4), act to promote disease development and progression towards adenocarcinomas.

MMP-9 can degrade type IV collagen and denatured collagens, and is associated with degradation of the basement membrane, which is a critical step in initial malignant invasion. Our results are not in line with a study, which reported a tumour suppressor function and protective role for MMP-9 in the AOM/DSS colitis-associated cancer model (Garg P et al., 2010). Although it remains to be determined whether MMP-9 is active and involved in tumour progression in our mouse model, we note that despite global colonic inflammation being present in both murine

models, tumours arising in the AOM/DSS model are not invasive and represent more polyp-like lesions. Therefore, it is possible that MMP-9 plays different roles depending on the tumour type (i.e. its mutation status) as well as the tumour stage. In CRC patients, MMP-9 expression is increased at the invasive front of primary tumours, but not in liver metastases, suggesting that it may contribute to initial invasion, but not in metastasis colonisation and establishment (Martin Illemann et al., 2006).

MMP-13 cleaves Type I, II and III collagens, with a preference for type II (Matthew P Vincenti et al., 2001). In CRC patients, expression of MMP-13 is higher in cancer tissue compared to the normal adjacent mucosae, and MMP-13 expression correlates with diminished survival (Leeman MF et al., 2002; Yamada T, et al 2010) and a higher risk of postoperative relapse (Ming-Yii Huang et al., 2010). Interestingly, MMP-13 expression is increased in tumour tissue from patients with liver metastasis as compared to those without metastatic disease. Therefore, MMP-13 gene expression may be a predictor of liver metastasis in patients with CRC. (Yamada T, et al 2010).

In addition to their ECM remodelling function, MMPs can also cleave adhesion proteins and activate growth factors such as TGF-β and VEGF (Yu Q, Stamenkovic I. 2009; Rundhaug JE. 2005), which is highly relevant in the context of tumour development. It is therefore possible that in our mouse model, Mmp9 and Mmp13 act together to release active TGF-β, given the upregulation of this cytokine in tumour-bearing animals and its role in tumourigenesis (Chapter 4). We also detect an increased expression of *Vegfa* in malignant tissue, which is linked to the promotion of angiogenesis, thus providing tumour cells with oxygen and nutrients.

Importantly, angiogenesis represents a critical step towards invasion and metastasis. In CRC patients, expression of VEGFA is increased and linked to disease localisation and long-term disease-specific survival (Bendardaf R et al., 2008). Anti-angiogenesis therapies, such as Bevacizumab, have proven useful for treatment of patients with late-stage CRC. Additional anti-angiogenesis drugs are currently being tested in the preclinical setting and in Phase I/II clinical trials and may represent new treatment opportunities. (Erika Martinelli et al., 2012).

We also detected increased levels of *Hif1α* (Hypoxia-inducible factor 1 alpha) in tumours vs inflamed tissue. Hypoxia (low oxygen tension) is a hallmark of cancer that influences tumour function and correlates with poor prognosis in CRC patients (Yoshifumi Baba et al., 2010). In addition, hypoxia is also an important component of tumour microenvironment as it can alter extracellular matrix, modulate anti-tumour immunity, and increase angiogenesis (reviewed in Edward L. LaGory and Amato J. Giaccia, 2016). HIF-1α and VEGF are frequently overexpressed in numerous types of cancer and are known to be important regulators of angiogenesis. A recent study has explored the prognosis of CRC patients depending on levels of expression of HIF-1α and VEGF, which is observed in more than 50% of the patients. HIF-1α and VEGF status significantly associate with tumour stage and metastasis to lymph nodes and liver. Besides, expression of both HIF-1α and VEGF in CRC patients serves as a poor indicator of overall survival. (Cao et al., 2009).

Given the upregulation of Areg in tumour-bearing mice, we also explored whether tumour tissue expresses increased levels of the EGF Receptor compared to inflamed

tissue. However, this was not the case. It remains to be determined whether Areg plays a role in tumourigenesis and whether blockade of the EGFR could dampen tumour burden. This question is especially interesting given the non-responsiveness of certain subtypes of CRC (mostly represented by KRAS mutant patients) to EGFR blockade therapy (Lièvre et al., 2008; Van Cutsem et al., 2015).

Finally, we identify Sox4 as specifically expressed in tumour tissue compared to the inflamed colon of tumour-bearing mice. In the $APC^{min/+}$ model, tumours develop rapidly in both small and large intestine in response to the somatic Apc mutation and consequent activation of Wnt signalling pathway. Comparison of the transcriptional profiles of adenomas arising from the duodenum, jejunum, and colon of $APC^{min/+}$ mice to those of normal and embryonic tissues from the gastrointestinal tract revealed genes that are upregulated in colonic adenomas, including *Sox4*. Moreover, stainings of Sox4 *in situ* shows that it is upregulated within tumour lesions compared to the normal epithelium (Reichling T et al., 2005).

Our *in situ* staining indicates that Sox4 is expressed in the normal epithelium and the inflamed mucosae. Interestingly, Sox4 expression seems to be increased in the invasive crypts compared to the inflamed epithelia, although quantitative studies are required to confirm this.

Altogether, these results suggest that tumours found in our mouse model of colorectal cancer display several critical invasive features and therefore resemble human CRC. Furthermore, we identify Sox4 upregulation as a feature of colonic adenocarcinomas.

5.3.3 SOX4 expression in human CRC

5.3.3.1 Primary CRC

As we detect Sox4 expression in adenocarcinomas in our mouse CRC model, and considering its reported expression in $APC^{min/+}$ adenomas, we were led to investigate SOX4 expression in human primary CRC and liver metastases.

First, we used a publically available dataset to probe *SOX4* expression in primary tumours, and report increased *SOX4* expression in primary colorectal cancer tumours compared to normal colon tissue. Informed by the numerous studies linking SOX4 to disease progression in various cancers, we have investigated its prognostic value. Using the Shaffer dataset, we link high expression of SOX4 to decreased disease-specific survival in CRC patients. However, our analyses included fewer than 200 hundred patients and therefore larger cohorts are required to fully understand the relationship between SOX4 expression and disease prognosis in CRC.

Other studies have addressed SOX4 expression in CRC over the course of our study. One study comprising 263 patients with colon cancer has looked at the association between SOX4 nuclear expression and various clinicopathologic parameters and patients survival. That study revealed that overexpression of nuclear SOX4 significantly correlates with depth of invasion, distant metastasis, and stage of disease. Moreover, patients with high expression levels of nuclear SOX4 achieve a significantly poorer disease-free survival rate, compared with patients with low SOX4 expression levels. Furthermore, using univariate Cox regression analysis, the authors show that overexpression of nuclear SOX4 is a clear prognostic marker for colon

cancer, and may be useful to predict the outcome for patients with colon cancer. (Lin et al., 2013).

Another study identified a number of deregulated transcription factors in CRC patients, including *SOX4*, and has evaluated the correlation between their expression and the recurrence of stage II CRC and overall survival. Using two independent cohorts of microsatellite-stable (MSS) stage II cancers, the study revealed that high *SOX4* transcript levels correlated with recurrence in CRC patients (Andersen et al., 2009).

Our ongoing research aims to answer three critical questions: whether SOX4 is preferentially enriched in certain CMS types, whether its expression correlates with key oncogenic drivers and mutations, and whether SOX4 expression is enriched in certain disease stages. Importantly, patient stratification in early colon cancer and consequent prediction of invasion risk is a major challenge that requires better understanding of molecular pathways and discovery of new biomarkers. Provided the association of *SOX4* in stage II MSS colon tumours and disease prognosis, we envisage that SOX4 expression may be an interesting biomarker that could help stratifying early stage patients, predict risk of invasion, and thus orientate treatment options.

5.3.3.2 Liver and lung metastases

Considering the striking invasive features of the tumours in our mouse model and *SOX4* correlation with poor prognosis in CRC patients, we sought to understand whether SOX4 may also be involved in the transition from primary tumour to metastasic dissemination.

Transcriptomics data combining both primary tumours and metastases samples is quite rare. To our knowledge, one study combines such attributes, along with matched healthy colon, liver and lung tissues. Employing the Shaffer et al dataset, we discover that *SOX4* expression is increased in polyps and primary tumours compared to normal colon, as previously reported. Interestingly, our analyses reveal an upregulation of *SOX4* expression in liver and lung metastases compared to their respective healthy tissues, but more importantly, this increase is also seen when comparing *SOX4* expression to primary tumours.

Through our collaboration with Ruth Muschel's lab, we confirm the data generated with the Shaffer dataset, and report increased SOX4 expression at the mRNA and protein levels in liver metastases tissue from CRC patients compared to matched-normal liver. Although our analyses are descriptive, we are also able to report SOX4 expression in all liver metastases samples from CRC patients (n=15), primarily noted in the invasive islets.

We now aim to confirm our findings in other CRC patient cohorts, with the specific goal of studying the correlation between SOX4 expression in primary tumour and liver metastases within the same patient. Despite its correlation with poor prognosis in CRC patients, it remains unknown whether *SOX4* is just a marker of the disease or whether its expression is linked to specific pro-oncogenic and invasive functions in primary tumours. More importantly, SOX4 function in metastatic disease is entirely unexplored. Considering that metastasis dissemination and colonisation are

inefficient processes since millions of circulating tumour cells escape their primary site but fail to colonise other tissues, shredded tumours are thought to acquire certain functions that enhance their ability to colonise specific organs as well as to proliferate, like for example by undergoing MET. The metastatic microenvironment and locally-produced cytokines, such as TGF-β and other cytokines, are thus also likely to play a critical role in fostering metastatic tumour growth, and the ability of tumour cells to adapt to these new environments represent the cornerstone of disease progression. Interestingly, *SOX4* expression is also reported in liver cancer where it could also correlate with poor prognosis (TCGA and Human Tissue Atlas public data). Together, we hypothesise that SOX4 expression may represent an environmental adaptation and may be involved in efficient liver colonisation. To endow cells with the capacity to colonise a secondary organs, SOX4 should confer certain lineage plasticity to tumour cells, and this may be commandeered by differential cytokine signalling. Our future studies of SOX4 function in murine models of liver and lung metastases will provide more certainty as to the exact function SOX4 holds in metastatic colorectal cancer.

5.3.4 Concluding remarks

Collectively, our data point towards a pathogenic role for SOX4 in colorectal cancer. To date, our study is the only one to investigate SOX4 function *in vivo*, and we hypothesise that SOX4 may operate as an EMT regulator, providing chemotherapy resistance and cancer stemness, similar to the case of breast cancer. Thus, our work may add to the growing body of evidence that SOX4 should be considered as a new member of the master regulators of EMT.

Our preliminary *in vitro* analysis of SOX4 upregulation shows that in Colo205 cells, TGF-β and IL-6 can augment SOX4 expression (data not shown). Moreover, considering that hypoxic stress can induce EMT programming and that *Hif1a* is upregulated in tumour tissue, we plan to investigate whether other signalling pathways than TGFβ can induce SOX4 and EMT features in CRC cells.

Furthermore, as far as the tumour microenvironment is concerned, analysis of cell populations infiltrating MC38 tumours will provide insights as to whether SOX4 overexpression is associated with the recruitment and promotion of a different type of immune response compared to SOX4-low tumours. In conclusion, describing cellular and molecular components of tumour microenvironment associated with SOX4-high tumours may lead to the identification of novel molecular predictors that will help to stratify CRC patients, with the aim of improving patient-targeted therapy and enhancing treatment efficacy.

6 General discussion

6.1 Summary of findings

In this study, we brought together two perspectives on tumour development to understand the mechanisms by which lack of immune cell regulation in the gut can drive the formation of colon adenocarcinomas. We explored the tumour microenvironment in Chapters 3 and 4, while in Chapter 5 we focused on tumour cells and how these can adapt to their microenvironment to favour their own growth and progression.

Using a mouse model of inflammation-driven colorectal cancer, we found that aberrant activity of Treg cells deficient in IL-10 can promote the development of mucinous adenocarcinomas in the colon. Our initial aim was to establish whether IL-10-deficient Tregs could mediate tumourigenesis by other means than failure to regulate pro-tumourigenic inflammatory immune responses. Several studies have highlighted that tissue-resident Tregs adapt to their microenvironment and mediate non-immune functions, such as participating in wound healing processes. We hypothesised that in the cancer setting, Treg might promote tumour growth by inducing an aberrant repair response. Our mouse model thus represented a unique setting to study how Treg cells could drive tumourigenesis. Transfer of WT Tregs into 129.RAG$^{-/-}$ mice followed by infection with *H. hepaticus* leads to minimal colitis as WT Tregs can control the *Hh*-driven innate inflammation and colitis, notably through IL-10 secretion. By contrast, as many other mouse models have reported, Treg cells that lacked IL-10 production were unable to control colonic inflammation, which led to colitis and ultimately favoured tumourigenesis. We hypothesised that if IL-10 deficient Tregs only participated to disease progression because of their inability to

suppress immune responses, injection of only IL-10 deficient effector $CD4^+$ T cells would similarly promote colitis development and tumourigenesis. Critically, we established that tumourigenesis was higher in mice that received IL-$10^{-/-}$ Tregs compared to mice receiving IL-$10^{-/-}$ effector $CD4^+$ T cells. This suggested that IL-10 deficient Tregs could mediate tumourigenesis through other mechanisms.

To determine by which mechanism IL-$10^{-/-}$ Tregs mediate tumourigenesis, we first compared their gene expression profile to WT Tregs, using qPCR. Our initial gene screen, comprising 30 targets, revealed two genes that were differentially expressed in splenic IL-$10^{-/-}$ Tregs: *Tgfb* and *Areg*, both of which expression remains to be confirmed at the protein level. Using flow cytometry analysis, we confirmed that the injected populations of WT and IL-$10^{-/-}$ Tregs were also different in terms of the transcription factors they expressed, as well as their proliferative state. WT Tregs were primarily Gata3 positive, expressed high amounts of Foxp3 and were of thymic origin. By contrast, IL-$10^{-/-}$ Tregs were composed of a small frequency Gata3- and Rorγt-expressing cells, were highly proliferative and were of shared thymic and peripheral origin. Taking an unbiased approach, we performed RNA sequencing on splenic Tregs, which revealed that very few genes were differentially expressed. Interestingly, we found and confirmed that IL-$10^{-/-}$ Tregs were enriched in transcripts for *Tlr1* and *Metrnl*, and expressed lower amounts of *Ldbh*. TLR1/2 signalling into Tregs was shown to be part of a metabolic programme that enhances glycolysis, promotes cell proliferation but is also linked to impair Treg cell suppressive capacity. This programme is balanced by Foxp3 expression, which orientates the metabolism towards the oxidative and catabolic pathways, and promotes regulatory function. Moreover, in macrophages, IL-10 was shown to inhibit mTORC1 and glycolysis,

favouring mitophagy, but it is unclear whether this is the case in Treg cells. The expression of Ldbh is linked to the catabolic pathway, and its downregulation in IL-$10^{-/-}$ Tregs may favour glycolysis, which further suggests that IL-$10^{-/-}$ Tregs may have a different metabolism. Whether the increased amounts of *Areg*, *Tgfb* and *Metrnl* are a direct consequence of IL-10 deficiency or whether it is linked to a difference in metabolism or expression of transcription factors remain to be determined.

Differences between WT and IL-$10^{-/-}$ Tregs were also found in the colon. Colonic WT Tregs expressed Gata3 and Rorγt, while IL-$10^{-/-}$ Tregs primarily expressed T-bet and were highly proliferative. The function of T-bet^{+} $Foxp3^{+}$ Tregs in colorectal cancer is unknown and this warrants further investigation. Furthermore, a population of $CD4^{+}$ $Foxp3^{-}$ T cell accumulated in the colon, and to date, it is unknown whether they originated from a cell contaminant or from the injected $Foxp3^{+}$ Tregs themselves, by way of lineage instability or intrinsic plasticity.

In Chapter 4, we analysed the colonic accumulation of various innate immune populations in colitic mice compared to tumour-bearing mice, to determine whether IL-$10^{-/-}$ Tregs may be driving a specific innate response involved in tumour development. As our results were not conclusive, we next explored the expression of various cytokines in the colon. We found that colonic protein expression of Areg, IL-6 and TGF-β was increased in tumour-bearing mice. Importantly, *in vivo* blockade of IL-6-R and TGF-β mediated decreased tumourigenesis in animals injected with IL-$10^{-/-}$ Tregs and infected with *H. hepaticus*, suggesting that these cytokines were necessary for tumour formation in this model. Tumourigenesis was associated with a marked stromal cell signature that is induced as a consequence of Treg deficiency in IL-10

production. Tumours were surrounded by a collagen network and were infiltrated by $Gp38^+$ expressing cells. We next identified $Gp38^+$ stromal cells as a primary source of IL-6, which suggested that these non-hematopoietic cells might be involved in tumour progression. E*x vivo* characterisation of these cells provided evidence of an imprint from the microenvironment, as elevated production of IL-6 and TNF was sustained in culture over time. Moreover, stromal cells from tumour-bearing mice expressed increased amounts of *Areg* and *Ereg*, chemokines and collagens, suggesting that they might provide tumour cells with growth factors, recruit pro-inflammatory cells, and remodel the ECM to promote tumour invasion.

In chapter 5, we focused on the role of SOX4 in mouse and human CRC. Using mice injected with IL-$10^{-/-}$ Tregs and infected with *H. hepaticus*, we detected increased amounts of Sox4 in tumours compared to inflamed tissue. As TGF-β signalling was linked to increased EMT in breast cancer through SOX4 expression, we sought to explore SOX4 expression in human CRC. Analysis of a publically available dataset revealed increased amounts of SOX4 in primary tumours compared to normal tissue, and further increased expression in liver and lung metastases compared to primary tumours. To date, it remains unclear whether high expression of SOX4 in primary tumours correlates with high expression in metastases, and further studies will aim at comparing expression in matched tumours and liver metastases in CRC patients. Critically, larger patient cohorts are required to validate the poor prognosis observed in CRC patients with high *SOX4* expression. Interestingly, SOX4 expression in metastases is largely unexplored. Can SOX4 mediate different processes to enable both tumour evasion and metastatic colonisation, such as through MET, depending

on microenvironmental clues? If this is the case, which cytokines mediate these different functions and what are the cellular pathways preferentially activated?

As we confirmed SOX4 expression in CRC patients, we went back to our mouse models and probed Sox4 function using combined *in vitro* and *in vivo* analyses. First, we confirmed that *in vivo*, Sox4 overexpression promoted tumour growth, using both human CRC lines and a murine CRC line. However, Sox4 expression itself was not sufficient to drive metastasis *in vivo* using these orthotopic models. Therefore, we now aim at determining whether Sox4 expression increases the metastatic colonisation of the liver and lung, using other mouse models. Investigation of the mechanisms by which Sox4 mediate tumour growth and potential metastasis is currently ongoing, but our analysis hinted towards a pro-mesenchymal function. Finally, SOX4 expression has gained a broad interest in the cancer community, as recent studies have suggested that SOX4 may be added to the family of EMT master regulators.

6.2 Conclusion

The **Figure 6.1** summarises our findings. Collectively, our findings suggest that Tregs and stromal cells act together to foster a microenvironment, characterised by increased amounts of Areg, IL-6 and TGF-β, that promotes disease progression potentially through the expression of Sox4 in tumour cells. These findings open an exciting avenue to explore the phenotype of tumour-promoting Tregs and to study Sox4 function in metastatic disease. Interestingly, our findings suggest that colonic mucinous adenocarcinomas develop in a context of elevated TGF-β signalling that is also associated with marked mesenchymal features, which together resembles the CMS4 subtype of CRC. Indeed, considering that some studies have suggested that

MC could represent a genetically distinct subtype of colorectal adenocarcinoma (Melis et al., 2010) that may develop along the sessile serrated pathway (Patai et al., 2013), and considering that this model involves a pro-tumourigenesis TGF-β signalling in the tumour microenvironment, this may orientate tumours from the sessile serrated pathway towards poor-prognosis CMS4 tumours (Fessler et al., 2016). Therefore, this model may prove to be useful to deepen our understanding of the stromal compartment in CRC and its associated tumour-promoting function, and may be used to test specific immunotherapies in the context of patient stratification.

Further investigation of the function of Meteorin-like expression by IL-10 deficient Tregs may add a new player to the pathogenic function of these cells. Importantly, although it is purely hypothetical, expression of Meteorin-like may represent a unique way by which IL-$10^{-/-}$ Tregs are capable of promoting a pro-inflammatory and pro-tumourigenic function in stromal cells. A few points have to be noted. First, the receptor for Meteorin-like is currently still unknown. Secondly, it is unclear whether IL-$10^{-/-}$ Tregs secrete Meteorin-like. If this is the case, simple blockade experiments and direct stimulation of stromal cell cultures with Meteorin-like should provide insights as to its function in mediating IL-6 production. Finally, more studies are required to characterise the cellular sources of Areg and the effect of this cytokine on tumour growth.

Current studies on Meteorin-like involve characterisation of its expression in various T cell populations, including $CD8^+$ T cells and Tregs, in several tissues such as the small intestine, colon, skin and spleen. This experiment will be performed using

Foxp3-GFP reporter mice and FACS sorting strategies to assess gene expression by qPCR. Protein expression will also be analysed using Meteorin-like FACS antibodies that are available. Moreover, we are also in the process of acquiring a floxed mouse strain for Metrnl, which will be crossed to Foxp3-Cre mice that are available at the KIR. First experiments will aim at characterise the Treg compartment in steady state animals to address whether development, frequencies and function are similar to WT Tregs. Further experiments will aim at inducing colorectal cancer *in vivo*, using the DSS AOM model, which tumours are infiltrating by Tregs, and assess whether Meteorin-like expression or not influence tumour development and progression. Finally, we aim at mining publically available datasets to determine whether Meteorin-like is expressed in human colorectal cancer and correlates with disease prognosis and survival.

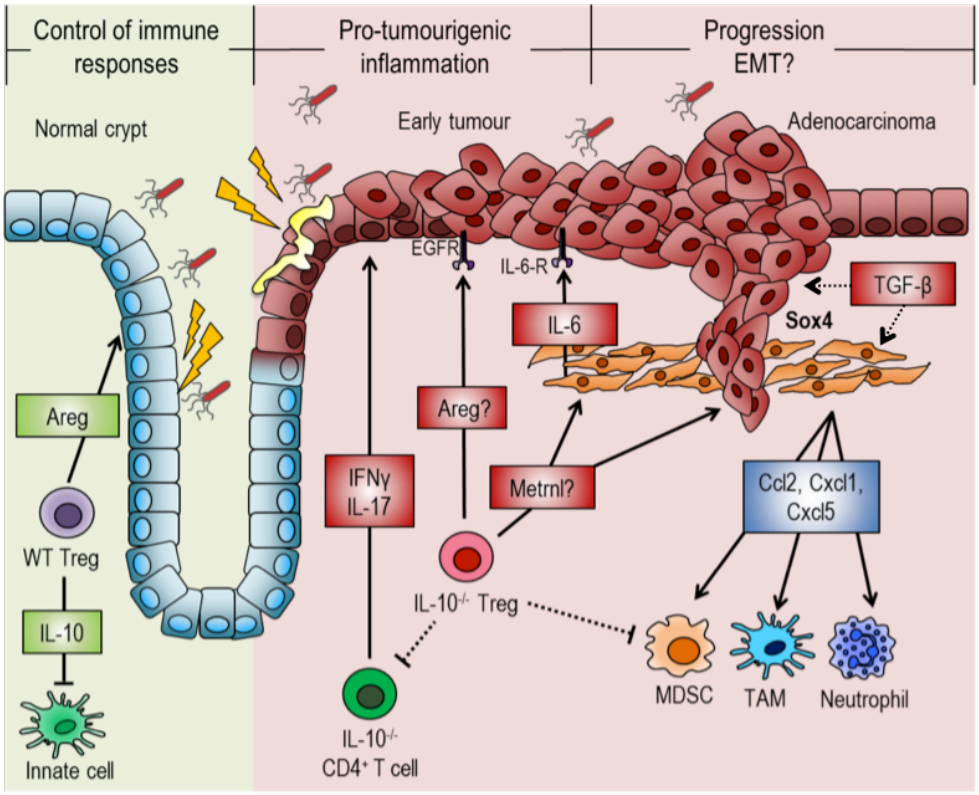

Figure 6.1: Working model for IL-10 deficient Treg-mediated tumourigenesis

In the colon, WT Tregs maintain immune homeostasis through the suppression of pro-inflammatory immune responses initiated by *H. hepaticus* infection, notably through IL-10 production. Moreover, WT Tregs express *Areg*, which may be involved in normal repair processes of the epithelium.

By contrast, IL-10$^{-/-}$ Tregs are unable to produce the immune suppressive cytokine IL-10, allowing pro-inflammatory cells to accumulate in the colon and mediate tissue damage, in conjunction with *H. hepaticus* infection. The chronic inflammation favours tumourigenesis over time and mucinous adenocarcinoma develop in the colon. Stromal cells are critical for disease development as they express the pro-tumourigenic cytokine IL-6 and can recruit several immune cells via the expression of Ccl2, Cxcl1 and Cxcl5. Stromal cells foster tumour growth by remodelling the ECM. These cells may acquire their function through TGF-β signalling, or perhaps through direct action of IL-10$^{-/-}$ Tregs, which express Metrnl. IL-10$^{-/-}$ Tregs may promote tumourigenesis through overexpression of Areg, directly influencing tumour cells.

Finally, tumour growth and invasion may be promoted by the expression of Sox4, which can be induced by various microenvironmental clues, such as TGF-β, although its cellular source remains unclear and may involve tumour cells and or stromal cells.

6.3 The future of Tregs in cancer immunotherapy

The incidence of colorectal cancer is increasing and the prognosis for patients with advanced or metastatic disease is relatively poor (Siegel et al., 2017). In the recent years, the development of several immunotherapies has gained wide interest and hold great promise. However, durable responses to immune checkpoints blockade, for instance, have only been obtained in a fraction of patients. Several factors are attributed to its limited success, such as the persistence of immunosuppressive mechanisms in the tumour microenvironment. As such, Tregs represent a critical immune population that suppresses aberrant immune responses against self-antigens, but also anti-tumour immune responses. Our understanding of the functional adaptations of Tregs to their environment, together with the discovery of tissue-Tregs and their non-immune capabilities have shed light onto their importance, and open new strategies to modulating their function in many diseases. However, the properties of tumour-infiltrating Tregs and their potential adapations to the tumour microenvironment are relatively unexplored. Importantly, this knowledge will address two critical points required to design better Treg targeted-immunotherapies. First, this may allow depleting tumour-Tregs specifically, while leaving untouched Treg cells in lymphoid organs and other tissues, which will reduce the risk of severe autoimmunity that occurs with a systemic depletion of Treg cells. Secondly, identifying specific markers of tumour-Tregs that distinguish them to effector $CD4^+$ T cells is critical to prevent the suppression of anti-tumour immune responses.

To date, two studies led by Rudensky and Pagani have addressed the gap of knowledge related to tumour-Tregs, respectively in breast cancer, and in both non-small-cell lung cancer and colorectal cancer (De Simone et al., 2016; Plitas et al., 2016). Using RNA sequencing and flow cytometry to characterise and compare tumour-Tregs to their tissue and peripheral Treg counterparts, they identify several markers uniquely expressed by tumour-Tregs. Both studies have identified expression of CCR8 as a unique feature of tumour-Tregs, which is specifically associated with poor prognosis and decreased patient survival. Furthermore, based on the human TCR repertoire (Plitas et al., 2016; Sherwood et al., 2013), previous studies have shown that tumour-Tregs are likely to be recruited *de novo* from lymphoid tissues and not from the adjacent tissue resident cells, despite exhibiting a phenotype similar to that of tissue-Tregs (Plitas et al., 2016). Altogether, these findings are critical to harness the full capacity of the next generation of immunotherapies. Finally, a recent study has validated the use of an anti-CD25 antibody with enhanced binding to activating FcγRs, capable of inducing antibody-dependent cell-mediated cytotoxicity, that targets tumour-Tregs and improves control of established tumours *in vivo* when combined with PD-1 blockade (Arce Vargas et al., 2017). This antibody may circumvent the use of specific antibodies targeting tissue-Tregs and represent a new therapeutic avenue to deplete tumour-Tregs in cancer patients.

In colorectal cancer patients, deploying immunotherapies effectively will require further knowledge of the complex cellular and molecular interactions that occur between intestinal tumours and the host immune system, where this organ is a

prime example of the bivalent function of Tregs. Treg cells can mediate the suppression of anti-tumour responses, while also suppressing pro-tumourigenic inflammatory responses, denoting a potential heterogeneity of tumour-Tregs that requires to be further investigated. Moreover, considering the finding that distinct Tregs subpopulations contribute in opposing ways to determining colorectal cancer prognosis (Saito et al., 2016), it is of utmost importance to effectively stratify patients and adapt therapies based on the type of Treg cells and their associated function in the tumour microenvironment.

Finally, the influence of the microbiota on the tumour immune microenvironment in CRC and its potential to augment or suppress therapeutic responses is currently an area of intense investigation (Drewes et al., 2016; Sears and Garrett, 2014). Notably, bacterial biofilms were found to be almost universally present on tumours in the proximal colon. These biofilms were associated with increased IL-6 production in the lamina propria and enhanced epithelial STAT3 activation, representing a novel driver of IL-6 production in human CRC (Dejea et al., 2014). Moreover, the microbiota composition has a profound effect on the colonic Treg populations, as reported by the multitude studies performed using germ-free and antibiotic-treated mice, which display decreased Treg numbers in the colon (Atarashi et al., 2011; Geuking et al., 2011). Moreover, certain microbial species or mixtures of bacteria can specifically induce or promote the accumulation of Tregs in the colon (reviewed in Tanoue et al., 2016). Altogether, these aspects of the microbiota could represent novel strategies for the modulation of the tumour microenvironment.

7 References

Abbas, A.K., Benoist, C., Bluestone, J.A., Campbell, D.J., Ghosh, S., Hori, S., Jiang, S., Kuchroo, V.K., Mathis, D., Roncarolo, M.G., et al. (2013). Regulatory T cells: recommendations to simplify the nomenclature. Nature Publishing Group *14*, 307–308.

Abreu, M.T. (2010). Toll-like receptor signalling in the intestinal epithelium: how bacterial recognition shapes intestinal function. Nature Publishing Group *10*, 131–144.

Ali, N., Zirak, B., Rodriguez, R.S., Pauli, M.L., Truong, H.-A., Lai, K., Ahn, R., Corbin, K., Lowe, M.M., Scharschmidt, T.C., et al. (2017). Regulatory T Cells in Skin Facilitate Epithelial Stem Cell Differentiation. Cell *169*, 1119–1123.e11.

Andersen, C.L., Christensen, L.L., Thorsen, K., Schepeler, T., Sørensen, F.B., Verspaget, H.W., Simon, R., Kruhøffer, M., Aaltonen, L.A., Laurberg, S., et al. (2009). Dysregulation of the transcription factors SOX4, CBFB and SMARCC1 correlates with outcome of colorectal cancer. British Journal of Cancer *100*, 511–523.

Annese, V. (2006). Multidrug resistance 1 gene in inflammatory bowel disease: A meta-analysis. Wjg *12*, 3636.

Arce Vargas, F., Furness, A.J.S., Solomon, I., Joshi, K., Mekkaoui, L., Lesko, M.H., Miranda Rota, E., Dahan, R., Georgiou, A., Sledzinska, A., et al. (2017). Fc-Optimized Anti-CD25 Depletes Tumor-Infiltrating Regulatory T Cells and Synergizes with PD-1 Blockade to Eradicate Established Tumors. Immunity *46*, 577–586.

Armaka, M., Apostolaki, M., Jacques, P., Kontoyiannis, D.L., Elewaut, D., and Kollias, G. (2008). Mesenchymal cell targeting by TNF as a common pathogenic principle in chronic inflammatory joint and intestinal diseases. J Exp Med *205*, 331–337.

Arnold, M., Sierra, M.S., Laversanne, M., Soerjomataram, I., Jemal, A., and Bray, F. (2017). Global patterns and trends in colorectal cancer incidence and mortality. Gut *66*, 683–691.

Arpaia, N., Green, J.A., Moltedo, B., Arvey, A., Hemmers, S., Yuan, S., Treuting, P.M., and Rudensky, A.Y. (2015). A Distinct Function of Regulatory T Cells in Tissue Protection. Cell *162*, 1078–1089.

Artis, D., Kane, C.M., Fiore, J., Zaph, C., Shapira, S., Joyce, K., Macdonald, A., Hunter, C., Scott, P., and Pearce, E.J. (2005). Dendritic cell-intrinsic expression of NF-kappa B1 is required to promote optimal Th2 cell differentiation. The Journal of Immunology *174*, 7154–7159.

Astarita, J.L., Acton, S.E., and Turley, S.J. (2012). Podoplanin: emerging functions in development, the immune system, and cancer. Front. Immunol. *3*, 1–11.

Atarashi, K., Tanoue, T., Shima, T., Imaoka, A., Kuwahara, T., Momose, Y., Cheng, G., Yamasaki, S., Saito, T., Ohba, Y., et al. (2011). Induction of Colonic Regulatory T Cells by Indigenous Clostridium Species. Science *331*, 337–341.

Awasthi, A., Riol-Blanco, L., Jäger, A., Korn, T., Pot, C., Galileos, G., Bettelli, E., Kuchroo, V.K., and Oukka, M. (2009). Cutting Edge: IL-23 Receptor GFP Reporter Mice Reveal Distinct Populations of IL-17-Producing Cells. The Journal of Immunology *182*, 5904–5908.

Baltgalvis, K.A., Berger, F.G., Pena, M.M.O., Davis, J.M., Muga, S.J., and Carson, J.A. (2008). Interleukin-6 and cachexia in ApcMin/+ mice. Am. J. Physiol. Regul. Integr. Comp. Physiol. *294*, R393–R401.

Barcellos-Hoff, M.H., Lyden, D., and Wang, T.C. (2013). The evolution of the cancer niche during multistage carcinogenesis. Nat Rev Cancer *13*, 511–518.

Bauler, T.J., Hendriks, W.J.A.J., and King, P.D. (2008). The FERM and PDZ Domain-Containing Protein Tyrosine Phosphatases, PTPN4 and PTPN3, Are Both Dispensable for T Cell Receptor Signal Transduction. PLoS ONE *3*, e4014–11.

Beck, K.E., Blansfield, J.A., Tran, K.Q., Feldman, A.L., Hughes, M.S., Royal, R.E., Kammula, U.S., Topalian, S.L., Sherry, R.M., Kleiner, D., et al. (2006). Enterocolitis in patients with cancer after antibody blockade of cytotoxic T-lymphocyte-associated antigen 4. J. Clin. Oncol. *24*, 2283–2289.

Beck, P.L., Rosenberg, I.M., Xavier, R.J., Koh, T., Wong, J.F., and Podolsky, D.K. (2010). Transforming Growth Factor-β Mediates Intestinal Healing and Susceptibility to Injury in Vitro and in Vivo Through Epithelial Cells. The American Journal of Pathology *162*, 597–608.

Bell, E.B., Sparshott, S.M., Drayson, M.T., and Ford, W.L. (1987). The stable and permanent expansion of functional T lymphocytes in athymic nude rats after a single injection of mature T cells. The Journal of Immunology *139*, 1379–1384.

Bennett, C.L., Christie, J., Ramsdell, F., Brunkow, M.E., Ferguson, P.J., Whitesell, L., Kelly, T.E., Saulsbury, F.T., Chance, P.F., and Ochs, H.D. (2001). The immune dysregulation, polyendocrinopathy, enteropathy, X-linked syndrome (IPEX) is caused by mutations of FOXP3. Nature Genetics *27*, 20–21.

Bennett, K.L., Plowman, G.D., Buckley, S.D., Skonier, J., and Purchio, A.F. (1992). Regulation of amphiregulin mRNA by TGF-beta in the human lung adenocarcinoma cell line A549. Growth Factors *7*, 207–213.

Berasain, C., and Avila, M.A. (2014). Amphiregulin. Seminars in Cell & Developmental Biology *28*, 31–41.

Berg, D.J., Davidson, N., Kühn, R., Müller, W., Menon, S., Holland, G., Thompson-Snipes, L., Leach, M.W., and Rennick, D. (1996). Enterocolitis and colon cancer in interleukin-10-deficient mice are associated with aberrant cytokine production and CD4(+) TH1-like responses. J. Clin. Invest. *98*, 1010–1020.

Biswas, S., Davis, H., Irshad, S., Sandberg, T., Worthley, D., and Leedham, S. (2015). Microenvironmental control of stem cell fate in intestinal homeostasis and disease. J.

Pathol. *237*, 135–145.

Blatner, N.R., Mulcahy, M.F., Dennis, K.L., Scholtens, D., Bentrem, D.J., Phillips, J.D., Ham, S., Sandall, B.P., Khan, M.W., Mahvi, D.M., et al. (2012). Expression of RORγt marks a pathogenic regulatory T cell subset in human colon cancer. Science Translational Medicine *4*, 164ra159–12.

Bohr, U.R.M., Selgrad, M., Ochmann, C., Backert, S., Konig, W., Fenske, A., Wex, T., and Malfertheiner, P. (2006). Prevalence and Spread of Enterohepatic Helicobacter Species in Mice Reared in a Specific-Pathogen-Free Animal Facility. Journal of Clinical Microbiology *44*, 738–742.

Bono, M.R., Fernández, D., Flores-Santibáñez, F., Rosemblatt, M., and Sauma, D. (2015). CD73 and CD39 ectonucleotidases in T cell differentiation: Beyond immunosuppression. FEBS Letters *589*, 3454–3460.

Boulard, O., Kirchberger, S., Royston, D.J., Maloy, K.J., and Powrie, F.M. (2012). Identification of a genetic locus controlling bacteria-driven colitis and associated cancer through effects on innate inflammation. J Exp Med *209*, 1309–1324.

Brahmer, J.R., Drake, C.G., Wollner, I., Powderly, J.D., Picus, J., Sharfman, W.H., Stankevich, E., Pons, A., Salay, T.M., McMiller, T.L., et al. (2010). Phase I Study of Single-Agent Anti–Programmed Death-1 (MDX-1106) in Refractory Solid Tumors: Safety, Clinical Activity, Pharmacodynamics, and Immunologic Correlates. Jco *28*, 3167–3175.

Brahmer, J.R., Tykodi, S.S., Chow, L.Q.M., Hwu, W.-J., Topalian, S.L., Hwu, P., Drake, C.G., Camacho, L.H., Kauh, J., Odunsi, K., et al. (2012). Safety and Activity of Anti–PD-L1 Antibody in Patients with Advanced Cancer. N Engl J Med *366*, 2455–2465.

Brennan, C.A., and Garrett, W.S. (2016). Gut Microbiota, Inflammation, and Colorectal Cancer. Annu. Rev. Microbiol. *70*, 395–411.

Brunkow, M.E., Jeffery, E.W., Hjerrild, K.A., Paeper, B., Clark, L.B., Yasayko, S.A., Wilkinson, J.E., Galas, D., Ziegler, S.F., and Ramsdell, F. (2001). Disruption of a new forkhead/winged-helix protein, scurfin, results in the fatal lymphoproliferative disorder of the scurfy mouse. Nature Genetics *27*, 68–73.

Brunner, S.M., Schiechl, G., Kesselring, R., Martin, M., Balam, S., Schlitt, H.J., Geissler, E.K., and Fichtner-Feigl, S. (2013). IL-13 signaling via IL-13Rα2 triggers TGF-β1-dependent allograft fibrosis. Transplant Res *2*, 16.

Buettner, M., and Lochner, M. (2016). Development and Function of Secondary and Tertiary Lymphoid Organs in the Small Intestine and the Colon. Front. Immunol. *7*, 186–11.

Buonocore, S., Ahern, P.P., Uhlig, H.H., Ivanov, I.I., Littman, D.R., Maloy, K.J., and Powrie, F. (2010). Innate lymphoid cells drive interleukin-23-dependent innate intestinal pathology. Nature *464*, 1371–1375.

Burzyn, D., Kuswanto, W., Kolodin, D., Shadrach, J.L., Cerletti, M., Jang, Y., Sefik, E., Tan, T.G., Wagers, A.J., Benoist, C., et al. (2013). A Special Population of Regulatory T Cells Potentiates Muscle Repair. Cell *155*, 1282–1295.

Butcher, D.T., Alliston, T., and Weaver, V.M. (2009). A tense situation: forcing tumour progression. Nat Rev Cancer *9*, 108–122.

Calon, A., Lonardo, E., Berenguer-Llergo, A., Espinet, E., Hernando-Momblona, X., Iglesias, M., Sevillano, M., Palomo-Ponce, S., Tauriello, D.V.F., Byrom, D., et al. (2015). Stromal gene expression defines poor-prognosis subtypes in colorectal cancer. Nature Publishing Group *47*, 320–329.

Cao, D., Hou, M., Guan, Y.-S., Jiang, M., Yang, Y., and Gou, H.-F. (2009). Expression of HIF-1alpha and VEGF in colorectal cancer: association with clinical outcomes and prognostic implications. BMC Cancer *9*, 905–909.

Caramalho, I., Lopes-Carvalho, T., Ostler, D., Zelenay, S., Haury, M., and Demengeot, J. (2003). Regulatory T Cells Selectively Express Toll-like Receptors and Are Activated by Lipopolysaccharide. J Exp Med *197*, 403–411.

Catalano, V., Loupakis, F., Graziano, F., Torresi, U., Bisonni, R., Mari, D., Fornaro, L., Baldelli, A.M., Giordani, P., Rossi, D., et al. (2009). Mucinous histology predicts for poor response rate and overall survival of patients with colorectal cancer and treated with first-line oxaliplatin- and/or irinotecan-based chemotherapy. British Journal of Cancer *100*, 881–887.

Chanmee, T., Ontong, P., Konno, K., and Itano, N. (2014). Tumor-Associated Macrophages as Major Players in the Tumor Microenvironment. Cancers *6*, 1670–1690.

Chaudhry, A., Rudra, D., Treuting, P., Samstein, R.M., Liang, Y., Kas, A., and Rudensky, A.Y. (2009). CD4+ regulatory T cells control TH17 responses in a Stat3-dependent manner. Science *326*, 986–991.

Chaudhry, A., Samstein, R.M., Treuting, P., Liang, Y., Pils, M.C., Heinrich, J.-M., Jack, R.S., Wunderlich, F.T., Brüning, J.C., Muller, W., et al. (2011). Interleukin-10 Signaling in Regulatory T Cells Is Required for Suppression of Th17 Cell-Mediated Inflammation. Immunity *34*, 566–578.

Chen, W., Jin, W., Hardegen, N., Lei, K.-J., Li, L., Marinos, N., McGrady, G., and Wahl, S.M. (2003). Conversion of peripheral CD4+CD25- naive T cells to CD4+CD25+ regulatory T cells by TGF-beta induction of transcription factor Foxp3. J Exp Med *198*, 1875–1886.

Cheroutre, H., Lambolez, F., and Mucida, D. (2011). The light and dark sides of intestinal intraepithelial lymphocytes. Nature Publishing Group *11*, 445–456.

Chu, V.T., Beller, A., Rausch, S., Strandmark, J., Zänker, M., Arbach, O., Kruglov, A., and Berek, C. (2014). Eosinophils Promote Generation and Maintenance of

Immunoglobulin-A-Expressing Plasma Cells and Contribute to Gut Immune Homeostasis. Immunity *40*, 582–593.

Chun, E., Lavoie, S., Michaud, M., Gallini, C.A., Kim, J., Soucy, G., Odze, R., Glickman, J.N., and Garrett, W.S. (2015). CCL2 Promotes Colorectal Carcinogenesis by Enhancing Polymorphonuclear Myeloid-Derived Suppressor Cell Population and Function. Cell Reports *12*, 244–257.

Chung, A.Y., Li, Q., Blair, S.J., De Jesus, M., Dennis, K.L., LeVea, C., Yao, J., Sun, Y., Conway, T.F., Virtuoso, L.P., et al. (2014). Oral Interleukin-10 Alleviates Polyposis via Neutralization of Pathogenic T-Regulatory Cells. Cancer Research *74*, 5377–5385.

Cipolletta, D., Feuerer, M., Li, A., Kamei, N., Lee, J., Shoelson, S.E., Benoist, C., and Mathis, D. (2012). PPAR-γ is a major driver of the accumulation and phenotype of adipose tissue Treg cells. Nature *18*, 363–11.

Cirri, P., and Chiarugi, P. (2011). Cancer associated fibroblasts: the dark side of the coin. Am J Cancer Res *1*, 482–497.

Clevers, H. (2013). The Intestinal Crypt, A Prototype Stem Cell Compartment. Cell *154*, 274–284.

Coletta, P.L. (2003). Lymphodepletion in the ApcMin/+ mouse model of intestinal tumorigenesis. Blood *103*, 1050–1058.

Collison, L.W., Workman, C.J., Kuo, T.T., Boyd, K., Wang, Y., Vignali, K.M., Cross, R., Sehy, D., Blumberg, R.S., and Vignali, D.A.A. (2007). The inhibitory cytokine IL-35 contributes to regulatory T-cell function. Nature *450*, 566–569.

Coombes, J.L., Siddiqui, K.R.R., Arancibia-Cárcamo, C.V., Hall, J., Sun, C.-M., Belkaid, Y., and Powrie, F. (2007). A functionally specialized population of mucosal CD103 +DCs induces Foxp3 +regulatory T cells via a TGF-β– and retinoic acid–dependent mechanism. J Exp Med *204*, 1757–1764.

Cua, D.J., Sherlock, J., Chen, Y., Murphy, C.A., Joyce, B., Seymour, B., Lucian, L., To, W., Kwan, S., Churakova, T., et al. (2003). Interleukin-23 rather than interleukin-12 is the critical cytokine for autoimmune inflammation of the brain. Nature *421*, 744–748.

Damiens, K., Ayoub, J.P.M., Lemieux, B., Aubin, F., Saliba, W., Campeau, M., and Tehfe, M. (2012). Clinical features and course of brain metastases in colorectal cancer: an experience from a single institution. Curr. Oncol. *19*, 1–5.

Danilova, E., Skrindo, I., Gran, E., Hales, B.J., Smith, W.A., Jahnsen, J., Johansen, F.E., Jahnsen, F.L., and Baekkevold, E.S. (2014). A role for CCL28-CCR3 in T-cell homing to the human upper airway mucosa. Mucosal Immunology *8*, 107–114.

David, C.J., Huang, Y.-H., Chen, M., Su, J., Zou, Y., Bardeesy, N., Iacobuzio-Donahue, C.A., and Massagué, J. (2016). TGF-β Tumor Suppression through a Lethal EMT.

Cell *164*, 1015–1030.

De Simone, M., Arrigoni, A., Rossetti, G., Gruarin, P., Ranzani, V., Politano, C., Bonnal, R.J.P., Provasi, E., Sarnicola, M.L., Panzeri, I., et al. (2016). Transcriptional Landscape of Human Tissue Lymphocytes Unveils Uniqueness of Tumor-Infiltrating T Regulatory Cells. Immunity *45*, 1135–1147.

de Souza, H.S.P., and Fiocchi, C. (2015). Immunopathogenesis of IBD: current state of the art. Nat Rev Gastroenterol Hepatol *13*, 13–27.

Deaglio, S., Dwyer, K.M., Gao, W., Friedman, D., Usheva, A., Erat, A., Chen, J.-F., Enjyoji, K., Linden, J., Oukka, M., et al. (2007). Adenosine generation catalyzed by CD39 and CD73 expressed on regulatory T cells mediates immune suppression. J Exp Med *204*, 1257–1265.

Dejea, C.M., Wick, E.C., Hechenbleikner, E.M., White, J.R., Mark Welch, J.L., Rossetti, B.J., Peterson, S.N., Snesrud, E.C., Borisy, G.G., Lazarev, M., et al. (2014). Microbiota organization is a distinct feature of proximal colorectal cancers. Proc Natl Acad Sci USA *111*, 18321–18326.

Delgoffe, G.M., Kole, T.P., Zheng, Y., Zarek, P.E., Matthews, K.L., Xiao, B., Worley, P.F., Kozma, S.C., and Powell, J.D. (2009). The mTOR Kinase Differentially Regulates Effector and Regulatory T Cell Lineage Commitment. Immunity *30*, 832–844.

Dennis, K.L., Wang, Y., Blatner, N.R., Wang, S., Saadalla, A., Trudeau, E., Roers, A., Weaver, C.T., Lee, J.J., Gilbert, J.A., et al. (2013). Adenomatous Polyps Are Driven by Microbe-Instigated Focal Inflammation and Are Controlled by IL-10-Producing T Cells. Cancer Research *73*, 5905–5913.

Dhainaut, M., Coquerelle, C., Uzureau, S., Denoeud, J., Acolty, V., Oldenhove, G., Galuppo, A., Sparwasser, T., Thielemans, K., Pays, E., et al. (2015). Thymus-derived regulatory T cells restrain pro-inflammatory Th1 responses by downregulating CD70 on dendritic cells. The EMBO Journal *34*, 1336–1348.

Drewes, J.L., Housseau, F., and Sears, C.L. (2016). Sporadic colorectal cancer: microbial contributors to disease prevention, development and therapy. British Journal of Cancer *115*, 273–280.

Duerr, R.H., Taylor, K.D., Brant, S.R., Rioux, J.D., Silverberg, M.S., Daly, M.J., Steinhart, A.H., Abraham, C., Regueiro, M., Griffiths, A., et al. (2006). A Genome-Wide Association Study Identifies IL23R as an Inflammatory Bowel Disease Gene. Science *314*, 1461–1463.

DuPage, M., and Bluestone, J.A. (2016). Harnessing the plasticity of CD4+ T cells to treat immune-mediated disease. Nature Publishing Group *16*, 149–163.

Dvorak, H.F. (1986). Tumors: wounds that do not heal. Similarities between tumor stroma generation and wound healing. N Engl J Med *315*, 1650–1659.

Elinav, E., Henao-Mejia, J., and Flavell, R.A. (2013). Integrative inflammasome activity in the regulation of intestinal mucosal immune responses. Mucosal Immunology *6*, 4–13.

Erdman, S.E., Rao, V.P., Poutahidis, T., Ihrig, M.M., Ge, Z., Feng, Y., Tomczak, M., Rogers, A.B., Horwitz, B.H., and Fox, J.G. (2003). CD4(+)CD25(+) regulatory lymphocytes require interleukin 10 to interrupt colon carcinogenesis in mice. Cancer Research *63*, 6042–6050.

Erdman, S.E., Sohn, J.J., Rao, V.P., Nambiar, P.R., Ge, Z., Fox, J.G., and Schauer, D.B. (2005). CD4+CD25+ regulatory lymphocytes induce regression of intestinal tumors in ApcMin/+ mice. Cancer Research *65*, 3998–4004.

Erreni, M., Mantovani, A., and Allavena, P. (2010). Tumor-associated Macrophages (TAM) and Inflammation in Colorectal Cancer. Cancer Microenvironment *4*, 141–154.

Facciabene, A., Peng, X., Hagemann, I.S., Balint, K., Barchetti, A., Wang, L.-P., Gimotty, P.A., Gilks, C.B., Lal, P., Zhang, L., et al. (2011). Tumour hypoxia promotes tolerance and angiogenesis via CCL28 and Treg cells. Nature *475*, 226–230.

Fearon, E.R., and Vogelstein, B. (1990). A genetic model for colorectal tumorigenesis. Cell *61*, 759–767.

Fessler, E., Drost, J., van Hooff, S.R., Linnekamp, J.F., Wang, X., Jansen, M., de Sousa E Melo, F., Prasetyanti, P.R., IJspeert, J.E., Franitza, M., et al. (2016). TGFβ signaling directs serrated adenomas to the mesenchymal colorectal cancer subtype. EMBO Mol Med. *8*, 745–760.

Feuerer, M., Hill, J.A., Mathis, D., and Benoist, C. (2009). Foxp3+ regulatory T cells: differentiation, specification, subphenotypes. Nature Publishing Group *10*, 689–695.

Fiala, E.S. (1977). Investigations into the metabolism and mode of action of the colon carcinogens 1,2-dimethylhydrazine and azoxymethane. Cancer *40*, 2436–2445.

Fichtner-Feigl, S., Strober, W., Kawakami, K., Puri, R.K., and Kitani, A. (2005). IL-13 signaling through the IL-13α2 receptor is involved in induction of TGF-β1 production and fibrosis. Nature Medicine *12*, 99–106.

Fontenot, J.D., Gavin, M.A., and Rudensky, A.Y. (2003). Foxp3 programs the development and function of CD4+CD25+ regulatory T cells. Nat Immunol *4*, 330–336.

Fournier, B.M., and Parkos, C.A. (2012). The role of neutrophils during intestinal inflammation. *5*, 354–366.

Frey, D.M., Droeser, R.A., Viehl, C.T., Zlobec, I., Lugli, A., Zingg, U., Oertli, D., Kettelhack, C., Terracciano, L., and Tornillo, L. (2010). High frequency of tumor-infiltrating FOXP3 +regulatory T cells predicts improved survival in mismatch repair-proficient colorectal cancer patients. Int. J. Cancer *353*, NA–NA.

Garín, M.I., Chu, C.-C., Golshayan, D., Cernuda-Morollón, E., Wait, R., and Lechler, R.I. (2007). Galectin-1: a key effector of regulation mediated by CD4+CD25+ T cells. Blood *109*, 2058–2065.

Gerber, B.O., Zanni, M.P., Uguccioni, M., Loetscher, M., Mackay, C.R., Pichler, W.J., Yawalkar, N., Baggiolini, M., and Moser, B. (1997). Functional expression of the eotaxin receptor CCR3 in T lymphocytes co-localizing with eosinophils. Current Biology *7*, 836–843.

Geremia, A., Arancibia-Cárcamo, C.V., Fleming, M.P.P., Rust, N., Singh, B., Mortensen, N.J., Travis, S.P.L., and Powrie, F. (2011). IL-23–responsive innate lymphoid cells are increased in inflammatory bowel disease. J Exp Med *208*, 1127–1133.

Gerriets, V.A., Kishton, R.J., Johnson, M.O., Cohen, S., Siska, P.J., Nichols, A.G., Warmoes, M.O., de Cubas, A.A., MacIver, N.J., Locasale, J.W., et al. (2016). Foxp3 and Toll-like receptor signaling balance Treg cell anabolic metabolism for suppression. Nat Immunol *17*, 1459–1466.

Gershon, R.K., and Kondo, K. (1970). Cell interactions in the induction of tolerance: the role of thymic lymphocytes. Immunology *18*, 723–737.

Geuking, M.B., Cahenzli, J., Lawson, M.A.E., Ng, D.C.K., Slack, E., Hapfelmeier, S., McCoy, K.D., and Macpherson, A.J. (2011). Intestinal Bacterial Colonization Induces Mutualistic Regulatory T Cell Responses. Immunity *34*, 794–806.

Ghoreschi, K., Laurence, A., Yang, X.-P., Tato, C.M., McGeachy, M.J., Konkel, J.E., Ramos, H.L., Wei, L., Davidson, T.S., Bouladoux, N., et al. (2010). Generation of pathogenic TH17 cells in the absence of TGF-β signalling. Nature *467*, 967–971.

Gibney, G.T., Kudchadkar, R.R., DeConti, R.C., Thebeau, M.S., Czupryn, M.P., Tetteh, L., Eysmans, C., Richards, A., Schell, M.J., Fisher, K.J., et al. (2015). Safety, correlative markers, and clinical results of adjuvant nivolumab in combination with vaccine in resected high-risk metastatic melanoma. Clinical Cancer Research *21*, 712–720.

Glocker, E.-O., Kotlarz, D., Boztug, K., Gertz, E.M., Schäffer, A.A., Noyan, F., Perro, M., Diestelhorst, J., Allroth, A., Murugan, D., et al. (2009). Inflammatory Bowel Disease and Mutations Affecting the Interleukin-10 Receptor. N Engl J Med *361*, 2033–2045.

Goldrath, A.W., Luckey, C.J., Park, R., Benoist, C., and Mathis, D. (2004). The molecular program induced in T cells undergoing homeostatic proliferation. Proc Natl Acad Sci USA *101*, 16885–16890.

Gondek, D.C., Lu, L.F., Quezada, S.A., Sakaguchi, S., and Noelle, R.J. (2005). Cutting Edge: Contact-Mediated Suppression by CD4+CD25+ Regulatory Cells Involves a Granzyme B-Dependent, Perforin-Independent Mechanism. The Journal of Immunology *174*, 1783–1786.

Gounaris, E., Blatner, N.R., Dennis, K., Magnusson, F., Gurish, M.F., Strom, T.B.,

Beckhove, P., Gounari, F., and Khazaie, K. (2009). T-Regulatory Cells Shift from a Protective Anti-Inflammatory to a Cancer-Promoting Proinflammatory Phenotype in Polyposis. Cancer Research *69*, 5490–5497.

Grady, W.M., and Carethers, J.M. (2008). Genomic and Epigenetic Instability in Colorectal Cancer Pathogenesis. Gastroenterology *135*, 1079–1099.

Green, D.R., and Webb, D.R. (1993). Saying the "S" word in public. Immunol. Today *14*, 523–525.

Griseri, T., Asquith, M., Thompson, C., and Powrie, F. (2010). OX40 is required for regulatory T cell-mediated control of colitis. J Exp Med *207*, 699–709.

Grivennikov, S.I., Greten, F.R., and Karin, M. (2010). Immunity, Inflammation, and Cancer. Cell *140*, 883–899.

Grossman, W.J., Verbsky, J.W., Barchet, W., Colonna, M., Atkinson, J.P., and Ley, T.J. (2004). Human T Regulatory Cells Can Use the Perforin Pathway to Cause Autologous Target Cell Death. Immunity *21*, 589–601.

Guinney, J., Dienstmann, R., Wang, X., de Reyniès, A., Schlicker, A., Soneson, C., Marisa, L., Roepman, P., Nyamundanda, G., Angelino, P., et al. (2015). The consensus molecular subtypes of colorectal cancer. Nature Medicine *21*, 1350–1356.

Guzman, M.J., Shao, J., and Sheng, H. (2012). Pro-Neoplastic Effects of Amphiregulin in Colorectal Carcinogenesis. J Gastrointest Canc *44*, 211–221.

Hanahan, D., and Weinberg, R.A. (2011). Hallmarks of Cancer: The Next Generation. Cell *144*, 646–674.

Hansen, J.J. (2015). Immune Responses to Intestinal Microbes in Inflammatory Bowel Diseases. Curr Allergy Asthma Rep *15*, 1907–1908.

Hapfelmeier, S., Lawson, M.A.E., Slack, E., Kirundi, J.K., Stoel, M., Heikenwalder, M., Cahenzli, J., Velykoredko, Y., Balmer, M.L., Endt, K., et al. (2010). Reversible Microbial Colonization of Germ-Free Mice Reveals the Dynamics of IgA Immune Responses. Science *328*, 1703–1705.

Harbaum, L., Pollheimer, M.J., Kornprat, P., Lindtner, R.A., Bokemeyer, C., and Langner, C. (2014). Peritumoral eosinophils predict recurrence in colorectal cancer. *28*, 403–413.

Harris, C.A., Haas, J.T., Streeper, R.S., Stone, S.J., Kumari, M., Yang, K., Han, X., Brownell, N., Gross, R.W., Zechner, R., et al. (2011). DGAT enzymes are required for triacylglycerol synthesis and lipid droplets in adipocytes. J. Lipid Res. *52*, 657–667.

Hase, K. (2002). Cell Differentiation Is a Key Determinant of Cathelicidin LL-37/Human Cationic Antimicrobial Protein 18 Expression by Human Colon Epithelium. Infection and Immunity *70*, 953–963.

Hataye, J. (2006). Naive and memory CD4+ T cell survival controlled by clonal abundance. Science *312*, 114–116.

Hayday, A., and Gibbons, D. (2008). Brokering the peace: the origin of intestinal T cells. Mucosal Immunology *1*, 172–174.

Herman, A.E., Freeman, G.J., Mathis, D., and Benoist, C. (2004). CD4 +CD25 +T Regulatory Cells Dependent on ICOS Promote Regulation of Effector Cells in the Prediabetic Lesion. J Exp Med *199*, 1479–1489.

Hori, S., Nomura, T., and Sakaguchi, S. (2003). Control of regulatory T cell development by the transcription factor Foxp3. Science *299*, 1057–1061.

Hsieh, C.-S., Lee, H.-M., and Lio, C.-W.J. (2012). Selection of regulatory T cells in the thymus. Nature Publishing Group *12*, 157–167.

Hu, H., Sun, L., Guo, C., Liu, Q., Zhou, Z., Peng, L., Pan, J., Yu, L., Lou, J., Yang, Z., et al. (2009). Tumor Cell-Microenvironment Interaction Models Coupled with Clinical Validation Reveal CCL2 and SNCG as Two Predictors of Colorectal Cancer Hepatic Metastasis. Clinical Cancer Research *15*, 5485–5493.

Huber, S., Gagliani, N., Zenewicz, L.A., Huber, F.J., Bosurgi, L., Hu, B., Hedl, M., Zhang, W., O'Connor, W., Murphy, A.J., et al. (2012). IL-22BP is regulated by the inflammasome and modulates tumorigenesis in the intestine. Nature *491*, 259–263.

Hugen, N., Simons, M., Halilović, A., van der Post, R.S., Bogers, A.J., Marijnissen-van Zanten, M.A., de Wilt, J.H., and Nagtegaal, I.D. (2014). The molecular background of mucinous carcinoma beyond MUC2. J Pathol Clin Res *1*, 3–17.

Iizuka, M. (2011). Wound healing of intestinal epithelial cells. Wjg *17*, 2161–11.

Ip, W.K.E., Hoshi, N., Shouval, D.S., Snapper, S., and Medzhitov, R. (2017). Anti-inflammatory effect of IL-10 mediated by metabolic reprogramming of macrophages. Science *356*, 513–519.

Isella, C., Terrasi, A., Bellomo, S.E., Petti, C., Galatola, G., Muratore, A., Mellano, A., Senetta, R., Cassenti, A., Sonetto, C., et al. (2015). Stromal contribution to the colorectal cancer transcriptome. Nature Genetics *47*, 312–319.

Itoh, M., Takahashi, T., Sakaguchi, N., Kuniyasu, Y., Shimizu, J., Otsuka, F., and Sakaguchi, S. (1999). Thymus and autoimmunity: production of CD25+CD4+ naturally anergic and suppressive T cells as a key function of the thymus in maintaining immunologic self-tolerance. The Journal of Immunology *162*, 5317–5326.

Ivanov, I.I., and Honda, K. (2012). Intestinal Commensal Microbes as Immune Modulators. Cell Host and Microbe *12*, 496–508.

Ivanov, I.I., Zhou, L., and Littman, D.R. (2007). Transcriptional regulation of Th17 cell differentiation. Semin. Immunol. *19*, 409–417.

Iwasaki, A., and Medzhitov, R. (2015). Control of adaptive immunity by the innate immune system. Nat Immunol *16*, 343–353.

Iyer, R.R., Pluciennik, A., Burdett, V., and Modrich, P.L. (2006). DNA Mismatch Repair: Functions and Mechanisms. Chem. Rev. *106*, 302–323.

Janeway, C.A. (1989). Approaching the asymptote? Evolution and revolution in immunology. Cold Spring Harbor Symposia on Quantitative Biology *54 Pt 1*, 1–13.

Janeway, C.A., Jr (1992). The T Cell Receptor as a Multicomponent Signalling Machine: CD4/CD8 Coreceptors and CD45 in T Cell Activation. Annu. Rev. Immunol. *10*, 645–674.

Jess, T., Rungoe, C., and Biroulet, L.P. (2012). Risk of Colorectal Cancer in Patients With Ulcerative Colitis: A Meta-analysis of Population-Based Cohort Studies. Yjcgh *10*, 639–645.

Johansson, M.E.V., Phillipson, M., Petersson, J., Velcich, A., Holm, L., and Hansson, G.C. (2008). The inner of the two Muc2 mucin-dependent mucus layers in colon is devoid of bacteria. 1–6.

Johansson-Lindbom, B., Svensson, M., Pabst, O., Palmqvist, C., Marquez, G., Förster, R., and Agace, W.W. (2005). Functional specialization of gut CD103 +dendritic cells in the regulation of tissue-selective T cell homing. J Exp Med *202*, 1063–1073.

Joller, N., Lozano, E., Burkett, P.R., Patel, B., Xiao, S., Zhu, C., Xia, J., Tan, T.G., Sefik, E., Yajnik, V., et al. (2014). Treg Cells Expressing the Coinhibitory Molecule TIGIT Selectively Inhibit Proinflammatory Th1 and Th17 Cell Responses. Immunity *40*, 569–581.

Josefowicz, S.Z., Niec, R.E., Kim, H.Y., Treuting, P., Chinen, T., Zheng, Y., Umetsu, D.T., and Rudensky, A.Y. (2012). Extrathymically generated regulatory T cells control mucosal TH2 inflammation. Nature *482*, 395–399.

Kabat, A.M., and Pearce, E.J. (2017). Inflammation by way of macrophage metabolism. Science *356*, 488–489.

Kain, M.J.W., and Owens, B.M.J. (2013). Stromal cell regulation of homeostatic and inflammatory lymphoid organogenesis. Immunology *140*, 12–21.

Kayama, H., Ueda, Y., Sawa, Y., Jeon, S.G., Ma, J.S., Okumura, R., Kubo, A., Ishii, M., Okazaki, T., Murakami, M., et al. (2012). Intestinal CX3C chemokine receptor 1high (CX3CR1high) myeloid cells prevent T-cell-dependent colitis. Proc Natl Acad Sci USA *109*, 5010–5015.

Khattri, R., Cox, T., Yasayko, S.-A., and Ramsdell, F. (2003). An essential role for Scurfin in CD4+CD25+ T regulatory cells. Nat Immunol *4*, 337–342.

Kim, K.S., Hong, S.-W., Han, D., Yi, J., Jung, J., Yang, B.-G., Lee, J.Y., Lee, M., and Surh,

C.D. (2016). Dietary antigens limit mucosal immunity by inducing regulatory T cells in the small intestine. Science *351*, 858–863.

Kirchberger, S., Royston, D.J., Boulard, O., Thornton, E., Franchini, F., Szabady, R.L., Harrison, O., and Powrie, F. (2013). Innate lymphoid cells sustain colon cancer through production of interleukin-22 in a mouse model. J Exp Med *210*, 917–931.

Kitani, A., Fuss, I., Nakamura, K., Kumaki, F., Usui, T., and Strober, W. (2003). Transforming Growth Factor (TGF)-β1–producing Regulatory T Cells Induce Smad-mediated Interleukin 10 Secretion That Facilitates Coordinated Immunoregulatory Activity and Amelioration of TGF-β1–mediated Fibrosis. J Exp Med *198*, 1179–1188.

Kitano, H., Kageyama, S.-I., Hewitt, S.M., Hayashi, R., Doki, Y., Ozaki, Y., Fujino, S., Takikita, M., Kubo, H., and Fukuoka, J. (2010). Podoplanin expression in cancerous stroma induces lymphangiogenesis and predicts lymphatic spread and patient survival. Arch. Pathol. Lab. Med. *134*, 1520–1527.

Knight, R. (2011). Microbial eukaryotes in the human microbiome: ecology, evolution, and future directions. 1–6.

Kobie, J.J., Shah, P.R., Yang, L., Rebhahn, J.A., Fowell, D.J., and Mosmann, T.R. (2006). T Regulatory and Primed Uncommitted CD4 T Cells Express CD73, Which Suppresses Effector CD4 T Cells by Converting 5'-Adenosine Monophosphate to Adenosine. The Journal of Immunology *177*, 6780–6786.

Koch, M.A., Tucker-Heard, G., Perdue, N.R., Killebrew, J.R., Urdahl, K.B., and Campbell, D.J. (2009). The transcription factor T-bet controls regulatory T cell homeostasis and function during type 1 inflammation. Nat Immunol *10*, 595–602.

Komatsu, N., Okamoto, K., Sawa, S., Nakashima, T., Oh-hora, M., Kodama, T., Tanaka, S., Bluestone, J.A., and Takayanagi, H. (2013). Pathogenic conversion of Foxp3+ T cells into TH17 cells in autoimmune arthritis. Nature Medicine *20*, 62–68.

Kontoyiannis, D., Boulougouris, G., Manoloukos, M., Armaka, M., Apostolaki, M., Pizarro, T., Kotlyarov, A., Forster, I., Flavell, R., Gaestel, M., et al. (2002). Genetic dissection of the cellular pathways and signaling mechanisms in modeled tumor necrosis factor-induced Crohn's-like inflammatory bowel disease. J Exp Med *196*, 1563–1574.

Krause, P., Morris, V., Greenbaum, J.A., Park, Y., Bjoerheden, U., Mikulski, Z., Muffley, T., Shui, J.-W., Kim, G., Cheroutre, H., et al. (2015). IL-10-producing intestinal macrophages prevent excessive antibacterial innate immunity by limiting IL-23 synthesis. Nature Communications *6*, 1–12.

Kretschmer, K., Apostolou, I., Hawiger, D., Khazaie, K., Nussenzweig, M.C., and Boehmer, von, H. (2005). Inducing and expanding regulatory T cell populations by foreign antigen. Nat Immunol *6*, 1219–1227.

Kuhn, K.A., Manieri, N.A., Liu, T.-C., and Stappenbeck, T.S. (2014). IL-6 Stimulates

Intestinal Epithelial Proliferation and Repair after Injury. PLoS ONE *9*, e114195–18.

la Cruz-Merino, de, L., Henao Carrasco, F., Vicente Baz, D., Nogales Fernández, E., Reina Zoilo, J.J., Codes Manuel de Villena, M., and Pulido, E.G. (2011). Immune Microenvironment in Colorectal Cancer: A New Hallmark to Change Old Paradigms. Clinical and Developmental Immunology *2011*, 1–9.

Langrish, C.L., Chen, Y., Blumenschein, W.M., Mattson, J., Basham, B., Sedgwick, J.D., McClanahan, T., Kastelein, R.A., and Cua, D.J. (2005). IL-23 drives a pathogenic T cell population that induces autoimmune inflammation. J Exp Med *201*, 233–240.

Le, D.T., Uram, J.N., Wang, H., Bartlett, B.R., Kemberling, H., Eyring, A.D., Skora, A.D., Luber, B.S., Azad, N.S., Laheru, D., et al. (2015). PD-1 Blockade in Tumors with Mismatch-Repair Deficiency. N Engl J Med *372*, 2509–2520.

Lee, J., Mo, J.-H., Katakura, K., Alkalay, I., Rucker, A.N., Liu, Y.-T., Lee, H.-K., Shen, C., Cojocaru, G., Shenouda, S., et al. (2006). Maintenance of colonic homeostasis by distinctive apical TLR9 signalling in intestinal epithelial cells. Nat Cell Biol *8*, 1327–1336.

Leoni, G., Neumann, P.-A., Sumagin, R., Denning, T.L., and Nusrat, A. (2015). Wound repair: role of immune–epithelial interactions. Mucosal Immunology *8*, 959–968.

Liang, B., Workman, C., Lee, J., Chew, C., Dale, B.M., Colonna, L., Flores, M., Li, N., Schweighoffer, E., Greenberg, S., et al. (2008). Regulatory T Cells Inhibit Dendritic Cells by Lymphocyte Activation Gene-3 Engagement of MHC Class II. The Journal of Immunology *180*, 5916–5926.

Lièvre, A., Bachet, J.-B., Boige, V., Cayre, A., Le Corre, D., Buc, E., Ychou, M., Bouché, O., Landi, B., Louvet, C., et al. (2008). KRAS Mutations As an Independent Prognostic Factor in Patients With Advanced Colorectal Cancer Treated With Cetuximab. Jco *26*, 374–379.

Lighvani, A.A., Frucht, D.M., Jankovic, D., Yamane, H., Aliberti, J., Hissong, B.D., Nguyen, B.V., Gadina, M., Sher, A., Paul, W.E., et al. (2001). T-bet is rapidly induced by interferon-gamma in lymphoid and myeloid cells. Proc Natl Acad Sci USA *98*, 15137–15142.

Lin, C.-M., Fang, C.-L., Hseu, Y.-C., Chen, C.-L., Wang, J.-W., Hsu, S.-L., Tu, M.-D., Hung, S.-T., Tai, C., Uen, Y.-H., et al. (2013). Clinical and Prognostic Implications of Transcription Factor SOX4 in Patients with Colon Cancer. PLoS ONE *8*, e67128–7.

Liston, A., and Gray, D.H.D. (2014). Homeostatic control of regulatory T cell diversity. Nature Publishing Group *14*, 154–165.

Liu, N., Phillips, T., Zhang, M., Wang, Y., Opferman, J.T., Shah, R., and Ashton-Rickardt, P.G. (2004). Serine protease inhibitor 2A is a protective factor for memory T cell development. Nat Immunol *5*, 919–926.

Liu, X., Das, A.M., Seideman, J., Griswold, D., Afuh, C.N., Kobayashi, T., Abe, S., Fang, Q., Hashimoto, M., Kim, H., et al. (2007). The CC Chemokine Ligand 2 (CCL2) Mediates Fibroblast Survival through IL-6. Am J Respir Cell Mol Biol *37*, 121–128.

Llosa, N.J., Cruise, M., Tam, A., Wicks, E.C., Hechenbleikner, E.M., Taube, J.M., Blosser, R.L., Fan, H., Wang, H., Luber, B.S., et al. (2015). The Vigorous Immune Microenvironment of Microsatellite Instable Colon Cancer Is Balanced by Multiple Counter-Inhibitory Checkpoints. Cancer Discovery *5*, 43–51.

Lorenz, R.G., and Newberry, R.D. (2004). Isolated Lymphoid Follicles Can Function as Sites for Induction of Mucosal Immune Responses. Annals of the New York Academy of Sciences *1029*, 44–57.

Lotz, M.M., Nusrat, A., Madara, J.L., Ezzell, R., Wewer, U.M., and Mercurio, A.M. (1997). Intestinal epithelial restitution. Involvement of specific laminin isoforms and integrin laminin receptors in wound closure of a transformed model epithelium. The American Journal of Pathology *150*, 747–760.

Lourenço, A.R., and Coffer, P.J. (2017). SOX4: Joining the Master Regulators of Epithelial-to-Mesenchymal Transition? TRENDS in CANCER *3*, 571–582.

Lynch, D., and Murphy, A. (2016). The emerging role of immunotherapy in colorectal cancer. Ann. Transl. Med. *4*, 305–305.

Mabbott, N.A., Donaldson, D.S., Ohno, H., Williams, I.R., and Mahajan, A. (2013). Microfold (M) cells: important immunosurveillance posts in the intestinal epithelium. Mucosal Immunology *6*, 666–677.

Macpherson, A.J. (2004). Induction of Protective IgA by Intestinal Dendritic Cells Carrying Commensal Bacteria. Science *303*, 1662–1665.

Maloy, K.J., and Kullberg, M.C. (2008). IL-23 and Th17 cytokines in intestinal homeostasis. Mucosal Immunology *1*, 339–349.

Maloy, K.J., and Powrie, F. (2011). Intestinal homeostasis and its breakdown in inflammatory bowel disease. Nature *474*, 298–306.

Maloy, K.J., Salaun, L., Cahill, R., Dougan, G., Saunders, N.J., and Powrie, F. (2003). CD4+ CD25+ T_R Cells Suppress Innate Immune Pathology Through Cytokine-dependent Mechanisms. J Exp Med *197*, 111–119.

Manousou, P., Kolios, G., Valatas, V., Drygiannakis, I., Bourikas, L., Pyrovolaki, K., Koutroubakis, I., Papadaki, H.A., and Kouroumalis, E. (2010). Increased expression of chemokine receptor CCR3 and its ligands in ulcerative colitis: the role of colonic epithelial cells in in vitro studies. Clinical & Experimental Immunology *162*, 337–347.

Massagué, J., and Obenauf, A.C. (2016). Metastatic colonization by circulating tumour cells. Nature *529*, 298–306.

McGeachy, M.J., Stephens, L.A., and Anderton, S.M. (2005). Natural Recovery and Protection from Autoimmune Encephalomyelitis: Contribution of CD4+CD25+ Regulatory Cells within the Central Nervous System. The Journal of Immunology *175*, 3025–3032.

McGeachy, M.J., Chen, Y., Tato, C.M., Laurence, A., Joyce-Shaikh, B., Blumenschein, W.M., McClanahan, T.K., O'Shea, J.J., and Cua, D.J. (2009). The interleukin 23 receptor is essential for the terminal differentiation of interleukin 17–producing effector T helper cells in vivo. Nat Immunol *10*, 314–324.

McHugh, R.S., Whitters, M.J., Piccirillo, C.A., Young, D.A., Shevach, E.M., Collins, M., and Byrne, M.C. (2002). CD4(+)CD25(+) immunoregulatory T cells: gene expression analysis reveals a functional role for the glucocorticoid-induced TNF receptor. Immunity *16*, 311–323.

Medrikova, D., Sijmonsma, T.P., Sowodniok, K., Richards, D.M., Delacher, M., Sticht, C., Gretz, N., Schafmeier, T., Feuerer, M., and Herzig, S. (2015). Brown Adipose Tissue Harbors a Distinct Sub-Population of Regulatory T Cells. PLoS ONE *10*, e0118534–13.

Medzhitov, R. (2001). Toll-like receptors and innate immunity. Nature Reviews Immunology *1*, 135–145.

Mekenkamp, L.J.M., Heesterbeek, K.J., Koopman, M., Tol, J., Teerenstra, S., Venderbosch, S., Punt, C.J.A., and Nagtegaal, I.D. (2012). Mucinous adenocarcinomas: Poor prognosis in metastatic colorectal cancer. European Journal of Cancer *48*, 501–509.

Melis, M., Hernandez, J., Siegel, E.M., McLoughlin, J.M., Ly, Q.P., Nair, R.M., Lewis, J.M., Jensen, E.H., Alvarado, M.D., Coppola, D., et al. (2010). Gene Expression Profiling of Colorectal Mucinous Adenocarcinomas. Diseases of the Colon & Rectum *53*, 936–943.

Mestecky, J., and Russell, M.W. (2009). Specific antibody activity, glycan heterogeneity and polyreactivity contribute to the protective activity of S-IgA at mucosal surfaces. Immunology Letters *124*, 57–62.

Miteva, L.D., Stanilov, N.S., Deliysky, T.S., and Stanilova, S.A. (2014). Significance of −1082A/G polymorphism of IL10 gene for progression of colorectal cancer and IL-10 expression. Tumor Biology *35*, 12655–12664.

Miyara, M., Yoshioka, Y., Kitoh, A., Shima, T., Wing, K., Niwa, A., Parizot, C., Taflin, C., Heike, T., Valeyre, D., et al. (2009). Functional Delineation and Differentiation Dynamics of Human CD4+ T Cells Expressing the FoxP3 Transcription Factor. Immunity *30*, 899–911.

Monticelli, L.A., Osborne, L.C., Noti, M., Tran, S.V., Zaiss, D.M.W., and Artis, D. (2015). IL-33 promotes an innate immune pathway of intestinal tissue protection dependent on amphiregulin–EGFR interactions. Proc Natl Acad Sci USA *112*, 10762–10767.

Morrissey, P.J., Charrier, K., Braddy, S., Liggitt, D., and Watson, J.D. (1993). CD4+ T cells that express high levels of CD45RB induce wasting disease when transferred into congenic severe combined immunodeficient mice. Disease development is prevented by cotransfer of purified CD4+ T cells. J Exp Med *178*, 237–244.

Mosmann, T.R., Cherwinski, H., Bond, M.W., Giedlin, M.A., and Coffman, R.L. (1986). Two types of murine helper T cell clone. I. Definition according to profiles of lymphokine activities and secreted proteins. The Journal of Immunology *136*, 2348–2357.

Motz, G.T., and Coukos, G. (2011). The parallel lives of angiogenesis and immunosuppression: cancer and other tales. Nature Publishing Group *11*, 702–711.

Mowat, A.M., and Agace, W.W. (2014). Regional specialization within the intestinal immune system. Nature Reviews Immunology *14*, 667–685.

Mowat, A.M. (2003). Anatomical basis of tolerance and immunity to intestinal antigens. Nature Reviews Immunology *3*, 331–341.

Möller, G. (1988). Do suppressor T cells exist? Scand. J. Immunol. *27*, 247–250.

Murai, M., Turovskaya, O., Kim, G., Madan, R., Karp, C.L., Cheroutre, H., and Kronenberg, M. (2009). Interleukin 10 acts on regulatory T cells to maintain expression of the transcription factor Foxp3 and suppressive function in mice with colitis. Nat Immunol *10*, 1178–1184.

Murphy, K.M., Ouyang, W., Farrar, J.D., Yang, J., Ranganath, S., Asnagli, H., Afkarian, M., and Murphy, T.L. (2000). Signaling and transcription in T helper development. Annu. Rev. Immunol. *18*, 451–494.

Müller, M.F., Ibrahim, A.E.K., and Arends, M.J. (2016a). Molecular pathological classification of colorectal cancer. Virchows Archiv 1–10.

Müller, M.F., Ibrahim, A.E.K., and Arends, M.J. (2016b). Molecular pathological classification of colorectal cancer. Virchows Archiv 1–10.

Nakayama, T., Hirahara, K., Onodera, A., Endo, Y., Hosokawa, H., Shinoda, K., Tumes, D.J., and Okamoto, Y. (2017). Th2 Cells in Health and Disease. Annu. Rev. Immunol. *35*, 53–84.

Niess, J.H., Brand, S., Gu, X., Landsman, L., Jung, S., McCormick, B.A., Vyas, J.M., Boes, M., Ploegh, H.L., Fox, J.G., et al. (2005). CX_3CR1-Mediated Dendritic Cell

Access to the Intestinal Lumen and Bacterial Clearance. Science *307*, 251–254.

Nishizuka, Y., and Sakakura, T. (1969). Thymus and reproduction: sex-linked dysgenesia of the gonad after neonatal thymectomy in mice. Science *166*, 753–755.

Nosbaum, A., Prevel, N., Truong, H.-A., Mehta, P., Ettinger, M., Scharschmidt, T.C., Ali, N.H., Pauli, M.L., Abbas, A.K., and Rosenblum, M.D. (2016). Cutting Edge:

Regulatory T Cells Facilitate Cutaneous Wound Healing. The Journal of Immunology *196*, 2010–2014.

Nusrat, A., Delp, C., and Madara, J.L. (1992). Intestinal epithelial restitution. Characterization of a cell culture model and mapping of cytoskeletal elements in migrating cells. J. Clin. Invest. *89*, 1501–1511.

O'Hara, R.J., Greenman, J., MacDonald, A.W., Gaskell, K.M., Topping, K.P., Duthie, G.S., Kerin, M.J., Lee, P.W., and Monson, J.R. (1998). Advanced colorectal cancer is associated with impaired interleukin 12 and enhanced interleukin 10 production. Clinical Cancer Research *4*, 1943–1948.

Ohnmacht, C., Park, J.H., Cording, S., Wing, J.B., Atarashi, K., Obata, Y., Gaboriau-Routhiau, V., Marques, R., Dulauroy, S., Fedoseeva, M., et al. (2015). The microbiota regulates type 2 immunity through ROR t+ T cells. Science *349*, 989–993.

Oldenhove, G., Bouladoux, N., Wohlfert, E.A., Hall, J.A., Chou, D., santos, Dos, L., O'Brien, S., Blank, R., Lamb, E., Natarajan, S., et al. (2009). Decrease of Foxp3+ Treg Cell Number and Acquisition of Effector Cell Phenotype during Lethal Infection. Immunity *31*, 772–786.

Ospelt, C., Reedquist, K.A., Gay, S., and Tak, P.P. (2011). Inflammatory memories: Is epigenetics the missing link to persistent stromal cell activation in rheumatoid arthritis? Autoimmunity Reviews *10*, 519–524.

Otte, J.-M., Rosenberg, I.M., and Podolsky, D.K. (2003). Intestinal myofibroblasts in innate immune responses of the intestine. Gastroenterology *124*, 1866–1878.

Owens, B.M.J., and Simmons, A. (2012). Intestinal stromal cells in mucosal immunity and homeostasis. *6*, 224–234.

Owens, B.M.J. (2015). Inflammation, Innate Immunity, and the Intestinal Stromal Cell Niche: Opportunities and Challenges. Front. Immunol. *6*.

Paget, S. (1889). The distribution of secondary growths in cancer of the breast. 1889.

Palm, N.W., de Zoete, M.R., Cullen, T.W., Barry, N.A., Stefanowski, J., Hao, L., Degnan, P.H., Hu, J., Peter, I., Zhang, W., et al. (2014). Immunoglobulin A Coating Identifies Colitogenic Bacteria in Inflammatory Bowel Disease. Cell *158*, 1000–1010.

Pan, L., Beverley, P.C., and Isaacson, P.G. (1991). Lactate dehydrogenase (LDH) isoenzymes and proliferative activity of lymphoid cells--an immunocytochemical study. Clinical & Experimental Immunology *86*, 240–245.

Pandiyan, P., Zheng, L., Ishihara, S., Reed, J., and Lenardo, M.J. (2007). CD4+CD25+Foxp3+ regulatory T cells induce cytokine deprivation–mediated apoptosis of effector CD4+ T cells. Nat Immunol *8*, 1353–1362.

Panduro, M., Benoist, C., and Mathis, D. (2016). Tissue Tregs. Annu. Rev. Immunol.

34, 609–633.

Panwala, C.M., Jones, J.C., and Viney, J.L. (1998). A novel model of inflammatory bowel disease: mice deficient for the multiple drug resistance gene, mdr1a, spontaneously develop colitis. The Journal of Immunology *161*, 5733–5744.

Patai, Á.V. (2013). Serrated pathway: Alternative route to colorectal cancer. Wjg *19*, 607–609.

Pearson, C., Thornton, E.E., McKenzie, B., Schaupp, A.-L., Huskens, N., Griseri, T., West, N., Tung, S., Seddon, B.P., Uhlig, H.H., et al. (2016). ILC3 GM-CSF production and mobilisation orchestrate acute intestinal inflammation. eLIFE *5*, e10066–21.

Persson, E.K., Scott, C.L., Mowat, A.M., and Agace, W.W. (2013). Dendritic cell subsets in the intestinal lamina propria: Ontogeny and function. Eur. J. Immunol. *43*, 3098–3107.

Pinchuk, I.V., Beswick, E.J., Saada, J.I., Boya, G., Schmitt, D., Raju, G.S., Brenmoehl, J., Rogler, G., Reyes, V.E., and Powell, D.W. (2011). Human colonic myofibroblasts promote expansion of CD4+ CD25high Foxp3+ regulatory T cells. Gastroenterology *140*, 2019–2030.

Plitas, G., Konopacki, C., Wu, K., Bos, P.D., Morrow, M., Putintseva, E.V., Chudakov, D.M., and Rudensky, A.Y. (2016). Regulatory T Cells Exhibit Distinct Features in Human Breast Cancer. Immunity *45*, 1122–1134.

Poutahidis, T., Haigis, K.M., Rao, V.P., Nambiar, P.R., Taylor, C.L., Ge, Z., Watanabe, K., Davidson, A., Horwitz, B.H., Fox, J.G., et al. (2007). Rapid reversal of interleukin-6-dependent epithelial invasion in a mouse model of microbially induced colon carcinoma. Carcinogenesis *28*, 2614–2623.

Powell, D.W., Pinchuk, I.V., Saada, J.I., Chen, X., and Mifflin, R.C. (2011). Mesenchymal Cells of the Intestinal Lamina Propria. Annu. Rev. Physiol. *73*, 213–237.

Powrie, F., and Mason, D. (1990). OX-22high CD4+ T cells induce wasting disease with multiple organ pathology: prevention by the OX-22low subset. J Exp Med *172*, 1701–1708.

Powrie, F., Leach, M.W., Mauze, S., Caddle, L.B., and Coffman, R.L. (1993). Phenotypically distinct subsets of CD4+ T cells induce or protect from chronic intestinal inflammation in C. B-17 scid mice. Int. Immunol. *5*, 1461–1471.

Prizment, A.E., Vierkant, R.A., Smyrk, T.C., Tillmans, L.S., Lee, J.J., Sriramarao, P., Nelson, H.H., Lynch, C.F., Thibodeau, S.N., Church, T.R., et al. (2016). Tumor eosinophil infiltration and improved survival of colorectal cancer patients: Iowa Women’s Health Study. *29*, 516–527.

Punt, C.J.A., Koopman, M., and Vermeulen, L. (2016). From tumour heterogeneity to advances in precision treatment of colorectal cancer. Nat Rev Clin Oncol *14*, 235–

246.

Rad, R., Cadiñanos, J., Rad, L., Varela, I., Strong, A., Kriegl, L., Constantino-Casas, F., Eser, S., Hieber, M., Seidler, B., et al. (2013). A Genetic Progression Model of BrafV600E-Induced Intestinal Tumorigenesis Reveals Targets for Therapeutic Intervention. Cancer Cell *24*, 15–29.

Rao, R.R., Long, J.Z., White, J.P., Svensson, K.J., Lou, J., Lokurkar, I., Jedrychowski, M.P., Ruas, J.L., Wrann, C.D., Lo, J.C., et al. (2014). Meteorin-like Is a Hormone that Regulates Immune-Adipose Interactions to Increase Beige Fat Thermogenesis. Cell *157*, 1279–1291.

Read, S., Greenwald, R., Izcue, A., Robinson, N., Mandelbrot, D., Francisco, L., Sharpe, A.H., and Powrie, F. (2006). Blockade of CTLA-4 on CD4+CD25+ Regulatory T Cells Abrogates Their Function In Vivo. The Journal of Immunology *177*, 4376–4383.

Rieder, F., Brenmoehl, J., Leeb, S., Scholmerich, J., and Rogler, G. (2007). Wound healing and fibrosis in intestinal disease. Gut *56*, 130–139.

Riihimäki, M., Hemminki, A., Sundquist, J., and Hemminki, K. (2016). Patterns of metastasis in colon and rectal cancer. Sci Rep 1–9.

Rosenberg, H.F., Dyer, K.D., and Foster, P.S. (2012). Eosinophils: changing perspectives in health and disease. Nature Publishing Group *13*, 9–22.

Rothenberg, M.E., and Hogan, S.P. (2006). THE EOSINOPHIL. Annu. Rev. Immunol. *24*, 147–174.

Rubtsov, Y.P., Rasmussen, J.P., Chi, E.Y., Fontenot, J., Castelli, L., Ye, X., Treuting, P., Siewe, L., Roers, A., Henderson, W.R., Jr., et al. (2008). Regulatory T Cell-Derived Interleukin-10 Limits Inflammation at Environmental Interfaces. Immunity *28*, 546–558.

Saada, J.I., Pinchuk, I.V., Barrera, C.A., Adegboyega, P.A., Suarez, G., Mifflin, R.C., Di Mari, J.F., Reyes, V.E., and Powell, D.W. (2006). Subepithelial myofibroblasts are novel nonprofessional APCs in the human colonic mucosa. The Journal of Immunology *177*, 5968–5979.

Saito, T., Nishikawa, H., Wada, H., Nagano, Y., Sugiyama, D., Atarashi, K., Maeda, Y., Hamaguchi, M., Ohkura, N., Sato, E., et al. (2016). Two FOXP3+CD4+ T cell subpopulations distinctly control the prognosis of colorectal cancers. Nature Medicine *22*, 679–684.

Sakaguchi, S., Sakaguchi, N., Asano, M., Itoh, M., and Toda, M. (1995). Immunologic self-tolerance maintained by activated T cells expressing IL-2 receptor alpha-chains (CD25). Breakdown of a single mechanism of self-tolerance causes various autoimmune diseases. The Journal of Immunology *155*, 1151–1164.

Sakaguchi, S., Takahashi, T., and Nishizuka, Y. (1982). Study on cellular events in post-

thymectomy autoimmune oophoritis in mice. II. Requirement of Lyt-1 cells in normal female mice for the prevention of oophoritis. J Exp Med *156*, 1577–1586.

Salama, P., Phillips, M., Grieu, F., Morris, M., Zeps, N., Joseph, D., Platell, C., and Iacopetta, B. (2009). Tumor-Infiltrating FOXP3 +T Regulatory Cells Show Strong Prognostic Significance in Colorectal Cancer. Jco *27*, 186–192.

Satoh-Takayama, N., Vosshenrich, C.A.J., Lesjean-Pottier, S., Sawa, S., Lochner, M., Rattis, F., Mention, J.-J., Thiam, K., Cerf-Bensussan, N., Mandelboim, O., et al. (2008). Microbial Flora Drives Interleukin 22 Production in Intestinal NKp46+ Cells that Provide Innate Mucosal Immune Defense. Immunity *29*, 958–970.

Schiering, C., Krausgruber, T., Chomka, A., Fröhlich, A., Adelmann, K., Wohlfert, E.A., Pott, J., Griseri, T., Bollrath, J., Hegazy, A.N., et al. (2014). The alarmin IL-33 promotes regulatory T-cell function in the intestine. Nature *513*, 564–568.

Schulz, O., Jaensson, E., Persson, E.K., Liu, X., Worbs, T., Agace, W.W., and Pabst, O. (2009). Intestinal CD103+, but not CX3CR1+, antigen sampling cells migrate in lymph and serve classical dendritic cell functions. J Exp Med *206*, 3101–3114.

Sears, C.L., and Garrett, W.S. (2014). Microbes, Microbiota, and Colon Cancer. Cell Host and Microbe *15*, 317–328.

Sefik, E., Geva-Zatorsky, N., Oh, S., Konnikova, L., Zemmour, D., McGuire, A.M., Burzyn, D., Ortiz-Lopez, A., Lobera, M., Yang, J., et al. (2015). Individual intestinal symbionts induce a distinct population of RORγ^{+} regulatory T cells. Science *349*, 993–997.

Sekiya, T., Kashiwagi, I., Inoue, N., Morita, R., Hori, S., Waldmann, H., Rudensky, A.Y., Ichinose, H., Metzger, D., Chambon, P., et al. (2011). The nuclear orphan receptor Nr4a2 induces Foxp3 and regulates differentiation of CD4+ T cells. Nature Communications *2*, 269–12.

Sellon, R.K., Tonkonogy, S., Schultz, M., Dieleman, L.A., Grenther, W., Balish, E., Rennick, D.M., and Sartor, R.B. (1998). Resident enteric bacteria are necessary for development of spontaneous colitis and immune system activation in interleukin-10-deficient mice. Infection and Immunity *66*, 5224–5231.

Sender, R., Fuchs, S., and Milo, R. (2016). Revised Estimates for the Number of Human and Bacteria Cells in the Body. PLoS Biol *14*, e1002533–14.

Seong, S.-Y., and Matzinger, P. (2004). Opinion: Hydrophobicity: an ancient damage-associated molecular pattern that initiates innate immune responses. Nature Reviews Immunology *4*, 469–478.

Shalapour, S., and Karin, M. (2015). Immunity, inflammation, and cancer: an eternal fight between good and evil. J. Clin. Invest. *125*, 3347–3355.

Shao, J., and Sheng, H. (2010a). Amphiregulin Promotes Intestinal Epithelial

Regeneration: Roles of Intestinal Subepithelial Myofibroblasts. Endocrinology *151*, 3728–3737.

Shao, J., and Sheng, H. (2010b). Amphiregulin Promotes Intestinal Epithelial Regeneration: Roles of Intestinal Subepithelial Myofibroblasts. Endocrinology *151*, 3728–3737.

Sharma, P., Wagner, K., Wolchok, J.D., and Allison, J.P. (2011). Novel cancer immunotherapy agents with survival benefit: recent successes and next steps. Nat Rev Cancer *11*, 805–812.

Shen, L., and Turner, J.R. (2006). Role of epithelial cells in initiation and propagation of intestinal inflammation. Eliminating the static: tight junction dynamics exposed. AJP: Gastrointestinal and Liver Physiology *290*, G577–G582.

Sher, A., and Coffman, R.L. (1992). Regulation of immunity to parasites by T cells and T cell-derived cytokines. Annu. Rev. Immunol. *10*, 385–409.

Sherwood, A.M., Emerson, R.O., Scherer, D., Habermann, N., Buck, K., Staffa, J., Desmarais, C., Halama, N., Jaeger, D., Schirmacher, P., et al. (2013). Tumor-infiltrating lymphocytes in colorectal tumors display a diversity of T cell receptor sequences that differ from the T cells in adjacent mucosal tissue. Cancer Immunol Immunother *62*, 1453–1461.

Shevach, E.M. (2009). Mechanisms of Foxp3+ T Regulatory Cell-Mediated Suppression. Immunity *30*, 636–645.

Shevach, E.M. (2011). The Resurrection of T Cell-Mediated Suppression. The Journal of Immunology *186*, 3805–3807.

Shimizu, J., Yamazaki, S., Takahashi, T., Ishida, Y., and Sakaguchi, S. (2002). Stimulation of CD25+CD4+ regulatory T cells through GITR breaks immunological self-tolerance. Nat Immunol *3*, 135–142.

Shull, M.M., Ormsby, I., Kier, A.B., Pawlowski, S., Diebold, R.J., Yin, M., Allen, R., Sidman, C., Proetzel, G., Calvin, D., et al. (1992). Targeted disruption of the mouse transforming growth factor-β1 gene results in multifocal inflammatory disease. Nature *359*, 693–699.

Siegel, R.L., Miller, K.D., and Jemal, A. (2017). Cancer statistics, 2017. CA: a Cancer Journal for Clinicians *67*, 7–30.

Singh, K., Hjort, M., Thorvaldson, L., and Sandler, S. (2015). Concomitant analysis of Helios and Neuropilin-1 as a marker to detect thymic derived regulatory T cells in naïve mice. Sci Rep *5*, 523–10.

Singh, N.J., and Schwartz, R.H. (2006). The Lymphopenic Mouse in Immunology: From Patron to Pariah. Immunity *25*, 851–855.

Sinicrope, F.A., Rego, R.L., Ansell, S.M., Knutson, K.L., Foster, N.R., and Sargent, D.J. (2009). Intraepithelial Effector (CD3+)/Regulatory (FoxP3+) T-Cell Ratio Predicts a Clinical Outcome of Human Colon Carcinoma. Gastroenterology *137*, 1270–1279.

Sonnenberg, G.F., Monticelli, L.A., Alenghat, T., Fung, T.C., Hutnick, N.A., Kunisawa, J., Shibata, N., Grunberg, S., Sinha, R., Zahm, A.M., et al. (2012). Innate Lymphoid Cells Promote Anatomical Containment of Lymphoid-Resident Commensal Bacteria. Science *336*, 1321–1325.

Spits, H., Artis, D., Colonna, M., Diefenbach, A., Di Santo, J.P., Eberl, G., Koyasu, S., Locksley, R.M., McKenzie, A.N.J., Mebius, R.E., et al. (2013). Innate lymphoid cells — a proposal for uniform nomenclature. Nature Reviews Immunology *13*, 145–149.

Stanilov, N., Miteva, L., Deliysky, T., Jovchev, J., and Stanilova, S. (2010). Advanced Colorectal Cancer Is Associated With Enhanced IL-23 and IL-10 Serum Levels. Lab Med *41*, 159–163.

Strum, W.B. (2016). Colorectal Adenomas. N Engl J Med *374*, 1065–1075.

Sun, C.-M., Hall, J.A., Blank, R.B., Bouladoux, N., Oukka, M., Mora, J.R., and Belkaid, Y. (2007). Small intestine lamina propria dendritic cells promote de novo generation of Foxp3 T reg cells via retinoic acid. J Exp Med *204*, 1775–1785.

Symonds, D.A., and Vickery, A.L. (1976). Mucinous carcinoma of the colon and rectum. Cancer *37*, 1891–1900.

Szurek, E., Cebula, A., Wojciech, L., Pietrzak, M., Rempala, G., Kisielow, P., and Ignatowicz, L. (2015). Differences in Expression Level of Helios and Neuropilin-1 Do Not Distinguish Thymus-Derived from Extrathymically-Induced CD4+Foxp3+ Regulatory T Cells. PLoS ONE *10*, e0141161–16.

Štros, M., Launholt, D., and Grasser, K.D. (2007). The HMG-box: a versatile protein domain occurring in a wide variety of DNA-binding proteins. Cell. Mol. Life Sci. *64*, 2590–2606.

Tan, W., Zhang, W., Strasner, A., Grivennikov, S., Cheng, J.Q., Hoffman, R.M., and Karin, M. (2011). Tumour-infiltrating regulatory T cells stimulate mammary cancer metastasis through RANKL-RANK signalling. Nature *470*, 548–553.

Tang, Q., and Bluestone, J.A. (2008). The Foxp3+ regulatory T cell: a jack of all trades, master of regulation. Nat Immunol *9*, 239–244.

Tanoue, T., Atarashi, K., and Honda, K. (2016). Development and maintenance of intestinal regulatory T cells. Nature Publishing Group 1–15.

Tauriello, D.V.F., Calon, A., Lonardo, E., and Batlle, E. (2017). Determinants of metastatic competency in colorectal cancer. Mol Oncol *11*, 97–119.

Thornton, A.M., Kilaru, G., Burr, P., Rieder, S., Muljo, S.A., and Shevach, E.M. (2016).

Helios expression defines two distinct populations of Foxp3⁺ regulatory T cells. J. Immunol. *196*, 125.6.

Thornton, A.M., Korty, P.E., Tran, D.Q., Wohlfert, E.A., Murray, P.E., Belkaid, Y., and Shevach, E.M. (2010). Expression of Helios, an Ikaros transcription factor family member, differentiates thymic-derived from peripherally induced Foxp3+ T regulatory cells. J. Immunol. *184*, 3433–3441.

Tiwari, N., Tiwari, V.K., Waldmeier, L., Balwierz, P.J., Arnold, P., Pachkov, M., Meyer-Schaller, N., Schübeler, D., van Nimwegen, E., and Christofori, G. (2013). Sox4 Is a Master Regulator of Epithelial-Mesenchymal Transition by Controlling Ezh2 Expression and Epigenetic Reprogramming. Cancer Cell *23*, 768–783.

Tomita, T., Kanai, T., Fujii, T., Nemoto, Y., Okamoto, R., Tsuchiya, K., Totsuka, T., Sakamoto, N., Akira, S., and Watanabe, M. (2008). MyD88-Dependent Pathway in T Cells Directly Modulates the Expansion of Colitogenic CD4+ T Cells in Chronic Colitis. The Journal of Immunology *180*, 5291–5299.

Topalian, S.L., Hodi, F.S., Brahmer, J.R., Gettinger, S.N., Smith, D.C., McDermott, D.F., Powderly, J.D., Carvajal, R.D., Sosman, J.A., Atkins, M.B., et al. (2012). Safety, Activity, and Immune Correlates of Anti–PD-1 Antibody in Cancer. N Engl J Med *366*, 2443–2454.

Totsuka, T., Kanai, T., Makita, S., Fujii, R., Nemoto, Y., Oshima, S., Okamoto, R., Koyanagi, A., Akiba, H., Okumura, K., et al. (2005). Regulation of murine chronic colitis by CD4+CD25- programmed death-1+ T cells. Eur. J. Immunol. *35*, 1773–1785.

Tseng, W., Leong, X., and Engleman, E. (2007). Orthotopic Mouse Model of Colorectal Cancer. JoVE (Journal of Visualized Experiments) e484–e484.

Tsuyada, A., Chow, A., Wu, J., Somlo, G., Chu, P., Loera, S., Luu, T., Li, A.X., Wu, X., Ye, W., et al. (2012). CCL2 Mediates Cross-talk between Cancer Cells and Stromal Fibroblasts That Regulates Breast Cancer Stem Cells. Cancer Research *72*, 2768–2779.

Turley, S.J. (2012). Podoplanin: emerging functions in development, the immune system, and cancer. 1–11.

Uhlig, H.H., Coombes, J., Mottet, C., Izcue, A., Thompson, C., Fanger, A., Tannapfel, A., Fontenot, J.D., Ramsdell, F., and Powrie, F. (2006). Characterization of Foxp3+CD4+CD25+ and IL-10-Secreting CD4+CD25+ T Cells during Cure of Colitis. The Journal of Immunology *177*, 5852–5860.

Ushach, I., Burkhardt, A.M., Martinez, C., Hevezi, P.A., Gerber, P.A., Buhren, B.A., Schrumpf, H., Valle-Rios, R., Vazquez, M.I., Homey, B., et al. (2015). METEORIN-LIKE is a cytokine associated with barrier tissues and alternatively activated macrophages. Clinical Immunology *156*, 119–127.

Valastyan, S., and Weinberg, R.A. (2011). Tumor Metastasis: Molecular Insights and

Evolving Paradigms. Cell *147*, 275–292.

Valvona, C.J., Fillmore, H.L., Nunn, P.B., and Pilkington, G.J. (2015). The Regulation and Function of Lactate Dehydrogenase A: Therapeutic Potential in Brain Tumor. Brain Pathology *26*, 3–17.

Van Cutsem, E., Lenz, H.-J., Köhne, C.-H., Heinemann, V., Tejpar, S., Melezínek, I., Beier, F., Stroh, C., Rougier, P., van Krieken, J.H., et al. (2015). Fluorouracil, Leucovorin, and Irinotecan Plus Cetuximab Treatment and RASMutations in Colorectal Cancer. Jco *33*, 692–700.

van der Flier, L.G., and Clevers, H. (2009). Stem Cells, Self-Renewal, and Differentiation in the Intestinal Epithelium. Annu. Rev. Physiol. *71*, 241–260.

Veldhoen, M., Hocking, R.J., Atkins, C.J., Locksley, R.M., and Stockinger, B. (2006). TGFβ in the Context of an Inflammatory Cytokine Milieu Supports De Novo Differentiation of IL-17-Producing T Cells. Immunity *24*, 179–189.

Vervoort, S.J., van Boxtel, R., and Coffer, P.J. (2012). The role of SRY-related HMG box transcription factor 4 (SOX4) in tumorigenesis and metastasis: friend or foe? Oncogene *32*, 3397–3409.

Vicente-Suarez, I., Larange, A., Reardon, C., Matho, M., Feau, S., Chodaczek, G., Park, Y., Obata, Y., Gold, R., Wang-Zhu, Y., et al. (2014). Unique lamina propria stromal cells imprint the functional phenotype of mucosal dendritic cells. Mucosal Immunology *8*, 141–151.

Vivier, E., van de Pavert, S.A., Cooper, M.D., and Belz, G.T. (2016). The evolution of innate lymphoid cells. Nat Immunol *17*, 790–794.

Walton, K.L.W., Holt, L., and Sartor, R.B. (2009). Lipopolysaccharide activates innate immune responses in murine intestinal myofibroblasts through multiple signaling pathways. AJP: Gastrointestinal and Liver Physiology *296*, G601–G611.

Wang, B., Li, Y., Tan, F., and Xiao, Z. (2016). Increased expression of SOX4 is associated with colorectal cancer progression. Tumor Biology 1–7.

Wang, D., Wang, H., Brown, J., Daikoku, T., Ning, W., Shi, Q., Richmond, A., Strieter, R., Dey, S.K., and DuBois, R.N. (2006). CXCL1 induced by prostaglandin E2 promotes angiogenesis in colorectal cancer. J Exp Med *203*, 941–951.

Wang, S., Xia, P., Chen, Y., Qu, Y., Xiong, Z., Ye, B., Du, Y., Tian, Y., Yin, Z., Xu, Z., et al. (2017). Regulatory Innate Lymphoid Cells Control Innate Intestinal Inflammation. Cell *171*, 201–216.e218.

Wehinger, J., Gouilleux, F., Groner, B., Finke, J., Mertelsmann, R., and Weber-Nordt, R.M. (1996). IL-10 induces DNA binding activity of three STAT proteins (Stat1, Stat3, and Stat5) and their distinct combinatorial assembly in the promoters of selected genes. FEBS Letters *394*, 365–370.

Weiss, A., and Attisano, L. (2012). The TGFbeta Superfamily Signaling Pathway. WIREs Dev Biol *2*, 47–63.

Weiss, J.M., Bilate, A.M., Gobert, M., Ding, Y., Curotto de Lafaille, M.A., Parkhurst, C.N., Xiong, H., Dolpady, J., Frey, A.B., Ruocco, M.G., et al. (2012). Neuropilin 1 is expressed on thymus-derived natural regulatory T cells, but not mucosa-generated induced Foxp3 +T reg cells. J Exp Med *209*, 1723–1742.

West, N.R., McCuaig, S., Franchini, F., and Powrie, F. (2015). Emerging cytokine networks in colorectal cancer. Nature Publishing Group *15*, 615–629.

West, N.R., Hegazy, A.N., Owens, B.M.J., Bullers, S.J., Linggi, B., Buonocore, S., Coccia, M., Görtz, D., This, S., Stockenhuber, K., et al. (2017). Oncostatin M drives intestinal inflammation and predicts response to tumor necrosis factor–neutralizing therapy in patients with inflammatory bowel disease. Nature Medicine *23*, 579–589.

Wildin, R.S., Ramsdell, F., Peake, J., Faravelli, F., Casanova, J.L., Buist, N., Levy-Lahad, E., Mazzella, M., Goulet, O., Perroni, L., et al. (2001). X-linked neonatal diabetes mellitus, enteropathy and endocrinopathy syndrome is the human equivalent of mouse scurfy. Nature Genetics *27*, 18–20.

Wilke, C.M., Wu, K., Zhao, E., Wang, G., and Zou, W. (2010). Prognostic significance of regulatory T cells in tumor. Int. J. Cancer *88*, n/a–n/a.

Wing, K., Onishi, Y., Prieto-Martin, P., Yamaguchi, T., Miyara, M., Fehervari, Z., Nomura, T., and Sakaguchi, S. (2008). CTLA-4 Control over Foxp3+ Regulatory T Cell Function. Science *322*, 271–275.

Wohlfert, E.A., Grainger, J.R., Bouladoux, N., Konkel, J.E., Oldenhove, G., Ribeiro, C.H., Hall, J.A., Yagi, R., Naik, S., Bhairavabhotla, R., et al. (2011). GATA3 controls Foxp3+ regulatory T cell fate during inflammation in mice. J. Clin. Invest. *121*, 4503–4515.

Wrzesinski, S.H., Wan, Y.Y., and Flavell, R.A. (2007). Transforming Growth Factor-beta and the Immune Response: Implications for Anticancer Therapy. Clinical Cancer Research *13*, 5262–5270.

Wu, S., Rhee, K.-J., Albesiano, E., Rabizadeh, S., Wu, X., Yen, H.-R., Huso, D.L., Brancati, F.L., Wick, E., McAllister, F., et al. (2009). A human colonic commensal promotes colon tumorigenesis via activation of T helper type 17 T cell responses. Nature Medicine *15*, 1016–1022.

Wynn, T.A., and Ramalingam, T.R. (2012). Mechanisms of fibrosis: therapeutic translation for fibrotic disease. Nature Medicine *18*, 1028–1040.

Xiao, H., Gulen, M.F., Qin, J., Yao, J., Bulek, K., Kish, D., Altuntas, C.Z., Wald, D., Ma, C., Zhou, H., et al. (2007). The Toll–Interleukin-1 Receptor Member SIGIRR Regulates Colonic Epithelial Homeostasis, Inflammation, and Tumorigenesis. Immunity *26*, 461–475.

Xie, Z., Chan, E.C., and Druey, K.M. (2015). R4 Regulator of G Protein Signaling (RGS) Proteins in Inflammation and Immunity. Aaps J *18*, 294–304.

Xue, Y., Johnson, R., DeSmet, M., Snyder, P.W., and Fleet, J.C. (2010). Generation of a Transgenic Mouse for Colorectal Cancer Research with Intestinal Cre Expression Limited to the Large Intestine. Molecular Cancer Research *8*, 1095–1104.

Yamada, M., Ichikawa, Y., Yamagishi, S., Momiyama, N., Ota, M., Fujii, S., Tanaka, K., Togo, S., Ohki, S., and Shimada, H. (2008). Amphiregulin Is a Promising Prognostic Marker for Liver Metastases of Colorectal Cancer. Clinical Cancer Research *14*, 2351–2356.

Yamamoto, M., Kikuchi, H., Ohta, M., Kawabata, T., Hiramatsu, Y., Kondo, K., Baba, M., Kamiya, K., Tanaka, T., Kitagawa, M., et al. (2008). TSU68 Prevents Liver Metastasis of Colon Cancer Xenografts by Modulating the Premetastatic Niche. Cancer Research *68*, 9754–9762.

Yang, B.-H., Hagemann, S., Mamareli, P., Lauer, U., Hoffmann, U., Beckstette, M., hse, L.F.O., Prinz, I., Pezoldt, J., Suerbaum, S., et al. (2015). Foxp3+ T cells expressing RORgammat represent a stable regulatory T-cell effector lineage with enhanced suppressive capacity during intestinal inflammation. Mucosal Immunology *9*, 444–457.

Yang, D. (1999). Beta-Defensins: Linking Innate and Adaptive Immunity Through Dendritic and T Cell CCR6. Science *286*, 525–528.

Zaiss, D.M.W., Gause, W.C., Osborne, L.C., and Artis, D. (2015). Emerging Functions of Amphiregulin in Orchestrating Immunity, Inflammation, and Tissue Repair. Immunity *42*, 216–226.

Zaiss, D.M.W., van Loosdregt, J., Gorlani, A., Bekker, C.P.J., Gröne, A., Sibilia, M., van Bergen en Henegouwen, P.M.P., Roovers, R.C., Coffer, P.J., and Sijts, A.J.A.M. (2013). Amphiregulin Enhances Regulatory T Cell-Suppressive Function via the Epidermal Growth Factor Receptor. Immunity *38*, 275–284.

Zamarron, B.F., and Chen, W. (2011). Dual roles of immune cells and their factors in cancer development and progression. Int. J. Biol. Sci. *7*, 651–658.

Zhang, D.H., Cohn, L., Ray, P., Bottomly, K., and Ray, A. (1997). Transcription factor GATA-3 is differentially expressed in murine Th1 and Th2 cells and controls Th2-specific expression of the interleukin-5 gene. Journal of Biological Chemistry *272*, 21597–21603.

Zhao, D.M. (2006). Activated CD4+CD25+ T cells selectively kill B lymphocytes. Blood *107*, 3925–3932.

Zhao, J., Ou, B., Han, D., Wang, P., Zong, Y., Zhu, C., Di Liu, Zheng, M., Sun, J., Feng, H., et al. (2017). Tumor-derived CXCL5 promotes human colorectal cancer metastasis through activation of the ERK/Elk-1/Snail and AKT/GSK3β/β-catenin pathways. Mol

Cancer *16*, 70.

Zheng, H., and Kang, Y. (2013). Multilayer control of the EMT master regulators. *33*, 1755–1763.

Zheng, S.-L., Li, Z.-Y., Song, J., Liu, J.-M., and Miao, C.-Y. (2016). Metrnl: a secreted protein with new emerging functions. Nature Publishing Group *37*, 571–579.

Zheng, Y., Chaudhry, A., Kas, A., deRoos, P., Kim, J.M., Chu, T.-T., Corcoran, L., Treuting, P., Klein, U., and Rudensky, A.Y. (2009). Regulatory T-cell suppressor program co-opts transcription factor IRF4 to control TH2 responses. Nature *458*, 351–356.

Zheng, Y., Josefowicz, S., Chaudhry, A., Peng, X.P., Forbush, K., and Rudensky, A.Y. (2010). Role of conserved non-coding DNA elements in the Foxp3 gene in regulatory T-cell fate. Nature *463*, 808–812.

Zhou, L., Chong, M.M.W., and Littman, D.R. (2009). Plasticity of CD4+ T Cell Lineage Differentiation. Immunity *30*, 646–655.

Zhou, Y., Lee, J.-Y., Lee, C.-M., Cho, W.-K., Kang, M.-J., Koff, J.L., Yoon, P.-O., Chae, J., Park, H.-O., Elias, J.A., et al. (2012). Amphiregulin, an Epidermal Growth Factor Receptor Ligand, Plays an Essential Role in the Pathogenesis of Transforming Growth Factor-β-induced Pulmonary Fibrosis. Journal of Biological Chemistry *287*, 41991–42000.

8 Appendix 1 – A Treg Tale

8.1 R Studio version and Session information

```
> sessionInfo()
R version 3.3.3 (2017-03-06)
Platform: x86_64-apple-darwin13.4.0 (64-bit)
Running under: OS X El Capitan 10.11.3

locale:
[1] en_GB.UTF-8/en_GB.UTF-8/en_GB.UTF-8/C/en_GB.UTF-8/en_GB.UTF-8

attached base packages:
[1] stats     graphics  grDevices utils     datasets  methods   base

other attached packages:
[1] biomaRt_2.30.0

loaded via a namespace (and not attached):
 [1] SummarizedExperiment_1.4.0 genefilter_1.56.0
 [3] locfit_1.5-9.1             splines_3.3.3
 [5] lattice_0.20-35            colorspace_1.3-2
 [7] htmltools_0.3.6            stats4_3.3.3
 [9] base64enc_0.1-3            blob_1.1.0
[11] survival_2.41-3            XML_3.98-1.9
[13] rlang_0.1.2                foreign_0.8-69
[15] DBI_0.7                    BiocParallel_1.8.2
[17] BiocGenerics_0.20.0        bit64_0.9-7
[19] RColorBrewer_1.1-2         plyr_1.8.4
[21] stringr_1.2.0              zlibbioc_1.20.0
[23] munsell_0.4.3              gtable_0.2.0
[25] DESeq2_1.14.1              htmlwidgets_0.9
[27] memoise_1.1.0              latticeExtra_0.6-28
[29] Biobase_2.34.0             knitr_1.17
[31] geneplotter_1.52.0         IRanges_2.8.2
[33] GenomeInfoDb_1.10.3        parallel_3.3.3
[35] AnnotationDbi_1.36.2       htmlTable_1.9
[37] Rcpp_0.12.12               acepack_1.4.1
[39] xtable_1.8-2               scales_0.4.1
[41] backports_1.1.0            checkmate_1.8.3
[43] S4Vectors_0.12.2           Hmisc_4.0-3
[45] annotate_1.52.1            XVector_0.14.1
[47] bit_1.1-12                 gridExtra_2.2.1
[49] ggplot2_2.2.1              digest_0.6.12
[51] stringi_1.1.5              GenomicRanges_1.26.4
[53] grid_3.3.3                 tools_3.3.3
[55] bitops_1.0-6               magrittr_1.5
[57] lazyeval_0.2.0             RCurl_1.95-4.8
[59] tibble_1.3.3               RSQLite_2.0
[61] Formula_1.2-2              cluster_2.0.6
[63] Matrix_1.2-11              data.table_1.10.4
[65] rpart_4.1-11               nnet_7.3-12
>
```

8.2 Total number of expressed genes for all samples

All genes with no reads in all samples were removed from the matrix count using the following code in PYCharm CE.

8.2.1 Main function

```
import pandas as pd
from auxiliary import *

def clean_data(file):
    df = pd.DataFrame.from_csv(file, sep='\t')
    df_zeros = df.loc[(df == 0).all(axis=1)]
    # loc is location, axis 0 would be column, while axis 1 is
a row
    df_clean = df.loc[(df != 0).any(axis=1)]
    num_del = len(df_zeros.index)
    num_values = df_clean[df_clean > 0].count()
    return [df_clean, num_del, num_values]


def main():
    file = 'refcoding.featurecountsmodified.tsv'
    res = clean_data(file)
    file_out = 'cleaned.csv'
    file_aux = 'nonzero_counts.csv'
    print(res[1])
    res[0].to_csv(file_out)
    res[2].to_csv(file_aux)


if __name__ == '__main__':
    main()
```

8.2.2 Auxiliary

```
import pandas as pd


def clean_data(file):
    df = pd.DataFrame.from_csv(file, sep='\t')
    df_zeros = df.loc[(df == 0).all(axis=1)]
    # loc is location, axis 0 would be column, while axis 1 is
a row
    df_clean = df.loc[(df != 0).any(axis=1)]
    num_del = len(df_zeros.index)
    num_values = df_clean[df_clean > 0].count()
    return [df_clean, num_del, num_values]
```

8.2.3 Addition

```
def add_(x):
    return sum(x)


def main():
    x = [int(y) for y in input('Enter shit: ').split(',')]
    z = [int(y) for y in input().split(',')]

    print(add_(x))
    print(add_(z))

if __name__ == '__main__':
    main()
```

8.2.4 Table of total genes with >1 read per sample

Sample ID	Total genes >1 read
treg-colonCD25KO-R1	10493
treg-colonCD25KO-R2	8934
treg-colonCD25KO-R3	11379
treg-colonCD25KO-R4	11924
treg-colonCD25negKO-R1	11239
treg-colonCD25negKO-R2	11300
treg-colonCD25negKO-R3	10953
treg-colonCD25negKO-R4	10973
treg-spleenCD25KO-R1	11667
treg-spleenCD25KO-R2	11887
treg-spleenCD25KO-R3	10504
treg-spleenCD25KO-R4	10646
treg-spleenCD25KO-R5	11062
treg-colonCD25WT-R1	10283
treg-colonCD25WT-R2	10893
treg-colonCD25WT-R3	11173
treg-colonCD25WT-R4	11918
treg-colonCD25WT-R5	11104
treg-colonCD25negWT-R1	9867
treg-colonCD25negWT-R2	11064
treg-colonCD25negWT-R3	10929
treg-colonCD25negWT-R4	12321
treg-colonCD25negWT-R5	11308
treg-spleenCD25WT-R1	12840
treg-spleenCD25WT-R2	12479
treg-spleenCD25WT-R3	12729
treg-spleenCD25WT-R4	8928
treg-spleenCD25WT-R5	10219

8.3 R Code used for this analysis

```
sessionInfo()

library(DESeq2)

countMatrix = read.table("matrix_counts.csv", header = T, row.names
= 1, sep=',')
countdata = as.matrix(countMatrix)

design2 <- read.csv("sample_table.csv", header=T, row.names=1)
coldata = data.frame(row.names = colnames(countdata), design2)

gsub("-",".",rownames(design2))==colnames(countdata)

dds = DESeqDataSetFromMatrix(countData = countMatrix, colData =
coldata, design = ~ Type)

(colData(dds) <- DataFrame(design2))

#------------ Differential expression analysis -------------#
dds <- estimateSizeFactors(dds)
dds <- estimateDispersions(dds, fitType = c("local"), maxit = 100,
quiet = FALSE, modelMatrix = NULL)
#local fit rather than parametric - use the locfit package to fit a
local regression of log dispersions
#over log base mean (normal scale means and dispersions are
#input and output for dispersionFunction).
#The points are weighted by normalized mean count in the local
regression.
dds <- nbinomWaldTest(dds)
pdf("DESeq2's dispersion estimates.pdf", width = 10, height = 10)
plotDispEsts(dds)
dev.off()

colData(dds)
resultsNames(dds)
counts(dds)

res <- results( dds )
res
mcols(res, use.names=TRUE)
summary(res)

res1 <- results(dds, contrast=c("Type", "SpleenTregWT",
"SpleenTregKO"))
res1
mcols(res1, use.names=TRUE)
summary(res1)

res2 <- results(dds, contrast=c("Type", "ColonTregWT",
"ColonTregKO"))
res2
mcols(res2, use.names=TRUE)
summary(res2)

res3 <- results(dds, contrast=c("Type", "ColonTcellWT",
"ColonTcellKO"))
```

```
res3
mcols(res3, use.names=TRUE)
summary(res3)

res4 <- results(dds, contrast=c("Type", "ColonTregKO",
"ColonTcellKO"))
res4
mcols(res4, use.names=TRUE)
summary(res4)

res5 <- results(dds, contrast=c("Type", "ColonTregWT",
"ColonTcellWT"))
res5
mcols(res5, use.names=TRUE)
summary(res5)

res6 <- results(dds, contrast=c("Type", "SpleenTregKO",
"ColonTregKO"))
res6
mcols(res6, use.names=TRUE)
summary(res6)

res7 <- results(dds, contrast=c("Type", "SpleenTregKO",
"ColonTcellKO"))
res7
mcols(res7, use.names=TRUE)
summary(res7)

res8 <- results(dds, contrast=c("Type", "SpleenTregWT",
"ColonTregWT"))
res8
mcols(res8, use.names=TRUE)
summary(res8)

res9 <- results(dds, contrast=c("Type", "SpleenTregWT",
"ColonTcellWT"))
res9
mcols(res9, use.names=TRUE)
summary(res9)


#----------- Vst analysis -----------#

vst <- varianceStabilizingTransformation(dds, blind=FALSE)
vst.fast <- vst(dds, blind=FALSE)
head(assay(vst), 3)

library("vsn")
meanSdPlot(assay(vst))

library("pheatmap")
select <-
order(rowMeans(counts(dds,normalized=FALSE)),decreasing=TRUE)[1:100]
df <- as.data.frame(colData(dds)[,c("Tissue","Genotype","Cell")])
pdf("Top 100 genes vst.pdf", width = 10, height = 10)
pheatmap(assay(vst)[select,], cluster_rows=FALSE,
show_rownames=FALSE,
         cluster_cols=FALSE, annotation_col=df)
dev.off()
```

```
#Heatmap of the sample-to-sample distances
sampleDists2 <- dist(t(assay(vst)))
library("RColorBrewer")
sampleDistMatrix2 <- as.matrix(sampleDists2)
rownames(sampleDistMatrix2) <- paste(vst, sep="-")
colnames(sampleDistMatrix2) <- NULL
pdf("sample_to_sample_distance_vst.pdf")
colors <- colorRampPalette( rev(brewer.pal(9, "Blues")) )(255)
pheatmap(sampleDistMatrix2,
         clustering_distance_rows=sampleDists2,
         clustering_distance_cols=sampleDists2,
         col=colors)
dev.off()

#Correlation matrix
cor2 <- cor(assay(vst))
pdf("pheatmap_correlation_matrix_vst.pdf")
pheatmap(1-cor2,
         clustering_distance_rows=sampleDists2,
         clustering_distance_cols=sampleDists2,
         col=colors)
dev.off()

#Scatter plot of sample 2 vs sample 1.
par( mfrow = c( 1, 2 ) )
plot( log2( 1+counts(dds, normalized=TRUE)[, 1:2] ),
col="#00000020", pch=20, cex=0.3 )
plot( assay(vst)[, 1:2], col="#00000020", pch=20, cex=0.3 )

#--- Other variations for matrix and clustering ---#

sampleDists <- dist( t( assay(vst) ) )
sampleDistMatrix <- as.matrix( sampleDists )
library( "gplots" )
library( "RColorBrewer" )
colours = colorRampPalette( rev(brewer.pal(9, "Blues")) )(255)
heatmap.2( sampleDistMatrix, trace="none", col=colours)
pdf("Sample_distance_vst.pdf", width = 10, height = 10)
heatmap.2(sampleDistMatrix, trace="none", col=colours, lhei =
c(0.05, 0.25), mar=c(18,12))
dev.off()

library( "genefilter" )
pdf("Top_var_genes_vst.pdf", width = 10, height = 10)
topVarGenes <- head( order( rowVars( assay(vst) ), decreasing=TRUE
), 100 )
heatmap.2( assay(vst)[ topVarGenes, ], scale="row",
           trace="none", dendrogram="column",
           col = colorRampPalette( rev(brewer.pal(9, "RdBu"))
)(255),
           mar=c(18,12)) #to have all text included on pdf, margins
dev.off()


#--- END OF other variations for clustering ---#
```

```
#-------- Principal component plot of the samples with vst --------#

library(ggplot2)
library(ggrepel)

Samples = (c(rep("ColonTregKO",3), rep("ColonTcellKO",4),
rep("SpleenTregKO",5), rep("ColonTregWT",5), rep("ColonTcellWT",2),
rep("SpleenTregWT",3)))
labelsample = c("R1",   "R3", "R4",
                "R1", "R2",   "R3", "R4",
                "R1", "R2",   "R3", "R4", "R5",
                "R1", "R2",   "R3", "R4", "R5",
                "R3",   "R5",
                "R1", "R2",   "R5")

# PCA with function prcomp
pca2 = prcomp(t(assay(vst)))
pcs2 <- data.frame(pca2$x)

# plot of observations
ggplot(data = pcs2, aes(x = PC1, y = PC2, color=Samples,
shape=Samples, geom_text(size=0.2))) +
  geom_hline(yintercept = 0, colour = "gray65") +
  geom_vline(xintercept = 0, colour = "gray65") +
  geom_point(size=1.5) +
  geom_text_repel(aes(label = labelsample))
ggsave("Vst_all_samples_pc1_vs_pc2.png")

ggplot(data = pcs2, aes(x = PC3, y = PC4, color=Samples,
shape=Samples, geom_text(size=0.2))) +
  geom_hline(yintercept = 0, colour = "gray65") +
  geom_vline(xintercept = 0, colour = "gray65") +
  geom_point(size=1.5) +
  geom_text_repel(aes(label = labelsample))
ggsave("Vst_all_samples_pc3_vs_pc4.png")

ggplot(data = pcs2, aes(x = PC5, y = PC6, color=Samples,
shape=Samples, geom_text(size=0.2))) +
  geom_hline(yintercept = 0, colour = "gray65") +
  geom_vline(xintercept = 0, colour = "gray65") +
  geom_point(size=1.5) +
  geom_text_repel(aes(label = labelsample))
ggsave("Vst_all_samples_pc5_vs_pc6.png")

#---- Scree plot for PCA using vst ----#
library(matrixStats)

# calculate the variance for each gene
rv <- rowVars(assay(vst))

# select the ntop genes by variance
select <- order(rv, decreasing=TRUE)[seq_len(min(500, length(rv)))]

# perform a PCA on the data in assay(x) for the selected genes
pca <- prcomp(t(assay(vst)[select,]))
```

```
# the contribution to the total variance for each component
percentVar <- pca$sdev^2 / sum( pca$sdev^2 )

#plot the "percentVar"
scree_plot=data.frame(percentVar)
scree_plot[,2]<- c(1:22)

colnames(scree_plot)<-c("variance","component_number")
pdf("Scree_plot.pdf", width = 10, height = 10)
ggplot(scree_plot, mapping=aes(x=component_number,
y=variance))+geom_bar(stat="identity")
dev.off()

#-------- MA plots --------#

pdf("SpleenTregWT vs SpleenTregKO.pdf", width = 10, height = 10)
plotMA(res1, main="SpleenTregWT vs SpleenTregKO", ylim=c(-5,5))
dev.off()

pdf("ColonTregWT vs ColonTregKO.pdf", width = 10, height = 10)
plotMA(res2, main="ColonTregWT vs ColonTregKO", ylim=c(-5,5))
dev.off()

pdf("ColonTcellWT vs ColonTcellKO.pdf", width = 10, height = 10)
plotMA(res3, main="ColonTcellWT vs ColonTcellKO", ylim=c(-5,5))
dev.off()

pdf("ColonTregKO vs ColonTcellKO.pdf", width = 10, height = 10)
plotMA(res4, main="ColonTregKO vs ColonTcellKO", ylim=c(-5,5))
dev.off()

pdf("ColonTregWT vs ColonTcellWT.pdf", width = 10, height = 10)
plotMA(res5, main="ColonTregWT vs ColonTcellWT", ylim=c(-5,5))
dev.off()

pdf("SpleenTregKO vs ColonTregKO.pdf", width = 10, height = 10)
plotMA(res6, main="SpleenTregKO vs ColonTregKO", ylim=c(-5,5))
dev.off()

pdf("SpleenTregKO vs ColonTcellKO.pdf", width = 10, height = 10)
plotMA(res7, main="SpleenTregKO vs ColonTcellKO", ylim=c(-5,5))
dev.off()

pdf("SpleenTregWT vs ColonTregWT.pdf", width = 10, height = 10)
plotMA(res8, main="SpleenTregWT vs ColonTregWT", ylim=c(-5,5))
dev.off()

pdf("SpleenTregWT vs ColonTcellWT.pdf", width = 10, height = 10)
plotMA(res9, main="SpleenTregWT vs ColonTcellWT", ylim=c(-5,5))
dev.off()
```

```
#------- New Version Annotating and exporting results -------#
library(biomaRt)

res1$ensembl <- sapply( strsplit( rownames(res1), split="\\+" ),
"[", 1 )
ensembl <- useMart("ensembl", dataset="mmusculus_gene_ensembl")
genemap <- getBM( attributes = c("ensembl_gene_id", "mgi_symbol",
"chromosome_name", "strand", "start_position", "end_position",
"gene_biotype"),
                  filters = "ensembl_gene_id",
                  values = res1$ensembl,
                  mart = ensembl )
idx <- match( res1$ensembl, genemap$ensembl_gene_id )
res1$entrez <- genemap$entrezgene[ idx ]
res1$mgi_symbol <- genemap$mgi_symbol[ idx ]
head(res1,4)
write.csv( as.data.frame(res1),
file="results_SpleenTregWT_vs_SpleenTregKO.csv" )

res2$ensembl <- sapply( strsplit( rownames(res2), split="\\+" ),
"[", 1 )
ensembl <- useMart("ensembl", dataset="mmusculus_gene_ensembl")
genemap <- getBM( attributes = c("ensembl_gene_id", "mgi_symbol",
"chromosome_name", "strand", "start_position", "end_position",
"gene_biotype"),
                  filters = "ensembl_gene_id",
                  values = res2$ensembl,
                  mart = ensembl )
idx <- match( res2$ensembl, genemap$ensembl_gene_id )
res2$entrez <- genemap$entrezgene[ idx ]
res2$mgi_symbol <- genemap$mgi_symbol[ idx ]
head(res2,4)
write.csv( as.data.frame(res2),
file="results_ColonTregWT_vs_ColonTregKO.csv" )

res3$ensembl <- sapply( strsplit( rownames(res3), split="\\+" ),
"[", 1 )
ensembl <- useMart("ensembl", dataset="mmusculus_gene_ensembl")
genemap <- getBM( attributes = c("ensembl_gene_id", "mgi_symbol",
"chromosome_name", "strand", "start_position", "end_position",
"gene_biotype"),
                  filters = "ensembl_gene_id",
                  values = res3$ensembl,
                  mart = ensembl )
idx <- match( res3$ensembl, genemap$ensembl_gene_id )
res3$entrez <- genemap$entrezgene[ idx ]
res3$mgi_symbol <- genemap$mgi_symbol[ idx ]
head(res3,4)
write.csv( as.data.frame(res3),
file="results_ColonTcellWT_vs_ColonTcellKO.csv" )

res4$ensembl <- sapply( strsplit( rownames(res4), split="\\+" ),
"[", 1 )
ensembl <- useMart("ensembl", dataset="mmusculus_gene_ensembl")
genemap <- getBM( attributes = c("ensembl_gene_id", "mgi_symbol",
```

```
"chromosome_name", "strand", "start_position", "end_position",
"gene_biotype"),
                  filters = "ensembl_gene_id",
                  values = res4$ensembl,
                  mart = ensembl )
idx <- match( res4$ensembl, genemap$ensembl_gene_id )
res4$entrez <- genemap$entrezgene[ idx ]
res4$mgi_symbol <- genemap$mgi_symbol[ idx ]
head(res4,4)
write.csv( as.data.frame(res4),
file="results_ColonTregKO_vs_ColonTcellKO.csv" )

res5$ensembl <- sapply( strsplit( rownames(res5), split="\\+" ),
"[", 1 )
ensembl <- useMart("ensembl", dataset="mmusculus_gene_ensembl")
genemap <- getBM( attributes = c("ensembl_gene_id", "mgi_symbol",
"chromosome_name", "strand", "start_position", "end_position",
"gene_biotype"),
                  filters = "ensembl_gene_id",
                  values = res5$ensembl,
                  mart = ensembl )
idx <- match( res5$ensembl, genemap$ensembl_gene_id )
res5$entrez <- genemap$entrezgene[ idx ]
res5$mgi_symbol <- genemap$mgi_symbol[ idx ]
head(res5,4)
write.csv( as.data.frame(res5),
file="results_ColonTregWT_vs_ColonTcellWT.csv" )

res6$ensembl <- sapply( strsplit( rownames(res6), split="\\+" ),
"[", 1 )
ensembl <- useMart("ensembl", dataset="mmusculus_gene_ensembl")
genemap <- getBM( attributes = c("ensembl_gene_id", "mgi_symbol",
"chromosome_name", "strand", "start_position", "end_position",
"gene_biotype"),
                  filters = "ensembl_gene_id",
                  values = res6$ensembl,
                  mart = ensembl )
idx <- match( res6$ensembl, genemap$ensembl_gene_id )
res6$entrez <- genemap$entrezgene[ idx ]
res6$mgi_symbol <- genemap$mgi_symbol[ idx ]
head(res6,4)
write.csv( as.data.frame(res6),
file="results_SpleenTregKO_vs_ColonTregKO.csv" )

res7$ensembl <- sapply( strsplit( rownames(res7), split="\\+" ),
"[", 1 )
ensembl <- useMart("ensembl", dataset="mmusculus_gene_ensembl")
genemap <- getBM( attributes = c("ensembl_gene_id", "mgi_symbol",
"chromosome_name", "strand", "start_position", "end_position",
"gene_biotype"),
                  filters = "ensembl_gene_id",
                  values = res7$ensembl,
                  mart = ensembl )
idx <- match( res7$ensembl, genemap$ensembl_gene_id )
res7$entrez <- genemap$entrezgene[ idx ]
```

```
res7$mgi_symbol <- genemap$mgi_symbol[ idx ]
head(res7,4)
write.csv( as.data.frame(res7),
file="results_SpleenTregKO_vs_ColonTcellKO.csv" )

res8$ensembl <- sapply( strsplit( rownames(res8), split="\\+" ),
"[", 1 )
ensembl <- useMart("ensembl", dataset="mmusculus_gene_ensembl")
genemap <- getBM( attributes = c("ensembl_gene_id", "mgi_symbol",
"chromosome_name", "strand", "start_position", "end_position",
"gene_biotype"),
                  filters = "ensembl_gene_id",
                  values = res8$ensembl,
                  mart = ensembl )
idx <- match( res8$ensembl, genemap$ensembl_gene_id )
res8$entrez <- genemap$entrezgene[ idx ]
res8$mgi_symbol <- genemap$mgi_symbol[ idx ]
head(res8,4)
write.csv( as.data.frame(res8),
file="results_SpleenTregWT_vs_ColonTregWT.csv" )

res9$ensembl <- sapply( strsplit( rownames(res9), split="\\+" ),
"[", 1 )
ensembl <- useMart("ensembl", dataset="mmusculus_gene_ensembl")
genemap <- getBM( attributes = c("ensembl_gene_id", "mgi_symbol",
"chromosome_name", "strand", "start_position", "end_position",
"gene_biotype"),
                  filters = "ensembl_gene_id",
                  values = res9$ensembl,
                  mart = ensembl )
idx <- match( res9$ensembl, genemap$ensembl_gene_id )
res9$entrez <- genemap$entrezgene[ idx ]
res9$mgi_symbol <- genemap$mgi_symbol[ idx ]
head(res9,4)
write.csv( as.data.frame(res9),
file="results_SpleenTregWT_vs_ColonTcellWT.csv" )

#-------- Volcano Plots --------#

library(dplyr)
library(magrittr)

vol1 <- data.frame(gene = row.names(res1),
                   pvalue = -log10(res1$padj),
                   lfc = res1$log2FoldChange)
```

```
# Remove rows that have NA values
vol1 <- na.omit(vol1)

# View table
head(vol1)

vol1 <- vol1 %>%
  mutate(color = ifelse(vol1$lfc > 0 & vol1$pvalue > 1.3,
                        yes = "TregKO",
                        no = ifelse(vol1$lfc < 0 & vol1$pvalue >
1.3,
                                    yes = "TregWT",
                                    no = "none")))

# Color corresponds to fold change directionality
colored1 <- ggplot(vol1, aes(x = lfc, y = pvalue)) +
  geom_point(aes(color = factor(color)), size = 1.75, alpha = 0.8,
na.rm = T) + # add gene points
  theme_bw(base_size = 16) + # clean up theme
  theme(legend.position = "none") + # remove legend
  ggtitle(label = "Volcano Plot", subtitle = "Splenic WT Tregs
versus IL10-/- Tregs") +  # add title
  xlab(expression(log[2]("Spleen TregKO" / "Spleen TregWT"))) + # x-
axis label
  ylab(expression(-log[10]("adjusted p-value"))) + # y-axis label
  geom_vline(xintercept = 0, colour = "black") + # add line at 0
  geom_hline(yintercept = 1.3, colour = "black") + # p(0.05) = 1.3,
p(0.1)=1
  annotate(geom = "text",
           label = "Spleen Treg WT",
           x = -3, y = 95,
           size = 4, colour = "black") + # add Untreated text
  annotate(geom = "text",
           label = "Spleen Treg KO",
           x = 3, y = 95,
           size = 4, colour = "black") + # add Treated text
  scale_color_manual(values = c("Spleen Treg KO" = "#E64B35",
                                "Spleen Treg WT" = "#3182bd",
                                "none" = "#636363")) # change colors

# Plot figure
colored1

plot(x = c(1:100),
     y = log1p(1:100),
     main = "log(1+x)")

# Scaled Y-axis with log1p function
colored1 + scale_y_continuous(trans = "log1p")
```

8.4 Differential expression analysis – gene details

8.4.1 An exploration of genes upregulated in splenic WT Tregs

Several genes found to be upregulated in splenic WT Tregs compared to IL-10$^{-/-}$ Tregs have no function described or lack characterisation in immune populations. These targets with unknown or poorly described function are listed in Appendix 1 (A Treg Tale).

For instance, *Tpm3-rs7* (tropomyosin 3, related sequence 7) is an uncharacterised protein that has potential functions in actin binding and filament organisation. *Tubb3* is an isotype of beta-tubulin that has been described in various cell types, but its precise function in non-neuronal cells is unknown. Similarly, *Nebl* (Nebulette) is an actin-binding protein with no described function in the immune system. *Gm10036* (predicted gene 10036) and *Gm9726* (predicted gene 9726) have no described expressions or functions thus far. Similarly, *Fxyd2* (FXYD domain-containing ion transport regulator 2) and *Akr1c12* (aldo-keto reductase family 1, member C12) have no known functions in lymphocytes. *Zfp330* (Zinc finger protein 330) has no function reported, however was found to be downregulated in tumour infiltrating CD8$^+$ T cells compared to splenic CD8$^+$ T cells, in a mouse model of melanoma (Katherine A. Waugh 2006, SI).

Several genes related to calcium-related processes were upregulated in WT Tregs, such as *Cacnb3*, *Ncald* and *Srl*. CD4$^+$ T cells express Cav1 family members (calcium channel, voltage-dependent), and functional β3 (*Cacnb3*) and β4 regulatory sub-units are necessary for normal TCR-triggered Ca^{2+} responses, nuclear translocation of NFAT and cytokine production (Badou, A. et al. 2006). *Cacnb3* function was also

explored in $CD8^+$ T cells, showing a previously unknown role for the β3 regulatory protein in the survival of $CD8^+$ T cells *in vitro* and *in vivo* (Mithilesh K Jha 2009 NI). *Srl* (Sarcalumenin) encodes a calcium-binding protein that is partially responsible for calcium buffering in the lumen of the sarcoplasmic reticulum, assisting calcium pump proteins (Yoshida M et al., 2005). Finally, *Ncald* (Neurocalcin delta) has no function reported in lymphocytes, but is involved in calcium signalling and vesicle trafficking (Daniel Ladant, 1995). Relatedly, *Sestd1* (SEC14 and spectrin domain containing 1) is a lipid-binding protein strongly expressed in aorta. It was found to interact with TRPC proteins, members of the mammalian transient receptor potential cation channel family (Susanne Miehe et al., 2009). Its expression was recently detected in human regulatory T cells (Alessandra Ferraro 2014), but no function has been reported.

Other genes upregulated in splenic WT Tregs relate to transport of metabolites and other proteins: *Vangl1*, *Mal2*, *Eepd1* and *Lrrc8d*. *Vangl1* (Vang-like 1) and *Vangl2* are part of the WNT/planar-cell-polarity (PCP) pathway, a key regulator of cell polarity and directional cell movements. No function has been described in lymphocytes, however Vangl2 and other PCP components are overexpressed in chronic lymphoid leukemia (Kaucka et al., 2013). *Mal2* (Myelin And Lymphocyte Protein 2) encodes a multispan transmembrane protein belonging to the MAL proteolipid family. It is required for transcytosis, an intracellular transport pathway used to deliver membrane-bound proteins and exogenous cargos from the basolateral to the apical surface. *Eepd1* (Endonuclease / exonuclease / phosphatase family domain containing 1) has no reported function in lymphocytes, however it was recently described as a novel target gene of cellular cholesterol homeostasis in macrophages, regulating the

expression of the cholesterol efflux transporters to promote cholesterol efflux (Jessica Kristine Nelson et al., 2017). Leucine-rich repeat-containing 8 (LRRC8) proteins, encoded by different isoforms, including *Lrrc8d*, have been identified as putative receptors involved in lymphocyte development and adipocyte differentiation. They comprise the volume-regulated anion channels (VRACs), which are key players in vertebrate cell volume regulation. VRACs have been studied biophysically and physiologically for decades, but the molecular composition of LRRC8 proteins, and the ability of particular LRRC8 heterodimers to transport certain metabolites and drugs has only been established recently (Thomas J. Jentsch, 2016). Another recent study provided experimental evidence that supports a role for LRRC8s in the transport of small molecules, such as those required for the import of the antibiotic blasticidin S (Clarissa C. Lee 2014).

8.4.2 An exploration of genes upregulated in splenic IL-10$^{-/-}$ Tregs

Dynlt1b and *Dynlt1c* (Dynein light chain Tctex-type 1B and 1C) encode for a dynein light chain that is known to bind to various cellular and viral proteins, and can function both as a molecular clamp and as a microtubule-cargo adapter. Similarly, *Fbxo41* (F-box protein 41) is a member of F-box protein family that play a role in phosphorylation-dependent ubiquitination. It has no function described in lymphocytes, however its expression was reported in lymphocyte-predominant Hodgkin lymphoma (Brune V 2008). *Slc41a3* (Solute carrier family 41, member 3), also known as 4F2HC, was identified as a novel player in magnesium homeostasis, demonstrated by the fact that in Slc41a3 deficient mice, serum and urine electrolyte determinations showed that animals suffer from hypomagnesemia. (Jeroen H.F. de Baaij, 2016). Its expression has been reported in human T lymphocytes, and was

linked to cell activation (Keith M. Gottesdiener et al., 1988), although no further characterization has been established more recently. *Ccdc38* encodes for Coiled-coil domain containing 38, which has no confirmed function. Finally, *Tpm3* (Tropomyosin 3, gamma) is part of the tropomyosin family of actin-binding proteins involved in the contractile system of striated and smooth muscles, and the cytoskeleton of non-muscle cells. No function reported in T cells.

A few receptors were also upregulated by IL-10$^{-/-}$ Tregs. The first, *Tmem181a* (Transmembrane protein 181A), also known as Gpr178, is a novel highly conserved GPCR identified in 2007, with no function known in the immune system. *Lilrb4a* (Leukocyte immunoglobulin-like receptor, subfamily B, member 4A), also known as Gp49b, is another receptor upregulated. Gp49B is a receptor of unknown function that is expressed on activated mast cells and natural killer (NK) cells. Generation of deficient mice for Gp49B showed that this receptor is not critical for the development, expansion, and maturation of mast cells and NK cells *in vivo* (Susana Rojo et al., 2000). More recently, expression of Gp49b was reported on DCs, which was linked to downregulation of cellular activity, preventing the excessive activation of T cells in vitro and in vivo (Satoshi Kasai et al., 2008). Overall, Gp49b function in immune responses and T cell function is currently unknown.

8.4.3 Colonic IL-10$^{-/-}$ Tregs

Several genes upregulated in colonic IL-10$^{-/-}$ Tregs were also upregulated in splenic cells: *Dynlt1b*, *Dynlt1c*, *Fbxo41*, *Slc41a3* and *Tlr1*. Furthermore, like splenic Tregs, a few genes have no reported function and are poorly characterised: *Fam189b*, *Hnrnpu* and *Trnt1*.

Fam189b (Family with sequence similarity 189, member B) is broadly poorly characterised and has no reported function in lymphocytes. *Hnrnpu* (Heterogeneous nuclear ribonucleoprotein U) encodes a member of a family of proteins that bind nucleic acids and function in the formation of ribonucleoprotein complexes in the nucleus with heterogeneous nuclear RNA (hnRNA). No function reported in lymphocytes. *Trnt1* (tRNA nucleotidyl transferase, CCA-adding, 1) encodes a protein involved in the maturation of all cytosolic and mitochondrial tRNAs. It functions to add CCA to the 3' terminus of tRNA molecules and is required for proper aminoacylation of all tRNAs. No specific function reported in lymphocytes.

Three upregulated genes have more defined functions: *Slc41a3*, *Crbn* and *Ccr3.*

Slc41a3 (Solute carrier family 41, member 3), also known as MCT6, belongs to the family of monocarboxylate transporters (MCTs). MCT6 has been suggested as bumetanide transporter and also transports various drugs but not L-lactate or L-tryptophan (Yuichi Murakami, 2005). Unlike other members of the MCT family, MCT6 has been poorly characterised and its function is unknown in T cells. *Crbn* (Cereblon) is a ubiquitously expressed E3 ligase protein and has been identified as the primary teratogenic target of thalidomide and other related antiproliferation drugs (A Lopez-Girona et al., 2012). Its expression is reported in lymphocytes, however no function has been associated.

9 Appendix 2: Extended Material and Methods

9.1 Antibodies used in flow cytometry and FACS sorting experiments

Specificity	Fluorochrome	Clone
Surface Markers		
CD11b	M1/70	V500, BV510
CD11c	3.9	BV605, eF450
CD25	7D4	AF647
CD3	17A2	BV650, BV510
CD31	390	FITC
CD4	BV650, BV785	BV650, BV785
CD44	IM7	APC, AF700
CD45	30-F11	AF700, BV
CD45RB	C363-16A	PE
CD62L	MEL-64	PE
CTLA-4	UC10-4F10-11	PE
EpCAM	G8.8	FITC, PeCy7
KLRG1	2FI/KLRG1	PerCP-Cy5.5
Ly6C	HK1.4	PeCy7
Ly6G (Gr1)	1A8	BV510, BV605, APC
MHCII	M5/114.15.2	AF700, eF450
PD-1	RMP1-30	PeCy7
Podoplanin	8.1.1	APC, PeCy7
Siglec-F	E50-2440	PE, BV421
ST2	101001B	Biotin
TCRb	H57-597	BV510, APC
Intracellular markers		
Foxp3	FJK-16s	PE-TxRed, eF450
Gata3	TWAJ	eFluor660
Helios	22F6	AF488
IFNγ	XMG1.2	PeCy7
IL6	MP5-20F3	FITC, PE
IL17A	TC11-18H10.1	FITC, APC
IL22	12-7221-82	PE
Ki67	SolA15	PerCP-eFluor710
Rorγt	Q31-378	PE, BV421
Tbet	4B10	BV711, BV605
TNF	MP6-XT22	AF700

9.2 Taqman probes used for gene expression

Gene Symbol	ABI Assay ID
Acta2	Mm00725412_s1
Areg	Mm00437583_m1
Ccl2	Mm00441242_m1
Cd31	Mm01242576_m1
Cd4	Mm00442754_m1
Cd45	Mm01293577_m1
Col1a1	Mm00801666_g1
Col3a1	Mm01254476_m1
Col5a1	Mm00489342_m1
Cxcl1	Mm00436450_m1
Cxcl5	Mm00436451_g1
Egf	Mm00438696_m1
Egfr	Mm00433023_m1
Epcam	Mm00493214_m1
Ereg	Mm00514794_m1
Fap	Mm01329177_m1
Fgf2	Mm01285715_m1
Foxp3	Mm00475162_m1
Gm-csf	Mm01290062_m1
Gp38	Mm01348912_g1
Ly6c	Mm03009946_m1
Hif1a	Mm01283760_m1
Hprt	Mm01545399_m1
Icam1	Mm00516023_m1
Ifng	Mm01168134_m1
Il11	Mm00434162_m1
Il17a	Mm00439618_m1
Il1b	Mm01336189_m1
Il6	Mm00446190_m1
Ldhb	Mm01267402_m1
Metrnl	Mm00522681_m1
Mmp10	Mm01168399_m1
Mmp13	Mm00439491_m1
Mmp2	Mm00439498_m1
Mmp9	Mm00442991_m1
Osm	Mm01193966_m1
Osmr	Mm01307326_m1
Pdgfra	Mm00440701_m1
Siglecf	Mm00523987_m1
Sox4	Mm00486320_s1
Tgfa	Mm00446231_m1
Tgfb1	Mm00441724_m1
Tlr1	Mm00495643_m1
Tnf	Mm00443258_m1
Vegfa	Mm01281449_m1